Towards Functional Analysis of Archaeological Objects through Reverse Engineering processes

Ph.D Thesis

Vera Moitinho de Almeida

UNIVERSITAT AUTÒNOMA DE BARCELONA
FACULTAT DE FILOSOFIA I LLETRES
Departament de Prehistòria
DOCTORADO OFICIAL D'ARQUEOLOGÍA PREHISTÒRICA

Towards Functional Analysis of Archaeological Objects through Reverse Engineering Processes

by

Vera da Silva Dias Moitinho de Almeida

Thesis submitted for the degree of Doctor in Prehistoric Archaeology

Supervisor
Doctor Juan Antonio Barceló Álvarez, *UAB*

2013

to Pedro and Tomás,

to Ana,

I haven't been everywhere, but it's on my list.

Susan Sontag

Aknowledgements

This cross-disciplinary research would not have been possible without the support and contribution of several people and institutions.

I would first and foremost like to thank my supervisor Juan Antonio Barceló. I am very grateful for his inspiring guidance and ability to truly think out of the box, which helped me a lot to push my own level of expertise. As well as his encouragement and great support during the writing process. I owe him much of chapter two. It has been really stimulating to work with him during these years!

I would also like to acknowledge to my colleagues and friends at UAB, especially to Florencia del Castillo, Giacomo Capuzzo, Hendaya Serrano, Igor Bogdanovich, Katia Achino, Laura Caruso, Laura Mameli, and Teresa Badia, for support and for creating a pleasant and inspiring atmosphere.

Many thanks to the following people and institutions for their kind availability and support (in alphabetical order):

Àngel Bosch, Antonio Nadal Gisbert, David Ortega, Edgard Camarós, Emili Bassols, Esteban Galindo Gali, Fátima Vaz, Hans Nottelmann, Helena Cruz, Ignacio Clemente, Igor Bogdanovich, Irene García, Jean Gaujoux, Jean Gerard, João Appleton, João Tereso, Joan Montserrat Reig, Joaquín Montón, Jordi Jürgens, José António Macedo, Josep Tarrús, Juan José Jiménez Iglesias, Juanjo Ibañez, Juan Serrahimas, Júlia Chinchilla, Laura Caruso, Lawrence G. Straus, Luís Afonso Carvalho, Luis Teira, Manuel Gonzaléz-Morales, Marco

Ansaloni, Maria Saña, Marian Cueto, Matías Monzó Pérez, Mercedes Farjas Abadía, Mériem Fournier, Millán Mozota, Montse Cucurella, Rafel Rosillo, Ramon Buxó, Raquel Piqué, Toni Palomo, Xavier Terradas.

A2P Consult; AgroParisTech Centre de Nancy: Laboratoire d'Etudes des Ressources Forêt Bois (LERFoB, UMR 1092 AgroParisTech INRA); Arqueolític; Atelier Afonso Carvalho; Centre d'Arqueologia Subaquàtica de Catalunya (CASC); Cimworks, Barcelona; Centre de Coopération Internationale en Recherche Agronomique pour le Développement (CIRAD), Département Performances des Systèmes de Production et de Transformation Tropicaux, Unité de Recherche Production et Valorisation des Bois Tropicaux et Méditerranéens, Montpellier; Consejo Superior de Investigaciones Científicas (CSIC), Catalonia: Institución Milà y Fontanals (IMF), Departamento de Arqueología y Antropología, Litoteca de Referència de Roques Silícies de Catalunya (LitoCAT); Digital Surf, Besançon; Laboratório Nacional de Engenharia Civil (LNEC), Lisbon: Departamento de Estruturas, Núcleo de Estruturas de Madeira; Museu Arqueològic Comarcal de Banyoles; Museu d'Arqueologia de Catalunya; Oficina Tècnica de Parcs Naturals de la Diputació de Barcelona; Parc de Montesquiu; Parc Natural de la Zona Volcànica de la Garrotxa, Àrea de Patrimoni Natural; Parcs i Jardis de Barcelona, del Ajuntament de Barcelona; Universitat Autònoma de Barcelona (UAB): Departament of Prehistòria, Laboratori d'Arqueologia Quantitativa (LAQU), Laboratorio de Arqueobotánica; Universidad de Cantabria (UC): Instituto Internacional de Investigaciones Prehistóricas de Cantabria (IIIPC); Universidade de Lisboa (UL): Instituto Superior Técnico (IST), Departamento de Engenharia Mecânica; Universidade do Porto (UP): Research Centre in Biodiversity and Genetic Resources (CIBIO); Universidad Politécnica de Madrid (UPM): Departamento de Ingeniería Topográfica y Cartografía; Universitat Politècnica de València (UPV), Alcoy campus: Departament d'Enginyeria Mecànica i de Materials.

I'm extremely grateful to Lawrence G. Straus and Manuel Gonzaléz-Morales, for giving me the opportunity to include archaeological materials from El Mirón Cave in this research. Rafel Rosillo and Antoni Palomo, from the Serra del Mas Bonet. And Àngel Bosch, Antoni Palomo, Josep Tarrús, Júlia Chinchilla, Maria Saña, Ramon Buxó, Raquel Piqué, and Xavier Terradas from La Draga.

IMF-CSIC for kindly providing the 3D scanner. Antonio Nadal (UPV) for the interesting discussions on the mechanics of bows, and for providing invaluable training and technical guidance whilst undertaking the material properties tests. Esteban Galindo Gali and Juan José Jiménez Iglesias (CimWorks), for their technical support and interesting discussions on the computer simulation of bows. And Digital Surf for their technical support.

Antonio Nadal (UPV); Lawrence G. Straus, Manuel Gonzaléz-Morales, and Luis Teira (IIIPC-UC); Rafel Rosillo (Arqueolític) and Antoni Palomo (UAB, Arqueolític); and Raquel Piqué (UAB), for their helpful comments and valuable criticism on different parts of the manuscript.

My family and friends, for being there. Especially my father António; Teresa and Carlos Madeira; André Moitinho, Maria Filipe, André and Diego; Natacha Moitinho; João Madeira; Rita Madeira, Rui and Alice; Tiago Madeira, Maria João, André and Mariana; Nuno Moitinho, Sofia, Joana, Vicente and Luísa. As well as

Alexandra Ribeiro Simões and Leonor; Ana Mota and Raúl; Ana Raposo and Nelson; Gero Hollberg, Babett, Helene and Alma; Isabel Aranda and Francisco; Isabel Vieira and Inês; João Paulo Simões; Luís Afonso Carvalho, Martim and Sebastião; Margarida Andrês; and Paulo Freitas.

Last and by no means least, I owe a very special thank to Pedro and our son Tomás, the *Stupendous Man*, for being understanding, supportive, and patient with me on this long journey. And for bringing lots of inspiration and joy to my life!

If I have, in any instance, failed to make proper acknowledgement, I offer my apologies.

This research has been financially supported by the Fundação para a Ciência e Tecnologia (FCT), Portugal, co-funded by the European Social Fund, through my Ph.D. grant [SFRH/BD/47609/2008], which I gratefully acknowledge; and by the Obra Social la Caixa and the Asociació d'Universitats Catalanes [Program RecerCaixa, RECER2010-05], through the funded project "PADICAT: Patrimoni Digital Arqueològic de Catalunya". It has also been supported by the following agencies and projects:

- "Experimentation and Development of Advanced Artificial Intelligence Techniques for the Computer Simulation of Social Dynamics and Historical Evolution" [HAR2009-12258, Spain];
- AGREST Research Group (UAB, IMF-CSIC), "Arqueología de la Gestió dels Recursos Socials i el Territori" [project 2009SGR734, Catalonia];
- "Ocupaciones lacustres y gestión de recursos en las primeras sociedades agrícola-ganaderas del NE peninsular: Tecnología de las producciones materiales y usos instrumentales. Estrategias agroforestales y ganaderas" [HAR2009-13494-C01 and C02, subprogram HIST, Spain] (project collaborator);
- "ETNOSIM: Etnicidad en el pasado. Un analisis causal de la etnogenesis en sociedades prehistoricas por medio de tecnicas avanzadas de simulacion computacional", Laboratory for Simulating Social and Historical Dynamics, UAB [HAR2012-31036, Spain].
- "Social and Environmental Transitions: Simulating the past to understand human behaviour (SimulPast)". CONSOLIDER-INGENIO 2010 program by Spanish Ministry of Science and Innovation [CSD2010-00034, Spain]. http://www.simulpast.es

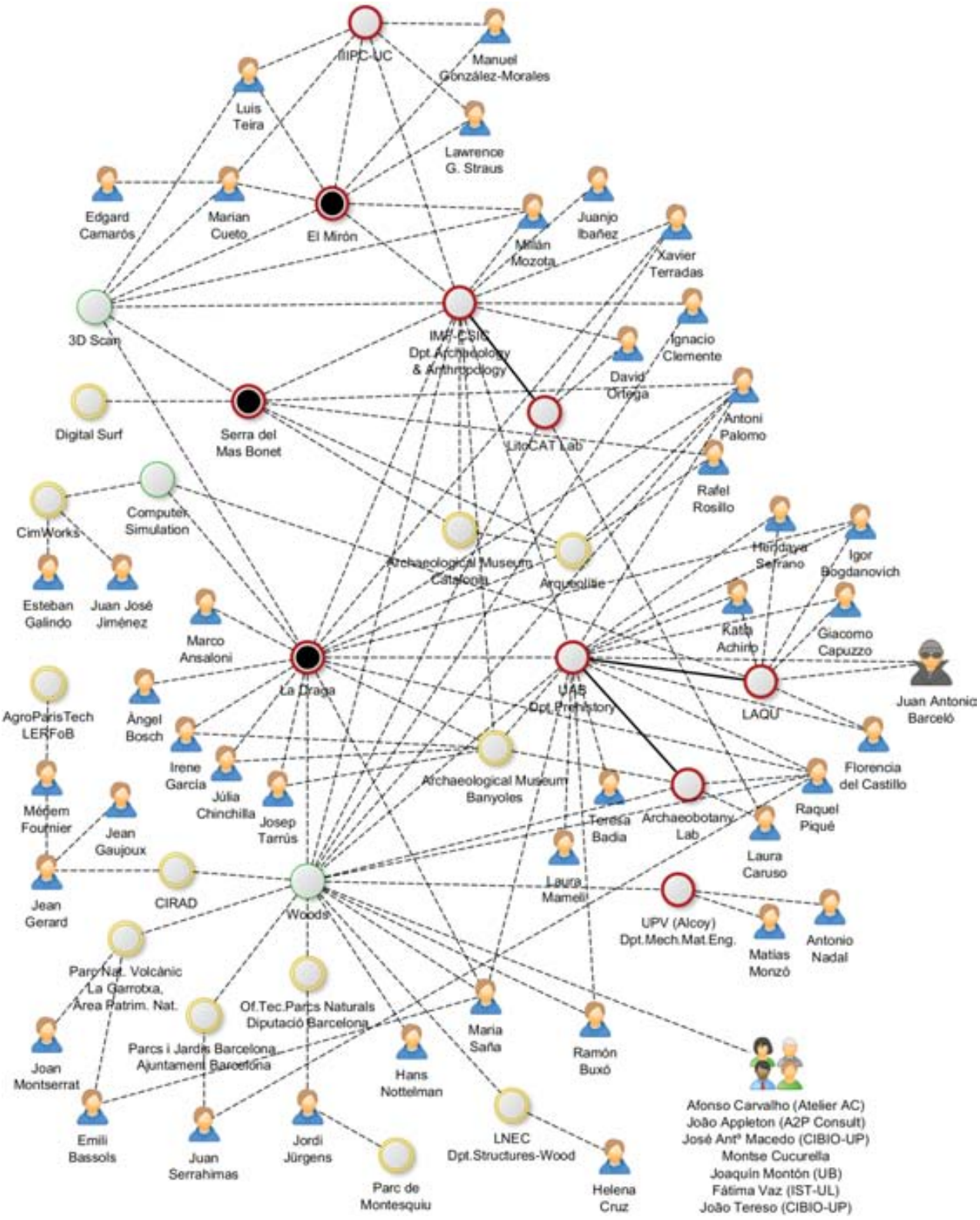
IIPC-UC
Manuel González-Morales
Luis Teira
Lawrence G. Straus
Edgard Camarós
Marian Cueto
El Mirón
Juanjo Ibañez
Milán Mozota
Xavier Terradas
3D Scan
IMF-CSIC Dpt.Archaeology & Anthropology
Ignacio Clemente
David Ortega
Digital Surf
Serra del Mas Bonet
LitoCAT Lab
Antoni Palomo
Rafel Rosillo
CimWorks
Computer Simulation
Archaeological Museum Catalogue
Arqueologia
Herdaya Serrano
Igor Bogdanovich
Esteban Galindo
Juan José Jiménez
Marco Ansaloni
Katia Achirio
Giacomo Capuzzo
La Draga
UAB Dpt.Prehistory
LAQU
Juan Antonio Barceló
AgroParisTech LERFoB
Àngel Bosch
Irene García
Júlia Chinchilla
Josep Tarrús
Archaeological Museum Banyoles
Florencia del Castillo
Médem Fournier
Jean Gaujoux
Teresa Badia
Archaeobotany Lab
Raquel Piqué
Laura Caruso
Jean Gerard
CIRAD
Woods
Laura Mameli
UPV (Alcoy) Dpt.Mech.Mat.Eng.
Matías Monzó
Antonio Nadal
Parc Nat. Volcànic La Garrotxa, Àrea Patrim. Nat.
Of.Tec.Parcs Naturals Diputació Barcelona
Parcs i Jardins Barcelona Ajuntament Barcelona
Maria Saña
Ramón Buxó
Joan Montserrat
Hans Nottelman
Afonso Carvalho (Atelier AC)
João Appleton (A2P Consult)
José Antª Macedo (CIBIO-UP)
Montse Cucurella
Joaquín Montón (UB)
Fátima Vaz (IST-UL)
João Tereso (CIBIO-UP)
Emili Bassols
Juan Serrahimas
Jordi Jürgens
LNEC Dpt.Structures-Wood
Parc de Montesquiu
Helena Cruz

Abstract

Archaeology seems to be a quintessentially 'visual' discipline, because visual perception makes us aware of such fundamental properties of objects as their size, orientation, form, colour, texture, spatial position, distance, all at once. I assume that human behaviour in the past can be asserted on the examination of archaeological observables in the present. In any case, I take into account that there are also non visual features characterizing ancient objects and materials. Information that should make us aware of many functional properties of objects is multidimensional in nature: size, which makes reference to height, length, depth, weight and mass; shape and form, which make reference to the geometry of contour, surfaces and volume; texture, which refers to microtopography (roughness, waviness, and lay) and visual appearance (colour variations, brightness, reflectivity and transparency); and finally material composition, meaning the combining of distinct elements to form a whole, and the manner in which such parts are combined.

This research is based on the more global idea of Perception (from the Latin *perceptio*, *percipio*), usually defined as the organization, identification, and interpretation of sensory information in order to represent and understand the environment. It should be understood not as the passive receipt of these signals, but the integration of learning, memory, and expectation. This research explores different ways of understanding the very idea of archaeological perception, which involves top-down effects as well as the bottom-up process of processing some sensory input. The bottom-up processing is basically low-level information that's used to build up higher-level information (e.g., shapes, forms and textures for object recognition and functional explanation). The top-down processing refers to an archaeologist's concept and expectations (knowledge)

that influence perception.

The approach adopted here is to follow current computational theories of object perception to ameliorate the way archaeology can deal with the explanation of human behaviour in the past (function) from the analysis of visual and non-visual data, taking into account that visual appearances and even compositional characteristics only constrain the way an object may be used, but never fully determine it.

I suggest that perceptual properties should be rigorously measured and coded if archaeologists intend to understand how objects were produced and/or used in the past. The insufficiency and lack of a clear consensus on the traditional methods of form description – mostly visual, descriptive, ambiguous, subjective and qualitative – have invariably led to ambiguous and subjective interpretations of its functions. It is thus strongly advisable to systematize, formalize and standardize methods and procedures more objective, precise, mathematical and quantitative, and whenever possible automated.

In this context, I intend to develop a framework based on three dimensional geometrical digital models to measure, describe, test and analyse the use and behaviour of archaeological artefacts. I try to understand the possible relationships between the geometry, material, and function(s) of archaeological artefacts by suggesting new ways of studying the way behaviour in the past can be asserted on the examination of archaeological observables in the present.

In this research, a novel framework is applied to three case studies which span a broad diachrony ranging from the Palaeolithic in Cantabria to the Neolithic in Catalonia, Spain. In respect to the archaeological objects, these encompass rock art, sculptures, lithics, and bows, as well as a wide variety of raw-materials. Each case study addresses its own archaeological questions, has particular aims, and therefore approaches. They are not intended to be exhaustive, but to provide a rounded picture in terms of the framework´s potentialities and effectiveness.

Resumen

La arqueología es una disciplina 'visual' por excelencia, ya que la percepción visual nos permite tomar conciencia de las propiedades fundamentales de los objetos: tamaño, orientación, forma, color, textura, posición en el espacio, distancia o todas estas características al mismo tiempo. En este trabajo se asume que la conducta humana en el pasado puede estudiarse a partir del examen de los elementos arqueológicos observables en el presente. De igual modo, se considera que también existen rasgos no visuales que caracterizan los objetos y materiales en el pasado. La información que nos permite entender muchas de las propiedades funcionales de los objetos es de naturaleza multidimensional: el tamaño refiere a la altura, longitud, profundidad, peso y masa; la forma, refiere a la geometría que define superficies y volúmenes; textura, a la microtopografía y aspecto visual; y por último a la composición del material, es decir, a la combinación de los distintos elementos que forman el total y la manera en que tales partes se combinan.

Esta investigación se basa en una idea más general de la percepción (del Latín *perceptio*, *percipio*), usualmente definida como la organización, identificación e interpretación de la información sensorial con el fin de representar y entender el entorno. No debe entenderse como una recepción pasiva de estas señales, más bien como la integración del aprendizaje, la memoria, y las expectativas. Esta investigación explora diferentes maneras de entender la idea de percepción arqueológica, que incluye el proceso *bottom-up* del procesamiento de información sensorial, así como los efectos *top-down*. El proceso *bottom-up* es básicamente la información de bajo nivel que se utiliza para construir la información de alto nivel (por ejemplo, formas y texturas para el reconocimiento de objetos y la explicación funcional). El proceso *top-down* se refiere al concepto y a

las expectativas (conocimiento) que influencian la percepción.

El enfoque adoptado sigue las teorías computacionales actuales sobre la percepción de objetos que intentan proponer nuevas vías explicativas acerca de las conductas humanas en el pasado, a partir del análisis de datos visuales y no visuales, teniendo en cuenta que las apariencias visuales y incluso las características de composición sólo limitan la forma en que un objeto puede ser utilizado, pero nunca lo determinan totalmente.

En este trabajo sugiero que las propiedades perceptivas deberían ser rigurosamente medidas y codificadas para poder llegar a entender cómo se produjeron y/o se utilizaron los objetos en el pasado. Hasta ahora, la insuficiencia y la falta de un consenso claro sobre los métodos tradicionales de descripción de los objetos - sobre todo visual, ambigua, subjetiva y cualitativa - han conducido invariablemente a unas interpretaciones ambiguas y subjetivas. Por consiguiente, es muy importante sistematizar, formalizar y estandarizar métodos y procedimientos más objetivos, exactos, matemáticos y cuantitativos, y siempre que sea posible automatizarlos.

Es en este contexto, se ha intentado desarrollar una metodología basada en modelos digitales tridimensionales para medir, describir cuantitativamente y analizar el uso y el comportamiento de los objetos arqueológicos. También, se intenta comprender las posibles relaciones entre la geometría, el material, y la(s) función(es) de los objetos arqueológicos al sugerir nuevas maneras de estudiar formas de comportamiento pasadas que puedan ser confirmadas a partir del examen de los observables arqueológicos en el presente.

Contents

List of Figures & Tables

3. Framework

4. Case Studies

4A. El Mirón Cave, Cantabria

4B. Serra del Mas Bonet, Catalonia

4C. La Draga, Catalonia

Ø1
Introduction

1.1 Problem Statement

Archaeology seems to be a quintessentially 'visual' discipline, because visual perception makes us aware of such fundamental properties of objects as their size, orientation, form, colour, texture, spatial position, distance, all at once. Visual cues often tell us about more than just optical qualities. We 'see' what we suppose are tools, rubbish generated by some past society, the remains of their houses… Are we sure that we are right? Why does this object look like a container? Why does this other seem an arrow point? Or are those stones being interpreted as the remains of a house? In which way an 'activity area' within an ancient hunter-gatherers settlement can be recognized as such?

Most of these questions seem out of order for when using, for instance, range-scanner or a photogrammetric camera. Current uses of technology in archaeology seem addressed to simply tell us what happens now at the archaeological site. They do not tell us what happened in the past, nor why or how.

What is being 'seen' in the present has been the consequence of human action in the past, interacting with natural processes through time. Human action exists now and existed in the past by its capacity to produce and reproduce labour, goods, capital, information, and social relationships. In this situation, the obvious purpose of what we 'perceive' in the present is to be used as evidences of past actions. It is something to be explained, and not something that explains social action in the past. In that sense, production, use and distribution are

the social processes which in some way have produced (cause) archaeologically observed properties (size, form, material, texture, place, time) (effect).

Archaeological artefacts have specific physical properties because they were produced so that they had those characteristics and not other. And they were produced in that way, at least partially, because those things were intended for some given uses and not to other: they were tools, or consumed waste material, or buildings, or containers, or fuel, etc. If objects appear in some locations and not in any other, it is because social actions were performed in those places and at those moments. Therefore, archaeological items have different forms, different sizes and materials. They also have different textures, and appear at different places and in different moments. That is to say, the changes and modifications in the form, size, texture, material and location that nature experiences as the result of human action (work) are determined somehow by these actions (production, use, distribution) having provoked its existence.

The real value of archaeological data should come from the ability to be able to extract meaningful information from them. This is only possible when all relevant information has been captured and coded. However, archaeologists usually tend to only consider very basic physical properties, like size and a subjective approximations to shape. Sometimes, texture, that is, the visual appearance of a surface, is also taken into account, or the mineral/chemical composition. The problem is that in most cases, such properties are not rigorously measured and coded. They are applied as subjective adjectives, expressed as verbal descriptions preventing other people will use the description without having seen the object. If the physical description of such visual properties is somewhat vague, then possibilities of discovering the function the artefact had in the past is compromised, we hardly can infer the object's physical structure. The insufficiency and lack of a clear consensus on the traditional methods of form description – mostly visual, descriptive, ambiguous, subjective and qualitative – have invariably led to ambiguous and subjective interpretations of its functions. It is thus strongly advisable to systematize, formalize and standardize methods and procedures more objective, precise, mathematical and quantitative, and whenever possible automated.

1.2 Aim of Research

In this sense, the scientific question which is intended to be solved can be expressed in the following terms:

Why the observed material entities have specific values of form, size, texture, material, and why they appear at some specific spatial and temporal location?

The main assumption is that some percept (archaeological description) should be related to a causal affirmation about the causal event (social event, work activity) having produced the perceived evidence (archaeological explanation). It has been suggested that there is a direct constraining relationship – sometimes even deterministic – between how a prehistoric artefact looks like in the present and its past function. That means that artefacts we see today at the archaeological site were produced in a specific way, at least partially, be-

cause those things were intended for some particular uses: they were tools, or consumed waste material, or buildings, or containers, or fuel, etc. Therefore, archaeological items have different forms, sizes, and materials. They also have different textures, and appear at different places and in different moments. That is to say, the changes and modifications in the form, size, texture, material, and location that object experiences as the result of human action (work) are determined somehow by these actions (production, use, distribution) having provoked its existence.

Computer simulation will allow us to predict the cause or formation process of some archaeological entity given some perceived evidence of the effect of this causal process. In its most basic sense, then, the task may be reduced to the problem of detecting localized key perceptual stimuli or features, which are unambiguous cues to appropriate causal events. For instance, a distinctive use wear texture on the surface of a lithic tool, and not on others, predicts that these tools have been used to process fresh wood, and we infer that at some moment a group of people was cutting trees or gathering firewood. Alternatively, we can consider that the form of some pottery vases predicts their past use as containers for wine, and then we have evidence of wine production and trade; the material of some graves predicts the social personality of the individual buried there and hence the existence of social classes. Here the output is not the object (trees or firewood, wine, social elite), but a causal affirmation: cutting trees or gathering firewood, wine production and trade, social power and coercion.

Archaeological objects must be documented in full using distinct types of information to determine their possible functions in the past. New ways of studying the way behaviour in the past can be asserted on the examination of archaeological observables in the present are proposed. In any case, it is taken into account that there are also non-visual features characterizing ancient objects and materials (i.e., compositional information based on mass spectrometry data, chronological information based on radioactive decay measurements, etc.). Information that should make us aware of many functional properties of objects is multidimensional in nature: size, which makes reference to height, length, depth, weight and mass; shape and form, which make reference to the geometry of contours and volumes; texture, which refers to the microtopography (roughness, waviness, and lay) and visual appearance (colour variations, brightness, reflectivity and transparency) of surfaces; and finally material, meaning the combining of distinct compositional and structural elements, and other properties, to form a whole. With the exception of material data, the other relevant aspects for functional reasoning have been traditionally described in archaeology in rather ambiguous terms, without taking into account the advantages of quantitative measurements of shape/form, and texture. Reasoning about the functionality of archaeological objects recovered at the archaeological site requires a cross-disciplinary investigation, which may also range from recognition techniques used in computer vision and robotics, to reasoning, representation, and computer simulation. The approach adopted here is to follow current computational theories of object perception to ameliorate the way archaeology can deal with the explanation of human behaviour in the past (function) from the analysis of visual and non-visual data, taking into account that visual appearances and even compositional characteristics only constrain the way an object may be used, but never fully determine it.

In a wide perspective, the aim of this research is to contribute to a better knowledge about the function of archaeological objects. In a more confined sense, the aim is to develop a comprehensive framework based on Reverse Engineering processes. In this context, the following objectives are set to be achieved:

1. To develop a framework based on specific methods and techniques used to generate three dimensional geometrical digital models; to measure and quantify shape, form, and texture features; to measure and quantify the physical and mechanical properties of materials; to test and analyse the use and behaviour of archaeological artefacts.

   In applying the framework to three distinct case studies, my ultimate goal is twofold:

   • To test the overall efficiency of the framework;

   • To test the flexibility of the framework, i.e., the possibility to generalize it to other archaeological contexts that can be similarly quantified.

2. To understand possible relationships between the geometry, material, and function(s) of archaeological artefacts.

3. To document multidimensional digital archaeological artefacts for future reuse and repurpose in conservation monitoring, preservation, digital archives, dissemination, and other future researches.

The results of this research are expected to make a considerable contribution on the current body of knowledge in the relevant field of study.

1.3 Work Dissemination

Earlier and short versions of this work have been disseminated through the following publications:

Moitinho de Almeida, V., Barceló, J.A., Rosillo, R., Palomo, A. (2013). Linking 3D Digital Surface Texture with Ancient Manufacturing Procedures. *IEEE Digital Heritage International Congress*, Marseille. A.C. Addison, G. Guidi, L. De Luca, S. Pescarin (eds.). pp.735-738. (ISBN:978-1-4799-3169-9/13)

Moitinho de Almeida, V., Barceló, J.A. (2013). Towards Reverse Engineering Archaeological Artefacts. *Proceedings of the Computer Applications and Quantitative Methods in Archaeology Congress* (CAA'12), Southampton. Amsterdam University Press (AUP), Pallas Publications. (*in press*)

Moitinho de almeida, V., Teira, L., Gonzaléz-Morales, M., Straus, L.G., Mozota, M., Blasco, A. (2013). (Re)seeing the engraved block of El Mirón Cave (Ramales de la Victoria, Cantabria, Spain). *Proceedings of the Computer Applications and Quantitative Methods in Archaeology Congress* (CAA'12), Southampton. Amsterdam University Press (AUP), Pallas Publications. (*in press*)

Moitinho de Almeida, V., Rosillo, R., Palomo, A. (2013). Analysis and Production. In *La Serra del Mas Bonet (Vilafant) i Els Banys de la Mercè (Capmany), dues ocupacions a l'aire lliure emmarcades en la pre-*

història recent a l'Alt Empordà. Monographic series on Archaeological Excavations in Catalonia. Archaeological Museum of Catalonia (MAC), Barcelona. (*in press*)

Barceló, J.A., Moitinho de Almeida, V. (2012). Functional Analysis from Visual and Non-visual Data. An Artificial Intelligence Approach. *International Scientific Journal of Mediterranean Archaeology & Archaeometry* 12(2):273-321.

Moitinho de Almeida, V., Barceló, J.A. (2012). Computer Simulation of Multidimensional Archaeological Artefacts. Proceedings of the 4th Congreso Internacional de Arqueología e Informática Gráfica, Patrimonio e Innovación, Arqueológica 2.0, Sevilla. *Virtual Archaeology Review – special issue on Virtual Museums* 3(7):77-81. (ISSN: 1989-9947)

Moitinho de Almeida, V., Barceló, J.A. (2012). Understanding Virtual Objects through Reverse Engineering. Proceedings of the 3rd Congreso Internacional de Arqueología e Informática Gráfica, Patrimonio e Innovación, Arqueológica 2.0 (2011), Sevilla. *Virtual Archaeology Review – special issue on Virtual Museums* 3(7):14-17. (ISSN: 1989-9947)

Moitinho de Almeida, V., Barceló, J.A. (2012). 3D Scanning and Computer Simulation of Archaeological Artefacts. *Proceedings of the 1st International Conference on Best Practices in World Heritage Archaeology*, Menorca, 384-399. A. Castillo (ed.), Editorial Complutense, Madrid. (ISBN: 978-84-695-6782-1)

Moitinho, V., Barceló, J.A. (2011). Para una Comprensión de los Artefactos Arqueológicos Mediante la Ingeniería Inversa. *Proceedings of the 3rd Congreso Internacional de Arqueología Experimental*, Banyoles, Girona. (*in press*)

Rosillo, R., Palomo, A., Moitinho de Almeida, V. (2011). Las Estelae con Cuernos Neolíticas de la Serra del Mas Bonet (Vilafant, Alt Empordà). *Proceedings of the 3rd Congreso Internacional de Arqueología Experimental, Banyoles*, Girona. (*in press*)

Moitinho, V., Barceló, J.A. (2011). Towards an Understanding of Archaeological Artefacts through Reverse Engineering. Paper presented at the *Scientific Computing & Cultural Heritage Conference* (SCCH'11), Heidelberg. [Best student paper award]

As well as the following conferences and presentations:

Moitinho de Almeida, V., Barceló, J.A., Rosillo, R., Palomo, A. (2013). Linking 3D Digital Surface Texture with Ancient Manufacturing Procedures. *Digital Heritage International Congress*, Marseille.

Barceló, J.A., Bogdanovic, I., Moitinho de Almeida, V., Vicente, O., Castillo, M.F. del (2013). The LAQU (Laboratori d'Arqueologia Quantitativa) and LSDS (Laboratory for Socio Dynamics Simulation) research lines. *Technology and Cultural Heritage Day*, UAB, Barcelona.

Moitinho de Almeida, V. (2012). Summer course on "Rock Art and New Technologies". Modules "Analysis of Rock Art using Structured Light 3D Scanners: theory and techniques", "3D Scanning of Rock Art: Hands-on training". Instituto Internacional de Investigaciones Prehistóricas de Cantabria, Universidad de Cantabria (IIIPC).

Moitinho de Almeida, V., Barceló, J.A. (2012). Postgraduate course on "Computational Intelligence in Archaeology". Module "Case studies. The analysis of shape and the visual appearance of archaeological artefacts. Using prehistoric tools: a computer simulation". LSDS, on behalf of the Department of Prehistory, UAB.

Moitinho de Almeida, V., Barceló, J.A. (2012). Computer Simulation of Multidimensional Archaeological Artefacts. *4th Congreso Internacional de Arqueología e Informática Gráfica, Patrimonio e Innovación, Arqueológica 2.0*, Sevilla.

Moitinho de Almeida, V., Barceló, J.A. (2012). 3D scanning and Computer Simulation of Archaeological Artefacts. *1st International Conference on Best Practices in World Heritage: Archaeology*, Menorca.

Moitinho de Almeida, V., Barceló, J.A. (2012). Towards Reverse Engineering Archaeological Artefacts. *Computer Applications and Quantitative Methods in Archaeology Congress* (CAA'12), Southampton.

Moitinho de almeida, V., Teira, L., Gonzaléz-Morales, M., Straus, L.G., Mozota, M., Blasco, A. (2012). (Re)seeing the engraved block of El Mirón Cave (Ramales de la Victoria, Cantabria, Spain). *Computer Applications and Quantitative Methods in Archaeology Congress* (CAA'12), Southampton (poster).

Moitinho de Almeida, V., Rosillo, R., Palomo, A. (2012). 3D Macrowear Analysis of Sculpture Techniques in the Manufacture of the Neolithic Stelae with Horns of the Serra del Mas Bonet (Vilafant, Catalonia). *Computer Applications and Quantitative Methods in Archaeology Congress* (CAA'12), Southampton (poster).

Moitinho de Almeida, V. (2012). Quantitative Data from 3D Digital Models. Shape, Form, and Texture. "Resource tools for Historical Research II: Introduction to Quantitative Archaeology" – 3rd year subject, Professor J.A. Barceló, Prehistoric Archaeology course, UAB.

Moitinho de Almeida, V., Rosillo, R., Palomo, A. (2012). 3D, Estelae & Arqueología Experimental. *Workshop "La Serra del Mas Bonet (Vilafant-Alt Empordà) – Diacronia Prehistòrica a l'Alt Empordà"*, Museu d'Arqueología de Catalunya, Barcelona.

Moitinho de Almeida, V., Barceló, J.A. (2011). Para una Comprensión de los Artefactos Arqueológicos Mediante la Ingeniería Inversa. *3rd Congreso Internacional de Arqueología Experimental*, Banyoles, Girona.

Rosillo, R., Palomo, A., Moitinho de Almeida, V. (2011). Las Estelae con Cuernos Neolíticas de la Serra del Mas Bonet (Vilafant, Alt Empordà). *3rd Congreso Internacional de Arqueología Experimental*, Banyoles, Girona (poster).

Moitinho, V., Barceló, J.A. (2011). Towards an Understanding of Archaeological Artefacts through Reverse Engineering. *Scientific Computing & Cultural Heritage Conference* (SCCH'11), Heidelberg.

Moitinhoa, V., Barceló, J.A. (2011). Understanding Virtual Objects through Reverse Engineering. *3rd Congreso Internacional de Arqueología e Informática Gráfica, Patrimonio e Innovación, Arqueológica 2.0*, Sevilla.

Moitinho, V., Gonçalves, C., Castillo, M.F. del (2011). Digital Technologies and Computational Methodologies in the Process of Archaeological Research. *4th Jornadas de Jovens Investigadores em Arqueologia* (JIA'11), Faro (session chair).

Moitinho, V. (2011). New Approaches for the Study of Archaeological Artefacts. *4th Jornadas de Jovens Investigadores em Arqueologia* (JIA'11), Faro.

Moitinho de Almeida, V. (2010). Shape Analysis in Archaeology. "Resource tools for Historical Research II: Introduction to Quantitative Archaeology" – 3rd year subject, Professor J.A. Barceló, Prehistoric Archaeology course, UAB.

1.4 Thesis Outline

This thesis is structured in five chapters, organized as follows:

Chapter 1 is an introduction. Here, the problem statement and general remarks have been presented, followed by the objectives of this research, work dissemination, and the outline of the thesis.

Chapter 2 presents a theoretical approach and new concepts which will form the basis of the succeeding chapters. Issues surrounding the functionality of archaeological artefacts through shape/form, texture, material, and interaction are here discussed. Throughout this chapter a relevant literature review is presented, likewise in view to guide the reader throughout the framework proposed in the succeeding chapter.

To address the issues discussed previously, **Chapter 3** deals with the fundamental knowledge that one should have in advance in order to be able to understand and implement the framework proposed in this thesis, by comprehensively describing each stage. The proposed framework includes unconventional approaches and research at the interface between different disciplines. New tools and new techniques require new workflows, to enable new researches which may permit new results and understandings. Some of the new trends and issues which characterize the various subjects presented and which bring their own archaeological and technological challenges are addressed.

In-depth description of the implementation of this framework and further technical details are given in **Chapter 4**, through the presentation of three case studies which span a broad diachrony ranging from the Palaeolithic in Cantabria to the Neolithic in Catalonia, Spain. In respect to the archaeological objects, these

encompass rock art, sculptures, lithics, and bows, as well as a wide variety of raw-materials. Each case study addresses its own archaeological questions, has particular aims, and therefore approaches. They are not intended to be exhaustive, but to provide a rounded picture in terms of the framework´s potentialities and effectiveness.

The **1st Case Study** is focused on the engraving block of El Mirón Cave (Ramales de La Victoria, Cantabria, Spain), where the ultimate goal of this ongoing work is to provide new information and a better knowledge about the engravings in such archaeological context. Different strategies for capturing geometric data are tested, to understand to what extent distinct technical choices determine the detection, characterization, and interpretation of the carvings. A preliminary geometric analysis of the signatures of engraving mechanisms is presented. In the one hand, to allow to infer possible types of engraving techniques and tools. On the other hand, to isolate the motifs of the palimpsest.

In the **2nd Case Study** is focused on the Neolithic stelae with horns from the Serra del Mas Bonet (Vilafant, Catalonia, Spain), and in a set of lithic tools that have been associated with them. This investigation is directed toward a better comprehension of the manufacturing procedures used mainly in the production of one of these stelae. Different strategies for the geometric analysis, description and comparison of the objects are presented.

The **3rd Case Study** is focused on a small selection of wooden artefacts from the Neolithic lakeside site of La Draga (Banyoles, Catalonia, Spain). More specifically, on three likely bows (if so, the oldest Neolithic bows in Europe, dated between 5.400 and 5.200 cal. AD). This investigation is directed toward the understanding of possible relationships between the form, material, and function(s) of these archaeological artefacts.

In **Chapter 5** an overall summary and final reflexions of the thesis are presented, followed by prospects for future works.

Unless otherwise indicated, all illustrations, graphics, and photographs presented were created by Vera Moitinho de Almeida.

Ø2
Theoretical Background

> *I am simply out of Lineland, that is to say,*
> *out of the Straight Line which you call Space,*
> *and in the true Space, where I can see things as they are.*
>
> Edwin A. Abbot (1838-1926), in Flatland. A Romance of Many Dimensions (1884)

Why archaeological artefacts are the way they are? In this chapter I will try to solve such a question by investigating the relationship between materiality and function. I suggest new ways of studying the way behaviour in the past can be asserted on the examination of archaeological observables in the present. In any case, I take into account that there are also non-visual features characterizing ancient objects and materials (i.e., compositional information based on mass spectrometry data, chronological information based on radioactive decay measurements, etc.). Information that should make us aware of many functional properties of objects is multidimensional in nature: *size*, which makes reference to height, length, depth, weight and mass; *shape* and *form*, which make reference to the geometry of contour, surfaces and volume; *texture*, which refers to microtopography (roughness, waviness, and lay) and *visual appearance* (colour variations, brightness, reflectivity and transparency); and finally *material composition*, meaning the combining of distinct elements to form a whole, and the manner in which such parts are combined. With the exception of compositional data,

the other relevant aspects for functional reasoning have been traditionally described in rather ambiguous terms, without taking into account the advantages of quantitative measurements of shape/form and texture. The approach adopted here is to follow current computational theories of object perception to ameliorate the way archaeology can deal with the explanation of human behaviour in the past (function) from the analysis of visual and non-visual data, taking into account that visual appearances and even compositional characteristics only constrain the way an object may be used, but never fully determine it.

2.1 Why Archaeological Artefacts Are the Way They Are?

A possible answer to this question would be: because objects have a distinctive 'appearance' for the sake of their proper 'functioning'. The meaning of functioning is always related with the idea of 'using'. An object's use can be defined as the exertion of control over a freely manipulable external object with the specific intention of: (1) altering the physical properties of another object, substance, surface or medium (the target, which may be the object user or another organism) via a dynamic mechanical interaction, or (2) mediating the flow of information between the tool user and the environment or other organisms in the environment (St. Amant and Horton 2008; see also Beck's 1980, McGrew 1993, Amant 2002, Bicici and Amant 2003).

According to Daniel Dennett (1987), the function of a certain item is – or should be – what it is best able to do (or be) given its physical constitution and its context. In accordance with Bonnet (1992), a function is taken as an activity, which can be performed by an object. Therefore, we can consider that the object's activity is in fact its operating mode or behaviour specification. Balachandran and Gero (1990) prefer to distinguish between 'function', 'structure', and 'behaviour' as three classes of properties of a design object: function properties would dictate the object's intended purpose and requirements, structure properties would represent the description of the whole and its constituents, while the behaviour properties would spell out how the structure of the object achieves its function". For example, consider the main physical features of a cup. We can assign different functions or actions (possible behaviours) to each part: the flat bottom is for standing the cup on a surface; the handle is for grasping the cup when lifting; the inside is for containing the liquid; the rim is for supporting the cup against the lips when drinking. The assignment of causal interactions to features defines the object as a cup (Leyton 1992, p. 163). We may argue, then, that the function of a cup is specified in terms of the actions applied to it, e.g., standing up, lifting, etc., and in terms of the resulting actions that the cup applies back to the environment, e.g., conveying the liquid upward. All that means that we are describing the cup in terms of five components:

1) Inputs

   e.g., standing up, lifting;

2) Outputs

   e.g., conveying liquid;

3) States

physical characteristics of the cup, e.g., its form;

4) First Causal Relationship

e.g., lifting (input) acts on form (state) → conveying liquid (output);

5) Second Causal relationship

e.g., lifting (input) acts on form (state) → form does not change (dynamics: next state).

The above definition of function would seem correct only in the case of objects like huts or hats, or any other tool-like things, which have been made according to a clearly defined purpose (Wright 1973, Millikan 1999, Neander 1991). Such definition would be also effective when dealing with objects with symbolic use, given that even style has a function (Wobst 1977). Martin Wobst disrupted the notion of a style-function dichotomy in archaeology when he described style as "that formal variability in material culture that can be related to the participation of artefacts in processes of information exchange" (1977, p.321). To Wobst, style is used actively and reflects intentional choices of individuals or groups to communicate particular messages. In other words, differences in style are used to communicate messages about group affiliation and identity. The purpose of creating prestige artefacts, for instance, may not be to perform a practical task, but to display wealth, success, and power, and such display is influenced by circumstances and people. Their purpose is to solve a social problem or accomplish a social task such as attracting productive mates, labour, and allies, or bonding members of social groups together via displays of success (Wiessner 1983, 1989, Binford 1989, Hayden 1998). Consequently, any attempt to create a rigid boundary between style and function will fail (see Bettinger et al. 1996, Hurt and Rakita 2001, Brantingham 2007, Kirsch 2009 about this discussion). Treating style and function as a dichotomy, arises from an oversimplified picture of human decision-making mechanisms.

The problem is that, although functional behaviours (symbolic or nonsymbolic) seem to be goal-directed activities, sometimes desirable ends are achieved through the incidental or even accidental use of an object, and consequently the use of archaeological artefacts can also be opportunistic. Objects can be used for purposes not intended by their designers and/or manufacturers and conversely, an object can be used in a specific way even if it was not designed as such initially (St. Amant 2002, Bicici and St. Amant 2003). In this way, the conclusions presented by Wobst were questioned by James R. Sackett (1985), who insisted in the difference between things that people do of their own free will from the things they do because they have to. Both Sackett and Wobst considered the meaning of function in the same terms: functional behaviours are the things people are constrained to do. Sackett considered also behaviours that people do when unconstrained. A presumably nonfunctional behaviour ('stylistic' in Sackett's terms; a wrong term for a correct concept in our view) would denote an action that does not have detectable intended purpose. The closer an action is unintended, the less likely it is to be functional, i.e., patterned by rational choice. Binford (1989, pp.52-53) has considered this functional/nonfunctional dichotomy as an opposition between conscious, explicitly-rational, problem-solving behaviour, on the one hand, and unconscious, rote-learned motor habits, and socially or symbolically-motivated behaviour, on the other. The distinction between 'functional' and 'nonfunctional'

seems to be established between material consequences that are subject to causal intentional explanation and material consequences that are not (Dunnell 1978).

To avoid the apparent many functions of the very word function, I prefer to insist in the idea of 'functional analysis', rather than in a single substantive with a single meaning. Functional analysis can be defined as the analysis of the object's disposition to contribute causally to the output capacity of a complex containing system of social actions (Cummins 1975, 2000, 2002). Such a definition includes the use of objects used in a direct way with a material purpose (instruments) and objects used in a metaphorical way with an ideological intention (symbols). No such pure-use functions suggest that neither design or natural (or artificial) selection is required for artefact function, but only an object's role in a human goal-directed activity. We suggest that we should attribute functions to archaeological objects because and only because it can be proved that they may exhibit certain behaviours under the appropriate conditions: two objects will be functionally equivalent (or analogous) if they *do* the same (or similar) things in the same (or similar) systems in the same (or similar) environment. The key is in the emphasis on the word 'do'. No other features of the archaeological materials are relevant, other than the fact that they do the same things under certain conditions, which is to say that it is their behaviour that is important. What archaeologists characteristically perceive are objects and changes in objects, and behaviours are reifications of these. Thus, an archaeological entity should be explained by the particular causal structure in which it is supposed to participate. The knowledge of the function of some perceived material element should reflect the causal interactions that someone has or can potentially have with needs, goals, and products in the course of using such elements.

According to such assumptions, if one wants to produce a specific tool that will be used in a distinct way, designers/manufacturers cannot violate the laws of physics, which might prevent using the object in some way, or facilitate its use in another way. We should consider how size and weight will affect what the object did in the past; its overall form (for holding or halting); the edge angle where cutting, scraping, or holding was important; the duration of its use, how specialized the working parts needed to be; whether it was at all desirable to combine two or more functions in the same tool; how reliable the tool needed to be; and how easily repaired or resharpened it needed to be (Hayden 1998).

Design theory has been defined as "a means of creating or adapting the forms of physical objects to meet functional needs within the context of known materials, technology, and social and economic conditions" (Horsfall, 1987, p.333). 'Design' should determine how easy an archaeologically identified artefact was used in the past, the sort of features that it was given, how it looks, and so on (Schiffer and Skibo 1987, Hayden 1998, Bejan 2000, Kirsh 2009). Design theory principles assume that there are different kinds of constraints operating in the developing of practical solutions for each behavioural problem, and that tradeoffs between constraints make it unlikely that there will be any single optimal solution to a problem, but rather a number of more or less equally acceptable solutions that can be conceptualized. Among the most powerful of these constraints are functional requirements, material properties, availability, and production costs. Once a field of acceptable solutions for a given problem has been identified (via trial and error, or actual planning), the choice of which solution is adopted may largely be a matter of culture tradition, ideological values, style, or idiosyn-

cratic behaviour. However, most of the design constraints leading up to this level of decision are much more consequential in nature and, in the case of practical technology, play an absolutely primary, determining role.

I sustain the view that archaeological functional explanation should be considered as a complex relational system that links physical structure, intention, settings, action, and use history. The term function can be defined as a causal explanation of behaviours the item was involved at some moment. We can argue that archaeological evidences' functional statements should provide an answer to the question "how does *S* work?" where S is a goal-directed system in which the material entity whose function we are interested in appears (Nagel 1961, Boorse 1976, 2002, Adams 1979, Cummins 1975, 2000, 2002). That means that what has to be determined is the history of social actions having used that solid entity for different purposes at different circumstances.

The present approach equates function with causal links or goal-directedness, rather than logical purpose. What underlies this idea of function is essentially historical in character. Humans possess a large amount of functionally relevant knowledge for any material category, which includes (a) the object's design history, (b) the object's physical structure and the physical settings in which it is found, and (c) the events that arise during the object's use, such as agent's actions, object's behaviours, and outcomes. Consequently, an object's function emerges from a relational system that links its physical structure with its use, background settings, and design history (Kitamura and Mizogouchi 1999, Chaigneau et al. 2004). Consequently, the proper function of an item is determined not by the present characteristics of that item, but by its history. According to Nagel (1961), a thing or event has to be explained in terms of the function it performs in some larger whole, or the role it plays in bringing something about. Functional explanation focuses attention on the culminations and end products of specific processes.

I am approaching archaeology as if it is a discipline dealing with events instead of mere objects. An event instance describes a state or a change in the state of specific object attributes and occurs at a specific time (Findler and Bickmore 1996). Archaeological events can be defined as an expression of the fact that some percept has some feature *f* in some space and temporal location *e*, that the perceived entity is in a state *s* and that the features defining state *s* of that entity are changing or not according to another space and temporal location *e'*. The fact that a vessel has form *x*, and the fact that a lithic tool has texture *t* are events, because a social action has been performed at this spatial and temporal location (event), resulting in some artefact with, among other things some specific form and texture properties. The fact that a bow has a specific form, and the fact that there are some engravings on the surface of a stela are also events, because a social action was performed at this spatial and temporal location (event), resulting in a modification of the physical space. In that sense, I am defining functional analysis as a problem solving task:

Why is present observation the way it is?
What action or process has caused what I'm seeing now?

In other words,

Why do the observed material entities have specific values of size, form, texture, composition, and why do they appear at some specific spatial and temporal location?

Explanation equals to solve such why-questions (van Fraasen 1980, Hintikka and Halonen 1995). In our opinion, the answer to a why question is a causal affirmation about the formation process of society. We will solve the why kind of problems in terms of how humans did it. It is easy to see then that the concept of productivity becomes the heart of this kind of causal explanation. Productivity has been called a type of cause, which makes things up from other things (Tubery 2004). It is the idea of productive capability, which is so important in the explanation of social events because the outcomes of any social action come from entities and actions being made up from old entities and old actions.

It is also important to distinguish between:

- **Causing social actions themselves**: which are processes and mechanisms capable of transforming reality;
- **Causal interactions**: which are events whereby the effect of a social action has induced a transformation by virtue of its own invariant change-relating capability (Glennan 1996, 2002, Tubery 2004). In some sense, those interactions are the factors explaining why a social action was performed at a specific time and place, which is, its motivation or reason.

In order to understand social causality, the 'automated archaeologist' (Barceló 2009) should also add an additional distinction:

- **Result of an action**: is the state of affairs that has to obtain for that action to have been carried out. The result of an action is conceptually linked to a causal interaction
- **Consequence of an action**: is a further state of affairs that has been brought about by the attempt to carry out the action. The consequences of an action are contingently related to the action, and are independent to the event in which the action was performed (Collins and Kusch 1998).

Social events may be explained by showing how their results and consequences fit into a causal structure, that is to say, a vast network of interacting actions and entities, where a change in a property of an entity dialectically produces a change in a property of another entity (transformation). What we need to compute is the definition of a complex system that produces the recognized evidence by the interaction of a number of actions and entities, where the interactions between them can be characterized by direct, invariant and change-relating generalizations.

Clearly, nothing is gained if we introduce as an explanation of how some *x* occurs, an indicator that some *y* occurred (where *x* and *y* refer to different acts, events or processes). Such descriptive mechanisms, even if true, are not explanations but are themselves something to be explained. Statistical regularities don't explain, but require explanation by appeal to the activities of individual entities and collections of entities. Studies offering models for the detection of event-related properties typically fail to distinguish between description and explanation. Usually the only explanation given for how the event in question was perceived was to describe some hypothetical mechanism which undergoes a given state transition whenever the event undergoes a correlated transition. For instance, the function of a table is not the fact that a board is fixed to four wood legs, and this appearance is regularly associated with what some people refer as 'table'. On the other hand,

the function of the table lies in the fact that a carpenter, in a specific place and time, did a work action whose goal was to establish a physical and durable relationship between a specific board and some specific wood legs. The wheel of the potter is not the cause of the form of a vessel; the condition for the existence of a vessel with that form is a work activity made by one or several social agents with a determined goal, and in specific circumstances in which certain techniques and instruments were used.

2.2 How We "See" Archaeological Artefacts The Way We Do?

By assuming that what we perceive in the present is simply the material effects of human work, we usually understand 'archaeological percepts' as material things that were products in some moment of their causal history. We have to analyse archaeological evidences within the context of social activity by identifying the ways people produced (and/or used) the artefact, the needs it served, and the history of its development. In that sense, production, use and distribution are the social processes which in some way have produced (cause) archaeologically observed properties (size, form/shape, composition, texture, place, time) (effect).

However, establishing the desired correspondence between the archaeological evidences and their causal explanation is not an easy task. A direct matching between a perceived input and explanatory stored patterns is insufficient for various reasons (Barceló 2009):

- The space of all possible visualizations of all causal events is likely to be prohibitively large. It therefore becomes impossible to test a shape for property *P* by simply comparing it against all the members of *S* stored in memory. To be more accurate, the problem lies in fact not simply in the size of the set *S*, but in what may be called the size of the *support* of *S*. When the set of supports is small, the recognition of even a large set of objects can still be accomplished by simple means such as direct template matching. This means that a small number of patterns is stored and matched against the figure in question. When the set of supports is prohibitively large, a template matching decision scheme will become impossible. The classification task may nevertheless be feasible if the set of shapes sharing the property in question contains regularities. This roughly means that the recognition of property *P* can be broken down into a set of operations in such a manner that the overall computation required for establishing *P* is substantially less demanding than the storing of all the shapes in *S*.
- Finding solutions may also seem an impossible task because of the non-uniqueness difficulties that arise. Non-uniqueness means that the true solution cannot be selected from among a large set of possible solutions without further constraints imposed (Thornton 2000). This undesirable behaviour is due to noise in the measurements, and insufficient number of measurements.
- The material evidences to be recognized will often not be sufficiently equivalent to any already known causal model. For instance, DVD players, computers, and shoeboxes have visual features (forms) that are about as unrevealing of their function as they could possibly be. Although we might be able to figure out their functions after extended viewing and interaction, if we didn't know them

already, its explanation will be impossible. Therefore, the relationship shape-function seems to be too ambiguous to base archaeological explanations.

- How to relate between them the many visual appearances that the same causal event can generate (Kersten et al. 2004)? That is to say, the ambiguity of visual data arises when several different causal events could have produced the same archaeological evidence description or visual features.
- The automated archaeologist generally does not know the most relevant factors affecting the form, size, texture, composition, and spatiotemporal location of material consequences of social action. Instead, it extracts from the environment sparse and noisy measurements of perceptual properties, and an incomplete knowledge of relational contexts. The trouble here includes which features are selected for correspondence, and how to determine the match between image and model features. What simple properties would distinguish, for example the territory of a hunter-gatherer society from the territory of a chiefdom-kind of society? How do the effects of economic intensification distinguish in terms of simple visual properties from the effects of self-subsistence? How do exchanged goods differentiate from stolen goods? To make such recognitions, it appears that a more precise description of visual features, rather than a restricted geometric invariance (form) would be necessary. In some cases, simple invariant properties may be common to all the archaeological observable material consequences of a single action. In other, less restricted cases, such invariance may not exist. In archaeological event recognition, there is no particular reason to assume the existence of relatively simple properties.
- There is a necessity to establish correspondence with not just one, but multiple internal models. To select the correct model, correspondence must be established between the viewed archaeological evidence and all the different candidate models that need to be considered.
- Specific to the archaeological case, we should take into account that the visible properties of the archaeological record are not always the result of purposeful human activity. The problem is that many types of social activities, actions, and operative behaviours leave memory, but there are many other types of processes that do not. In fact, there are many types of processes whose effect is to actually wipe out memory. An aggregation of bones or artefacts may not reflect past human social action, but rather post depositional processes: fluvial, transport, solifluction, rodent activity, contemporary farming, etc. Most post-depositional processes have the effect of disordering artefact patterning in the archaeological record, and increasing entropy. Loss, discard, reuse, decay, and archaeological recovery are numbered among the diverse formation processes that in a sense, mediate between the past behaviours of interest and their surviving traces in the present.

At the end, one may question whether perception is driving problem solving (explanations) or vice versa. Two different ways of solving perception problems have resulted (Arkin 1998, pp.265-266):

- **Action-oriented perception**: in which problem solving needs to determine the perceptual strategies used. Action-oriented perception requires that perception be conducted in a top down manner, with perceptual control and resources determined by an already defined causal theory. The underlying principle is that perception is predicated in the structure of explanation: Only the information

germane for a particular explanation need be extracted from the input data. Instead of attempting to interpret almost everything a percept contains, an advantage is gained by recognizing that perceptual needs depend on what an agent is required to do within the world. This is in contrast to more traditional computer vision research, which to a large extent takes the view that perception is an end in itself or that its sole purpose is to construct a model of the world without any understanding of the need for such a model.

- **Active perception**: in which perceptual requirements dictate the automated archaeologist's problem solving strategy. It focuses primarily on the needs of perception, rather the needs of action. The question changes from the action-oriented perspective of "how can perception provide information necessary for problem solving? to "how can problem solving support perceptual activity"? An active perceptual system is a system that is able to manipulate its incoming sensory information in a controlled manner in order to extract useful data, based on evidences gathered from other input data and with the aim of efficiently accomplishing an explanation with respect to the available resources (Fernmüller and Aloimonos 1995, Tsontos 1990, 2001). Therefore, an active approach is a selective one, and the issues of planning causal sequences become of primary importance, as well as focusing the attention on useful pieces of information. Active perception is thus defined as an intelligent data acquisition process, intelligent in its use of sensors guided by feedback and a priori knowledge.

These two viewpoints are not mutually exclusive; indeed active perception and action-oriented perception are intimately related. What the automated archaeologist needs to know to accomplish its tasks still dictates perceptual requirements, but active perception provides the perceptual processes with the ability to control the problem solving system to make its task easier as well.

According to this way of thinking, a social action is archaeologically recognized according to a stepwise and expectation-bound differentiation of visual information in which each given state defines the starting conditions for the generation of further information.

Archaeological perception (automated or not) is not a clear window into past realities The reason is that perception is under specified (or under constrained or under determined) by the visual data captured from the empirical world. That means that archaeological explanation cannot be reduced to a mere 'see' and 'understand' because what we, or the robots, perceive is not necessarily identical to what the robots (or we) *see*. In order to perceive, one must understand the world. To recognize objects, the automated archaeologist must know what it is looking at. To know what it is looking at, it must already be able to see it, but it couldn't if it does not know what to see. In other words, to recognize some pottery sherds as a vase, the automated archaeologist must know what a vase is, and which kind of vase was. To explain archaeological evidences from a grave, the robot has to know why such an individual was buried with those grave goods, who was she, and who were the people that performed such a funerary ritual.

The world is not data, but a set of perceptual information waiting for an observer that imposes order by recognizing an object and by describing it. Global percepts are constructed from local information, and such a

construction process depends on the interaction of the automated archaeologist with the external context and is constructed according to its individual history of practical experiences (Florian 2002). Hence, the perception problem is reduced to recognizing what situation(s) we are in and then choosing one action (or perhaps many) to undertake. As soon as the observer finds itself in a new situation, it selects a new and more appropriate action. That means that, what is recognized, is always known in terms directly related to an agent's current possibilities for future action (Anderson 2003).

The idea that perception depends on the interaction of the observer with the world is now a popular one (Gibson 1979, Clancey 1997, Pfeiffer and Scheier 1999, O'Reagan and Noë 2001, Purves and Lotto 2003, among many others). Perceiving is an act, not a response; an act of attention, not a triggered impression; an achievement, not a reflex (Gibson 1979). As a mechanical system, robots may seem to lack perceptual capabilities at all; that is, they do not *know* anything about the scenes they record. Photographic images merely contain information, whereas sighted people and animals acquire knowledge about their environments. It is this knowledge that should enable cognitive robots to act appropriately in a given perceived situation.

Perceptions are internal constructions of a hypothesized external reality. Unless the perceiver makes assumptions about the physical world that gave rise to a particular image, perception just is not possible (Vision 1997, p.22). It should be axiomatic then that perception is not passive but active. Automated perception should be conducted on a need-to-know basis. That means that automated perception has to be considered as a holistic, synergistic process deeply intertwined with the complete agent's cognitive system, because perceptual needs are predicated upon the agent's motivational and behavioural requirements (Arkin 1998, p.238).

Sensorial experience is a mode of activity involving practical knowledge about currently possible behaviours and associated sensory consequences. Visual experience rests on know-how, the possession of skills. The experience of seeing occurs when the outside world is being probed according to the visual mode. In this sense, seeing is a way of acting. As the automated archaeologists look at archaeological visual data, it should question different aspects of the scene. As soon as it does so, each thing it asks about springs into awareness, and is perceived because knowledge is now available about how the external world will change when it manipulates the thing it sees. Perceiving the world is not a reflection of the content of some knowledge base, but rather, is due to the structure of the world itself and the robot's ability to act intelligently with respect to it.

Perception and cognitive problem solving are then closely linked. If perception has to be tied to action, then an artificial archaeologist should be an entity situated and surrounded by the real world. It should not operate upon abstract representations of reality, but rather upon reality itself. That means that an observer should have a physical presence (a body), which influences its dynamic interactions with the world. Situated activity means that robot's actions are predicated upon the situations in which it finds itself.

Is it possible to build a machine to perceive automatically? Will it be capable of avoiding the problem of subjectivity in perceptual description? The so called 'intelligent' machines incite instinctive fear and anger by resembling ancestral threats - a rival for our social position as more or less respected specialists. Critics

of technology seem to think that hardware/software that imitate human activity (seeing, touching, etc.) are guilty of excessive simplification, of forcing knowledge, or distorting it, and of failing to exploit fully the knowledge of the expert.

Computer perception has been defined as a process of recognizing elements of interest in an image, and it can be described as the automatic logical deduction of structures or properties of the three-dimensional objects from either a single image or multiple images and the recognition of objects with the help of these properties (Kulkarni 2001). As such, computer perception should be considered as an interpretive process. Any reasonable sophisticated perceptual system must involve a set of processes that extract a variety of types of information from the input image about the visual scene it comes from. This information is captured in a variety of internal intermediate-level representations (e.g., neural networks) which form the basis for higher-level recognition processes.

Our first task is to decide what sort of distinctive visual marks we must seek to understand why what we see is the way it seems to be. And what we 'see' or 'perceive' can be reduced to the size, form, texture, composition and location of material consequences of social activity. Relevant questions to an automated archaeologist are then:

How can it be discovered what makes such form a container?
How can it be discovered what makes that use-wear texture a knife?
How can it be discovered what makes an artefact with that composition a foreign production?
How can it be discovered what makes such locations an activity area?

Current computational theories of visual perception tend to break down the perception of meaningful stimuli into three functional stages. It is common to categorize visual process into low, intermediate, and high levels. Low-level information is typically about the spatial relationships among primitive, two-dimensional visual features such as observed shape, texture, and composition variability patterns. Intermediate information describes the properties arising from forms of organization of the low-level primitives, such as texture or shape differences, and may include descriptions of the three-dimensional spatial relationship (location) among visual properties.

In his most influential essay, David Marr (1982) suggested that there are different mechanisms by which any sensing agent (a human or a machine) transforms visual data into an identification of the cause of visual variation. He saw perception essentially as building larger and larger structures from elementary sensory features. First, primitive visual features (e.g. location of shape and texture components) are extracted from empirical data. Second, these features are used to construct a description of the structure of the input information (texture and/or compositional variation). Third, the constructed description is matched against stored descriptions. The line between perception and cognition should be drawn between stages two and three. Specifically, cognitively derived expectations and beliefs do not interact with visual processing up to the construction of a visual description, but may influence the matching stage, perhaps by modulating the threshold amount of activation necessary to trigger a match to a particular object type.

Archaeological perceptual explanation is then a gradual process that proceeds from the general to the specific and that overlaps with, guides and constrains the derivation of a causal explanation from an image or visual representation of some archaeological evidences (Marr 1982, Palmer 1999). Following modern studies of computer object-recognition (Grimson 1991, Palmer 1999, Bernardini and Rushmeier 2002, Carbonetto et al. 2005, Ponce et al. 2007), we should consider specialized archaeological perception essentially as building larger and larger explanatory structures from elementary visual features.

The overall explanatory process is thus broken down into the extraction of a number of different observable physical properties (low-level analysis: form, texture, composition and location), followed by a final decision based on these properties (High-level analysis). The idea is then to build an automated observer in terms of a hierarchy of feature detectors and specialized problem-solvers. At the lowest level in the hierarchy, there is what is called retinal units, or visual feature detectors. These detectors encode primitive visual features, namely, form or texture basic parts. The retinal units provide a vector description of the stimulus in terms of a spatial co-ordinate system. These units activate all appropriate mapping units to which they are connected, and in turn, the mapping units activate all of their super ordinate object-based units. The receptive field properties of low-level detectors would encode the salient features of the input image in order to generate a preliminary model of the external world. This first level encodes information, which will be processed and eventually decoded by middle and higher-order mechanisms. The middle-level contains mapping mechanisms building a mapping between image defined and explanation-centered descriptions. What the mapping mechanisms are doing is to impose a frame of reference on the visual features, so that these features can be matched up with the same features specified in the definition of explanations. Specialized problem-solvers (higher-level mechanisms) represent particular solutions or explanatory concepts looking for particular combinations of features from the feature detectors. At the highest level, a decision mechanism selects the concept corresponding to that represented by the specific problem-solver activated by the highest quantity of features.

This approach to non-linear pattern matching suggests that, instead of casting object recognition as a massive dynamic search problem, we can think of it in terms of gradual sequences of transformations (operating in parallel) that emphasize certain distinctions and collapse across others. If the result of this sequence of transformations retains sufficient distinctions to disambiguate different possible explanations, but collapses across irrelevant differences produced by individual variability, then functional determination has been achieved. This approach is considerably simpler because it does not try to recover the complete 3D structural information or form complex internal models.

In so doing, perceptual features should be viewed as emergent properties of sensory fields, not static things in the environment that are merely detected, selected, or picked up. In this conception of perceptual problem solving, the automated archaeologist should see its empirical significance, or more formally, the probability distribution of the possible sources of the stimulus, in response to any given stimulus. Understanding what a robot can see and why will depend on understanding the probabilistic relationship between stimuli and their sources during the automated archaeologist past experience. As a result, the percepts that are entertained would accord with the accumulated experience of what the visual and non-visual inputs in question had typi-

cally signified in the history of this individual automated archaeologist.

These ideas suggest that the perceptual structure underlying object recognition may be described as expectations of certain stimulations at certain locations in a still unstructured global stimulus distribution (Hoffman 1996).

2.2.1 What is Shape & Form?

Archaeology has been traditionally considered as a quintessentially visual discipline (Shelley 1996). Among all features that describe archaeological evidences, some of them, the most important for the recognition and/or the discovery of the way an item was produced and or used in the past, have something to do with what we have been trained to 'see' in the archaeological record. Unfortunately, there is no universal method of searching for informative visual marks. They can be extracted from any archaeological record almost *ad infinitum*, but one usually fails to formalize the significant criterion for what is intrinsically visual. An additional difficulty is that different visual features will almost definitely be of importance for different explanations. To cope with this problem, archaeologists have traditionally assumed that there is a roughly fixed set or vocabulary of 'supposed' descriptive visual regularities shared by a single population of objects, which are also distinctive enough. Archaeologists believe that what they see is a 'seed', a 'bone', a 'bowl', a 'knife', the 'wall of a house', a 'prince burial', etc., and they can distinguish between different kinds of 'bowls', different kinds of 'prince burials', and so on. This way of identification-based explanation seems then a tricky way of solving any archaeological research problem. It pretends to explain what has been 'seen', not in terms of their visual characteristics, but in terms of subjective recognition.

Compositional data are a good example of well defined, properly acquired and effectively represented data. Visual features are fast never formalized, and most archaeologists do not even recognize the problem. If the physical description of archaeological observables is somewhat vague, then possibilities of discovering the function the artefact had in the past is compromised, we hardly can infer the object's physical structure. The attempts at formally defining the terms 'form' or 'shape' are often based on the idea of any single, distinct, whole or united visual entity; in other words, it is the structure of a localized field constructed around an object (Koenderink 1990, Small 1996, Costa and Cesar 2001, Leymarie 2011). Therefore, the shape/form of an object located in some space could be expressed in terms of the geometrical description of the part of that space occupied by the object – abstracting from location and orientation in space, size, and other properties such as colour, content, and material composition (Johansson 2008, 2011, Rovetto 2011). According to USAITA (n.a.), form includes shape, size, dimensions, mass, weight, and other visual parameters which uniquely characterize an object. Shape can be regarded as the external contour or silhouette of an object – this is to say, two dimensions (2D) –, while form describes the three-dimensional (3D) arrangement of the component parts (Ingram and Hudson 1994). Henceforth 'shape' will refer to 2D, and 'form' to 3D.

We may call surfaces the boundaries of separation between two phases. A phase is a homogenous mass of substance possessing a well-defined boundary. When we have two phases in mutual contact we have an inter-

facial boundary, i.e., an interface. The surface of a solid, kept in atmosphere, is in fact an air-solid interface; although it is often simply referred to as a solid surface. We can also conceive of a solid-solid interface that occurs when two solids or solid particles are brought in mutual contact. By combining surfaces and discovering discontinuities between boundaries we recognize shapes/forms in objects, so to speak, and this is how we linguistically understand shape and form as properties. These physical or organic shapes/forms do not reflect the exact specifications of geometrical descriptions of the part of space occupied by each object. They approximate geometric shapes/forms. We may treat the geometrical description of the part of space occupied by each object as if existed independently, but common sense indicates that it is an abstraction with no exact mind-external physical manifestation, and it would be a mistake to betray that intuition. That which we consider to be shape/form is intimately dependent on that which has the shape/form. In the mind-external world, shapes and forms, it seems, are properties of things. They (things) must have a form, i.e. be delineated by a shape. We say that a physical object exhibits a form. Thus, shapes/forms must always be shapes/forms of something in the mind-external world. Outside idealized geometric space, it does not make sense to posit the existence of an independently existing shape, a shape with no bearer. The shape cannot exist, but as an idea, without an entity that bears, exhibits, or has that shape (Rovetto 2011). Shape/form so delineated is a property dimension, which is quite consistent with the fact that some shapes/forms in turn have (second-order) properties such as 'being symmetric', 'being regular', 'being polyhedral', and as having mathematical properties such as 'eccentricity' (Johansson 2008). If shapes or forms are defined as having a particular number of sides (as with polygons) or faces (as with polyhedrons), a particular angle or curvature (as with curved shapes, such as the circle and the ellipse; or forms, e.g., sphere, ellipsoid), specific relations between them, then it should be apparent that we are describing properties of properties of things. We might be inclined to say that it is the shape/form that has a certain amount of sides/faces and angles/curvatures, rather than the object bearing the shape/form in question, but this is not entirely accurate (Rovetto 2011). The distinction between geometric and physical space, between ideas and ideal or cognitive constructions and material mind-external particulars is significant.

Consequently, the idea of shape and form should be understood as a process by which our mind 'builds' a definition of some observable input (Barceló 2010a, Leymarie 2011). Within this paradigm, the form of things appears to be a physical representation of the content of information associated with each thing. The word information itself comes from the Latin *in forma* meaning 'in form' and implies that 'information' is what you need to know in order to put things into a proper form/shape (Gammaitoni 2011).

The conceptual structure of these new foundations has been elaborated by Michael Leyton (1992, 2005). The first fundamental concept is that so-called Generative Geometry defines shape/form by the sequence of operations needed to create it. One should recover from the form the history of embryological development and subsequent growth which the body underwent. The form is full of its history. Similarly, the form of a tree gives us information about how it grew. A scar on a person's face tells us that, in the past, the surface of the skin was cut. A crack in a vase informs us that, in the past, the vase underwent some impact; i.e., this information is retrievable from the crack. In the same way, the vertical height of the vase is information about the past process that pushed the clay upwards; and the outline of the vase, curving in and out, is information of the

past changing pressure that occurred in the potter's hands. Therefore, the crack is a memory store of hitting which sits on the vase which is a memory store of clay-manipulation. According to Leyton's foundations for geometry, every feature of the world is a memory store. The recovery of such a memory can be carried out by simple procedure of partitioning the presented situation into its asymmetries and symmetries and following some inference rules to understand why an originally symmetric formation ended in asymmetry.

This is not the proper place to develop the approach of form as a process, but it gives us some very important cues. To completely characterize a form means to be able to recreate its configuration using only the measurements made over the interfacial boundaries. Read (2007) formalizes this requirement in the following definition: An ordered *n*-tuple of measurements completely characterizes a shape without redundancy if (a) there is a set of drawing rules that permits reconstruction of the shape outline using only this ordered *n*-tuple of measures, and (b) there is no ordered *k*-tuple of measures, $k<n$, such that the shape outline can be reconstructed from the ordered *k*-tuple (Read 2007, p.157). We can also refer to a set of measures that completely characterizes a shape or form as satisfying the archival property: the shape/form can be reconstructed from the measures that have been taken. The archival property is a weaker requirement of non-redundancy in that a set of measurements satisfying the archival property may possibly be a redundant set of measures.

This implies to consider perceived variation in the interfacial boundary of an artefact to arise from successive modification by the craftsperson through a sequential, conceptual process going from an initial abstract ideal form to the final geometry of the set of surfaces defining the finished artefact (Van der Leeuw 2000). In some instances, the particular morphology of the boundary may be determined from physical constraints acting on the process underlying its formation process (craftsperson work, user action) – such as distribution of forces acting on the formation of the boundary of an artefact, as occurs with the hands of the potter making pottery with a pottery wheel – but in most cases the underlying physics may be too complex to model if there is no single pattern that constrains the interfacial boundaries.

By virtue of the properties of the raw material and the features of human labour or action, many objects from the past have a constructed shape. This can be the case of pottery containers or most built structures (pit holes, graves, walls, buildings). Nevertheless, in many cases, the actual geometry of perceived interfacial boundaries may be the result of taphonomic processes or all what passed at the site since the time of the deposition of material evidences. The actual form of a wall, as it is perceived in the moment of the archaeological excavation, is the result of the destruction of the original wall, in such a way that the original ordering of building blocks may be lost. The same is true for a broken pottery vessel, transformed into an amount of fragments whose individual form is not the result of human labour in the past. Mounds resulting from the accumulation of stones, debris or animal bones also can be defined in terms of edges and boundaries explaining the formation (or deformation) processes involved (Mameli et al. 2001). As a result, the precise form of any archaeological deposition should be analysed to understand the formation process of the archaeological site (Barceló et al. 2003, 2009). At higher perceptual scales, in the case of soil and landscape features, as territories, valleys, drainage basins etc, the geometry of their interfacial boundaries may also be the result of natural processes or social events having contributed to its actual appearance. In general, and following Leyton

(1992, p. 73) if boundaries (or edges) are understood as perceived discontinuities or asymmetries generated through time, we should be able to recover the history of the perceived (and 'differentiated') archaeological entity from the perception of change. In other words, archaeologists use shape/form information, that is to say data on geometric discontinuities, as memories of process-history.

However, the precise relationship between form and formation processes is not always direct and easy to explain. In the case of prehistoric stone tools made of retouched flint, for instance, the form of the tool is simply the mechanical consequence of the flake removal, in such a way that the edge of such tools does not necessary represent a cognized form on the part of the craftspeople (Bisson 2000, Collins 2008). However, a thrusting spear point is likely to be squat and short with a wide tip angle. This design combines relatively long cutting edges with a short blade and a relatively wide base suitable for hafting with a strong, robust shaft. A throwing spear point, in contrast, needs to optimise the requirements for aerodynamics, killing power and accuracy. A slim, elongated point combines mass with a relatively acute tip angle and a small presentation area and base. A smaller base means that a smaller shaft can be used and this leads to a lower overall weapon mass. According to Newtonian mechanics, a lighter missile can be launched at a higher velocity with a flatter trajectory resulting in a faster, more powerful projectile weapon (Crompton 2007).

The insufficiency and lack of a clear consensus on the traditional methods of visual description – mostly based on spoken language, descriptive, ambiguous, subjective and qualitative – have invariably led to rhetoric, ambiguous and subjective interpretations of its functions. It is thus strongly advisable to systematize, formalize and standardize methods and procedures more objective, precise, mathematical and quantitative, and whenever possible automated (O'Brien 2002, Read 2007, Barceló 2009, Moitinho et al. 2011). If visual features – which include shape description – of archaeological observables are not formalized, then possibilities of discovering the function the artefact had in the past is compromised.

Traditionally, archaeologists have referred to diameters and heights when speaking about shape and form. The conventional method for capturing the artefact's morphology has been to take linear measurements with callipers at fixed loci along an arbitrary line of maximum bilateral symmetry, generally defined as length. Such linear measurements, however, are absolute quantities reflecting only size. No geometric information is provided on the relative position of the various breadth and thickness measurements. Accordingly, the variables sampled constitute an abstract collection of relative size measurements. There is no assurance that two archaeological artefacts with identical size values at different parts of their extension will have similar shapes/forms. The shape of every square, for example, is the same whether it is a large square or a small square; and the same goes for cubes.

Most of the ways of representing shape in terms of the object physical boundaries have been developed in terms of extracted 2D contours or silhouettes (see Barceló 2010a for an overview of such methods). For some time, computer specialists thought that it would be very easy to adapt linear contour (Nelson and Selinger 1998), landmark (Dryden and Mardia 1998, Adams et al. 2004, Slice 2007, Elewa 2010), or decompositional (Biederman 1987, 1995; Edelman 1994, Palmer 1999, Edelman and Intrator 2000, 2002, Binford and Levitt

2003, Jang et al. 2006, Cao et al. 2008) approaches of shape to the analysis of form (Ingram and Hudson 1994), that is, 3D, but modern research has proved that we need much more than a mere adaptation.

The third dimension is much more important than many archaeologists tend to think, it isn´t just a matter of realism in the representation of enhanced aesthetic qualities. In fact, it opens up new possibilities for incorporating movement and dynamics into a model, in the effort to understand the use and function of archaeological artefacts. A rigid body in three-dimensional space has several degrees of freedom for movement, where it can: go left or right, up or down, forward or background; translate and rotate. Each of coordinates represents the set of all possible orientations about some axis. Any movement we make must be some combination of these degrees of freedom. Down-up motions are hard, because we are tied to the surface of the Earth by gravity. Hence it is not hard for us to walk along the surface anywhere not obstructed by objects, but we find it difficult to soar upwards and then downwards: many archaeologists prefer paper-and pencil, or digital pictures to resume what they can see. But such flat representations do not allow studying movement.

Is it possible to build a machine to 'see' automatically? Fortunately for us, technology has produced a diversity of 3D scanner systems, and the like. Such 'instrumental-observers' are able to capture the form of an archaeological object. The generated output data is composed by a point cloud with thousands of three-dimensional Cartesian coordinates – besides x,y,z coordinates, each point can also have colour, normal vector, or image texture information –, which describe the overall scanned surfaces of an object. However, working with hundreds of thousands or even millions of points is difficult, because surfaces cannot be distinguished and the meaningful information that can be extracted may seem quite limited, and we have already suggested that shape/form is basically information. This leads us to digitally reconstruct the surface of the object from captured sets of coordinates, which can be done by converting the point cloud into a 3D polygonal mesh, and thereafter into a 3D surface model.

The resulting surface models are with no doubt quite impressive, and contain most relevant geometric information we will need to calculate the particular relationship between form and function. However, we should consider these surface models as an intermediate step in the process of quantifying form, because they cannot be used directly for explanatory purposes. The relevant information should be extracted before being used for inferring the object's function in the past.

2.2.2 What is Texture?

Texture is usually defined as those attributes of an object's surface having either visual or tactile variety, and defining the appearance of the surface (Tuceryan and Jain 1998, Fleming 1999, Mirmehdi, Xie and Suri 2008, Barceló 2009, Engler and Randle 2009). A texture perceived by humans is a visualization of complex patterns composed of spatially organized, repeated subpatterns, which have a characteristic, somewhat uniform appearance (Szczypinski et al. 2009). It is useful to distinguish between 'visual appearance' (colour variations, brightness, reflectivity, and transparency), from 'tactile appearance', which refers to microtopography (i.e.,

roughness, waviness, and lay).

Texture has always been used to describe archaeological materials. It is possible to distinguish between different archaeological materials, because of the appearance of the raw material they are made of. For example, based on textural characteristics, we can identify a variety of materials such as carved lithic tools, stripped bones, polished wood, dry hide, painted pottery, etc.

Because surfaces cover everything, in the same way as when using shape and form cues to infer functional capabilities of archaeological objects, texture data can also be used to recognize function. This is usually called a texture classification problem, whose goal involves deciding to which functional category the observed texture variation belongs. In order to accomplish this, we need to have prior knowledge of the functions to be recognized, and to delete all texture features observed in the object that were not related with labour induced variations. In fact this is a popular approach in archaeology. Whitehouse (1978, p.179) considers texture "a 'fingerprint' of the whole of the manufacturing process; it is a very sensitive end product of a long sequence of operations. Any deviation in the manufacture reflects itself in the texture. So, simply making sure that the surface texture is within certain bounds ensures similar manufacture which, in turn, ensures similar performance of the workpiece".

Some texture features of an artefact's surface are consequences of the modifications having experimented that object along its history. After all, the surface of solids plays a significant role in any kind of dynamic process. Solid surfaces are generally not equipotential, because surface energy varies from point to point, given the number of asperities and irregularities (Rao 1972, Lüth 1993). When a surface interacts with another surface, higher points may have more intense effects (higher energy) than lower areas (Rao 1972, Lüth 1993); and when a surface is plane and uniform, all surface points have the same interfacial contribution, that is, all points have the same potential to induce changes on a contacting surface. Major types of wear phenomena include abrasion, friction (adhesion and deformation), erosion, corrosion, and fatigue. Along these lines, tribology deals with the design, friction, wear, and lubrication of interacting surfaces in relative motion, whereas a tribological system considers the resistance against motion (friction), or against the surface damage (wear) of a material in a dry or lubricated system, in a given environment (Bowden and Tabor 1964, Whitehouse 1978, Blau 1992, Hutchings 1992, Bhushan 2001, Myshkin et al. 2005, Friedrich and Schlarb 2008, Heshmat 2010).

When we analyse macro or microscopically an object's surface, we should recognize some differential features (striations, polished areas, scars, particles, undifferentiated background) which are the consequence of an action (human, animal, natural) having modified the original appearance of that surface. Consequently, the main assumption is that artefacts have surface properties because of the way they have been made, or the way they have been used. That is, we should distinguish two kinds of perceptual appearances, one of them is inherent to the artefact raw material, and the other one is the result of modifications on the surface generated by work activities.

For instance, making and/or using an object produces important alterations in its surface features, so we can

use a description of such changes to understand how the object was made and/or used. Texture variations due to human work are observable, and may vary according to different causal factors, among them:

- Movement: longitudinal (cutting), transversal (scrapping), etc.
- Surface of friction: the effects of worked material (wood, bone, shell, fur, etc.)

By replicating lithic tools and performing some activity (e.g., cutting green wood) for a certain period of time, enables to test the relationship between kinematics, worked material and observed use-wear on the surface of the tool (Semenov 1964, Hayden 1979, Anderson 1981, Grace 1989, Clemente et al. 2002, González and Ibáñez 2003, Pijoan-López 2007, Longo et al., 2009). For further relevant tribological studies in archaeology see OUP (n.a.), Cotterell and Kamminga (1990), Burroni et al. (2002), Astruc et al. (2003, 2011), Anderson et al. (2006), Vargiolu et al. (2007), Evans and Donahue (2008), Gluchy et al. (2008), Evans and Macdonald (2011), d'Incau et al. (2012).

In the same way, decoration should be understood in its physical nature, and not only stylistically. Engraved, carved or painted, decorative patterns are man-made modifications on the surface of some objects, and they can be considered as an example of induced texture (Maaten et al. 2006). Preservation also alters surface features. It implies a third factor for texture origin: not only original visual appearances of raw material and man-made surface modifications should be taken into account, but also taphonomic and post-depositional modifications.

Therefore, it is easy to see that the problem of texture variation is a complex one. And acquiring perceptual data for a proper analysis of those attributes of an object's surface having either visual or tactile variety is of topmost relevance

Regarding visual variability, the study of colour variations has a long tradition in archaeology – essays in formalizing colour description using Munsell codes or related approaches are very old, while more recent technologies, such as colorimeters and spectrophotometers, already permit to describe objectively colour properties with great precision. But in archaeology texture has been traditionally measured in terms of transforming grey-level image information into a map of bumps within a surface. Texture analysis has been then essentially the operation of detecting significant local changes among luminance values in a visually perceived scene and its translation into a geometric language. In other words, texture as a consequence of anisotropic reflection, given the underlying assumption that light waves undergo reflection when they encounter a solid interface (surface), and this reflection is irregular depending on the heterogeneity of the surface (Haralick 1979). Texture properties are then represented as a bidimensional mapping of points (p_i,q_i) with a specific luminance value (r_i). Texture is then described as the relationships of luminance values in one pixel with luminance values in neighbouring pixels. Crudely stated, the goal was to establish a minimal set of statistical measurements such that two textures are identical in appearance if and only if they agree on these measurements. Such an approach has produced good results in archaeology (Pijoan-Lopez 2008, Barceló 2009), but it is no more tenable because it is still based on the probably wrong assumption that digital pictures (coded in pixels) are surrogates of real objects. Luminance variations not always allow distinguishing differentiated texture variations because they can be an effect of the perceptual acquisition mechanism (the microscope, the eye, the

camera, the sensor), and consequently images not only show features of the object being analysed but they mix this variation with variability coming from the context of observation and the mechanical characteristics of the observation instrument. There are always shadows and reflections which are not the result of original irregularities of the surface, but generated by the light source, the instrument, or other objects in the scene. That means that an image texture not only contains the object surface irregularity data, but additional information which in the best cases is just random noise, and in many other cases makes difficult to distinguish what belongs to the object from what belongs to the observation process.

Nowadays, the high resolution precision of many modern systems allows accurate measurements of tiny details of complex microstructures. Some non-contact close-range 3D scanners can capture surface data points with less than 50 microns between adjacent points. In addition, atomic force, confocal, digital holography, focus variation, interferometric, or scanning tunneling microscopy, optical focus sensing, Nomarski differential profiler, phase shifting or coherence scanning interferometry, angle resolved SEM, SEM stereoscopy, just to name some other non-contact instruments, can generate 3D representations of surface irregularities with even higher detail, and thus allowing finer measurements. In this way, instead of using grey-level values measured at pixel resolution, we have proper measurements of depth and height at well localized points within the surface (Stytz and Parrott 1993, Swan and Garraty, 1995, Lark 1996, van der Sanden and Hoekman 2005).

The textural character of the surface often depends on the spatial size of texture constituents, in such a way that coarse texture can be decomposed in large areas, while small areas give fine texture surfaces. Leung and Malik (2001) have developed further this decomposition approach by building a small, finite vocabulary of microstructures, which they call 3D textons. Theoretically, once a universal vocabulary of 3D primitive components of texture is defined, the surface of any material such as marble, concrete, leather, or rug can be represented as a spatial arrangement (perhaps stochastic) of symbols from this vocabulary (Cula and Dana 2004, Varma and Zisserman 2005, Dong and Chantler 2005). For an archaeological application, see Beyries et al. (1988).

In simple terms, tactile variation can be understood as the geometrical irregularities that emerge when considering roughness, waviness, and lay. At some level, this microvariation may be an intrinsic feature of an individualized surface, its topography. In a three-dimensional approach, we basically perceive surface geometric irregularities in terms of planes variations or curvature variability (angle and distribution). But, as before, we do not have enough with a simple spatial invariant measurement of heights and depths at the micro-level of a single surface. Since texture should be regarded as a similarity grouping in the visual and tactile constituents of a surface, the idea would be to decompose the analysed surface into regions which differ in the statistical variability of their constitutive features.

2.2.3 What is Material?

Visual features are not enough for an exhaustive documentation of archaeological material. Among non-visual data we can mention compositional data, which are most frequently understood as the enumeration

of basic or fundamental elements and properties defining a material. Although in the historical beginnings of the discipline, the enumeration of the substances an archaeological object was made of was regarded as a visual inference based on the scholar previous experience (in terms of the colour or texture of different materials like 'pottery', 'stone', 'bone'), nowadays, mineralogical and physicochemical compositions are measured objectively using appropriate instruments, such as x-ray and μ-Raman spectrometry, neutron activation analysis for elemental composition information, neutron scattering for revealing alloys and organic material; particle accelerator, Laser Induced Breakdown Spectroscopy (LIBS). Archaeometry provides an unquestionable valuable source of data for inferring possible functional behaviours of ancient and prehistoric artefacts. Nevertheless, we should take into account that the material components of any archaeological object can be defined and delimited at a variety of scales (e.g., atomic, molecular, cellular, macroscopically), what prevents taking compositions as magnitudes. Instead, we have different compositions at different analytical scales.

Archaeometric data have proved difficult to handle statistically, because of the awkward constraint that compositions are not mere lists of substances but multi-component vectors, where the addition of components is a constant in the population under study. Compositional vectors should fulfil two conditions:

a) The components should be 'generic', in the sense that all objects can be described as different combinations of the same components. For instance, the chemical components of a knife can be decomposed in steel and wood; the components of a pottery vase can be decomposed into Al, Mg, Fe , Ti, Mn, Cr, Ca, Na, Ni.

b) The components should be expressed as a proportion of the total sum of components, which defines the composition of the entity. Compositions should be expressed as vectors of data, which sum up to a constant, usually proportions or percentages. To say that there is steel and wood in this object, is not a true decomposition of the knife. Instead, we have to say that 13% of the object consists in wood for the grip, and the remaining 87% is composed of steel. In this case the components sum a constant (100), and composition is measured against this total.

This special characteristic of compositional data means that the variables involved in the study occur in constrained space defined by the simplex, a restricted part of a mathematical space, implying dangers that may befall the analyst who attempts to interpret correlations between ratios whose numerators and denominators contain common parts. It is important for archaeologists to be aware that the usual multivariate statistical techniques are not applicable to constrained data (Aitchison, 1986, 1994, 1997, Aitchison and Barceló-Vidal 2002, Barceló-Vidal et al. 2001, Billheimer et al. 1998).

In any case, what we seek it is not only an enumeration of the substances (at the atomic, molecular or composite levels) the archaeological object is made of, but a specific combination of non-visual features central to the direct interaction with solid materials – a material's "property profile" (Ashby 2005) – that allows to make inferences about the past function and behaviour of the artefact. These additional properties make reference to the biological, chemical, physical, thermal, mechanical or other constraints any substance may experiment (Markwardt 1930, 1935; Winandy 1994; Ashby 2005; FPL 2010; Siegismund and Snethlage 2011).

It is surprising the lack of research on the physical and mechanical properties of materials in mainstream archaeological and archaeometric studies. Archaeologists insist in documenting ancient artefacts, but such documentation seldom takes into account these properties of ancient materials, when without such information any effort in functional analysis is impossible. It is undoubtedly reasonable the impossibility to 'use' in the present, or even 'to touch', prehistoric or other ancient objects in order to preserve its integrality, may be the cause for the delay in this area of investigation. Imagine the answer of any museum director when asked to break a prehistoric object so we may measure its physical and mechanical properties.

2.3 Why Archaeological Artefacts Look the Way They Look?

2.3.1 Inferring Function

Functional analysis in archaeology is a fast perfect example of an inverse problem. That is, the answer is known, but not the question. The problem we want to solve can always be represented in the motto:

Guessing how the object was used from the object's visual appearance and material composition.

Here the past function is the unknown question we are looking for, and the form, texture, material properties are the raw data we have measured. The more precise and quantitative are such perceptual features, the more reliable the inferences about past behaviour.

2.3.1.1 Classificatory Approaches for Functional Explanation

Functional analysis can be carried out conjecturing unobservable mechanisms that link the input (observation) with the output (explanation). It can be defined as the recognition of observed patterns or the prediction to a larger set of circumstances of unobserved outcomes, by generalizing from a group of measurements for which the desired outcome is known. Since Aristotle, generalization has been the paradigmatic form of inductive inference. In our case, the task would be to find the common structure in a given sequence, under the assumption that: structure that is common across many individual instances of the same cause-effect relationship must be definitive of that group (Holland et al. 1986, Thagard 1989, Triantaphyllou and Felici 2006, Kowalski 2011, Flach 2012).

Consequently, certain characteristics or properties should be more probable than others when the object was manufactured to fulfil a specific function. That means that the characteristic perceptual properties of a precise function will be more probable when the more characteristics are 'frequent' in objects that performed such action, and the less characteristics are 'infrequent' in the same set of objects. The propensity, inclination, or

tendency of certain properties of form, texture and material to appear together is then, what we need to learn how perceptual data can be related with concrete functions. That is, we should learn a mapping from the hypothetical function to the measured values of form, size and material provided some instances of such a mapping are already known or can be provided by direct experience in the world. When subsequently asked to determine whether novel instances belong to the same function, those instances that are similar to instances characteristic of a single event of a single class of events will tend to be accepted.

This way of understanding functional analysis lead us directly to the concepts of clustering and classification, because we always can understand functional analysis as the partitioning of an observation set according to a similarity criterion and generating class descriptions from these partitions.

Clustering is the process of grouping input samples in similarity classes partitioning the input space, so that diversity may be explicitly recognized and encoded. The starting point is the formal description of each object as an ordered set of features. Similar objects are those that have nearly the same values for different features. Thus, one would like to group samples to minimize intra-cluster distances while maximizing inter-cluster distances, subject to the constraints on the number of clusters that can be formed. This approach is popular within statistics: Principal Component Analysis, Cluster Analysis, etc., are good examples. A more 'artificial intelligence' approach to unsupervised learning, beyond classical statistical procedures is vector quantization methods, a general term used to describe the process of dividing up space into several connected regions, using spatial neighbourhood as an analogue of similarity (Kohonen 2001, Barceló 2009). Every point in the input space belongs to one of these regions, and it is mapped to the corresponding nearest vector. For example, the attributes for *object A* are mapped to a particular output unit or region, such that it yields the highest result value and is associated with that object, while the attributes for *object B*, etc., are mapped to different regions (Engel and van der Broeck 2001). There are many applications of self-organization or unsupervised learning for functional analysis (Mayorga and Ludeman 1991, 1994, Jain and Karu 1996, Ruiz del Solar 1998, Kulkarni 2001, Acebrón-Linuesa et al. 2002, Chandraratne et al. 2003, Valiente-González 2001, Bhakar et al. 2004). And relevant examples of unsupervised analysis of functional analysis based on archaeological texture data have been published (Fulcher 1997, Bell and C. Croson 1998, López Molinero et al. 2000, Ma et al. 2000, Novic et al. 2001, Petrelli et al. 2001, 2003, Chang et al. 2002, Grudzinski et al. 2003, Lletí et al. 2003, Ma 2003, Fermo et al. 2004, Kadar et al. 2004, Beardah and Baxter 2005, Grudzinski and Karwowski 2005, Baxter 2006, Toyota et al. 2009).

Classification is a form of categorization where the task is to take the descriptive attributes of an observation (or set of observations), and from this to label or identify the observation within a different phenomenological domain. The descriptive attributes may themselves be drawn from different data domains, each domain effectively contributing an axis to a combined feature space of all possible object descriptions. Hence, the task of the classifier is somehow to partition this feature space into disjoint regions that each represents a particular class, cluster, or pattern. The goal in a classification problem is to develop an algorithm which will assign any artefact, represented by a vector x, to one of *c* classes (functional assignments). The problem is to find the best mapping from the input patterns (descriptive features) to the desired response (classes). Some finite or

infinite set of patterns (binary or real valued vectors) are partitioned into classes, and a particular problem is specified by a set of selected training patterns, which are given together with their corresponding class names, and the goal is to classify all patterns as correctly as possible. The problem is of dividing the set of possible input vectors into two sets, one for which its output is positive, and the other for which its output is negative. The classes will be said to be linearly separable when the separation of different input-output patterns is better than if no decision rule was used, In the other case, when it seems there is no clear decision rule to separate examples from counterexamples, we say that classes are not separable.

Whereas Clustering equals self-organized or unsupervised learning, Classification tasks are a kind of supervised learning problem, on the grounds that the known instances of a cause-effect relationship are like information given by a teacher or supervisor. In this way, we learn to classify visual and non-visual data as members of contrastive functional categories through trial and error with corrective feedback (the teacher).

Differences with the classical statistical or clustering approach are obvious. In a clustering approach to functional analysis, a set of functional assignments will be modelled by first describing a set of prototypes, then describing the objects using these prototypical descriptions. In such an unsupervised or self-organized task, the goal is to identify clusters of patterns that are similar, thus identifying potential generalizations. Functional assignments are based on the assumption there is a structure to the input space such that certain patterns occur more often than others, and it would look for what generally happens and what does not. The trouble is that with clustering approaches we are not discovering how to instantiate a specific function on the basis of some perceptual information. Whereas supervised learning involves learning some mapping between observed values of shape, texture and/or composition and their hypothesized functions, much unsupervised learning can be viewed as learning a mapping between observations and themselves. It is important to understand the difference between clustering and classification, and between learning and partitioning or clustering. A good functional classification should both impose structure and reveal the structure already present within the data. The outcome from a clustering of a set of archaeological objects may have little meaning since the resulting clusters are not associated (by design) with any functional assignment arising from the domain of study (although they may be as a consequence of inherent structure in the data). Automated explanation cannot be possible if the automated archaeologist cannot distinguish positive and negative instances of the explanation to be learnt. That is to say, if it has not any knowledge that will ensure that its causal predictions tend to be plausible and relevant to some predefined goals. Consequently, the acquisition of explanatory knowledge cannot be reduced to clustering, because such methods are limited by the natural grouping of the input data, and they are based on restricting knowledge production to finding regularities in the input. Such regularities are not generalizable out of the specific limits of the input data used.

On the other hand, a supervised classification approach to functional analysis will imply that instrumental functions as ‘cutting’, ‘scraping’, ‘containing’, or symbolic functions like ‘visualizing the idea of violence’, ‘representing the idea of dominance’ or any other are to be learnt in an objective way, provided we have enough known instances for the underlying function, and a general background knowledge about how in this situation a human action has generated the observed modification of visual appearances. When subsequently

asked to determine whether novel instances belong to the same function, those instances that are visually (or non-visually) similar to instances characteristic of a single function or a single class of functions will tend to be accepted. For instance, we will understand what a house, a castle, a burial, a tool are when we learn how a prototypical house, a prototypical castle, a prototypical burial, a prototypical tool have been made, under which social and economic conditions they have existed.

The approach we are suggesting is a surrogate of experiment design. Experimental analysis is the process whereby the antecedents of a phenomenon are manipulated or controlled and their effects are measured. An obvious archaeological example is modern use wear analysis. By replicating lithic tools and using them a determined period of time performing some activity (e.g., cutting fresh wood) we will be able to test the relationship between kinematics, worked material, and observed use wear on the surface of the tool. When laboratory replication is not possible (i.e., not all social activities performed in the past can be replicated in the present), archaeologists are limited to mere observation. Ethnoarchaeological data can be also used to generalize observations and learn explanatory general principles.

Computer scientists are intensively exploring this subject and there are many new mechanisms and technologies for knowledge expansion through iterative and recursive revision. Artificial Intelligence (AI) offers powerful methods and techniques to bring about this task, namely fuzzy logic, rough sets, genetic algorithms, neural networks and Bayesian networks. Although statistical reasoning is still giving its support to all these methods, it is not classical statistical inference. AI paradigms differ from usual classification and clustering methods, in that they are (in comparison at least) robust in the presence of noise, flexible as to the statistical types that can be combined, able to work with feature (attribute) spaces of very high dimensionality, they can be based on non-linear and non monotonic assumptions, they require less training data, and make fewer prior assumptions about data distributions and model parameters. The huge number of learning algorithms and data mining tools make impossible that I can review the entire field in a single section (Langley 1996, Han and Kamber 2001, Witten and Frank 2005).

The most basic supervised learning algorithms are designed to find a conjunctive description for a single concept *C* that covers positive instances of *C* and that fails to cover negative instances. In this way, we can represent the solution to an inverse problem as a logical conjunction of boolean features, values of nominal attributes, limits on the values of numeric attributes, or some combination of them. It is usual to refer to each component of such conjunction as a condition or a test. Alternatively, functional hierarchies provide a framework for knowledge organization, and a considerable amount of machine learning research has taken this approach. Such hierarchies can be represented as a decision tree consisting of nodes and branches. Each node represents a separate function, typically with its own associated intentional definitions. The links connecting a node to its children specify an 'is-a' or subset relation, indicating that the parent's extension is a superset of each child's extension. Typically, a node covers all of the instances covered by the union of its descendents. In fact, such a decision tree can be seen as a collection of rules, with each terminal node corresponding to a specific decision rule.

Inductive decision trees have been applied in archaeology. Applications range from sex determination of buried human bodies to the discrimination of geo-archaeological soil data. In any case, it is in archaeometry where these methods have found its greatest popularity in the recent years (Baxter 2006). More details on applications are given in Barceló (2009, 2010b).

Alternatively, one can use Artificial Neural Networks (ANN) as a non-linear fitting mechanism to find regularities in a set of data. Application of ANN include: rock-art research (Barceló 1993, Díaz and Castro 2001), lithic arrow-point shape classification (Lohse et al. 2004, Keogh et al. 2010, Koutsoudis et al. 2010), reconstruction of whole pottery vessels (Zweig 2006, Kleber and Sablatnig 2009), historical classification of ancient Mesopotamian seals or Egyptian scarabs (Camiz and Venditti 2004), recognition of written characters in ancient documents, coins and epigraphic inscriptions (Kashyap et al., 2003, Maaten and Boon 2006, Maaten et al. 2006), human and animal bone materials found in archaeological sites (Gibson 1993, 1996, Schmitt et al. 2001, Bell and Jantz 2002, Corsini et al. 2005, Bignon et al. 2005, Gil-Pita and Sala-Burgos 2006, Coppa et al. 2007), classification of different properties of wheat grains based on image morphology (Li and Flenley 1999, Wang et al. 2002), and in the identification of mineral inclusions and petrographic information from thin sections of geologic or archaeological samples (Fueten 1997, Fueten et al. 2001, Thompson et al. 2001, Drolon et al. 2003, Marmo et al. 2005). Those examples give us a clue about how to apply neural networks for shape identification in palaeobotanical or archaeometric analysis (for instance, microscopy recognition). For more archaeological applications and examples of this paradigm see Barceló (2009, 2010b).

Such an associative memory, however, is not limited to the association of only those specific individual objects whose functional properties have been experimented before. If such was the case, the mechanisms underlying archaeological automatic explanation would be of limited use. We must identify a range of novel data as corresponding to a given type of object. Generalization is part of our ability to identify objects and events; we typically can identify social actions having been performed in the past even when the visual appearance of its material consequences in the present does not exactly matches what we know of previously memorized cause/effect associations. The capability for archaeological recognition implies then the existence of some previous form of learning, in which the abstract potentially explanatory categories have been created and defined. The goal of recognition is to perform these identifications correctly, in the sense that identification reflects a meaningful property of the world that is independent of the particular data that is being interpreted.

2.3.1.1.1 Limitations of Classificatory Approaches for Functional Analysis

Methods of functional explanation reviewed up to here are not entirely trustworthy. Functional explanation cannot be reduced to the task of finding the common structure in a given perceptual sequence, because such methods are limited by the natural grouping of the input data, and they are based on restricting knowledge production to finding literal regularities in the input. Such regularities are not generalizable out of the specific limits of the input data used. If the archaeological evidence happens to be atypical, or for instance the neural network misidentifies the relevant conditions, predicted behaviour may be permanently warped. Even human experts are vulnerable to inappropriate learning. We may be victims of self-reinforcing phobias or obsessions,

instilled by a few experiences.

Therefore, we should take into account that AI inductive techniques that rely only on the input are of limited utility, and we should integrate techniques that compare the functional assignments generated using different inferential mechanisms. Functional analysis is an inference process, whose very nature is beyond a mere mapping out of the statistical correlation present in the descriptive features of material evidences.

First of all, we should explore the possibilities of a different kind of learning which goes beyond standard induction. This is the case of relational learning. One way of understanding such idea is in equivalence terms: two objects are functionally equivalent (or analogous) if they do the same (or similar) things in the same (or similar) systems although they do not have the same form, texture or composition. No other features of the objects should be relevant other than the fact that they do the same things under certain conditions: it is their potential behaviour what matters.

Therefore not only communalities are necessary for learning the past function of archaeological objects, but also some kind of contingent relationship between the observed examples, which will determine the type of association learned. The central problem of functional analysis is then to specify constraints that will ensure that the predictions drawn inductively are plausible and relevant to our general explanatory goals. Functional explanation is thus highly context dependent, being guided by prior knowledge activated in particular situations that confront the automated system as it seeks to achieve its goals.

The trouble with functional analysis based on implicit relationships is that this kind of input data is not always apparent. On the other hand, the number of potential relationships in a given scenario is generally unbounded, implying that the number of possible relational regularities is infinite. Given the fact that everything may be related with everything, this is, in principle, an infinitely hard operation. It is a good example of an ill-defined problem, whose problem space is infinite. To solve this situation there are only three approaches:

a) The experimental replication;

b) The controlled observation;

c) Or the simulation of the related factors.

Regrettably, not all social activities performed in the past can be replicated in the present. What cannot be replicated, in many occasions can be observed or has been observed and someone has witnessed it. Ethnoarchaeology has been defined as the observation in the present of actions that were probably performed in the past. Ethnographic and historically preserved ancient written sources can be used as observational situations in which some causal events took place and were described.

According to the theoretical framework discussed at the beginning, the focus should be on processes, and not only on visual/non-visual characteristics. Actions and intentions can have subtle relationships in the context of tool use. It is not sufficient to simply assign objects to roles in specific actions and call the behaviour object use (Kitamura & Mizoguchi, 2004, Erden et al. 2008, St. Amant and Horton 2008). Therefore, function can-

not be reduced to a linear relationship between input and output, but a non-linear and non-monotone causal connection between changing intentions, design and uses. This constant interaction between task and object, between what users can do and what they want to do is what can be called the artefact-task cycle. The net effect is that a change in the design of an artefact may not only change practices and tasks, but lead to a change in the environments where it is being used and a change in the sub-populations who now make use of it. This regularly causes speciation of artefact and segmentation of user community (Kirsh 2009).

Archaeological observables should be explained by the particular causal structure in which they are supposed to have been participated. The knowledge of the function of some perceived material element should reflect the causal interactions that someone has or can potentially have with needs, goals and products in the course of using such elements. This approach has been called the affordances view of function, because it can be traced back to Gibson's formulation of affordance theory (Gibson, 1979, Norman, 1989). This theory states that information available from the perception of an object gives clues as to its function and possible manipulations. According to Turvey (1992), affordances are dispositional properties of the environment, that is to say, 'tendencies' to manifest some other property in certain circumstances. 'Being fragile' is a common dispositional property. Something is fragile just in case it would break in certain circumstances, particularly circumstances in which it is struck sharply. Thus dispositional properties are conceivable only when paired with circumstances in which the disposition becomes manifest – the glass is fragile only if there are possible circumstances in which it might shatter. That means that an object's physical structure and an agent's action specify an affordance jointly, constituting the immediate causes of a perceived function.

On the other hand, the term affordance designates the range of possible actions which objects or other elements of the surrounding offer to an agent. Therefore, it may also refer to relationships between structural properties of objects and specific components of their use (Bozeat et al. 2002, Chaigneau et al. 2004). In tool use, however, the function determined by structural properties may concern interactions of the tool with other tools, recipients or material rather than with the animate actors themselves. Comprehension of such interactions has been conceptualized as 'mechanical reasoning' or 'mechanical problem solving' (Hegarty 2004). Consequently, affordances are not properties, or at least not always properties (Chemero 2003). Affordances are relations between the abilities of people, physical characteristics of solids, and features of the environment. Therefore, affordances are partly constituted by functional properties.

To put it shortly, archaeological entities should be described not only in terms of their intrinsic properties (form, size, texture, colour, and material properties) but also in terms of their affordances: relationships between these properties and the properties/abilities of the intended users. The affordances of any archaeological evidence become obvious in its use and/or formation process. Both involve establishing and exploiting constraints: between the user/producer and the artefact, the user/producer and the environment, and the artefact and the environment. Physical affordances, closely related to constraints, are mutual relationships that involve both the agent and the artefacts she/he manipulates (and the environment he/she operates). An object's function should reflect the actions that can be performed on it, given both its physical structure and the physical structure of the agent interacting with it. Consequently, reasoning about the affordances of physi-

cal artefacts depends on the following factors and senses (Bicici and St. Amant 2003):

- **Form/Texture/Material**. For many tools, these are decisive factors in their effectiveness.
- **Planning**. Appropriate sequences of actions are basic to tool use. The function of a tool usually makes it obvious what kinds of plans it takes part in.
- **Dynamics**. Kinematic and physic relationships between the parts of tools, and between the tools and their targets provide cues for proper usage. For reasoning about a tool's interactions with other objects, and measuring how it affects other artefacts, we need to have a basic understanding of the physical rules that govern the objects.
- **Causality**. Causal relationships between the parts of tools, and their corresponding effects on other physical objects, help us understand how we can use them and why they are efficient.
- **Work space environment**. a tool needs enough work space to be effectively applied.
- **Design requirements**. Using a tool to achieve a known task requires close interaction with the general design goal and requirements of the specific task.

A possibility to add affordance knowledge into archaeological functional analysis would be through the decomposition of use-behaviour processes into chains of single mechanisms or operations, each one represented by some part of the studied object. Zlateva and Vaina (1991) have noted that decomposed parts relate to the most obvious operations an object may be submitted. They claimed that in order to know the use of an object, we need to infer its proper usage position, the direction of the action, and the pressure to be applied by a prospective user. These cannot be learned without spatial relations between parts and sub-parts, which imply that the parts and sub-parts directly relate to behaviours made with the object. Changing the direction of forces, torques, and impulses, and devising plans to transmit forces between parts are two main problems that arise in this framework. To solve these, we need to integrate causal and functional knowledge to see, understand, and be able to manipulate past use scenarios. We have already defined functional analysis as the application of an object in a specific context for the accomplishment of a particular purpose. Thus, we should consider the modality of the operation, which will be reflected by the task description and context of application (Bogoni 1995, Brand 1997). That means, we should add the rules of physics that govern interactions between objects and the environment to recognize functional capabilities. The functional outcome cannot occur until all of the conditions in the physical environment are present, namely the object(s), its material, kinematics and dynamics. Once these conditions exist, they produce and process the relevant behaviours, followed by the outcome (Barsalou et al. 2005). That means we need to integrate material, form, and texture models with representations of dynamic physical relationships to recognize the function(s) of objects. The recognition process is enhanced by the consideration of causal relationships between objects, such as the predictable or observable effect on some target object, by carrying out an action with a tool or object.

DiManzo et al. (1989) regarded functional reasoning as the ability to integrate visual/non-visual data and function with the help of planning. They described the difficulty of separating the function of a tool from the plan it takes part in, since plans and tools evolve together, and differentiate with time. More research on this domain of integrating knowledge of physics, the mechanics of the task, and perceptual data (visual and non-

visual: shape, texture and/or material) has been advanced by Far (1992), Deshmukh et al. (1993), Cooper et al., (1995), Hodges (1995), Rivlin et al. (1995), Froimovich et al. (2002), Zhang et al. (2002), Peursum et al. (2003, 2005, 2007), Pechuk et al. (2005), Erden et al. (2008). Alternatively, it is possible to build a model of function based on a description of the physical structure (shape/form) of the known ancestors of this object, namely certain reproduced physical dispositions. In that sense, both the artefact and its ancestors are part of a genetic reproduction history and are thus products of processes. In some cases, it can be proved that the physical structure of the element is approximately similar to the physical structure of those ancestors, including the dispositions that correspond to the proper functions ascribed to the artefact. Only malformed, and consequently malfunctioning, are an exception of the principle that the genetic structure of the causal history provides partial justification for the belief that: artefact A has the physical disposition (form) that corresponds to the ascribed function (Vermaas and Houkes 2003). Obviously this approach cannot be applied in all circumstances, because it is wrong in the case of new objects and the introduction of novelty and revolutionary changes, but it can be useful for understanding the causal history (or 'genetic' reproduction) of a historically connected series of objects.

2.3.1.2 Object Interaction

The purpose of documenting archaeological objects is to be able to 'use' them in the same way they were used in the past. More than integrating knowledge of physics with the appearance of the archaeological object in a deductive way, we need to interact with the object to learn more properly what we can do with it. Interacting means here using, that is to intervene in the empirical world changing and modifying the solids around us. As it has been suggested many times in psychology, to interact directly with a solid material entity gives much more information than simply seeing it (Lacey et al. 2007, Deshpande et al. 2010).

The major interest in object direct interaction lies in the recognition of additional properties, which determine the possibilities and limits of what can be done with the object (Johnson-Frey 2004, Goldenberg and Spatt 2009). Where each property tells us something about the reaction an artefact would have gone through, in case prehistoric people brought it into a certain environment and used it in a certain way.

Obviously, archaeological objects cannot be used in a real way, because they must be preserved. But we can approach them in a virtual way, by manipulating digital solid surrogates of tools, structures, or any other object. Form, shape, size, and texture data are indeed necessary, yet clearly insufficient to understand functional issues. Including mass and assigning the raw-materials' physical and mechanical properties to an artefact's digital solid model can benefit reasoning about the behaviour of archaeological objects. In fact, these are properties whose values should be included – along with, for example, geometry, texture, colour, weight, or name of the raw-material – whenever describing an artefact (Moitinho de Almeida and Barceló 2012, Barceló et al. 2012). The use of physical laws and measured quantities in constitutive relations yields mathematical equations (Kooi 1991). These multidimensional digital models permit theoretical experiments on computers to gain new insight into the function and behaviour of archaeological artefacts.

Once created the virtual model integrating all observed and measured properties of the real object, we can recognize the function of an object interactively, by observing the deformations that happen on the model when submitted to simulated forces (Stark and Bowyer, 1996, Stark et al., 1996). The causal effect of such forces can be efficiently represented algorithmically using physical and mechanical equations. In this domain, we should mention pioneering work by Ernest Davis (Davis 1990, 1993) formalizing the kinematics of cutting solid objects, among other functions. He showed the geometric aspects of various cutting operations: slicing an object in half, cutting a notch into an object, stabbing a hole through an object, and carving away the surface of an object. He also gave a list of geometric relations between the shapes and motions of the blades and targets – for example, suggested that a blade needs to be sufficiently thin and hard, but he does not discuss its elasticity or sharpness (see also Duric, Fayman and Rivlin 1996, or Atkins 2009, for a more exhaustive analysis of the mechanics of cutting). In archaeology, Kamminga and Cotterell (1990) applied mechanical sciences to understand the kinematics and dynamics of shaping, throwing, pressing, cutting, heating, etc., in prehistoric and ancient times. Although such an approach is not at the core of mainstream archaeology, there are already important and relevant applications (Kilikoglou et al. 1997, 2000, Tite et al. 2001, Richmond et al. 2005, Miller 2007, Hopkins 2008, Kuzminsky and Gardiner 2012, O'Higgins et al. 2012).

Computer simulation can reveal to be a key aspect of archaeological documentation, because it allows exploring ancient artefacts as dynamic entities and not just seeing them as passive objects (Moitinho de Almeida and Barceló 2012). Computer simulation algorithms permit to test different features and replicate distinct behaviours on a specific multidimensional digital model of an archaeological artefact – here described as a mathematical model that incorporates several variables. That is to say, the use of computer simulation as an experimentation and validation tool towards a better understanding of archaeological artefacts, by endowing 3D digital models with both physical and mechanical properties, and thereafter manipulate virtually these enhanced multidimensional models (Reichenbach and Kovačić 2003, Kamat and Martinez 2007, Perros 2009).

When the use behaviour and the corresponding mechanical process are simple, we can suggest a linear model using parameters that are constant over the entire simulation and independent of each other. Nevertheless, the physical world where objects were once produced and used is not a flat, linear domain where the objects' responses are always proportional to the applied forces. Parameters are always dependent upon other parameters to some degree, but in many cases the dependency is so small it can be well neglected. In other cases, we can decide for a non-linear model to bypass such difficulties, by introducing dependent parameters that are allowed to vary throughout the course of a simulation run – parameters are updated at each iteration, recalculating displacements, reaction forces, strains, and stresses at incrementally varying levels of forces and restraints. Non-linearities generally arise from two major sources: non-linear materials and non-linear geometries. Such non-linearities can occur due to large displacements, large strains, or large rotations, and these enter the formulation through the strain-displacement relations as well as the equations of motion. Non-linear boundary conditions are often included in non-linear geometries because the area of contact is a function of the deformation (Reddy 2004).

While the term non-linear primarily refers to the nature of an object's physical response, the forces and

boundary conditions that elicit non-linear responses can either be static or dynamic in nature. When the applied force is a function of time, and the material response is a function of displacement or temperature, an object can respond in ways that are difficult to predict. Predicting the impact of time-varying forces and other load-related effects, such as damping and inertia, which can occur with alternating forces, sudden applied forces, or intermittent loads, requires dynamic analysis capabilities.

Of course, an archaeologist should face this kind of challenges. We may analyse an elastic material – such as a prehistoric bow made of flexible wood, although it can be considered having a ductile compression behaviour and a brittle tensile behaviour at the same time – in a form that constitutes both material non-linearities, where the response varies disproportionately to the applied forces; and geometric non-linearities, where displacements alter the structure's stiffness. The practical applications of non-linear materials analysis vary widely. In a non-linear analysis of a component, 'failure' may be defined by the extent that a material yields rather than if the materials yields, as in linear analysis. We may also want to examine different failure modes. Many ancient materials, such as bone, shell, ceramic, stone, or wood have unique properties that require non-linear materials analysis to capture their complex load response behaviour. When we are dealing with non-linear materials in a flexible structure, we will need to combine large displacement and non-linear material analysis. An important consideration for these simulations is that as the part changes form, it can experience a phenomenon known as 'stress stiffening'. Stress stiffening can either increase or decrease the components stiffness, depending upon the applied loads and the component geometry. At times – as is the case with membrane effects – a relatively small change in form results in a substantial change in stiffness. Such complexities and non-linearities do not mean that functional problems are beyond the scope of computer simulation.

Hitherto we have seen that interaction modalities in conjunction with the form and dimension of the model, the properties of the materials, including weight and density, the relation between the artefacts' components, kinematics, the type of medium, and physics, are all to be considered when conducting simulation tests, analysing, and predicting how the virtual archaeological artefact would have behaved as a physical object in possible scenarios of real world operating conditions. If necessary, one can modify characteristics of the model, redefine parameters, assign new values and settings, or any other input data, select another simulation study or run a new simulation test, to troubleshoot problems or question the validity of the model itself. After all, these analyses are based on experiments of both functional hypothesis and knowledge obtained so far.

Investigating prehistoric or ancient mechanics through computer simulation may provide new insights into the complex dynamics of certain phenomena, such as event-based motion or kinematics. The analysis of the used mechanics allows us to understand how the behaviour with the object was performed in the past, quantifying the needed forces to activate a specific mechanism, or to exert mechanical forces to study certain phenomena and processes.

2.3.2 Functional Analysis as Reverse Engineering

Function-based reasoning can be seen as a constraint satisfaction problem where functional descriptions constrain visual appearance and structure, or visual appearance and structure constrains functional possibilities. Available mappings between perception and function are actually many-to-many, and recovering an object by matching previously recognized functional capabilities may experience exponential growth, what may constrain us not to infer the actual function in the past, but some more improbable action(s) or behaviour(s).

Model-based recognition has been thought as a possible solution. Another view may consider reasoning about function as a planning module that is composed of helper procedures for recognition. In this view, the functional description is done at a higher level discarding the complete representation. A complete representation of the physical world could attempt to represent the forces governing the universe, and reach from gravitational forces between planets to forces between chemical compounds and atoms.

Engineering is the process of turning a top level abstraction and logical design specification into a product for performing to it. The alternative presented here is Reverse Engineering (RE), which, as the name implies, is the reverse of this (Musker 1998). RE can be defined by the process of extracting missing knowledge from anything man-made, by going backwards through its development cycle and analysing its structure, function and operation (USAITA n.a., Dennet 1991, Eilam 2005, Raja 2008, Wang 2011). It is the attempt to recapture the top level specification by disassembling or analysing in detail an object. 'Attempt' because it may simply not be possible to recapture all original and valuable information – i.e., the concepts and/or procedures involved in the manufacture or use of an object – by analysing its shape, form, texture, material, and interaction (Pennestrì et al. 2006, El-Khoury 2008, Hopkins 2008, Benoit et al. 2009).

RE has been widely used for distinct applications, namely: in the development of competing products in the aerospace, automotive, medical, and software industries; product inspection and quality control; architectural and construction documentation and measurement; fitting clothing or footwear to individuals and determining the anthropometry of a population; generating data to create dental or surgical prosthetics, tissue engineered body parts, or for surgical planning; documentation and reproduction of crime scenes; competitive technical intelligence (to uncover the uncoordinated features of commercial products); as a learning tool for academic and other learning purposes; to recover lost documentation (the original design documentation is inadequate, has been lost, or never existed); product analysis and data acquisition (to examine how a product works; the components it consists of and its features; the interoperability between all the component parts of an object); replacement of archaic parts in long-lived equipment (e.g., nuclear reactors, airliners, and ships); digital update/correction (to update obsolete materials or antiquated manufacturing processes; to match an 'as-built' condition; to improve product performance and features; to strengthen the good features of a product based on long-term usage of the product). Examples of applications in cultural heritage can be found in Cotte et al. (2007) and Menna et al. (2011); in paleontology, Marcé-Nogué et al. (2011); in cognitive and brain sciences Schierwagen (2012). Similar inroads can be made into the archaeological community.

Investigating prehistoric and ancient mechanics through computer simulation may provide new insights into the complex dynamics of certain phenomena. Would the object have behaved as expected? As we have been discussing, this depends on several interrelated issues, for these determine possible outcomes. Its form, its texture, its material, for many properties have been characterized by hypothetical statements, it is then important to quantify them. But the object must also be used in a certain manner. An object having the required properties therefore functions in the intended manner, only if used in the environment and in the way the craftsperson has thought up and prescribed. The use of an object is not a given for the craftsperson, like the function, but is thought up – together with the form and material of the object – and thus comprises an essential part of the solution to the design problem.

The functioning, or actual behaviour of an object, depends both on its form and structure, as well as on the mode and conditions of its use. Given the form, the material properties, and the use of an object, then, by physical or virtual experiment, we should try to evaluate the implied functional behaviour(s). Given a desired function, the craftsperson must think up the form and its use. The reasoning from perceptual data to function is usually called analysis, whereas the reasoning from function to perceptual data is called synthesis. In spite of the importance of analysis, in design the essential mode of reasoning is synthesis, for without an idea of perceptual data (material, form, texture) and use (kinematics and dynamics) there is nothing to analyse (Chakrabarti 2002). This reasoning from what we 'see' in the archaeological present to function in the past – or from structure to behaviour – is based on deduction (Roozenburg 2002).

The present approach can be related with M. Schiffer's recent proposal for a 'behavioural analysis' of technological choices (Schiffer 2003): this discussion has concerned the material properties, a product of technical choices, which can be defined and measured without reference to post-manufacture activities. In addition to directly affecting material properties, functional analysis also determines such measurable attributes of an artefact as form, size, weight and so forth, what Schiffer denotes as Formal properties. I have tried to show how material properties can influence formal properties, but also how formal properties can influence on material ones, not only through technological choices, but also as a result of goal-direct intention.

Logically speaking, perception of function, and categorization, should be independent of one another. One can perceive that an object is throwable, for instance, without knowing that it is an arrow. Conversely, one can know that an object is an arrow without necessarily knowing what it is for. In practice, however, knowing how to categorize an object generally implies knowing what it is for, as well where it is likely to be found and when. In this sense, we can argue that rather that "form determines function", it is better to say that "function causally explains form, and texture, and material, and any other property of the artefact".

References

Acebrón-Linuesa, F., López-García, F., Valiente-González, J.M. (2002). Surface Defect Detection on Fixed Ceramic Tiles. *Proceedings of the 2nd IASTED International Conference on Visualization, Imaging, and Image Processing*.

Adams, F.R. (1979). A Goal-State Theory of Function Attributions. *Canadian Journal of Philosophy* 9:493-518.

Adams, D.C.F., Rohlf, J., Slice, D.E. (2004). Geometric Morphometrics: Ten Years of Progress Following the 'Revolution'. *Italian Journal of Zoology* 71:5-16.

Adan, M., Barceló, J.A., Pijoan-Lopez, J., Piqué, R., Toselli, A. (2003). Spatial Statistics in Archaeological Texture Analysis. In *The Digital Heritage of Archaeology, Computer Applications and Quantitative Methods in Archaeology*. M. Doerr and A. Sarris (ed.), Hellenic Ministry of Culture. Archive of Monuments and Publications.

Adán, A., Adán, M., Salamanca, S., Merchán, P. (2008). Using Non Local Features for 3D Shape Grouping. In *Structural, Syntactic, and Statistical Pattern Recognition*. N. da Vitora Lobo, T. Kasparis, F. Roli, J.T. Kwok, M. Georgiopoulos, G.C. Anagnostopoulos, M. Loog (eds.), Springer-Verlag, Berlin/Heidelberg, *Lecture Notes in Computer Science* 5342:644-653.

Aitchison, J. (1986). *The Statistical Analysis of Compositional Data*. Chapman and Hall, London.

Aitchison, J. (1994). Principles of Compositional Data Analysis. In *Multivariate Analysis and its Applications*. T.W. Anderson, I. Olkin, K.T. Fang (eds.), Institute of Mathematical Statistics, Hayward (CA), pp.73-81.

Aitchison, J. (1997). The One-Hour Course in Compositional Data analysis or Compositional Data Analysis is Easy. *Proceedings of the 3rd Annual Conference of the International Association for Mathematical Geology*. Pawlowsky Glahn, V. (ed.), CIMNE, Barcelona, pp.3-35.

Aitchison, J., Barceló-Vidal, C. (2002). Compositional Processes: A Statistical Search for Understanding. *Proceedings of the 3rd Annual Conference of the International Association for Mathematical Geology*. V. Pawlowsky-Glahn (ed.), CIMNE, Barcelona.

Anderson, P.C. (1981). *Contribution méthodologique à l'analyse des micro-traces d'utilisation sur les outils préhistoriques*. M.Sc. Thesis. Université de Bordeaux I.

Anderson, P.C., Georges, J.-E., Vargiolu, R., Zahouani, H. (2006). Insights from a Tribological Analysis of the Tribulum. *Journal of Archaeological Science* 33:1559-1568.

Ankerst, M., Kastenmueller, G., Kriegel, H.-P., Seidl, T. (1999). 3D Shape Histograms for Similarity Search and Classification in Spatial Databases. *Proceedings of the 6th International Symposium on Large Spatial Databases* (SSD`99), Hong Kong.

Asahina, D., Taylor, M.A. (2011). Geometry of irregular particles: Direct surface measurements by 3-D laser scanner. *Powder Technology* 213, 70-78. Elsevier.

Ashby, M.F. (2005). *Materials Selection in Mechanical Design*. 3rd ed. Elsevier (1992, Pergamon Press).

ASME (2010). *ASME-B46.1-2009 - Surface Texture (Surface Roughness, Waviness, and Lay)*. American Society of Mechanical Engineers (ASME), New York (NY).

Astruc, L., Vargiolu, R., Ben Tkaya, M., Balkan-Atli, N., Özbaşaran, M., Zahouani, H. (2011). Multiscale tribological analysis of the technique of manufacture of an obsidian bracelet from Aşıklı Höyük (Aceramic Neolithic, Central Anatolia). *Journal of Archaeological Science* 38:3415-3424.

Astruc, L., Vargiolu, R., Zahouani, H. (2003). Wear Assessments of Prehistoric Instruments. *Wear* 255:341-347.

Atkins, T. (2009). *The science and engineering of cutting: the mechanics and processes of separating, scratching and puncturing biomaterials, metals and non-metals*. Oxford, Butterworth.

Balachandran, M., Gero, J.S. (1990). Role of prototypes in integrated expert systems and CAD systems. In *Applications of Artificial Intelligence in Engineering*. V. Gero, J.S. (ed.), Springer-Verlag, Berlin, 1:195-211.

Barceló, J.A. (2000). Visualizing what might be. An introduction to Virtual Reality in Archaeology. In *Virtual Reality in Archaeology*. J.A. Barceló, M. Forte and D. Sanders (eds.). Archaeopress, Oxford. *BAR International Series* 843:9-36.

Barceló, J.A. (2009). *Computational Intelligence in Archaeology*. The IGI Group, Hershey, New York (NY).

Barceló, J.A. (2010a) Visual Analysis in Archaeology. An Artificial Intelligence Approach. In *Morphometrics for Nonmorphometricians*. A.M.T. Elewa (ed.), Springer Verlag, Berlin. *Lecture Notes in Earth Sciences* 124:51-101.

Barceló, J.A. (2010b). *Computational Intelligence in Archaeology. State of the Art*. In *Making History Interactive*. Frischer, B., Webb, J., Koller, D. (eds.), ArcheoPress (BAR Int. Series, S2079), Oxford, pp.11-22.

Barceló, J.A., Moitinho de Almeida, V. (2012). Functional Analysis from Visual and Compositional Data. An Artificial Intelligence Approach. *Mediterranean Archaeology & Archaeometry* 12(2):273-321.

Barceló, J.A., Pijoan-Lopez, J. (2004). Cutting or Scrapping? Using Neural Networks to Distinguish Kinematics in Use Wear Analysis". In *Enter the Past*. The E-way into the Four Dimensions of Culture Heritage. Magistrat der Stadt Wien (ed.), ArcheoPress (BAR Int. Series, S1227), Oxford, pp.427-431.

Barceló-Vidal, C., Martín-Fernández, J.A., Pawlowsky-Glahn, V. (2001). Mathematical foundations for compositional data analysis. *Proceedings the Annual Conference of the International Association for Mathematical Geology* (IAMG'01), Cancún.

Barsalou, L.W., Sloman, S.A., Chaigneau, S.E. (2005). The HIPE theory of function. In *Representing Functional Features for Language and Space: Insights from Perception, Categorization and Development*. L. Carlson, E. van der Zee (eds.), Oxford University Press, pp.131-147.

Baxter, M.J. (2006). A Review of Supervised and Unsupervised Pattern Recognition in Archaeometry. *Archaeometry* 48(4):671-694.

Beardah, C.C., Baxter, M.J. (2005). An R Library for Compositional Data Analysis in Archaeometry. *2nd Compositional Data Analysis Workshop* (CoDaWork'05), Girona.

Beck, B.B. (1980). *Animal Tool Behaviour: The Use and Manufacture of Tools*. Garland Press, New York (NY).

Bejan, A. (2000). *Shape and Structure, from Engineering to Nature*. Cambridge University Press.

Bell, S., Croson, C. (1998). Artificial Neural Networks as a tool for Archaeological Data Analysis. *Archeometry* 40(1):139-151.

Bell, S., Jantz, R. (2002). Neural Network Classification of Skeletal Remains. In *Archeological Informatics: Pushing the Envelope*. G. Burenhult (ed.), ArcheoPress (BAR Int. Series, S1016), Oxford, pp.205-212.

Benoit, S., Kilouchi, A., Michel, A.P., Pouyllau, St. (2009). Usines 3D. La simulation pour questionner les sources et les vestiges de l'histoire industrielle. *Proceedings of the Colloque Virtual Retrospect*, Pessac.

Bettinger, R.L., Boyd, R., Richerson, P.J. (1996). Style, Function, and Cultural Evolutionary Processes. In *Darwinian Archaeologies*. Maschner HDG (ed.), Plenum Press, New York (NY), pp.133-164.

Beyries, S., Delamare, F., Quantin, J.-C. (1988). Tracéologie et Rugosimétrie Tridimensionnelle. In *Industries Lithiques, Tracéologie et Technologie*. S. Beyries (ed.), Hadrian Books (BAR Int. Series, 411-1),

Oxford, pp.115-132.

Bhakar, S. *et al.* (2004). Textiles, Patterns and Technology: Digital Tools for the Geometric Analysis of Cloth and Culture. *Textile: The Journal of Cloth and Culture* 2(3):308-327.

Bhushan, B. (ed.) (2001). *Modern Tribology Handbook*. CRC Press, Boca Raton (FL).

Bicici, E., St. Amant, R. (2003). *Reasoning about the Functionality of Tools and Physical Artefacts*. Technical Report TR-2003-22. Department of Computer Science, North Carolina State University.

Biederman, I. (1987). Recognition-by-components: A Theory of Human Image Understanding. *Psychological Review* 94(2):115-147.

Biederman, I. (1995). *Visual Object Recognition. In An Invitation to Cognitive Science - Visual Cognition*. S.F. Kosslyn, D.N. Osherson (eds.), MIT Press, 2(4):121-165.

Bignon, O. *et al.* (2005). Geometric Morphometrics and the Population Diversity of Late Glacial Horses in Western Europe (*Equus caballus arcelini*): Phylogeographic and Anthropological Implications. *Journal of Archaeological Science* 32:375-391.

Billheimer, D., Guttorp, P., Fagan, W.F. (1998). *Statistical Analysis and Interpretation of Discrete Compositional Data*. NRCSE Technical Report, Series 011.

Billmeyer, F.W., Saltzman, M. (1981). *Principles of Colour Technology*. John Wiley & Sons, New York (NY).

Binford, L.R. (1989). Styles of style. *Journal of Anthropological Archaeology* 8:51-67.

Binford, T.O., Levitt, T.S. (2003). Evidential Reasoning for Object recognition. *IEEE Transactions on pattern Analysis and Machine Intelligence* 25(7):837-851.

Blau, P.J. (ed.) (1992). *ASM Handbook on Friction, Lubrication, and Wear Technology*. ASM International.

Bogoni, L. (1995). *Identification of Functional Features through Observations and Interactions*. Ph.D. Thesis. University of Pennsylvania, Philadelphia (PA).

Bonnet, J.C. (1992). *Towards a Formal Representation of Device Functionality*. Report KSL 92-54. Stanford University Knowledge Systems Laboratory.

Bonet, J., Wood, R.D. (1997). *Nonlinear Continuum Mechanics for Finite Element Analysis*. Cambridge University Press.

Boorse, C. (1976). Wright on Functions. *Philosophical Review* 85:70-86.

Boorse, C. (2002). A Rebuttal on Functions. In *Functions. New Essays in the Philosophy of Psychology and Biology*. A. Ariew, R. Cummins, M. Perlman (eds.), Oxford University Press.

Bosch, A., Chinchilla, J., Tarrús, J. (ed.) (2006). Els objectes de fusta del poblat neolític de la Draga. Excavacions de 1995-2005. Museu d'Arqueologia de Catalunya (MAC), Centre d'Arqueologia Subaquàtica de Catalunya (CASC), Girona. *Monografies del CASC* 6.

Bowden, F.P., Tabor, D. (1964). *Friction and Lubrication of Solids*. Oxford University Press, Oxford.

Bozeat, S. *et al.* (2002). When objects lose their meaning: What happens to their use? *Cognitive, Affective, & Behavioural Neurosciences* 2(3):236-251.

Brand, M. (1997). Physics-Based Visual Understanding. *Computer Vision and Image Understanding, CVIU* 65(2):192-205.

Brantingham, P.J. (2007). An Unified evolutionary model of archaeological style and function based on the Price equation. *American Antiquity* 72(3):395-416.

Bribiesca, E. (2000). A Measure of Compactness for 3D Shapes. *Computers & Mathematics with Applications* 40(10–11):1275–1284. Elsevier.

Burroni, D., Donahue, R.E., Pollard, A.M. (2002). The Surface Alteration Features of Flint Artefacts as a Record of Environmental Processes. *Journal of Archaeological Science* 29:1277-1287.

Camiz, S., Venditti, S. (2004). Unsupervised and Supervised Classifications of Egyptian Scarabs Based on Typology Qualitative Characters. *Proceedings of the Computer Applications and Quantitative Methods in Archaeology Conference* (CAA'04), Prato. F. Nicolucci (ed.), ArchaeoLingua, Budapest.

Cao, F. *et al.* (2008). A Theory of Shape identification. *Lecture Notes in Mathematics* 1948.

Carcagni, P., Daffara, C., Fontana, R., Gambino, M.C., Mastroianni, M., Mazzota, C., Pampaloni, E., Pezzati, L. (2005). Optical Micro-profilometry for Archaeology. In *Optical Methods for Arts and Archaeology*. R. Salimbeni, L. Pezzati (eds.), Proceedings of the SPIE 5857:118-128.

Castro, D., Diaz, D. (2004). Kohonen Networks Applied to Rincón del Toro Rock Art Site Analysis. *Proceedings of the Computer Applications and Quantitative Methods in Archaeology Conference* (CAA'04), Prato. F. Nicolucci (ed.), ArchaeoLingua, Budapest.

Chaigneau, S.E., Barsalou, L.W., Sloman, A. (2004). Assessing the Causal Structure of Function. *Journal of Experimental Psychology: General* 133(4):601-625.

Chakrabarti, A. *et al.* (2002). An Approach to Compositional Synthesis of Mechanical Design Concepts Using Computers. In *Engineering Design Synthesis: understanding, approaches, and tools*. A. Chakrabarti (ed.), Springer.

Chandraratne, M. R. *et al.* (2003). Determination of Lamb Grades using Texture Analysis and Neural Networks. *Proceedings of the 3rd IASTED International Conference Visualization, Imaging and Image Processing*. M.H. Hamza (ed.), Benalmadena.

Chang, H.-C., Kopaska-Merkel, D., Chen, H.C. (2002). Identification of Lithofacies using Kohonen Self-Organizing Maps. Computers & Geosciences 28:223-229.

Chaouch, M., Verroust-Blondet, A. (2006). Enhanced 2D/3D Approaches Based on Relevance Index for 3D-Shape Retrieval. *Proceedings of the IEEE International Conference on Shape Modeling and Applications* (SMI'06).

Chaouch, M., Verroust-Blondet, A. (2007). 3D Model Retrieval Based on Depth Line Descriptor. *Proceedings of the IEEE International Conference on Multimedia and Expo*, pp.599-602.

Chemero, A. (2003). An Outline of a Theory of Affordances. *Ecological Psychology* 15(2):181-195.

Clemente, I., Risch, R., Gibaja, J.F. (eds.) (2002). *Análisis Functional. Su Aplicación al Estudio de Sociedades Prehistóricas*. Hadrian Books, ArcheoPress (BAR Int. Series, 1073), Oxford.

Cooper, P.R., Birnbaum, L.A., Brand, M.E. (1995). Causal Scene Understanding. *Computer Vision and Image Understanding* 62(2):215-231.

Coppa, A. *et al.* (2007). Evidence for new Neanderthal teeth in Tabun Cave (Israel) by the application of Self-Organizing Maps (SOMs). *Journal of Human Evolution* 52(6):601-661.

Corney, J. *et al.* (2002). Coarse filters for shape matching. *IEEE Computer Graphics and Applications* 22(3):65-74.

Corsini, M.M., Schmitt, A., Bruzek, J. (2005). Aging Process Variability on the Human Skeleton: Artificial Network as an Appropriate Tool for Age at Death Assessment. *Forensic Science International* 148:163-167.

Costa, L.F., César, R.M. (2001). *Shape Analysis and Classification: Theory and Practice*. CRC Press, Boca Raton (FL).

Cotte, M., Kerouanton, J.-L., Bernard, A. (2007). L'histoire, un medium de didactique aux Nouvelles Technologies. Proceedings of the 3ème Journées ReForEHST-Recherches et Formation en Epistémologie et Histoire des Sciences et des Techniques, Caen.

Cotterell, B., Kamminga, J. (1990). *Mechanics of Pre-Industrial Technology. An introduction to the me-*

chanics of ancient and traditional material culture. Cambridge University Press.

Cula, O.G., Dana, K.J. (2004). 3D Texture Recognition Using Bidirectional Feature Histograms. *International Journal of Computer Vision* 59(1):33-60.

Cummins, R. (1975). Functional Analysis. *Journal of Philosophy* 72(20):741-765.

Cummins, R. (2000). "How does it work?" vs. "What are the laws?" Two conceptions of psychological explanation. In *Explanation and Cognition*. F. Keil, R. Wilson (eds.), MIT Press, pp.117-145.

Cummins, R. (2002). Neo-Teleology. In *Functions. New Essays in the Philosophy of Psychology and Biology.* A. Ariew, R. Cummins, M. Perlman (eds.), Oxford University Press.

David, S.E. *et al.* (1994). *Texturing and Modeling: a Procedural Approach*. Academic Press Professional, San Diego (CA).

Davis, E. (1990). *Representations in Commonsense Knowledge*. Morgan Kaufmann Publishers, San Mateo (CA).

Davis, E. (1993). The Kinematics of Cutting Solid Objects. *Annals of Mathematics and Artificial Intelligence* 9(3-4):253-305.

Dennett, D.C. (1987). *The Intentional Stance*. The MIT Press, Cambridge (MA).

Dennett, D.C. (1991). Cognitive Science as Reverse Engineering: Several Meanings of 'Top-Down' and 'Bottom-Up'. *Proceedings of the 9th International Congress of Logic, Methodology and Philosophy of Science*. D. Prawitz, B. Skyrms, D. Westerstahl (eds.).

Deshmukh, A., Yung, J.P., Wang, H.P. (1993). Automated generation of assembly sequence based on geometric and functional reasoning. *Journal of Intelligent Manufacturing* 4(4):269-284.

Deshpande, G. *et al.* (2010). Object familiarity modulates effective connectivity during haptic shape perception. *NeuroImage* 49(3):1991-2000.

Diaz, D., CAstro, D. (2001). Pattern Recognition Applied to Rock Art". In *Archaeological Informatics: Pushing the Envelope*. G. Burenhult (ed.), ArcheoPress (BAR Int. Series, S1016), Oxford, 463-468.

Dimanzo, M. *et al.* (1989). FUR: Understanding FUnctional Reasoning. International *Journal of Intelligent Systems* 4:431-457.

Domanski, M., Webb, J.A., Boland, J. (1994). Mechanical properties of stone artefact materials and the effect of heat treatment. *Archaeometry* 36(2):177-208.

Dong, J., Chantler, M. (2005). Capture and Synthesis of 3D Surface Texture. *International Journal of Computer Vision* 62(1-2):177-194.

Drolon, H. *et al.* (2003). Multiscale Roughness Analysis of Particles: Application to the Classification of Detrital Sediments. *Mathematical Geology* 35(7):805-817.

Dryden, I.L., Mardia, K. (1998). *Statistical Shape Analysis*. John Wiley & Sons, Chichester (UK).

Dunnell, R.C. (1978). Style and Function: A Fundamental Dichotomy. *American Antiquity* 43(2):192-202.

Duric, Z., Fayman, J., Rivlin, E. (1996). Function from Motion. *IEEE Transactions on Pattern Analysis and Machine Intelligence* 18:579-591.

Edelman, S. (1999). *Representation and Recognition in Vision*. MIT Press, Cambridge (MA).

Edelman, S., Intrator, N. (2002). Visual Processing of Object Structure". In *The Handbook of Brain Theory and Neural Networks*. M. A. Arbib (ed.), MIT Press, Cambridge (MA).

Edelman, S., Intrator, N. (2003). Towards Structural Systematicity in Distributed, Statically Bound Visual Representations. *Cognitive Science* 27:73-110.

Eilam, E. (2005). *Reversing: Secrets of Reverse Engineering*. Wiley Publishing, Indianapolis (IN).

El-Khoury, N. (2008). *Proposition et simulation de modèles numériques de compréhension d'un patrimoine : le théâtre romain de Byblos au Liban*. PhD thesis, Université de Montréal.

Elewa, E.M.T. (ed.) (2010). Morphometrics for Non-Morphometricians. Springer, Berlin. *Lecture Notes in Earth Sciences* 124.

Engel, A. Van den Broeck C. (2001). *Statistical Mechanics of Learning*. Cambridge University Press.

Engler, O., Randle, V. (2009). *Introduction to Texture Analysis: Macrotexture, Microtexture, and Orientation Mapping*. CRC Press, Boca Ratón (FL).

Erden, M.S. *et al.* (2008). A review of function modeling: Approaches and applications. *Artificial Intelligence for Engineering Design, Analysis and Manufacturing* 22:147-169.

d'Errico, F., Backwell, L. (2009). Assessing the Function of Early Hominin Bone Tools. *Journal of Archaeological Science* 36(8):1764-1773.

Evans, A.A., Donahue, R.E. (2008). Laser Scanning Confocal Microscopy: a potential technique for the study of lithic microwear. *Journal of Archaeological Science* 35:2223-2230.

Evans, A.A., Macdonald, D. (2011). Using metrology in early prehistoric stone tool research: further work and a brief instrument comparison. *Scanning* 33(5):294-303.

Falconer, K. (2003). *Fractal Geometry*. John Wiley, London.

Far, B.H. (1992). *Functional Reasoning, Explanation and Analysis*. Technical Report JAERI-M 91-225. Japan Atomic Energy Research Institute.

Fermo, P. *et al.* (2004). Classification of Ancient Etruscan Ceramics Using Statistical Multivariate Analysis of Data. *Applied Physics A: Materials Science & Processing* 79(2):299-307.

Flach, P. (2012). *Machine Learning: The Art and Science of Algorithms that Make Sense of Data*. Cambridge University Press.

Fleming, B. (1999). *3D Modeling and Surfacing*. Morgan Kaufmann Publishers, San Francisco (CA).

FPL (2010). *Wood Handbook – Wood as an Engineering Material*. General Technical Report FPL-GTR-190. U.S. Department of Agriculture, Forest Service, Forest Products Labouratory (FPL). Centennial Edition, Madison (WI).

Friedhoff, R.M., Benzon, W. (1989). *Visualization: The Second Computer Revolution*. Abrahams, New York.

Friedrich, K., Schlarb, A.K. (ed.) (2008). *Tribology of Polymeric Nanocomposites: Friction and Wear of Bulk Materials and Coatings*. Elsevier.

Froimovich, G., Rivlin, E., Shimshoni, I. (2002) Object Classification by Functional Parts. *Proceedings of the 1st Symposium on 3D Data, Processing, Visualization and Transmission*, 648-655.

Fueten, F. (1997). A Computer Controlled Rotating Polarizer Stage for the Petrographic Microscope. *Computers and Geosciences* 23:203-208.

Fueten, F., Hynes, K., Vanluttikhuisen, R.L. (2001). An Experimental Setup for the Analysis of Analogue Deformation Experiments using the Rotating Polarizer Stage. *Journal of Structural Geology* 24:241-245.

Fulcher, J. (1997). Neural Networks for Archaeological Provenancing. In *Handbook of Neural Computation*. E. Fiesler, R. Beale (eds.), Institute of Physics, Oxford University Press.

Gal, R., Shamir, A., Cohen-Or, D. (2007). Pose-Oblivious Shape Signature. *IEEE Transactions on Visualization and Computer Graphics* 13(2):261-271.

Gammaitoni, L. (2011). Shape is Physical. In SHAPES 1.0. The Shape of Things. *Proceedings of the 1st Interdisciplinary Workshop on SHAPES*. J. Hastings, O. Kutz, M. Bhatt, S. Borgo (eds.), Karlsruhe.

Gaspar, P., Cummings, A., Hubbard, C. (2000). Topographical Studies in the Conservation of Statuary Materials. *Conservation Journal* 36. http://www.vam.ac.uk/content/journals/conservation-journal/issue-36/topographical-studies-in-the-conservation-of-statuary-materials/

Gibson, P. (1993). The Potentials of Hybrid Neural Network Models for Archaeological Ageing and Interpre-

tation. In *Computing the Past*. T. Madsen, J. Andresen (eds.), University of Aarhus Press.

Gibson, P. (1996). An archaeofaunal ageing comparative study into the performance of Human analysis versus hybrid neural network analysis. *Analecta Prehistorica Leidensia* 28(1):229-232.

Gibson, J.J. (1979). *The Ecological Approach to Visual Perception*. Houghton Mifflin, Boston (MA).

Gil-Pita, R., Sala-Burgos, N. (2006). Using Neural Networks to Detect Microfossil Teeth in Somosaguas Sur Paleontological Site. In Intelligent Data Engineering and Automated Learning (IDEAL'06). *Lecture Notes in Computer Science* 4224:496-503.

Gluchy, A., Vargiolu, R., Mordant, C., Zahouani, H. (2008). Tribology's Contribution to Archaeology. *Surface Engineering* 24(2):154-161.

Goldenberg, G., Spatt, J. (2009). The Neural Basis of Tool Use. *Brain – A Journal of Neurology* 132:1645-165.

González, J.E., Ibáñez, J.J. (2003). The quantification of use-wear polish using image analysis. First results. *Journal of Archaeological Science* 30:481-489.

Grace, R. (1989). *Interpreting the function of stone tools. The quantification and computerisation of microwear analysis*. Hadrian Books (BAR Int. Series, 497), Oxford.

Grenander, U. (1993) *General Pattern Theory*. Oxford University Press.

Grudzinski, K., Karwowski, M., Duch, W. (2003). Computational Intelligence Study of the Iron Age Glass Data. *International Conference on Artificial Neural Networks* (ICANN), and *International Conference on Neural Information Processing* (ICONIP), Istanbul.

Grudzinski, K., Karwowski, M. (2005). The Analysis of the Unlabelled Samples of the Iron Age Glass Data. In *Intelligent Information Processing and Web Mining*. Proceedings of the International IIS - IIPWM'05. M.A. Klopotek, S.T. Wierzchon, K. Trojanowski (eds.), Advances in Soft Computing Series, Springer.

Han, J., Kamber, M. (2001). *Data Mining. Concepts And Techniques*. San Francisco, Morgan Kaufmann.

Haralick, R.M. (1979). Statistical and Structural Approaches to Texture. *Proceedings of the IEEE* 67(5):786-804.

Hayden, B. (ed.) (1979). *Lithic Use-Wear Analysis*. Academic Press, New York (NY).

Hayden, B. (1998). Practical and Prestige Technologies: The Evolution of Material Systems. *Journal of Archaeological Method and Theory* 5:1-55.

Hegarty, M. (2004). Mechanical Reasoning as Mental Simulation. *Trends in Cognitive Science* 8:280-285.

Hermon, S., Niccolucci, F., D'Andrea, A. (2005). Some Evaluations of the potential Impact of Virtual Reality on the Archaeological Scientific Research. *Proceedings of the 11th International Conference on Virtual Systems and Multimedia, VSMM2005*, Ghent. Archaeolingua, Budapest.

Heshmat, H. (2010). *Tribology of Interface Layers*. CRC Press, Boca Ratón (FL).

Hodges, J. (1995). Functional and Physical Object Characteristics and Object Recognition in Improvisation. *Computer Vision and Image Understanding: CVIU* 62(2):147-163.

Holland, J.H., Holyoak, K.J., Nisbett, R.E., Thagard, P.R. (1986). *Induction. Processes of Inference, Learning, and Discovery*. The MIT Press, Cambridge (MA).

Hopkins, H. (2008). Using Experimental Archaeology to Answer the Unanswerable: A case study using Roman Dyeing. In *Experiencing Archaeology by Experiment*. P. Cunningham, J. Heeb, R.P. Paardekooper (eds.). Oxbow Books, Oxford. pp.103-118.

Horsfall, G. (1987). Design Theory and Grinding Stones. In *Lithic Studies Among the Contemporary Highland Maya*. B. Hayden, (ed.), University of Arizona Press, Tucson, pp.332-377.

Hüllermeier, E. (2007). *Case-Based Approximate Reasoning*. Springer Verlag (Theory and Decision Library B), New York/Berlin.

Hummel, J.E., Biederman, I. (1992). Dynamic Binding in a Neural Network for Shape Recognition. *Psychological Review* 99(3):480-517.

Hunt, R.W.G., Pointer, M.R. (2001). *Measuring Colour*. Ellis Horwood.

Hunter, R.S., Harold, R.W. (1987). *The Measurement of Appearance*. John Wiley & Sons, New York (NY).

Hurt, T.D., Rakita, G.F.M. (eds.) (2001). *Style & Function: Conceptual Issues in Evolutionary Archaeology*. Bergin & Garvey, Westport (CT).

Hutchings, I.M. (1992). *Tribology: friction and wear of engineering materials*. Edward Arnold, London.

d'Incau, E., Couture, C., Maureille, B. (2012). Human Tooth Wear in the Past and the Present: Tribological mechanisms, scoring systems, dental and skeletal compensations. *Archives of Oral Biology* 57:214-229.

Ingram, D.S., Hudson, A. (eds.) (1994). Shape and Form in Plants and Fungi. *Linnean Society Symposium Series* 16, Linnean Society of London, Academic Press.

Jain, A.K., Karu, K. (1996). Learning Texture Discrimination Masks. *IEEE Transactions on Pattern Analysis and Machine Intelligence* 18(2):195-205.

Jang, J. *et al.* (2006). Punctuated simplification of man-made objects. *Visual Computer* 22(2):136-145.

Jayanti, S., Kalyanaraman, Y., Ramani, K. (2009). Shape-based clustering for 3D CAD objects: A comparative study of effectiveness. *Computer-Aided Design* 41:999-1007.

Johansson, I. (2008). Functions and Shapes in the Light of the International System of Units Metaphysica. *International Journal for Ontology & Metaphysics* 9:93-117.

Johansson, I. (2011). Shape is a Non-Quantifiable Physical Dimension. In *SHAPES 1.0. The Shape Of Things*. Proceedings of the 1st Interdisciplinary Workshop on SHAPES. J. Hastings, O. Kutz, M. Bhatt, S. Borgo (eds.), Karlsruhe.

Johnson-Frey, S.H. (2004). The Neural Bases of Complex Tool Use in Humans. *Trends in Cognitive Sciences* 8(2):71-78.

Jones, A. (2004). Archaeometry and Materiality: Materials-based Analysis in Theory and Practice. *Archaeometry* 46(3):327-338.

Kadar, M., Ileana, I., Joldes, R. (2004). Artificial Neural Networks used in Forms Recognition of the Properties of Ancient Copper based Alloys. *Proceedings of the Computer Applications and Quantitative Methods in Archaeology Conference* (CAA'04), Prato. F. Nicolucci (ed.), ArchaeoLingua, Budapest.

Kashyap, H.K., Bansilal, P., Koushik, A.P. (2003). Hybrid Neural Network Architecture for Age Identification of Ancient Kannada Scripts. *Proceedings of the IEEE International Symposium on Circuits and Systems* (ISCAS'03), 3:423-426.

Kazhdan, M., Funkhouser, T., Rusinkiewicz, S. (2003). Rotation Invariant Spherical Harmonic Representation of 3D Shape Descriptors. *Eurographics Symposium on Geometry Processing*. L. Kobbelt, P. Schröder, H. Hoppe (eds.). The Europgraphics Association.

Keogh, E., Ye, L., Rampley, T., Lee, S.-H. (2010). Automatic Construction of Typologies for Massive Collections of Projectile Points. In *Making History Interactive*. B. Frischer, J. Webb, D. Koller (eds.), ArcheoPress (BAR Int. series, S2079), Oxford, pp.146-157.

Kilikoglou, V. *et al.* (1998). Mechanical performance of quartz tempered ceramics: part 1, strength and toughness. *Archaeometry* 40:261-79.

Kilikoglou, V., Vekkinis, G. (2002). Failure Prediction and Function Determination of Archaeological Pottery by Finite Element Analysis. *Journal of Archaeological Science* 29:1317-1325.

Kirsh, D. (2009). Explaining Artefact Evolution. In *Cognitive Life of Things: Recasting the Boundaries of the Mind.* L. Malafouris (ed.), McDonald Institute for Archaeological Research, Cambridge University press.

Kitamura, Y., Mizogouchi, R. (1999). *An Ontology of Functional Concepts of Artefacts*. Artificial Intelligence Research Group, The Institute of Scientific and Industrial Research, Osaka University (AI-TR-99-1).

Kitamura, Y., Mizogouchi, R. (2004). Ontology-based systematization of functional knowledge. *Journal of Engineering Design* 15(4):327-351.

Kleber, F., Sablatnig, R. (2009). Scientific Puzzle Solving: Current Techniques and Applications. *Proceedings of the Computer Applications and Quantitative Methods in Archaeology Conference* (CAA'09), Williamsburg (VA).

Koenderink, J.J., Van Doorn, A.J. (1992). Surface Shape and Curvature Scales. *Image and Vision Computing* 10(8), 557-564. K.D. Baker (ed.), Butterworth-Heinemann Newton (MA).

Kohonen, T. (2001). *Self-Organizing Maps*. (3rd ed.) Springer, Berlin.

Kolodner, J. (1993). *Case-Based Reasoning*. Morgan Kaufmann Publishers, San Francisco (CA).

Koutsoudis, A. *et al.* (2010). 3D Pottery content-based retrieval based on pose normalisation and segmentation. *Journal of Cultural Heritage* 11(3):329-338.

Kowalski, R. (2011). *Computational Logic and Human Thinking: How to be Artificially Intelligent*. Cambridge University Press.

Krotkov, E. (1994). Perception of Material by Robotic Probing: Preliminary Investigation. In *The Role of Functionality in Object Recognition*. CVPR Workshop.

Kulkarni, A.D. (2001). *Computer Vision and Fuzzy Neural Systems*. Prentice Hall, Upper Saddle River (NJ).

Kuzminsky, S.C., Gardiner, M.S. (2012). Three-dimensional laser scanning: potential uses for museum conservation and scientific research. *Journal of Archaeological Science* 39(8):2744–2751

Lacey, S., Campbell, C., Sathian, K. (2007). Vision and touch: Multiple or multisensory representations of objects? *Perception* 36(10):1513-1521.

Laga, H., Takahashi, H., Nakajima, M. (2006). Spherical wavelet descriptors for contentbased 3D model retrieval. *Proceedings of the IEEE International Conference on Shape Modeling and Applications* (SMI'06), pp.75-85.

Langley, P. (1996). *Elements Of Machine Learning*. Morgan Kaufmann Publ, San Francisco (CA).

Lark, R.S. (1996). Geostatistical description of texture on an aerial photograph for discriminating classes of land cover. *International Journal of Remote Sensing* 17(11):2115-2133.

Lee, T.S. (1996). Image representation using 2D Gabor wavelets. *IEEE Transactions on Pattern Analysis and Machine Intelligence* 18(10):959-971.

Leung, T., Malik, J. (2001). Representing and Recognizing the Visual Appearance of Materials using Three-dimensional Textons. *International Journal of Computer Vision* 43(1):29-44.

Leymarie, F.F. (2011). On the Visual Perception of Shape - Analysis and Genesis through Information Models. In *SHAPES 1.0. The Shape of Things*. Proceedings of the 1st Interdisciplinary Workshop on SHAPES. J. Hastings, O. Kutz, M.l Bhatt, S. Borgo (eds.), Karlsruhe.

Leyton, M. (1992). *Symmetry. Causality, Mind*. The MIT Press, Cambridge (MA).

Leyton, M. (2005). Shape as Memory Storage. In *Ambient Intelligence for Scientific Discovery*. In *Lecture Notes in Artificial Intelligence* 3345. C. Young (ed.), Springer, Berlin.

Li, P., Flenley, J.R. (1999). Pollen Texture Identification using Neural Networks. *Grana* 38:59-64.

Lian, Z., Rosin, P.L., Sun, X. (2010) Rectilinearity of 3D Meshes. *International Journal of Computer Vision - IJCV* 89(2-3):130-151.

Lletí, R. *et al.* (2003). Application of the Kohonen Artificial Neural Network in the Identification of Protein-

aceous Binders in Samples of Panel Painting Using Gas Chromatography-Mass Spectrometry. *Analyst* 128:281-286.

Lohse, E.S. *et al.* (2004). Automated Classification of Stone Projectile Points in a Neural Network. In *Enter the Past. The e-way into the four dimensions of Culture Heritage*. Magistrat der Stadt Wien-Referat Kulturelles Erbe-Städtarhchäologie Wien (ed.). ArcheoPress (BAR Int. series, S1227), pp.431-437.

Longo, L., Dalla Riva, M., Saracino, M. (eds.) (2009). *Prehistoric Technology. 40 years later: Functional Analysis and the Russian Legacy*. Hadrian Books (BAR Int. series).

Lopez Molinero, A. *et al.* (2000). Classification of Ancient Roman Glazed Ceramics using the neural network of self-organizing maps. *Fresenius Journal of Analytical Chemistry* 367:586-589.

Ma, Q.L. (2003). Application of EDXRF and artificial neural networks to provenance studies of the archaeological pottery sherds during Neolithic Age in Gansu Province. *China Journal of Lanzhou University (Natural Sciences)* 39(1):47-53.

Ma, Q.L. *et al.* (2000). Principal component analysis and artificial neural networks applied to the Classification of Chinese pottery of Neolithic age. *Analytica Chimica Acta* 406:247-256.

Maaten, L.J.P. van der, Boon, P.J. (2006). COIN-O-MATIC: A Fast and Reliable System for Coin Classification. *Proceedings of the MUSCLE Coin Workshop*, Berlin, pp.7-17.

Maaten, L.J.P. van der *et al.* (2006). Computer Vision and Machine Learning for Archaeology. *Proceedings of the Computer Applications and Quantitative Methods in Archaeology Conference* (CAA'06), Fargo (ND).

MacAdam, D.L. (1985). *Colour Measurement: Theme and Variations*. Springer-Verlag, New York (NY).

Mademlis, A. *et al.* (2009). Ellipsoidal Harmonics for 3-D Shape Description and Retrieval. *IEEE Transactions on Multimedia - TMM* 11(8):1422-1433.

Marcé-Nogué, J., Fortuny, J., Gil, L.L., Galobar, À (2011). Using Reverse Engineering to Reconstruct Tetrapod Skulls and Analyse its Feeding Behaviour. *Proceedings of the 13th International Conference on Civil, Structural and Environmental Engineering Computing*, Chania. B.H.V. Topping, Y. Tsompanakis (ed.). Civil-Comp Press, Stirlingshire, Scotland.

Markwardt, J.L. (1930). *Comparative strength properties of woods grown in the United States*. Technical Bulletin 158. U.S. Department of Agriculture, Washington D.C.

Markwardt, J.L. (1935). *Strength and related properties of woods grown in the United States*. Technical Bulletin 479. U.S. Department of Agriculture, Washington D.C.

Marmo, R. *et al.* (2005). Textural Identification of Carbonate Rocks by Image Processing and Neural Network: Methodology Proposal and Examples. *Computers & Geosciences* 31:649-659.

Martin, D.H., Fowlkes, C.C., Malik, J. (2004). Learning to Detect Natural Image Boundaries Using Local Brightness, Colour, and Texture Cues. *IEEE Transactions on Pattern Analysis and Machine Intelligence* 26(5):530-549.

Martinez-Ortiz, C., Žunić, J. (2009). Measuring Cubeness of 3D Shapes. Progress in Pattern Recognition, Image Analysis, Computer Vision, and Applications. *Lecture Notes in Computer Science* 5856:716–723. E. Bayro-Corrochano, J.-O. Eklundh (eds.), Springer-Verlag, Berlin, Heidelberg.

Marwan, N. *et al.* (2004). *3D measures of complexity for the assessment of complex trabecular bone structures*. http://www.pik-potsdam.de/members/kurths/publikationen/2004/3d-measures-of-complexity-for-the-assessment-of-complex-trabecular-bone-structures.

Masad, E., Al-Rousan, T., Little, D. (2007). *Test Methods for Characterizing Aggregate Shape, Texture, and Angularity*. NCHRP Report 555, National Cooperative Highway Research Program. Transportation Research Board of the National Academies, Washington D.C.

Mayorga, M.A., Ludeman, L.C. (1991). Neural Nets for Determination of Texture and its Orientation. *Proceedings of the International Conference on Acoustics, Speech, and Signal Processing* (ICASSP'91) 4:2689-2692.

Mayorga, M.A., Ludeman, L.C. (1994). Shift and Rotation Invariant Texture Recognition with Neural Nets. *Proceedings of the IEEE World Congress on Computational Intelligence* 6, 4:078-4083.

McGrew, W.C. (1993). The Intelligent Use of Tools: Twenty Propositions. In *Tools, Language, and Cognition in Human Evolution*. K. R. Gibson, T. Ingold (eds.), Cambridge University Press, pp.151-170.

Menna, F., Nocerino, E., Scamardella, A. (2011). Reverse Engineering and 3D Modelling for Digital Documentation of Maritime Heritage. *International Archives of Photogrammetry, Remote Sensing and Spatial Information Sciences* 38(5/W16).

Miller, H. M.-L. (2007). *Archaeological Approaches to Technology*. Academic Press.

Millikan, R.G. (1999). Wings, Spoons, Pills and Quills: A Pluralist Theory of Function. *Journal of Philosophy* 96:192-206.

Mirmehdi, M., Xie, X., Suri, J. (eds.) (2008). *Handbook of Texture Analysis*. Imperial College Press, London.

Moitinho de Almeida, V., Barceló, J.A. (2012a). Towards Reverse Engineering Archaeological Artefacts. *Proceedings of the Computer Applications and Quantitative Methods in Archaeology Congress* (CAA'12), Southampton. Amsterdam University Press (AUP), Pallas Publications. (*in press*)

Moitinho de Almeida, V., Barceló, J.A. (2012b). 3D Scanning and Computer Simulation of Archaeological Artefacts. *Proceedings of the 1st International Conference on Best Practices in World Heritage: Archaeology*, Menorca.

Moitinho, V., Barceló, J.A. (2011). Understanding Virtual Objects through Reverse Engineering. Paper presented at the *III Internacional de Arqueología, Informática Gráfica, Patrimonio e Innovación*, Sevilla.

Musker, D.C. (1998). Protecting & Exploiting Intellectual Property in Electronics. *IBC Conferences*.

Myshkin, N.K., Petrokovets, M.I., Kovalev, A.V. (2005). Tribology of Polymers: adhesion, friction, wear, and mass-transfer. *Tribology International* 38:910-921.

Nagel, E. (1961). *The Structure of Science*. New York and Burlingame, Harcourt, Brace and World Inc.

Neander, K. (1991). The Teleological Notion of Function. *Australian Journal of Philosophy* 69:454-68.

Nelson, R.C., Selinger, A. (1998). A Cubist Approach to Object Recognition. *Proceedings of the International Conference on Computer Vision* (ICCV98), pp.614-621.

Norman, D.A. (1989). *The Psychology of Everyday Things*. Basic Books, New York (NY).

Novič, M. *et al.* (2001). The application of the combination of chemical (ICP-OES and ICP-MS) and chemometric analytical procedures for the tracing of the geologically predetermined composition of archaeological pottery. *Proceedings of the 12th International Symposium Spectroscopy in Theory and Practice*. Thinkshop "In search of the Metrological Basis of Spectroscopic Measurements", Bled, Slovenia.

Novotni, M., Klein, R. (2003). 3D Zernike descriptors for content based shape retrieval. *Proceedings of the 8th ACM Symposium on Solid Modeling and Applications* (SM'03), ACM, New York (NY), pp.216-225.

O'Brien, M.J., Lyman, R.L. (2002). *Seriation, Stratigraphy, and Index Fossils. The Backbone of Archaeological Dating*. Kluwer Academic Publishers.

O'Higgins, P. *et al.* (2012). Virtual Functional Morphology: Novel Approaches to the Study of Craniofacial Form and Function. *Evolutionary Biology* 39. http://link.springer.com/article/10.1007/s11692-012-9173-8/fulltext.html

Ohbuchi, R., Hata, Y. (2006). Combining Multiresolution Shape Descriptors for Effective 3D Similarity Search. *Proceedings of the WSCG'06*, Plzen, Czech Republic.

Oñate, E. (1995). *Calculo de Estructuras por el Metodo de Elementos Finitos. Analisis estático lineal*. Centro Internacional de Métodos Numéricos en Ingeniería, UPC, Barcelona.

Osada, R. *et al.* (2002). *Shape Distributions*. ACM Transactions on Graphics 21(4):807- 832.

OUP (n.a.). *Obsidian Use Project*. CNRS/IFEA/TCIU/LTDS/ANR. http://www.obsidianuseproject.org/OUP/?cat=71

Outram, A.K. (2008). Introduction to Experimental Archaeology. *World Archaeology* 40(1):1-6.

Palmer, S. (1999). *Vision Science. Photons to Phenomelogy*. The MIT Press, Cambridge (MA).

Paquet, E. *et al.* (2000). Description of shape information for 2-D and 3-D objects. *Signal Process: Image Communication* 16:103–122.

Pawlowsky-Glahn, V., Egozcue, J.J, Tolosana-Delgado, R. (2007). *Lecture Notes on Compositional Data Analysis*. University of Girona Technical Report. DUGidocs.

Pechuk, M., Soldea, O., Rivlin, E. (2005). Function-Based Classification from 3D Data via Generic and Symbolic Models. *Proceedings of the 20th National Conference on Artificial Intelligence* (AAAI'05), Pittsburgh, Pennsylvania (PA).

Pennestrì, E., Pezzuti, E., Valentini, P.P., Vita, L. (2006). Computer-aided Virtual Reconstruction of Italian Ancient Clocks. *Computer Animation and Virtual Worlds* 17(5):565-572.

Peng, L.W., Shamsuddin, S.M. (2004). Modeling II: 3D object reconstruction and representation using neural networks. *Proceedings of the 2nd International Conference on Computer Graphics and Interactive Techniques in Australasia and Southeast* (GRAPHITE '04). Academy of Computing Machinery Press.

Petrelli, M. *et al.* (2001). A Simple System based on Fuzzy Logic and Artificial Neural Networks to Determine Travertine Provenance from Ancient Buildings. *Proceedings of the Workshop Artificial Intelligence for the Cultural Heritage and Digital Libraries*. L. Bordoni, G. Semeraro (eds.), Dipartimento di Informatica, Università degli Studi di Bari. Associazione Italiana per l'Inteligenza Artificiale.

Petrelli, M. *et al.* (2003). Determination of Travertine Provenance from Ancient Buildings Using Self-Organizing Maps and Fuzzy Logic. *Applied Artificial Intelligence* 7(8-9):885-900.

Peursum, P. *et al.* (2003). Object Labeling from Human Action Recognition. *Proceedings of the IEEE International Conference on Pervasive Computing and Communications*, Dallas-Fort Worth, Texas, pp.399-406.

Peursum, P. *et al.* (2005). Robust Recognition and Segmentation of Human Actions using HMMs with Missing Observations. *EURASIP Journal of Applied Signal Processing* 13:2110-2126.

Peursum, P., Venkatesh, S., Wes, G. (2007). Tracking-as-Recognition for Articulated Full-Body Human Motion Analysis. *Proceedings of the IEEE International Conference on Computer Vision and Pattern Recognition* (CVPR). IEEE CS Press.

Pijoan-López, J. (2008). *Quantificació de traces d'ús en instruments lítics mitjançant imatges digitalitzades: Resultats d'experiments amb Xarxes Neurals I Estadística*. Ph.D. Thesis. Universitat Autònoma de Barcelona.

Popper, K. (1963). *Conjectures and Refutations: The Growth of Scientific Knowledge*. London, Routledge & Kegan Paul.

Raja, V., Fernandes, K.J. (eds.) (2008). *Reverse Engineering: An Industrial Perspective*. Springer-Verlag, London.

Rao, S. (2005). *The Finite Element Method in Engineering*. Elsevier, Amsterdam.

Read, D. (2007). *Artefact Classification. A Conceptual and Methodological Approach*. Left Coast Press, Walnut Creek (CA).

Reddy, J.N. (2004). *An Introduction to Nonlinear Finite Element Analysis*. Oxford University Press.

Richmond, B.G. *et al.* (2005). Finite element analysis in functional morphology. The Anatomical Record Part A: Discoveries in Molecular, Cellular, and Evolutionary Biology. *Finite Element Analysis in Vertebrate Biomechanics (special issue)* 283A(2):259-274.

Rivlin, E., Dickinson, S., Rosenfeld, A. (1995). Recognition by Functional Parts. *Computer Vision and Image Understanding* 62(2):164-176.

Roozenburg, N.F.M. (2002). Defining Synthesis: on the senses and the logic of design synthesis. In *Engineering Design Synthesis: understanding, approaches, and tools*. A. Chakrabarti (ed.), Springer.

Rovetto, R. (2011). The Shape of Shapes: An Ontological Exploration. In *SHAPES 1.0. The Shape Of Things*. Proceedings of the 1st Interdisciplinary Workshop on SHAPES. J. Hastings, O. Kutz, M. Bhatt, S. Borgo (eds.), Karlsruhe, Germany.

Ruggeri, M., Saupe, D. (2008). Isometry-invariant matching of point set surfaces. *Eurographics'08, Workshop on 3D Object Retrieval*, Crete.

Ruiz del Solar, J. (1998). TEXSOM: Texture Segmentation using Self-Organizing Maps. *Neural Networks* 21:7-18.

Russ, J.C. (1990). *Computer-assisted microscopy: The measurement and analysis of images*. Plenum Press, New York (NY).

Russell, B. (1967). *The Problems of Philosophy*. Oxford University Press (1st ed. 1912, Home University Library).

Sackett, J.R. (1985). Style and ethnicity in archaeology: the case for isochrestism. In *The Uses of Style in Archaeology*. M. Conkey, C. Hastorf (eds.), Cambridge University Press, pp.32-43.

Sanden, J.J., Hoekman, D.H. (2005). Review of relationships between grey-tone co-occurrence, semivariance, and autocorrelation based image texture analysis approaches. *Canadian Journal of Remote Sensing* 31(3):207-213.

Schierwagen, A. (2012). On Reverse Engineering in the Cognitive and Brain Sciences. *Natural Computing* 11:141-150.

Schiffer, M., Skibo, J. (1987). Theory and Experiment in the Study of Technological Change. *Current Anthropology* 28:595-622.

Schiffer, M. (2003). Properties, performance characteristics and behavioural theory in the study of technology. *Archaeometry* 45(1):163-183.

Schmitt, A. *et al.* (2001). Les résaux de neurones artificiels. Un outil de tratitement de donnés prometteur pour l'Anthropologie. *Bulletin et Mémoirs de la Société d'Anthropologie de Paris* 13(1-2):143-150.

Semenov, S.A. (1964). *Prehistoric technology: an experimental study of the oldest tools and artefacts from traces of manufacture and wear*. Cory, Adams & Mackay, London.

Shelley, C.P. (1996). Visual Abductive Reasoning in Archaeology. *Philosophy of Science* 63:278-301.

Shilane, P., Min, P., Kazhdan, M., Funkhouser, T. (2004). The Princeton Shape Benchmark. *IEEE Computer Society - Shape Modeling International*, pp.167-178.

Siegismund, S., Snethlage, R. (eds.) (2011). *Stone in Architecture – Properties, durability*. (4th ed.) Springer.

Slice, D.E. (2007). Geometric morphometrics. *Annual Review of Anthropology* 36.

Small, C.G. (1996). *The Statistical Theory of Shape*. Springer, Berlin.

St. Amant, R. (2002). *A Preliminary Discussion of Tools and Tool Use*. NCSU Technical Report TR-2002-06.

St. Amant, R., Horton, T.E. (2008). Revisiting the definition of animal tool use. *Animal Behaviour* 75:1199-1208.

Stark, L., Bowyer, K. (1996). Generic Object Recognition using Form and Function. *Machine Perception and Artificial Intelligence* 10. World Scientific Press, Singapore.

Stark, L. et al. (1996). Recognizing Object Function Through Reasoning About Partial Shape Descriptions and Dynamic Physical Properties. *Proceedings of the IEEE* 84(11):1640-1658.

Strang, G. (2008). *An Analysis of the Finite Element Method*. Wellesley-Cambridge Press.

Stytz, M.R., Parrott, R.W. (1993). Using Kriging for 3D Medical Imaging. *Computerized Medical Imaging and Graphics* 17(6):421-442.

Sundar, H. *et al.* (2003). Skeleton based shape matching and retrieval. *Proceedings of the IEEE Shape Modeling International*, pp.130-139.

Swan, A.R.H., Garraty, J.A. (1995). Image analysis of petrographic textures and fabrics using semivariance. Mineralogical Magazine 59:189-196.

Szczypinski, P.M. *et al.* (2009). A software package for image texture analysis. Computer Methods and Programs in Biomedicine 94(1):66-76.

Thagard, P. (1988). *Computational Philosophy of Science*. The MIT Press, Cambridge (MA).

Thompson, S., Fueten, F., Bockus, D. (2001). Mineral Identification using Artificial Neural Networks and the Rotating Polarizer Stage. *Computers in Geosciences* 27:1081-1089.

Tite, M.S., Kilikoglou, V., Vekinis, G. (2001). Review article: ´Strength, toughness and thermal shock resistance of ancient ceramics, and their influence on technological choice'. *Archaeometry* 43(3):301–24.

Toyota, R.G. *et al.* (2009). Neural network applied to elemental archaeological marajora ceramic compositions. *Proceedings of the International Nuclear Atlantic Conference* (INAC'09), Rio de Janeiro, Associação Brasileira de Energia Nuclear (ABEN).

Triantaphyllou, E. Felici, G. (eds.) (2006). *Data Mining and Knowledge Discovery Approaches Based on Rule Induction Techniques*. Berlin, Springer.

Tuceryan, A., Jain, A.-K. (1998). Texture Analysis. In The Handbook of Pattern Recognition and Computer Vision. C. H. Chen, L. F. Pau, P. S. P. Wang (eds.). *World Scientific Publishing*, pp.207-248.

Turvey, M. (1992). Affordances and prospective control: An outline of the ontology. *Ecological Psychology* 4:173-187.

Umeda, Y., Tomiyama, T. (1997). Functional Reasoning in Design. *IEEE Expert* 12(2):42-48.

Ungar, P.S., Brown, C.A., Bergstrom, T.S., Walker, A. (2003). Quantification of Dental Microwear by Tandem Scanning Confocal Microscopy and Scale-sensitive Fractal Analyses. *Scanning* 25:185–193.

USAITA - U.S. Army Information Technology Agency (n.a.). *Glossary*. U.S. Army Information Technology Agency. http://ita.army.mil/CatalogService.aspx?service_Id=122&serviceGroup_Id=9

Valiente-González, J.M. (2001). Object Comparison in Structural Analysis of Decorative Patterns in Textile Design. *Proceedings of the 12th International Conference on Design Tools and Methods in Industrial Engineering* 1(B1).

Váradi, K. *et al.* (2004). 3D Characterization of Engineering Surfaces. *Budapest Tech Jubilee Conference*.

Vargiolu, R., Morero, E., Boleti, A., Procopiou, H., Pailler-Mattei, C., Zahouani, H. (2007). Effects of Abrasion During Stone Vase Drilling in Bronze Age Crete. *Wear* 263:48-56.

Varma, M., Zisserman, A. (2005). A Statistical Approach to Texture Classification from Single Images. *International Journal of Computer Vision* 62(1-2):61-81.

Venkatesh, Y.V, Raja, S.K., Ramya, N. (2006). Multiple Contour Extraction From Graylevel Images Using an Artificial Neural Network. *IEEE Transactions on Image Processing* 15(4):892-899.

Vermaas, P.E., Houkes, W. (2003). Ascribing Functions to Technical Artefacts: A Challenge to Etiological

Accounts of Functions. *British Journal for the Philosophy of Science* 54:261-289.

Vranic, D.V. (2005). DESIRE: A Composite 3D-Shape Descriptor. *Proceedings of the IEEE International Conference on Multimedia and Expo* (ICME'05), pp.962-965.

Wadell, H. (1935). Volume, Shape, and Roundness of Quartz Particles. *Journal of Geology* 43(3):250-280.

Wang, N., Dowell, F., Zhang, N. (2002). Determinig Wheat Vitreousness using Image Processing and a Neural Network. *Proceedings of the ASAE International Annual Meeting/CIGR 15th World Congress*.

Wang, W. (2011). *Reverse Engineering: Technology of Reinvention*. CRC Press, Boca Ratón (FL).

Wiessner, P. (1983). Style and social information in Kalahari San projectile points. *American Antiquity* 48:253-276.

Wiessner, P. (1989). Style and Changing Relations Between the Individual and Society. In *The Meanings of Things: Material Cultural and Symbolic Expression*. I. Hodder (ed.), Unwin Hyman, London.

Whitehouse, D.J. (1978). Surfaces - A Link between Manufacture and Function. *Proceedings of the Institution of Mechanical Engineers* 192:179-188.

Whitehouse, D.J. (2002). *Handbook of Surface Metrology*. Institute of Physics, Bristol.

Winandy, J.E. (1994). Wood Properties. *Encyclopedia of Agricultural Science* 4:549-561. C. J. Arntzen (ed.), Academic Press, Orlando (FL)

Wittek, I.H., Frank, E. (2005). *Data Mining: Practical Machine Learning Tools and Techniques*. (2nd ed.). Morgan Kaufmann, San Francisco (Ca).

Wobst, H.M. (1977). Stylistic Behaviour and Information Exchange. In *For the Director: Research Essays in Honor of James B. Griffen*. E.H. Cleland (ed.), University of Michigan Museum of Anthropology, Anthropological Papers, Ann Arbour, pp.317-342.

Wright, L. (1973). Functions. *Philosophical Review* 82:139-68.

Wyszeki, G., Stiles, W.S. (1982). *Colour Science: Concepts and Methods, Quantitative Data and Formulae*. John Wiley & Sons, New York (NY).

Zaharia, T.B., Prêteux, F.J. (2003). Descripteurs de forme pour l'indexation de maillages 3D. *Technique et Science Informatiques* 22(9):1077-1105.

Zahouani, H., Guinet, A., Mathia, T. (1993). Analysis of 3D-pattern Topography of Manufactured Surfaces in Regard to Tribological Situations. *Proceedings of the 6th International Congress on Tribology*, Budapest, pp.284-289.

Zhang, C., Chen, T. (2001). Efficient feature extraction for 2D/3D objects in mesh representation. *Proceedings of the IEEE International Conference on Image Processing* 3(3):935-938.

Zhang, C. *et al.* (2002). A Domain-Specific Formal Ontology for Archaeological Knowledge Sharing and Reusing. In *Practical Aspects of Knowledge Management*. Proceedings of the 4th International Conference (PAKM'02). D. Karagiannis, U. Reimer (eds.), Springer-Verlag, Berlin, *Lecture Notes in Computer Science* 2569:213-225.

Zlateva, S.D., Vaina, L.M. (1991). From object structure to object function. *Proceedings of SPIE: Applications of Artificial Intelligence IX*, 1468:379-393.

Zweig, Z. (2006). *Using Data-Mining Techniques for Analysing Pottery Databases*. Mst. Thesis. Department of Land of Israel Studies & Archaeology, Bar-Ilan University.

Ø3
Framework

> *When my Grandson entered the room I carefully secured the door. Then, sitting down by his side and taking our mathematical tablets, – or, as you would call them, Lines - I told him we would resume the lesson of yesterday. I taught him once more how a Point by motion in One Dimension produces a Line, and how a straight Line in Two Dimensions produces a Square. After this, forcing a laugh, I said, "And now, you scamp, you wanted to make me believe that a Square may in the same way by motion Upward, not Northward' produce another figure, a sort of extra Square in Three Dimensions. Say that again, you young rascal.*

Edwin A. Abbot (1838-1926), in Flatland. A Romance of Many Dimensions (1884)

Following the issues discussed in the previous chapter, this chapter deals with the fundamental knowledge that one should have in advance in order to be able to understand and implement the proposed framework, by comprehensively describing each stage. Some of the new trends and issues which characterize the various subjects presented and which bring their own archaeological and technological challenges are addressed.

In-depth description of the implementation of this framework and further technical details are finally given in the case studies presented in Chapter 4.

3.1 Reverse Engineering

Reverse Engineering (RE) is the process of extracting missing knowledge from anything man-made, by going backwards through its development cycle and analysing its structure, function and operation (USAITA n.a., Dennet 1991, Eilam 2005, Raja 2008, Wang 2011). The process may be used by a diversity of specialists and for many different purposes. It involves examining an object under different scales or taking it apart and figuring out what each piece does (Eilam 2005). RE consists of a series of iterative steps, each addressing different questions regarding, in this case, an overall object. These steps may be repeated as often as needed until all steps are sufficiently satisfied.

The introduction of any technological or methodological advances should assume a new step for archaeological research (Lock 2003, Evans 2006). The framework proposed herein is based on RE processes, as it also enables being applied to a wide variety of objects, from different archaeological sites or chronologies (Moitinho et al. 2011). In this context, to RE requires a combination of skills and a thorough understanding and integration of different disciplines, from archaeology, to engineering and computer science.

Although there are various approaches to Reverse Engineering (USAITA n.a., Dennet 1991, Varaday et al. 1997, Musker 1998, Eilam 2005, Raja 2008, Wang 2011), it may comprise the following stages:

a) Reason for RE

The reasons for RE should be set clearly right from the beginning. What is the archaeological problem one is attempting to address? Does it involve, for instance, understanding possible relations between artefacts or within their components; the interoperability between user and artefact; working or production processes; function, behaviour, and ways of using an object (i.e., kinematics, dynamics); object's life-cycle?

b) Planning

Strategic planning gives the operational planning process coherence and direction. Strategy should be based on an understanding of the broader context. Whereas operability should be based on the plan of action for putting the framework into practice, considering the overall strengths and weaknesses (e.g., human resources, equipment, software, logistics, budget, time), as well as which are the alternatives.

This step, then, consists in developing a mental picture of how to implement RE processes. To do this, it is useful to start with a simplistic graphic. Then, as the complexity of the processes grows, so does the importance of a good and detailed planning.

c) Physical-to-digital process

It includes the choice of an adequate 3D data acquisition system or modelling technique, knowing that

each one has its own strengths and weaknesses. When using 3D scanners, and the like, it is necessary to first capture 3D digital data of the real surface and then post-process it. The resultant 3D digital surface model is not perceptual, but metric. It is a digital representation of the real object in certain conditions, generated in accordance to the characteristics of the measurement system and used procedures.

Before generating 3D digital models, every project should set clearly why is three-dimensional information required; what for is it needed; what resolution, accuracy and outputs are required; if all the necessary equipment, software and know-how are available; and what are the alternatives.

d) Extracting knowledge

It consists in 'dissecting' and studying the digital model, in order to obtain meaningful information. This stage is strongly dependent on the previous one, meaning that the quality of both captured and processed data will always constrain the reliability and usefulness of the information.

- **Information extraction from 3D digital surface model**: in this research, it refers only to the extraction of shape, form, and texture geometrical information from the 3D digital surface model.
- **Data integration** and **computer simulation**: the former consists in endowing the 3D digital models, by integrating additional data (e.g., material properties, mass, kinematics and dynamics) (Figure 3.1). The latter, consists in manipulating virtually these enhanced multidimensional models, to simulate possible uses and behaviours of the archaeological object.

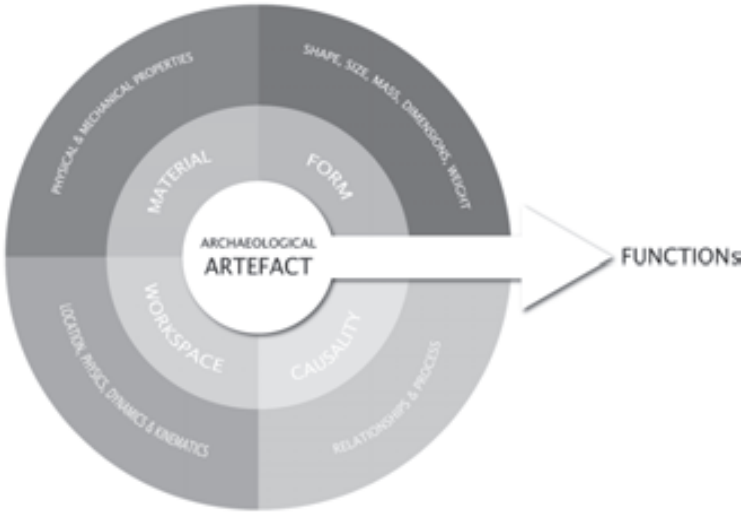

Fig. 3.1 Functional capabilities from an enhanced virtual multidimensional model (Moitinho de Almeida and Barceló 2012a).

A full specification may not only specify what the object can do, but also specify performance criteria it needs to meet along the way.

Technically, these two steps are independent of each other. As such, the order in which they are implemented does not affect their results. Depending on the reason for reverse engineering, only one of these steps may eventually be skipped. Though a full implementation of the framework is herein proposed,

because it may permit a more complete analysis, and therefore provide a better knowledge and comprehension of the archaeological object in question

e) Interpretation

The results should be able to respond or contribute to the initial reasons for RE (Figure 3.2). In this research, the aim is towards the understanding of possible working processes and function(s) of archaeological objects.

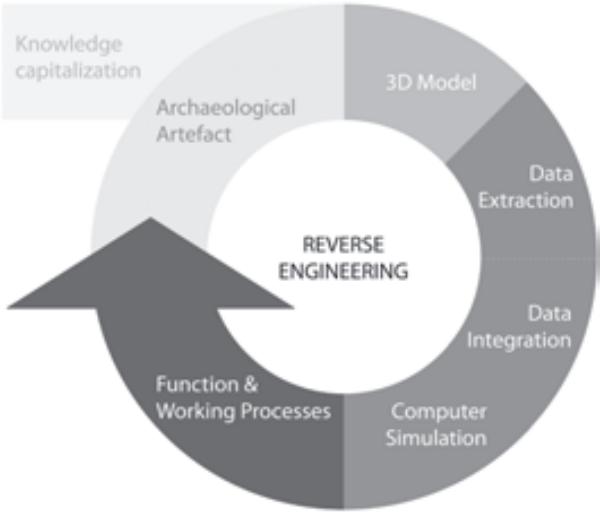

Fig. 3.2 Framework for Reverse Engineering archaeological objects.

Dealing with various equipment and computer programs throughout the framework may not be straightforward. A full operability between hardware-software and software-software urges for a fast solution. Considering that during most of this framework one will often be dealing with large amounts of data, as those frequently generated for many archaeological research purposes, hardware and software capacities should not be overestimated. On the contrary, it is undoubtedly a very critical technical issue – as they presently are a common working tool, thus part of the research process – and almost likely the Achilles heel of the present framework.

There is a challenge for standardization of policies and strategies for long-term digital preservation and access to 3D digital data (DCMI 1995, CIDOC-CRM 2006, 3D-COFORM 2009, London Charter 2009, CARARE 2012, Ronzino et al. 2012). Metadata (i.e., data about the data content) and paradata (i.e., data about the process of survey data collection) (Couper 1998) can provide more insight into the models and connected files, by overlaying them with increasing meaningful information. The procedures for creating the final dataset of all the generated digital files connected to each virtual archaeological object is partially ensured, by following specific international recommendations. During this research I followed the 3D-COFORM (2009) recommendations in conjunction with tDAR (tDAR 2009), English Heritage (Bryan et al. 2009), and GeoMetaVerse (Adam 2011) data fields. In the near future I intend to start converting the dataset to the CARARE's metadata schema (CARARE 2012), which takes into account additional requirements for 3D models, as well as including it in the PADICAT system (Patrimoni Digital Arqueològic de Catalunya).

In the following sections I will describe this framework in more detail and often in a step by step fashion, though the order can be on occasion rearranged. And in a few cases some steps can even be skipped or let in stand-by for later studies. In between the planning and the final results is the implementation process, which involves an increasing degree of automation. It is convenient to think in terms of 'stages' and 'steps' of planning or implementation. Often, the same planning can be implemented in many different ways – for instance, by using different 3D scanners, software or techniques. Considering the fact that each device, software, and version, has its specific technical procedures in operation of capturing, processing, and measuring data, one should look up the corresponding manuals for further details.

3.2 3D Digital Surface Model Generation

There is a growing trend towards 3D digital models of archaeological objects, as already highlighted in the previous chapter. Several really impressive technologies and devices are available in the market. But technology is useless if it's not actually solving anyone's problems. And without method and planning it is all to easy to get the wrong answer.

Besides the archaeological questions behind and the nature of the objects to be recorded, there are technical considerations, operational imperatives and environmental conditions which must be taken into account when planning survey strategies (3D-COFORM 2009), so as to prevent or troubleshoot problems. Likewise, on the one hand, it is fundamental to have a thorough understanding and knowledge of how the workflow functions, since each stage of the process depends on the outcome of the previous ones and determines the subsequent ones. On the other hand, to set clear objectives when tailoring each step's parameters. The 3D scan workflow comprises the following steps (Figure 3.3):

a) 3D Digital Data Acquisition System

It consists of choosing the appropriate system (or integration of systems) for a particular archaeological project requirements.

b) Workspace

It consists of preparing the workspace for an optimal 3D data acquisition of the subject.

c) 3D Digital Data Acquisition

It consists of capturing 3D coordinates (point cloud) from the surface of an object.

d) 3D Digital Data Post-processing

It consists of processing the unordered point clouds previously captured.

e) 3D Digital Surface Model

It consists of generating a 3D digital surface model of the subject, and exporting deliverables.

Fig. 3.3 3D Scan workflow: from choosing a 3D data acquisition system to generating a 3D digital model.

All raw data should always be saved at a specified repository for archiving purposes and to enable potential re-processing (3D-COFORM 2009). Deliverables may include from higher-resolution files for scientific research to lower-resolution files for general dissemination. Specially in research projects, it is recommended to create a traceability chain of the 3d digital model – a 3D modelling chain. Meaning that in every key step of the project's workflow its own reference dataset file(s), including metadata and paradata, are saved. On the one hand, this will latter reveal to be time saving, while permitting to test distinct procedures and parameters more efficiently. On the other hand, ensure subsequent data coherency, by providing a better understanding of the outcome data and allowing comparisons (Kreuter et al. 2010, Bentkowska-Kafel 2012).

3.2.1 3D Scanners

The potentialities of 3D scanning and some of the advantages of working and conducting experiments with 3D digital models in the cultural heritage sector are already well-known. Archaeological documentation and archival, conservation monitoring, preservation, restoration, replicas, virtual reconstruction, visualization, virtual reality, and dissemination are quite firmly established as some of the applications where 3D data capture can unquestionably provide real benefits (Reilly 1992, Fowles 2000, Pieraccini et al. 2001, Guipert 2003, Scopigno et al. 2003, Beraldin 2004, Guidi et al. 2004, Mara et al. 2004, Hermon et al. 2005, La Pensée et al. 2006, Pieraccini et al. 2006, Skar et al. 2006, Moitinho de Almeida 2007, Pescarin 2007, Farjas et al. 2008, 2013, Frischer et al. 2008, Arnold et al. 2008, Bathow et al. 2008, Forte at al. 2009, Georgopoulos et al. 2010, André et al. 2012, Guidazzoli et al. 2012, Amendas et al. 2013, Creté et al. 2013, Tapete 2013; see also proceedings of CAA - 'Computer Applications & Quantitative Methods in Archaeology', VSMM - 'Conference on Virtual Systems and MultiMedia', VAST - 'Symposium on Virtual Reality, Archaeology and Cultural Heritage', among others). Though, in spite of the potentialities, there seem to be few relevant archaeological scientific investigations that go in further directions while making use of 3D digitized models as a research tool (Friess et al. 2002, Astruc et al. 2003, 2011, Carcagni et al. 2005, Karasik et al. 2005, 2008, Kampel et al. 2006, Zapassky et al. 2006, Pereira et al. 2006, Moitinho 2007, 2010, Moitinho et al. 2011, 2013, Diaz-Andreu et al. 2008, d'Errico et al. 2009, El Zaatari 2010, Lin et al. 2010, Stemp et al. 2011, Sessen et al. 2013).

Since archaeological objects encompass a wide range of characteristics (e.g., size, form, texture, material, colour), there is no single system 'perfect' for all tasks. Every 3D scanner has a unique spectrum for resolution, accuracy and data quality. For that reason, it is important to determine the most appropriate system (or integration of systems) for a particular archaeological project, by assessing namely: the nature and volume of the objects to be scanned; logistics, workspace, time constraints, budget, technical know-how; the requirements for resolution, accuracy, automation, and portability. Figure 3.4 synthesizes the main 3D Data acqui-

sition systems (Beraldin et al. 2004, Blais 2004, Remondino et al. 2006, Moitinho 2007, 2010, Chen at al. 2008, Lanman et al. 2009, Sansoni et al. 2009, Remondino 20011, Guidi et al. 2012).

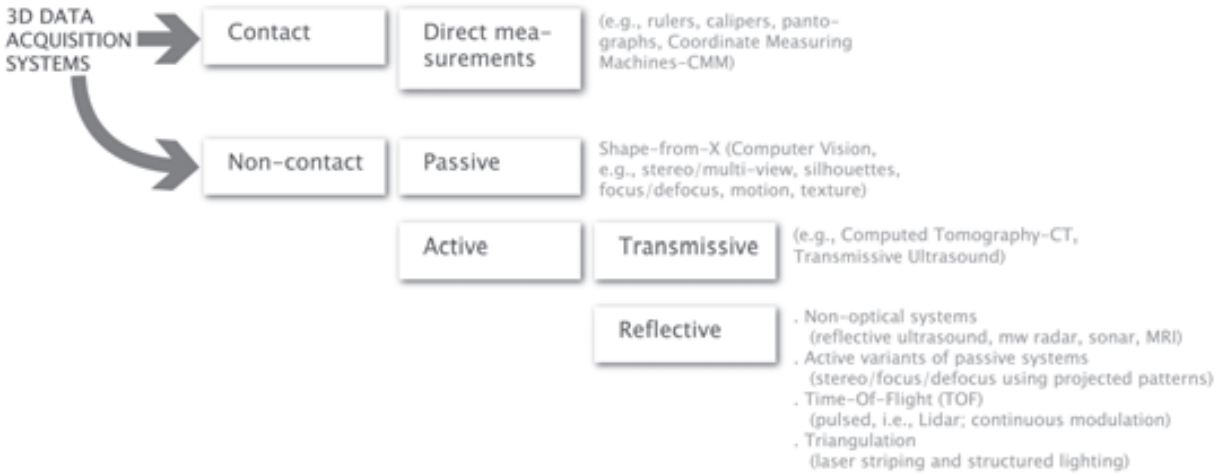

Fig. 3.4 3D Data acquisition systems.

Although all measurements are subject to error, when planning the 3D data capture strategy it is fundamental to consider measurement error and uncertainty of measurement results issues (Figure 3.5) (Boehler et al. 2003, Beraldin et al. 2004, Remondino et al. 2006, JCGM 2008a, 2008b, Georgopoulos et al. 2010, Li 2011, Havemann 2012).

Fig. 3.5 Example of sources of measurement error that lead to uncertainty of measurement results.

Three-dimensional "scanning differs from illustration in that no interpretation is incorporated into the resulting image" (EH 2010). However, using inadequate 3D scanning systems and data processing methods or techniques may generate unreliable 3D digital model, leading to erroneous interpretations.

3.2.1.1 Structured Light Scanner

In the course of this investigation an approach based on close-range non-contact (active, reflective) system to capture three-dimensional digital data from archaeological objects was used. The focus is on structured light scanners, since this type of system also permits to achieve the overall objectives and the equipment – SmartSCAN3D Duo System, Breukmann – was kindly provided by IMF-CSIC, Barcelona. However, depending on the archaeological goals, other non-invasive and non-destructive systems may as well be used in some stages (e.g., 3D laser scanning, CT) without jeopardizing the overall framework and sometimes even enhancing it.

Structured light scanners project a set of periodical patterns of light on the object's surface, which are used as internal vectors of information – the SmartSCAN3D Duo System is based on a combination of Moiré-topography, phase shift and grey code techniques (Slizewski et al. 2010) to maximize the measurement resolution. After that, the camera captures the deformation of the coded light patterns reflected by the surface. Then, using basic trigonometric principles (Thales, 6th century BC) – i.e., geometric triangulation method

$$d = (½\ a) / tan\ (½\ \alpha)$$

where a is the known distance between the projector and the camera, and α is the known angle formed by the projector, the object's surface and the camera – the computer calculates the 3D coordinate triplets (x,y,z) of each point (d) in the known pattern of light sequence (Figure 3.6) and obtains the range data, this is to say, the point cloud (Inokushi et al. 1984, Pagès et al. 2003, Blais 2004, Salvi et al. 2004, Chen at al. 2008, Sansoni et al. 2009, Gorthi et al. 2010, Zhang 2010, Breukmann 2013). This principle is essentially the same as that of laser scanners.

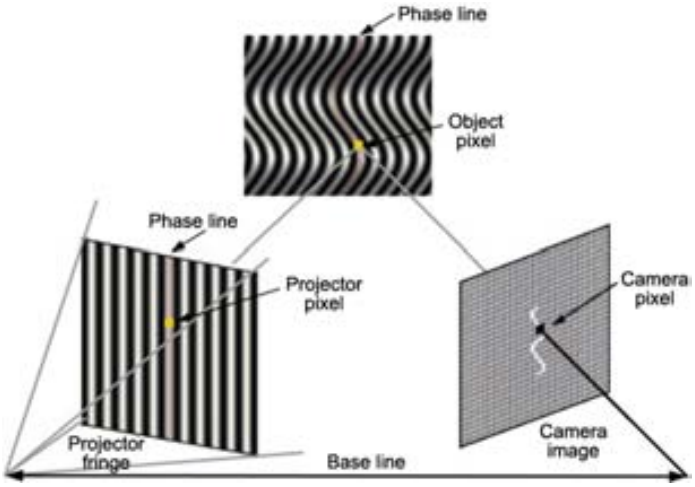

Fig. 3.6 Typical setup of a digital fringe projection and phase shifting system (Zhang 2010).

Some sensor systems can be scaled for a wide range of Field Of Views (FOV) in order to respond to specific demands of a given measuring task, by changing the baseline distance and/or set/specifications of lenses. Calibrating the sensor hardware setup with camera, projection unit and selected set of lenses *in situ* may be necessary to guarantee a sufficient sharpness in the complete measurement volume (Breukmann 2009) and to further process reliable output data. Consequently, this step has to be performed prior to 3D data acquisition.

3.2.2 Workspace

This stage consists of preparing the workspace for an optimal 3D data acquisition of the object, whenever possible it should be studied in advance. It comprises setting up efficiently all the necessary equipment – ideally small, compact, and lightweight, also for ease of transportation. Besides both scanner (plus components) and computer, in some cases it may for instance be necessary to include a portable power supply (batteries,

generator), extension cords, a tent or piece of fabric to block interfering light; or even to build a structure to ensure a complete scanning of the surfaces of interest (Baracchini et al. 2006, Gernat et al 2007, Bathow et al 2008, Bianco et al. 2010).

3.2.3 3D Data Acquisition

This stage consists in capturing the point cloud, i.e., the 3D coordinates (*x*,*y*,*z*) of each point of the geometry of the object's surface, as described previously. This captured data is a digital representation of the real surface in certain condition produced at a certain phase of a measurement.

There are further technical reasons that can explain the complexity of scanning, namely: the object's dimension, overall geometry, surface microtopography, surface opacity/reflectivity, and type of raw-material; required levels of accuracy and resolution of measurements; and hardware-software issues (Georgopoulos et al. 2010, Moitinho de Almeida et al. 2012, 2013).

Each sensor FOV determines the resolution of the registered data, as well as the scanning volume and working distance. In general, the higher the FOV, the lower the number of scans needed to cover an entire area. However, the resolution also tends to diminish leading to less fine density 3D meshes. The opposite is also true.

As to the scanning ambient light conditions, for better results, capturing data with structured light scanners should be done in a dark environment – when outdoors, preferably during the night – because the more contrasted the projected and reflected patterns are, the more consistent data we get.

The amount of overlapping area between scans should be set to approximately one third, to facilitate the matching procedure and minimize measurement error. To overcome most self-occlusion problems one can use multiple viewing angles during scans, by reorienting the scanner's position in respect to the object or vice-versa. In some cases, a manual or automated turntable can be used for small and/or fragile portable archaeological objects to avoid handling them further, as well as to reduce the amount of time and work during scanning and data post-processing. Three-dimensional data registration *in situ* often has time constraints. In these cases, at least a rough pre-alignment of the point clouds acquired from multiple views should be accomplished *in situ*, to check the completeness of the scanned surface and the general quality of the recorded data.

In general, it is important to acquire the best data as possible to enable different scientific uses or others. Notwithstanding, determining the optimal resolution for capturing 3D data will always depend on the characteristics of the object, on the scale of observation and on the type of information required. Likewise, it is significant to previously consider that capturing image texture during scans, oversampling points during alignment, reducing data noise, increasing data reliability, among other settings, easily yield an overwhelming of computing resources. More than data quantity (which also raise data storage issues), it is data quality and adequacy that is needed.

3.2.4 3D Data Post-processing

The 3D surface data post-processing stage consists of processing the 3D data formerly captured (i.e., the unordered point cloud) by the acquisition system. This is often a cumbersome process, as it still requires much semi-automatic and manual work. In addition, working with large data sets can be very difficult for the computer to manage. This stage generally comprises the following steps:

a) Data Cleaning

It consists of removing extraneous, erroneous or other unwanted points.

b) Point Clouds Final Alignment

It consists of performing a concluding fine alignment to bring the scans in a common reference system, and optimise the matching of all single patches at the end.

c) Scans Merging

It consists of merging the previous aligned patches into a common data set.

Usually, scans should be merged using 'maximum reliability' options, and avoiding any type of smooth filtering. At the end of the merging process, overlapping areas and similar vertices are semi-automatically removed. Data redundancy of overlapping points can work for the advantage of uncertainty reduction on data merging (Sitnik et al. 2012). Then, the data structure is automatically optimized, and vertex normals are automatically calculated.

d) Polygonal Mesh Generating

It consists of generating a polygonal mesh. The final outcome and overall accuracy of the mesh depends intrinsically on all previous steps.

Filling holes generates non measured points, meaning that the software must be able to handle non measured points seamlessly, and simultaneously be able to calculate parameters on surfaces with missing data points. This process can be performed not only during polygonal mesh generating, but also after this step is concluded.

The quality of the final 3D digital model should be analysed by using quality inspector tools – potent statistical tools that compare between raw data and final mesh – usually available on 3D processing data software (Farjas et al. 2010).

The 3D digital surface model can now be exported in the file format that better suits the objectives.

It should be borne in mind that from the 3D acquisition data stage to the 3D data post-processing stage and final exporting deliverable some geometric changes are likely to take place. As above mentioned, since each stage of the process depends on the outcome of the previous ones and determines the following ones, all parameters and procedures must be tailored accordingly. Certain scanning and post-processing techniques (e.g., subsampling, noise reduction, smoothing and other filters, filling holes, mesh decimation, compression) may

conceal, distort or eliminate relevant data. If not at a macro level, at least at a micro level. Moreover, used algorithms for processing data may differ between software and within versions, eventually yielding distinct results. Then, we may ask how accurate is the captured data in respect to the original object and how will this level of accuracy affect the analysis, classification, and interpretation of the archaeological object. These issues and more make no longer possible to clearly distinguish between raw measured data and 'invented' data, leading to loss of authenticity of the model and erroneous interpretations (Havemann 2012, Moitinho de Almeida and Barceló 2012) – once more addressing the importance of linking source, process and other meaningful information to the data when dealing with it.

3.3 Geometric Information Extraction from 3D Digital Surface Models

The real value of 3D digital data comes from the ability to be able to extract meaningful information from it. This is only possible when all relevant information has been captured and coded. Yet, best practices often involve methods that are simply not practical manually. Proper equipment and software are therefore essential, along with automatic procedures whenever possible.

In this section I describe a number of analytical techniques based only on the geometric features from 3D digital surface model, which aim to contribute with significant information on the study of archaeological objects.

3.3.1 Describing Shape and Form

It has been argued that neither shape nor form can be fully quantified (Johansson 2008, 2011). However, we consider that an approach towards the statistical analysis of shapes and forms is technically possible and even recommendable to archaeologists. In other words, even in the case the object's shape or form cannot be reduced to a single measure, shape-and-form variability can be effectively estimated and even explained in functional terms.

In this vein, we should extract a number of different shape/form descriptors from the generated 3D model. That means integrating some parameters related with the 3D geometry of the objects' interfacial boundaries in a set of relational coefficients. The fundamental role of such composite measures is that they allow evaluating archaeological observables from a population as similar or different.

This approach has some tradition in 2D shape analysis (Kuo and Freeman 2000, Russ 2002, Gilboa et al. 2004, Rousan 2004, Masad 2007). Shape indices allow the integration of all parameters related with the 2D geometry of the objects' contour or silhouette into single measurements, in a way that a statistical comparison of such parameters allows a complete description of visual variability in a population of material evidences (Barceló 2010a). Accordingly, the form of the archaeological artefact is defined as an *n*-dimensional vector

space (where *n* represents the number of shape coefficients), and whose axes represent global shape-and-form parameters, or further vector spaces denoting different domains of the same idea of "shape".

Table 3.1 lists a few shape descriptors, some of which can be easily calculated after extracting basic geometric data from a 3D digital model. A wider list with corresponding descriptions can be read in Rousan (2004).

Elongation is perhaps the simplest shape index. It uses the ratio between length and width to measure the elongation of an object.

Roundness measures the degree to which an object resembles a circle. The roundness calculation is constructed so that the value of a circle equals 1, while departures from a circle result in values less than 1. For instance, an isosceles triangle has a roundness value of approximately 0,492. In the equation, *p* is the perimeter, and *Area* is a measure of the surface of the object.

Quadrature measures the degree of quadrature of a shape, where 1 is a square and 0,8 an isosceles triangle.

Shape factor is similar to *Roundness*, but emphasizes the configuration of the perimeter rather than the length relative to object area, i.e., it varies with surface irregularities, but not with overall elongation. It is based on the mathematical fact that a circle, compared to all other shapes (regular or irregular), has the smallest perimeter relative to its area. Because every object has a perimeter length and an area, this mathematical relationship can be used to quantify the degree to which an object's perimeter departs from that of a smooth circle, resulting in a value less than 1. Squares are approximately 0,78. A thin thread-like object would have the lowest shape factor approaching 0.

Table 3.1 2D Shape descriptors.

2D Shape Descriptor	Equation	Reference
Angularity Index	$AI = \frac{\sum_{i=1}^{3}(Angularity_i \times Area_i)}{\sum_{i=1}^{3} Angularity_i}$	(Masad 2007)
Angularity Parameter	$Angularity\ Parameter = (P_{Convex} / P_{Ellipse})^2$	(Kuo and Freeman 2000)
Aspect Ratio	$ASPCT = MaxCaliperDimension / MinCaliperDimension$	(Russ 2002)
Compactness	$Compactness = [\sqrt{(4/\pi)Area}] / MaxDiameter$	(Russ 2002)
Convexity	$Convexity = ConvexPerimeter / Perimeter$	(Russ 2002)
Convexity	$Con = \sqrt{(A_{Particle} / A_{Convex})}$	(Rousan 2004)
Curl	$Curl = Length / FibreWidth$	(Russ 2002)
Elongation	$Elongation = Length / Width$	(Russ 2002)

2D Shape Descriptor	Equation	Reference
Flat-Elongation Ratio	$FER = LongestDimension / ShortestPerpendicularDimension$	(Masad 2007)
Fourier Series Analysis of Angularity	$\alpha_r = \sum_{j=5}^{25} \left[\left(\frac{a_n}{a_0}\right)^2 + \left(\frac{b_n}{a_0}\right)^2 \right]_{5 \le n \le 25}$	(Wang 2003)
Hough Transform (Angularity)	$HTSI = 1 - A / A_{Max}$	(Wilson 2007)
Modification Ratio	$Modification\ Ratio = InscribedDiameter / CircumscribedDiameter$	(Russ 2002)
Quadrature	$Q = Perimeter / 4\sqrt{Area}$	-
Roundness	$Roundness = (4 \cdot Area) / (\pi \cdot MaxDiameter^2)$	(Russ 2002)
Shape Factor (or Formfactor)	$Shape\ Factor = (4\pi A) / p^2$	(Russ 2002)
Shape Index	$2D\ Shape\ Index = \sum_{\theta=0}^{\theta=360-\Delta\theta} \lvert R_\theta + \Delta_\theta - R_\theta \rvert / R_\theta$	(Rousan 2004)
Symmetry	$Symm = 1/2\ [1 + min\ (r_1 / r_2)]$	(Rousan 2004)
Solidity	$Solidity = Area / ConvexArea$	(Russ 2002)

Unfortunately, many of the coefficients cannot be directly generalized to 3D (Lian et al. 2010), and it has already bee argued the relevance of a proper 3D analysis. Up to now, just a few global form descriptors with direct meanings for 3D models have been proposed, where each of them describes 3D objects in a quite different manner, thereby providing new and independent information. A compactness coefficient for example, may describe the extent to which a 3D object is spherical (Wadell 1935, Asahina 2011). The sphericity of a sphere is 1 and, by the isoperimetric inequality, any form which is not a sphere will have sphericity less than 1. Sphericity (Ψ) is expressed by the equation shown in Table 3.2, where *Vp* is volume of the archaeological object or building structure and *Ap* is its surface area.

Cubeness refers to the extent to which a 3D object is a cube (Martinez-Ortiz et al. 2009). The cubeness of a cube is 1, thus any form which is not a cube will have cubeness less than 1. The cubeness *Cd(S)* of an observed entity is the ratio of the surface area *A(S)* of a cube with the same volume as the given entity to the surface area of the entity. If the form is subdivided into faces, then *n(S)* represents the number of different faces.

Likewise, similar indices can be calculated for other forms (e.g., cylinders, ellipsoids).

Table 3.2 3D Form descriptors.

3D Form Descriptor	Equation	Reference
Cubeness	$Cd(S) = [n(S) - A(S) / 6] / [n - \sqrt[3]{n(S)}]^2$	(Martinez-Ortiz et al. 2009)
Curvedness	$Cp = \sqrt{[(k_1^2 + k_2^2) / 2]}$	(Koenderink et al. 1990, 1992, Dorai et al. 1997)
Shape Index	$3D\ SI = 1/2 - (2/\pi) \arctan [(k_1 + k_2) / (k_1 + k_2)]$	(Koenderink et al. 1992, Dorai et al. 1997)
Shape Spectrum	$\sum_{i-1}^{N_{bins}} SSD\ (i) = 1$	(Dorai et al. 1997, Bober et al. 2001)
Sphericity	$\Psi = [\pi^{1/3} (6Vp)^{2/3}] / A_p$	(Wadell 1935, Asahina 2011)

There are indeed many other form descriptors on the available literature – often more complex and frequently requiring specific software or programming for efficient calculations – that can be here mentioned, namely: the compactness measure proposed by Bribiesca (2000), which corresponds to the sum of the contact surface areas of the face-connected 3D form primitives. To measure rectilinearity, Lian et al. (2010) have used a genetic algorithm, which is an optimization technique. Kazhdan et al. (2003) have presented a 3D objects' reflective symmetry descriptor as a 2D function associating a measurement of reflective symmetry to every plane through the model's centroid. In addition, several other numerical methods to compute form descriptors have been proposed. Among them are: Volume-Area Ratio, Statistical Moments, and Fourier Transform Coefficients (Zhang and Chen 2001a, 2001b), Bounding Box (Paquet et al. 2000), Convex-hull based coefficients like hull crumbliness, hull packing, and hull compactness (Corney et al. 2002), 3D Shape Histograms, where the space in which the objects reside is decomposed, i.e., a complete and disjoint decomposition into cells which correspond to the bins of the histograms (Ankerst et al. 1999), a shape distribution sampled from a shape function measuring global geometric properties of the object (Osada et al. 2002), Spherical Harmonic Descriptor (Kazhdan et al. 2003), Skeleton based shape descriptor (Sundar et al. 2003), and other view-based methods used to extract 2D descriptors – e.g. 3D Zernike Moments (Novotni and R. Klein 2003), Fourier Coefficient, Elevation Descriptor, etc. – from the silhouettes or depth buffers captured around 3D models (Chen et al. 2003, Chaouch and Verroust-Blondet 2006, 2007), 3D Spherical Harmonics (Jayanti 2009), Ellipsoidal Harmonics (Mademlis et al. 2009), 3D-Shape Index (Marwan et al. 2004), Cone-Curvature Descriptor (Adan et al. 2008), 3D Hough Transform, Canonical 3D Hough Transform Descriptor (C3DHTD) (Zaharia and Prêteux 2003), and 3D Shape Histogram-Solid Angle Histogram (Jayanti 2009).

However, since no single descriptor outperforms others in all situations (Shilane et al. 2004), a well suited approach is to construct composite form descriptors (Vranić 2005, Ohbuchi and Hata 2006, Laga et al. 2006, Gal et al. 2007, Ruggeri and Saupe 2008).

3.3.2 Describing Texture

The surface texture properties of 3D digital models of archaeological objects have so far not been much investigated, and conclusions based on qualitative descriptions must hence be considered no more than hypotheses awaiting testing. In this vein, I suggest an approach based on both standards and advanced soft computing measuring techniques to describe and quantify the surface texture of archaeological objects as a means of inferring manufacturing processes and/or functional performance. Surface texture is, ergo, a key parameter in archaeological materials where its study is central to use-wear research.

As aforementioned, texture is usually defined as those attributes of an object's surface having either visual or tactile variety, and defining the appearance of the surface.

Among visual irregularities, colour variations can be measured and described in an objective and precise way, benefitting the analysis of the surface texture of archaeological objects, as well as their conservation and monitoring. By assigning a specific numeric value to each colour property, differences or distances between samples can be consistently compared (Wyszeki and Stiles 1982, Billmeyer and Saltzman 1981, MacAdam 1985, Hunter and Harold 1987, Hunt and Pointer 2011). Just to mention some of the most followed international standards are the ISO/CIE (International Standard Organization / Commission Internationale de l'Eclairage) and the ASTM (American Society for Testing and Materials; E12.04 on Colour and Appearance Analysis, E12.06 on Image Based Colour Measurement, E12.07 on Colour Order Systems, E12.11 on Visual Methods, and E12.14 on Multidimensional Characterization of Appearance). Colour measurement systems can be divided in colorimeters and spectrophotometers:

- **Colorimeters**: measure tristimulus data, that is, lightness (value), chromaticity (saturation), and hue (rainbow or spectrum of colours) of a sample colour. The colour's numeric value is then visually determined using a specific three-dimensional colour model or three-valued system. Among the most widely used colour space graphs for defining and mathematically expressing colour attributes are the CIE's Yxy, established in 1931; the 1976 CIELAB, L*a*b* colour space; the 1994 L*C*h; and the CIEDE2000. Other three-dimensional colour spaces, such as CIELUV, Hunter Lab, and the Munsell colour notation system, are also in use. The disadvantage of these measured data is that they are fully dependent upon viewing conditions (viewer or image capture device, type of lighting, object´s microtopography/finishing). These instruments provide measurements that correlate with human eye-brain perception (psychophysical), which can be a disadvantage in some archaeological analysis.
- **Spectrophotometers**: measure spectral data. That is to say, the amount of spectral reflectance, transmitting, and/or emitting properties of a sample colour at each wavelength on the visible spectrum continuum, without interpretation by a human. The measured data has the advantage of not being dependent upon light, object microtopography/finishing, and viewer. By gathering such complete colour information, it provides the most accurate description of the actual coloured object. Furthermore, it is able to indirectly calculate colorimetric information.

However, in the course of this investigation I will focus on the real surface of an object, which is defined as a set of features which physically exist and separate the entire workpiece from the surrounding medium (ISO 14460-1 1996), where the texture of the surface – here, its topography, as a scale limited complex combination of spatial frequencies – is just one of its key features. In a mechanical sense, the surface texture of a part may affect its function. Hence, the real surface geometry of an object can be so complex and diverse that a small number of parameters cannot provide a full description. Yet, a more accurate description can be obtained, if the set of parameters used is adequate or the number of parameters is increased. This is one of the reasons for introducing advanced metrology methods, techniques, and new parameters for assessment of surface texture (Gadelmawla et al. 2002).

For instances, differential geometry introduces curvatures. Measuring curvature at a surface point permits analysing the bending energy of surface irregularities, i.e., the surface texture. Curvedness is specified by a quantitative measure, its value is invariant to translation and rotation, and describes how much the surface in the neighbourhood of a considered point deviates from a plane (Pressley 2001, Ho and Gibbins 2009, Faresin et al 2012). Briefly speaking, this allows, on the one hand, detecting and analysing in a semi-automatic way edges and patterns, and possible use-wear traces and working surfaces – considering that the manufacturing process and functions affect certain areas, as well as the overall form of the artefact. On the other hand, predicting paleostress and areas favourable for natural fractures (Chopra, and Marfurt 2007).

Another method may consist of using surface roughness, waviness and lay parameters. ASME B46.1-2009 (ASME 2010) (Figure 3.7) defines:

- **Roughness**: the finer spaced irregularities of the surface texture that usually result from the inherent action of the production or material conditions;
- **Waviness**: the more widely spaced component of the surface texture. Roughness may be considered as superimposed on a wavy surface;
- **Lay**: the predominant direction of the surface pattern, ordinarily determined by the production method used.

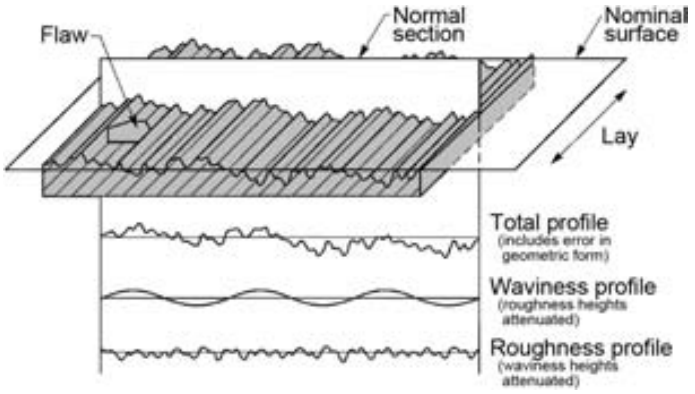

Fig. 3.7 Schematic diagram of surface characteristics (adapted from ASME 2010).

Many of these parameters are currently regulated by ISO International Standards (technical committee TC213, working groups WG 15 "GPS (Geometric Product Specification) extraction and filtration technique" and WG 16 "Areal and profile surface texture"), which describes terms, materials and methods, and how they can be used to consistently measure and analyse surfaces. There are several 2D profile and 3D areal surface texture parameters and constituents. These can be characterized either from physical or digital surfaces, from macroscale to nanoscale, using advanced metrology methods and techniques, and by means of 2D profilers or 3D areal contact (e.g., stylus, atomic force microscopy) or non-contact instruments (e.g., optical interference, optical scatting, capacitance, ultrasound, Scanning Probe Microscope - SPM, 3D scanners), which span a wide range and resolution.

Because archaeological objects are intrinsically three-dimensional, their surface texture should be able to be both characterized and analysed in 3D so as to improve the understanding of functional phenomena. The ISO 25178 series (2012) define more than 40 areal parameters for measuring surface texture, which are grouped in:

- **Height**: calculates the statistical distribution of height values along the z axis. Height parameters are dependent on the level of detail of the captured 3D data;
- **Spatial**: calculate the spatial periodicity of the data, specifically its direction. Spatial parameters are primarily dependent on the level of detail of the captured 3D data;
- **Hybrid**: calculates the spatial form of the data. Hybrid parameters are based upon both amplitude and spatial information;
- **Functional volume**: are calculated on the basis of the surface bearing area ratio curve (Abbott-Firestone curve). Indicated for bearing and fluid retention properties;
- **Features**: significant features are identified by a segmentation of the surface into valleys and peaks (watersheds algorithm and Wolf pruning). Then, parameters are calculated to quantify only the characteristics of the selected features.

The advantage of applying 3D areal surface metrology methods and parameters is that these are calculated on the entire or sampled surface and not upon averaging estimation calculations derived from 2D profilometric methods and parameters (Blunt and Jiang 2003, Blateyron 2006, Blanc et al 2011, Deleanu et al. 2012). Table 3.3 lists some commonly reported 3D areal surface texture parameters.

In addition, many archaeological patterns are fractal. Fractal geometry refers to the study of the form and structure of complex, rough and irregular phenomena (Brown et al. 2005). Because fractals demonstrate self-similarity and scale-invariance, it can be an adequate approach to quantitatively measure the surface's texture at different scales (Mandelbrot 1977, 1982, Brown et al. 2005): from archaeological remote sensing, to settlement pattern analysis, or even patterns on artefacts caused by fragmentation or use-wear. The ASME B46.1 "Surface texture (surface roughness, waviness, and lay)" (2002) introduces fractal based analysis, which gives an informative global measure of surface texture – related terminology and procedure for evaluation of surface texture using fractal analysis are given in this standard. Stemp and Stemp (2003) used fractal analysis to demonstrate quantitatively that tools used on the same material for differing lengths of time produced

surfaces with different fractal properties. Once again, since this parameter does not completely describe a surface and may not be able to differentiate some important feature variations, additional analysis may be required to fully describe the surfaces. In another more recent study, Stemp and Chung (2011) suggested coupling with the F-test in order to discriminate used from unused surfaces on individual tools, as well as the wear histories of tools used on different contact materials. In spite of the interest of 3D fractal geometry analysis as a quantitative approach in use-wear analysis, there seem to be very few relevant archaeological studies (Stemp et al. 2003, 2011, 2013, El Zaatari 2010, 2011, Sessen et al. 2013).

Table 3.3 List of some commonly reported 3D areal parameters for measuring the surface texture (ASME B46.1-2009 2010, ISO 25178-2 2012, Blateyron 2013, Image Metrology n.a.).

Areal Parameter		Description	Equation
Height	***Sa***	Average roughness [µm, mm]. Arithmetic average of the absolute values of the measured height deviations from the mean surface taken within the evaluation area. It indicates significant deviations in the texture characteristics.	$Sa = 1/A \int_A \lvert z(x,y) \rvert dxdy$
	Sq	Root mean square roughness [µm, mm]. Root mean square (rms) average of the measured height deviations from the mean surface taken within the evaluation area.	$Sq = (1/A \iint_A z^2(x,y)dxdy)^{-1/2}$
	Ssk	Skewness [unitless]. A measure of the asymmetry of surface heights about the mean surface. A negative value indicates that the surface is composed of mainly one plateau and deep and fine valley (i.e., the distribution is sloping to the top). A positive value indicates a surface with a lot of peaks on a plane (i.e., the distribution is sloping to the bottom). Due to the large exponent used, this parameter is very sensitive to sampling and noise of measurement.	$Ssk = 1/Sq^3 \, [1/A \iint_A z^3(x,y)dxdy]$
	Sku	Kurtosis [unitless]. A measure of the peakedness of the surface heights about the mean surface. It qualifies the flatness of the height distribution. Because of the large exponent used, this parameter is very sensitive to sampling and noise of measurement.	$Sku = 1/Sq^4 \, [1/A \iint_A z^4(x,y)dxdy]$
	Sp	Maximum area peak height [µm, mm]. The maximum height in the evaluation area with respect to the mean surface.	$Sp = Z_{max}$
	Sv	Maximum area valley depth [µm, mm]. The absolute value of the minimum height in the evaluation area with respect to the mean surface.	$Sv = Z_{min}$
	Sz	Maximum height of the surface [µm, mm]. Height between the highest peak and the deepest valley.	$Sz = Sp + \lvert Sv \rvert = Sp - Sv$
	St	Area peak-to-valley height [µm, mm]. The vertical distance between the maximum height and the maximum depth in the evaluation area.	$St = Sp - Sv$
	Sds	Density of summits [1/µm², 1/mm²]. The number of area peaks per unit area. Additional parameters can be defined that include the mean area peak spacing and parameters that count either area peaks, whose heights are above a selected reference surface, or area valleys, whose depths are below a selected reference surface.	$Sds = (Number\text{-}of\text{-}peaks) \, / \, Area$

Areal Parameter		Description	Equation
Spatial	***Str***	Texture aspect ratio [% or (0≤Str≤1)]. Indicator of surface isotropy. *Rmin* and *Rmax* correspond to the min and max radii calculated with respect to the perimeter of the central lobe. An isotropic surface will be close to 1 (100%), while a strongly anisotropic surface will be close to 0.	$Str = Rmin / Rmax$
	Sal	Fastest decay auto-correlation rate [µm, mm]. Horizontal distance of the autocorrelation function (tx, ty) which has the fastest decay to a specified value *s* (0 ≤ *s* ≤ 1; default value *s* = 0,2). This parameter expresses the content in wavelength of the surface. A high value indicates that the surface has mainly high wavelengths (i.e., low frequencies).	$Sal = min\sqrt{(tx^2 + ty^2)}$
	Std	Texture direction [deg.]. Angular direction (anticlockwise) of the dominant lay comprising a surface. It is determined by the angular power spectral density function (APSD, the square of the amplitude of the Fourier transform of the measured topography).	$Std = Major\text{-}direction\text{-}of\text{-}lay\text{-}derived\text{-}from\text{-}APSD$
	Sfd	Fractal dimension. Reflects the complexity of the surface texture. It is designed to correlate with human visual perception of roughness. The rougher the perceived surface, the higher the value of the fractal dimensional parameter. It is the ratio of the log of the number of linear or areal elements *N* with respect to the log of the reciprocal of the linear scaling ratio *r*.	$Sfd = (\log N) / [(\log (l / r)]$
Hybrid	***Sdq***	Area rms slope [deg.]. The rms surface slope comprising the surface, evaluated over all directions.	$Sdq = \sqrt{1/A \iint [(\delta z^2 / \delta x) + (\delta z^2 / \delta y)]dxdy}$
	Sdr	Developed surface area ratio [% or unitless positive number]. The developed interfacial ratio.	$Sdr = [(Total\text{-}surface\text{-}area\text{-}of\text{-}all\text{-}the\text{-}triangles) - (Lx \cdot Ly)] / (Lx \cdot Ly)$
Functional	***mr***	Material ratio [%]. The ratio of the intersecting area of a plane (i.e. parallel to the mean plane) passing through the surface at a given height to the cross sectional area of the evaluation region. The Areal Material Ratio Curve (aka Bearing Area Curve or Abbot Firestone Curve) is established by evaluating *mr* at various levels from the highest peak to the lowest valley.	$mr = 100\% \times (A+B+C+D) / L$
	Smr	Surface bearing area ratio [%]. The ratio of the cross sectional area of the surface at a height *c* relative to the evaluation cross sectional area.	$Smr = (Area\text{-}of\text{-}intersection\text{-}of\text{-}measured\text{-}topography\text{-}with\text{-}surface\text{-}parallel\text{-}to\text{-}mean\text{-}surface) / (Evaluation\text{-}Area)$
	Sk	Core roughness depth [µm, mm]. The core roughness (peak-to-valley) of the surface with the predominant peaks and valleys removed.	(ISO 25178-2 2012)
	Sxp	Extreme peak height [µm, mm]. The difference in heights on the surface from the areal material ratio value of *p* and the areal material ratio of *q*.	$Sxp = Smc(2{,}5\%) - Smc(50\%)$
	Vm	Material volume [ml/m², µm³/mm², µm³/mm²]. The volume of material comprising the surface from the height corresponding to *mr* to the highest peak of the surface.	$Vm = [V_m(h_{0,10})] / A$
	Vv	Void volume [ml/m², µm³/mm², µm³/mm²]. The volume of space bounded by the surface texture from a plane at a height corresponding to a chosen *mr* value to the lowest valley (default value 80-100%).	$Vv = [V_v(h_{0,80}) - V_v(h_{1,00})] / A$
	Vmp	Material volume of peaks [ml/m², µm³/mm², µm³/mm²]. The volume of material comprising the surface from the height corresponding to a *mr* level *p* to the highest peak.	$Vmp = Vm(mr1)$
	Vmc	Material volume of the core [ml/m², µm³/mm², µm³/mm²]. The volume of material comprising the texture between heights corresponding to the *mr* values of *p* and *q*.	$Vmc = Vm(mr2) - Vm(mr1)$
	Vvc	Void volume of the core [ml/m², µm³/mm², µm³/mm²]. The volume of space bounded by the texture at heights corresponding to the *mr* values of *p* and *q* (default value 10-80%).	$Vvc = [V_v(h_{0,10}) - V_v(h_{0,80})] / A$

	Areal Parameter	Description	Equation
(cont.)	***Vvv***	Void volume of the valleys [ml/m^2, µm^3/mm^2, µm^3/mm^2]. The volume of space bounded by the surface texture from a plane at a height corresponding to *mr* level *p* to the lowest valley.	*Vvv = Vv(mr2)*
Features	***Spd***	Density of peaks [1/mm^2]. Number of peaks per unit area. Wolfprune Nesting Index *X*% (default value *X*%=5%)	*Spd = (Number-of-peaks) / (Segmented-Area)*
	Spc	Arithmetic mean peak curvature [1/mm^2]. Wolfprune Nesting Index *X*% (default value: *X*% = 5%).	(ISO 25178-2 2012)
	S5p	5 point peak height [µm, mm]. Average value of the heights of the five peak with the largest global peak height, within the definition area. Wolfprune Nesting Index *X*% (default value *X*% = 5%).	(ISO 25178-2 2012)
	S5v	5 point valley height [µm, mm]. Average value of the heights of the five valleys with the largest global valleys height, within the definition area. Wolfprune Nesting Index *X*% (default value *X*% = 5%).	(ISO 25178-2 2012)
	Sda	Closed dales area [mm^2]. Average area of dales connected to the edge at height *c*.	(ISO 25178-2 2012)
	Sha	Closed hills area [mm^2]. Average area of dales connected to the edge at height *c*.	(ISO 25178-2 2012)
	Sdv	Closed dales volume [mm^3]. Average volume of dales connected to the edge at height *c*.	(ISO 25178-2 2012)
	Shv	Closed hills volume [mm^3]. Average volume of hills connected to the edge at height *c*.	(ISO 25178-2 2012)

Some of these parameters (or their 2D profile equivalent) have been for several years widely used in several industrial sectors – such as aerospace, automotive, cosmetics, electronics, energy, metallurgy, paper, plastics and printing –, namely to investigate surface characteristics, use in product and process design, detect local defects, monitor manufacturing processes and tool performance, control surface quality, or predict surface behaviour during operational use (Blateyron 2006). This quantitative approach is becoming increasingly used in archaeology (Zahouani 1993, Astruc et al. 2003, 2011, Carcagni et al. 2005, Evans and Donahue 2008, d'Errico and Backwell 2009, Mélard 2010, Faulks 2011, Stemp et al. 2003, 2011, 2013), in palaeontology in dental microwear analysis to reconstruct evolutionary animal adaptation, palaeodiets, and paleoenvironments (Ungar et al. 2003, Schulze and Kaiser 2007, Schulze et al. 2010, Kaiser et al. 2011), as well as for conservation and monitoring cultural heritage objects (Gaspar et al. 2000).

Although there are different ways to assess surface texture (Scott 1988, Muralikrishnan and Raja 2008, Li 2011, Qi et al. 2012), it generally comprises the following steps (Figure 3.8):

a) Choice of metrological solution

It consists of choosing the measurement instrument, knowing that each type has its own strengths and weaknesses, and in accordance to the complexity and other characteristics of the measuring surface, required level of detail, scale of analysis, sampling method, analytical methods and parameters.

b) Digital data acquisition / Sampling

It consists of using the same workflow described in section *3.2 3D Digital Surface Model Generating*. It can be just a sample area or the whole surface and then extracting surface samples. Sampling should be adequate and consistent, in the sense that it represents the whole surface area of evaluation. This captured data is a digital representation of the real surface in certain condition produced at a certain phase of a measurement.

c) Digital surface pre-processing

It may include surface levelling, form removal, data manipulation (e.g., truncation, rotation, inversion, sub-area extraction), and filtering.

d) Digital surface description, comparison, and analysis

This step includes using texture parameters to describe quantitatively, compare, and analyse the surface. Characterization techniques can be scale-dependent (i.e. the results depend on the measurement scale) or scale-independent (e.g., using a fractal dimension).

Fig. 3.8 3D Surface texture workflow: from choosing a 3D data acquisition system to describing the 3D digital surface texture.

When planning the surface texture measurement strategy it is fundamental to consider measurement error and uncertainty of measurement results issues (Figure 3.9) (Li 2011).

Fig. 3.9 Example of sources of measurement error in surface texture that lead to uncertainty of measurement results.

Once again, depending on the object of study – including the type of surface (layered, opaque, translucent, transparent, reflective) that is being measured, specific measurement´s scale and desired level of accuracy, scale of interest (e.g., cm, mm, microns) – and the archaeological question behind, one should select the most suitable metrology strategy, technique, and parameters. For details on technical procedures see Whitehouse (2002), Varadi et al. (2004), Masad et al. (2007), ASME (2010), ISO 25178 series (2012).

Linked to these considerations, further research also based on the analysis of surface texture can be easily foreseen. For instances, by:

- Adding a fourth dimension to the 3D digital model – *x*,*y*,*z* plus *T*, where *T* can stand for ‘time’, ‘tem-

perature', 'pressure', etc. – to study and monitor surface change with respect to any other dynamic or physical dimension;

- Extending it to a tribological system (Figure 3.10). As prior mentioned, tribology deals with the design, friction, wear, and lubrication of interacting surfaces in relative motion. Here, wear is restricted to the surface damage involving loss of material (i.e., remove or displacement, which can be dominated by shear fracture, extrusion, chip formation, tearing, brittle or fatigue fracture, dissolution or diffusion, erosion, or interaction between corrosion and fracture), gain of material (i.e., adherence, which can be from the transfer of material from one of the surfaces to the other, from dust particles or other extraneous material, or lubrication and finishing materials), and plastic deformation or cracking. Notwithstanding, surface damage may yet occur without wear, this is to say, when deterioration of the function of the surface happens but no material is lost. The behaviour of both external surface layer and sub-surface layers can be better understood if the material properties and manufacturing procedures are also well known;

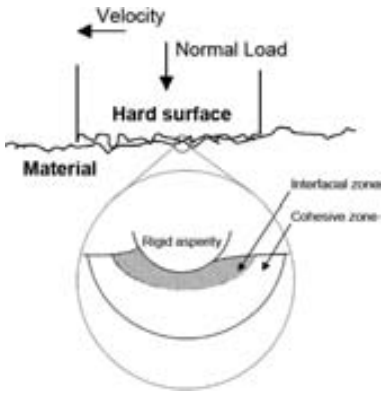

Fig. 3.10 Two-term model of friction and wear processes (adapted from Briscoe and Sinha 2002). Kinematics, loading, sliding velocity and distance, frictional heating and contact temperature, environment, chemical reactions, time dependance and their functional duration, are all functional combinations that make part of the Tribological System, which yield to specific wear marks and tracks.

- Studying the effect which a manufactured surface generated by a certain working process has on the functional performance of that same object. Griffiths (2001), Blunt and Jiang (2003) define Surface Integrity as the state and attributes (including the external aspects of topography, texture, and surface finish, as well as the internal sub-surfaces aspects) of a manufactured surface which influence performance. Meaning that, if the surface integrity is low the functional performance will be poor, and conversely.

Hence, the texture of an archaeological object can be defined as an *n*-dimensional vector space whose axes represent distinct states and attributes. The technological complexity of such system encompasses many disciplines, namely from chemistry and physics, to material science and mechanical engineering, some of which will be briefly tackled in the next sections.

3.4 Describing Material Properties

Archaeological materials from prehistoric sites comprise natural elements and constitute the physical matter of artefacts. Understanding the properties of solid materials, their role, and their combinations, allows on the one hand insight to the interrelationships between form and function, on the other to predict its utility (strengths and limitations) in a new context, beholding that differences in the kinds of knowledge required from a given material, or group of materials, are related to the scale at which one intends to interact with the object.

For this reason, it seems unequivocal the need and concern to characterize these materials with respect to their properties and behaviours, by means of reliable procedures and techniques internationally accepted. "In its most general context, the term materials measurements denotes principles, techniques and operations to distinguish qualitatively and to determine quantitatively the characteristics of materials" (Czichos et al. 2006, p.95). Suffice it to recall that it is the archaeological question one wishes to answer which determines the key properties that need to be characterized.

Properties that are germane and central to the direct interaction with solid materials can be broadly classified into the following categories, which may include but are not restricted to the listed characteristics (Markwardt 1930, 1935, Winandy 1994, Askeland 1998, Dinwoodie 2000, Hoadley 2000, Ashby 2005, Callister 2007, FPL 2010, Siegismund and Snethlage 2011):

a) **Chemical properties**

Are defined by its chemical elements (or compounds) and structure, and determine how a substance changes into a completely different substance. Environmental resistances, such as flammability and corrosion or oxidation, are examples of these.

b) **Biological properties**

Are defined by the structure of a specific organic material, and determine all the other types of properties. Some archaeological objects were made of raw materials from the living world: bone, wood, vegetal fibre, leather, etc. For instance, in the case of wooden artefacts the fundamental structure of wood, from the molecular to the cellular (types, sizes, proportions, pits, and arrangements of different cells) or anatomical level, determines the mechanical properties and, thus, possible behaviours of artefacts.

c) **Physical properties**

Here referring to macroscopic physical properties, are those whose particular values can be determined without changing the identity of the substance, i.e. the chemical nature of matter, but are a consequence of constraints at lower levels. Besides, physical properties may constrain other material properties (e.g., thermal, mechanical). Among the physical properties, other than visual appearance, we can mention:

- **Density**: in wood, is a function of the ratio of cell wall thickness to cell diameter. It is calculated

by the ratio of its mass per unit volume (symbol: ρ. The International System (SI) unit for density is g/cm^3 or Mg/m^3)

$$\rho = m / v$$

- **Specific gravity**: is the ratio of the density of a material per density of water (symbol: *G*)

$$G = \rho / \rho w$$

- **Moisture content**: is the ratio of the mass of water contained in a sample to the mass of the same sample dried, usually expressed as a percentage (symbol: *MC,* ω);
- **Permeability**: is the moisture-excluding effectiveness, expressed as a percentage (symbol: *K*);
- **Shrinkage**: meaning here the degree of reduction or downsizing (symbol: *S*). It is as well expressed as a percentage. Shrinkage can be affected by several variables, such as density, rate of drying, or even the size and form of the object.

Taking the example of an inorganic material such as minerals, these have been commonly classified according to their chemical and physical properties, besides other characteristics. Quartz, for instance, is a nonmetallic mineral and is chemically identified as SiO_2, for Silicon dioxide, is a compound of one part silicon and two parts of oxygen. Its crystal structure is hexagonal, and its crystal system is trigonal. Density (measured: 2.65 - 2.66 g/cm^3; calculated: 2.66 g/cm^3) is a physical property, whereas hardness (7) refers to a mechanical property. Other characteristics may include colour (colourless, various colours), streak (white), luster (vitreous; cryptocrystalline: waxy to dull, vitreous if polished), diaphaneity (transparent to translucent), cleavage (poor/indistinct), fracture (conchoidal), index of refraction (n_o=1.54422; n_e=1.55332; cryptocrystalline: n=approximately 1.54) (Schlumberger 1990, Crossman 1997, Barthelmy 2010, MatWeb 2013). Likewise, when studying compound materials, such as ceramics or metal alloys, each of its elements and the transformation due to the action of heat and subsequent cooling into new elements, structure, and composition, should be considered.

d) Thermal properties

Their values may vary as a result of the prior mentioned properties inherent to each material, describing how it will respond to the application of heat. Thermal properties include thermal conductivity, heat capacity, thermal diffusivity, and thermal expansion. These can be highly important when analysing archaeological materials, in order to reason about certain technological strategies. Many materials become weaker at high temperatures, yet materials which retain their strength at high temperatures, i.e. refractory materials, are useful for many purposes. For example, glass-ceramics have become extremely useful for cooking, as they exhibit excellent mechanical properties and can sustain repeated and quick temperature changes up to 1000 °C. Some wooden artefacts were hardened with heat; in others, the drying processes were well controlled (swelling, shrinkage, flexibility) for intentional form deformation.

e) Mechanical properties

Their values may vary as a result of the physical properties inherent to each material, describing how

it will react to physical forces (Newton 1687, Record 1914, Feynman et al. 1963, Gordon 1978, Cotterell, and Kamminga 1990, Hoadling 2000, Goldstein 2001). Mechanical properties may be divided in elastic, strength, friction, and vibration properties.

e1. Elastic Properties

Materials that behave elastically generally do so when the applied stress is less than a yield value. When the applied stress is removed, all deformation strains are fully recoverable and the material returns to its undeformed state, i.e., volume or form. In continuum mechanics, deformation refers to the transformation of a body from an initial reference configuration to a new reference configuration.

- **Elastic modulus**: or modulus of elasticity, is an elastic constant which measures the stiffness of a given material (symbols: *E*, *K*, *G*; *v*, unitless; SI unit: GPa, MPa, or N/mm²; 1 MPa=10^6 N/$m^{2;}$). Is defined by the ratio of stress to strain, and it can be obtained by:

  Young's modulus – describes the material's response to tensile or compressive loading,

  $$E = (F/A) / (\Delta L/L_0)$$

  where F/A is force per unit area, ΔL is change in length, i.e. elongation, and L_0 is initial length;

  Bulk modulus – describes the material's response to hydrostatic pressure,

  $$K = -V(\Delta P/\Delta V) \quad \text{or} \quad K = -\rho(\Delta P/\Delta \rho)$$

  where V is volume, P is pressure, $\Delta P/\Delta V$ is the derivative of pressure with respect to volume; or ρ is density, and dP/dρ denotes the derivative of pressure with respect to density;

  Shear modulus – or modulus of rigidity, describes the material's response to shear loading,

  $$G = (F/A) / (\Delta x/L_0)$$

  where $\Delta x/L_0$ is the transverse displacement.

- **Poisson´s ratio**: when a material is compressed in one direction, it usually tends to expand in the other two directions perpendicular to the direction of compression. Therefore, another important elastic constant is the Poisson's ratio, which is dimensionless. The Poisson's ratio (symbol: *v*) is defined by the ratio of lateral strain to axial strain, in axial loading

  $$v=-\varepsilon_y/\varepsilon_x \quad \text{and} \quad \varepsilon=\Delta L/L_0$$

  where ε_y and ε_x are strains in the *y* and *x* directions resulting from an applied stress in the *x* direction.

Nevertheless, besides elasticity, an object can also respond to force by viscoelasticity, plasticity or fracture.

- **Yield strength**: refers to the point on the stress-strain curve (Figure 3.11) beyond which the solid starts to deform plastically and cannot be reversed upon removal of the loading, thus producing

permanent plastic deformation, but still remaining in one piece (symbol: σ_y; SI unit: MPa). Prior to the yield point the material will deform elastically and will return to its original shape when the applied stress is removed. When the stress is greater than the yield stress, the material behaves plastically and does not return to its previous state, and fracture can occur.

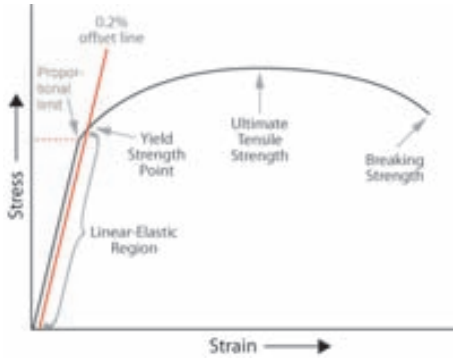

Fig. 3.11 Schematic representation of stress-strain curve.

Non-linearities in mechanical properties can be due to non-linear material behaviour or be caused by changes in geometry. Material non-linearity is originated by non-linear relationships between properties arising from the kinetic and kinematic variability. A material is said to be linear if some specified influence (e.g., stress) produces a response (e.g., strain) proportional to the influence,

$$\sigma = E\epsilon$$

as described by Hooke's law. In this case, a linearly elastic material deforms proportionally to the applied load, returning to its original shape and size upon removal of the load, as discussed above. For instance, glass is a linear material. Conversely, wood is definitely a non-linear material, because it does not comply with Hook's law. So are soils, and anisotropic metals, ceramics and stones (Reddy 2004, Ashby 2005).

e2. Strength Properties

The material's mechanical strength properties refer to the ability to withstand an applied stress without failure, by measuring the extent of a material's elastic range, or elastic and plastic ranges together. Loading refers to the applied force to an object, which can be by tension, compression, bending, torsion, or fatigue.

e2.1 **Tension** – Involves pulling or elongating two sections of a material on either side of a plane (Figure 3.12).

Fig. 3.12 Mechanical strength property: tension.

- **Ultimate Tensile Strength**: (UTS. Symbol: σ_u; SI unit: MPa or psi) is the maximum amount of tensile stress (force per unit area) a material can withstand while being stretched or pulled before failure.
- **Tensile stress**: (symbol: σ; SI unit: MPa) is defined by the ratio of the instantaneous load (F) applied perpendicular to a cross-section of a material to the original cross-section (A_0) before any load is applied (m^2).

$$\sigma = F/A_0$$

- **Tensile strain**: (symbol: ϵ; unitless, but can be expressed in meters per meter or as a percentage, in which the strain value is multiplied by one hundred) is defined by the equation

$$\epsilon = (L_i - L_0)/L_0 = \Delta L_i/L_0$$

where L_0 is the initial length before load is applied, and L_i is the instantaneous length. $L_0 - L_i$ can be denoted as ΔL_i, meaning the deformation elongation or change in length.

- **Ductility**: is the ability of a material to undergo large strains before failure (Figure 3.5). It can be measured in percentage of elongation of a tensile sample after breaking.

$$\epsilon = (L_f - L_0)/L_0 = \Delta_L/L_0$$

where L_f is the final length in m/m.

- **Brittleness**: is the ability of a material to fracture with very little or no previous detectable deformation (Figure 3.13). It is measured by the Brittleness Index (BI), and the resulting value is scaled from 0 to 100 (Grieser and Bray 2007, Rickman et al. 2008)

$$BI = \left[\frac{100\,(E_v - E_{v\_min})}{(E_{v\_max} - E_{v\_min})} + \frac{100\,(\mu_v - \mu_{v\_max})}{(\mu_{v\_min} - \mu_{v\_max})}\right]/2$$

where E_{v_min} and E_{v_max} are the minimum and maximum vertical Young's Modulus in interval of interest (psi), respectively; and μ_{v_min} and μ_{v_max} are the minimum and maximum vertical Poisson's ratio in interval of interest (psi), respectively.

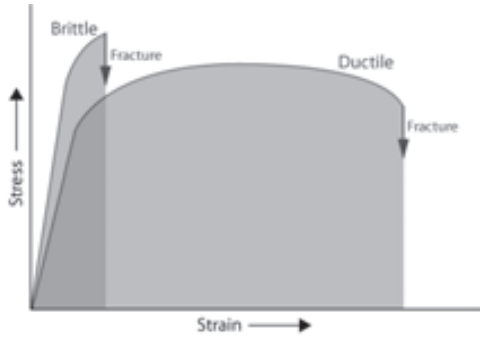

Fig. 3.13 Schematic representation of tensile stress-strain curve behaviour: ductile and brittle materials loaded to fracture.

e2.2 **Compression** – Involves pressing the material together. It is the opposite of tensile loading (Figure 3.14).

Fig. 3.14 Mechanical strength property: compression.

- **Compressive strength**: (symbol: σ_c; SI unit: MPa) is the maximum amount of compressive stress a material can withstand while being compressed before failure.

  The equations for computing **compressive stress** and **compressive strain** are the same of their tensile counterparts, only here the computed compressive strain is negative.

- **Hardness**: (symbol: *H*; SI unit: Vickers, Brinell, Janka, Rockwell, Mohs scales), and nanoindentation hardness, is the ability to withstand surface indentation. A measure for material hardness can also be the degree of abrasion, which is the resistance to grinding force.

e2.3 **Bending** – Involves applying a load that causes a material to curve, resulting in compressing the material on one side and stretching it on the other (Figure 3.15).

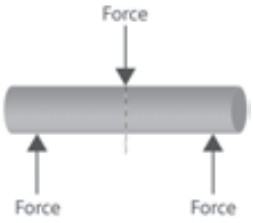

Fig. 3.15 Mechanical strength property: bending.

It can be quantified as:

- **Bending strength**: (symbol: σ; SI unit: MPa), flexural strength, or modulus of rupture (MOR). Even though it reflects the maximum load-carrying capacity of a material in bending, its computed formula is valid only to the elastic limit.

e2.4 **Shear** – Involves applying a load parallel to a plane, causing the material on one of the sides of the plane to want to slide across the material on the other side (Figure 3.16).

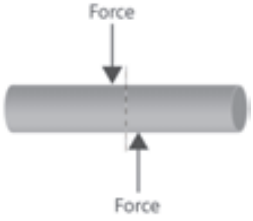

Fig. 3.16 Mechanical strength property: shear.

It can be quantified as:

- **Shear modulus**: (symbol: G; SI unit: Pa, MPa, GPa) or modulus of rigidity, is defined by the ratio of shear stress to shear strain. It measures the stiffness of materials indicating the resistance to deflection of a member caused by shear stresses. It is concerned with the deformation of a solid when it experiences a force parallel to one of its surfaces while its opposite face experiences an opposing force, as in friction. The modulus of rigidity is defined by the equation

$$G = \tau/\gamma$$

where τ is shear stress, and γ is the transverse displacement $(\Delta x/L_0)$. In torsion $\gamma = \theta r/l$ (see *e2.5 Torsion strength*).

- **Shear strength**: (symbol: τ; SI unit: MPa) is the maximum amount of shear stress a material can withstand before failure.
- **Shear stress**: (symbol: τ; SI unit: MPa) is defined by the ratio of the load or force (F) parallel to opposite faces, each of which has an area of A_0

$$\tau = F/A_0$$

- **Shear strain**: refers to the displacement per unit sample length. The units for shear stress and strain are the same of their tensile counterparts.

e2.5 **Torsion** – Involves applying a torque that causes a material to twist. It is a variation of pure shear.

- **Torsion strength**: (symbols: τ; SI unit: MPa) refers to the maximum stress a material can withstand under torsional load before rupture (Figure 3.17).

Fig. 3.17 Mechanical strength property: torsion.

It is defined by the equation

$$\tau = G\theta r/l$$

where θ is the angle of twist in radians, r is the distance between the rotational axis and the stressed surface in a given position, and l is the length of the object the torque is being applied to or over.

e2.6 **Fatigue** – Involves resistance to failure under particular combinations of repeated loading conditions, such as frequency and number of cycles, and ratio of maximum to minimum stress.

- **Fatigue limit**: (symbol: σ_e, S_e; SI unit: MPa) refers to the maximum stress a material can withstand under cyclic loading without breaking.

e3. Friction properties

Refer to the force resistance to interacting surfaces in relative motion. Friction is a dimension-

less scalar value, is expressed by the ratio of the magnitude of the friction force (F_f; or maximum friction force, when static friction) per the magnitude of the normal force (F_n), and is measured in Newtons (N). They include the coefficients (μ) of static, kinetic, and rolling friction, which depend on the moisture content, the surface roughness, and the opposing surface's characteristics. Although related with the visual appearance of texture (microtopography) they should not be confounded.

e4. Vibration Properties

Internal friction and speed of sound are of most importance in structural materials, or even in the study of archaeological musical instruments. Speed of sound is a function of the modulus of elasticity and density. Internal friction is the term used for when solid material is strained and some mechanical energy is dissipated as heat, i.e. damping capacity (symbol: η).

Although nowadays there is a vast number of publications and digital material libraries available with the values of several material properties, for less common materials in modern life, notably some of the most used in prehistory and ancient times, it can be difficult, or even impossible, to measure how their chemical composition, biological structure, or physical properties constrained their mechanical properties. In those cases, when there is no available literature or library with the required material properties, it can be necessary to conduct real-world tests in order to obtain the necessary values for a particular material that a given archaeological object is made of. Depending on the material sample as well as on the type of property to be determined, these tests can be destructive (e.g., mechanical methods using Universal Testing Machine – UTM) or non-destructive (e.g., resonance frequency and ultrasonic techniques) (Green et al. 2003).

Taking the example of wood, to measure such values with a UTM implies the direct manipulation of real wood samples. Here, modern material samples of the same family or specie need to be arranged, prepared, and tested in a controlled manner, meaning that:

- The tests can be replicated with reasonable accuracy;
- Measures can be taken and used as the material´s properties reference values. If the assigned property values of modern materials are sufficiently homogeneous, they can then be used as reference data for archaeological material properties datasets (ISO/IEC 2007).

On the subject of sampling, its major purpose is to obtain information that represents the whole material batch as well as possible. It is a very important part of the measurement process, considering that the quality of the subsequent measurements is intrinsically related to the quality of the sampling upon which it is based, followed by the level of care and attention paid to the instrumental measurements. The procedures for a correct material sampling are ensured, by following the appropriate standards. It is important to state all the followed standards for sampling, to clarify the results. There are a number of authoritative and detailed texts on various aspects of sampling and measuring uncertainties (ASME, ASTM, BSI, ISO, UNE; Czichos 2006).

3.5 Data Integration: A Computer Simulation

Computer simulation was pioneered as a scientific tool in meteorology and nuclear physics in the period directly following World War II. Since then it has become indispensable in a growing number of disciplines - from astrophysics, materials science, engineering, fluid mechanics, climate science, to evolutionary biology, ecology, economics, decision theory, sociology. Chaos theory and complexity theory emerged alongside the development of the computational models they study (Winsberg 2009, 2010, 2013).

According to Winsberg (2009, 2010, 2013), computer simulation is, in the broad sense, a comprehensive method for studying the entire process of complex systems. This method is used to make inferences about the target system that one tries to model, as well as the procedures used to sanction those inferences. The process may be iterative at any step, and comprises (Figure 3.18):

a) Hypothesis

It consists of a hypothesis (or theory) that attempts to explain the phenomenon of interest.

b) Model

It consists of choosing a model of a real-world, imaginary, or hypothetical system.

c) Treatment

It consists of implementing the model in a form that can be run on a computer, namely by assigning values to basic parameters and assigning initial values to the variables.

d) Solver

Model and treatment are combined to create a solver, which calculates the output of the algorithm.

e) Results

It consists of visualizing and studying the output data.

Fig. 3.18 Computer simulation workflow: from hypothesis to resultant data (adapted from Winsberg 2010).

Hence, simulations can be used for different purposes: heuristic, i.e., to represent scientific information to oneself, or to communicate knowledge to others; to predict data that one does not have; or to generate understanding of data that one does already have.

Computational Mechanics (CM) is a core discipline in computational science and engineering, and considered as a sub-discipline of Theoretical and Applied Mechanics (TAM). It is concerned with the use of computational methods to characterize, predict, simulate, and understand physical events governed by the laws of mechanics. Along these lines, Continuum Solid Mechanics is a branch of mechanics which deals with

the analysis of the kinematics and the mechanical behaviour of materials modelled as a continuum mass, by disregarding the molecular structure of matter and picturing it as being without gaps or empty spaces. CM is usually interdisciplinary in nature, and has had a profound impact over the past decades in science and technology. Briefly speaking, it comprises generating a mathematical model of the physical event. After that, the mathematical equations are converted into forms which are suitable for digital computation. Finally, computer packages and coding are used to solve the discretization equations by means of direct or iterative methods (USNCTAM et al. 1991, Mase and Mase 1999, Oden et al. 2003, Berger 2010).

3.5.1 3D Solid Model

Requicha (1980) refers that a solid must have an interior, which must be determined unequivocally by the solid's boundary; the form of any solid model is invariant to location or orientation; applying boolean operations to a solid produces other solids; and that a solid model must have finite aspects, for instance, a finite number of faces.

Whereas a 3D continuous surface model is generated after a 3D faceted surface model – which in turn is based on a polygon mesh, generated from an initial point cloud – and represents the exterior geometry only; a solid model lies on a volumetric mesh, which describes both the exterior surface and the interior volume of an object. A solid model can be defined in terms of a computer representation, i.e. a digital model, of a physical entity, with computable mathematical properties which allows emulating the physical systems behaviour of the real-world artefacts and processes. This definition is to be true as long as it follows the premises that any constructed representation should (Shapiro 2001):

- Be valid in the sense that it corresponds necessarily to some real physical object;
- Represent unambiguously the corresponding physical object;
- Support, at least in principle, any geometric queries that may be asked of the corresponding physical object.

In other words, solid models emphasize on informational completeness, physical fidelity, and universality of representations.

The objective of this stage is, thus, to convert the 3D digital surface model into a 3D digital solid model. It comprises the following steps:

a) Preparing the surface mesh

It may include noise and extraneous data removal, global or local simplification, and global, local or boundary smoothing. The imported surface model needs to be watertight.

Mesh density has a direct impact on the accuracy of results. The smaller the elements, the lower the discretization error. However, the meshing and solving time both take longer, besides the fact that there is not always enough computer processing capacity to deal with such huge amount of data. The objec-

tive is to produce a mesh capable of providing acceptable discretization errors, while keeping solution times reasonably short (Kurowski 2011).

b) Creating a 3D continuous surface model

It may include adjusting surface resolution, controlling surface shapes, and fixing surface errors;

c) Converting the continuous surface model into a solid model

The process involved in this step can generate different types of elements, namely parabolic tetrahedral solid elements. The meshing technique depends on three factors: the meshing options of the chosen simulation study, the mesh control specifications (including defining the element sizes at different regions in the model), and the contact or connections between models or components.

Extending this argument takes a brief introduction to Finite Elements.

3.5.1.1 Finite Elements

Before inserting the digital model in a simulated interaction, it has to be first subdivided into a finite set of connected elements. This fundamental theory was outlined by the mathematician Richard Courant in 1943 and developed independently. Put to practical use on computers during the 1950's by aerospace and nuclear power engineers, the term Finite Element Method (FEM) was first coined and used by Clough in 1960 (Clough 1960). Since then, the Finite Element Analysis (FEA) computational technique has been widely used in various disciplines that draw on solid mechanics (Dwyer 1972, Niklas 1999, Zhang et al. 2001, Alkin et al. 2005, Richmond et al. 2005, Subic et al. 2005, Moreo et al. 2007, Moazen et al. 2008, Dumont et al. 2009, Panagiotopoulou 2009, Smevik 2009, Cheng et al. 2010, Curtis et al. 2010, Degrange et al. 2010, Fletcher et al. 2010, Wroe et al. 2010, Archangelo et al. 2011, Bright and Rayfield 2011, Cheng at al. 2011, Fortuny et al. 2011, Gentilini and Shimada 2011, Fortuny et al. 2012). Given its powerful tool in the prediction of functional, mechanical, or structural behaviours, archaeology should not be an exception as it has already been demonstrated by a small number of works (Baker and Pelcin 1998, Baker 2000, Kilikoglou 2002, Vila et al. 2007, Hopkins 2008, Levy and Dawson 2009, Lacanette and Malaurent 2010, Perucchio and Brune 2010).

FEM is a general numerical method for approximating solutions of partial differential or integral equations associated with specific physical problems on complicated geometries (Zienkiewicz and Chung 1967, Cook et al. 1989, Bonet and Wood 1997, Larson and Bengzon 2000, Reddy 2004, Zienkiewicz 2005, Morris 2008). The basic concept lies in that a body or structure may be considered as an assemblage of many smaller cells, typically parabolic tetrahedral solid elements (Figure 3.19), which are second-order or higher-order elements, here defined by four corner nodes, six mid-side nodes, and six curved or straight edges.

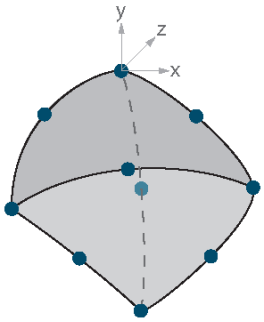

Fig. 3.19 Parabolic tetrahedral Finite Element (FE), defined by: 4 corner nodes, 6 mid-side nodes, and 6 curved or straight edges. Each node has 12 variables and degrees of freedom: 3 variables take care of translation, 3 of rotation, leaving 6 to describe the deformation.

The original body or structure is then decomposed into finite dimensions, whose elements are connected at a finite number of joins called nodes or nodal points, with determinable degrees of freedom. Nodes are assigned at a certain density throughout the digital model, depending on the hypothetical stress levels of each particular area. Regions which will receive large amounts of stress are modelled having a higher node density than those which experience little or no stress. Points of interest may consist of: fracture point perceived at the archaeological object, corners, complex detail, and high stress areas, among others.

The resulting mesh of finite elements acts like a spider web carrying the material and structural properties for each region in which we have decomposed the object, so that those properties can be formulated and combined to obtain the properties of the entire artefact. Equilibrium equations, which relate inner tensions of the solid with the applied loads, for the entire artefact are then obtained by combining the equilibrium equation of each element, and ensuring the continuity at each node. Besides equilibrium equations, constitutive or compatibility equations can also be applied. The necessary governing and boundary conditions are then imposed and, depending on the problem to analyse, the corresponding equations are solved to obtain the required values. The end result of the assembly process are the master equations

$$[K]\ \{u\} = \{f\}$$

where K is the master property matrix (elastic: stiffness; thermal: conductivity; fluid: viscosity; electrostatic: dialectri permittivity), which include the mesh geometry and the material, u is the unknown behaviour (elastic: vector or node displacements; thermal: temperature; fluid: velocity; electrostatic: electric potential), and f is the action (elastic: vector or node forces; thermal: heat source; fluid: body force; electrostatic: charge).

Additionally, such dynamic decomposition of the model enables the analysis of how each node or the whole assembly will react to distinct forces and magnitudes. Thus, instead of solving the problem for the entire structure or body in one operation, the attention is mainly devoted to the formulation of properties of the constituent elements. In this way, we increase the prediction accuracy in important or critical areas, by reducing it in others not so relevant functionally speaking (Rao 2005, Strang 2008).

Yet, one must keep in mind that although the geometry of the model has to be optimized before a simulation

can be achieved, the final solid model must necessarily carry all the relevant information. The accuracy of the simulation results is intrinsically linked to the quality of this new finite element model, while being easier to handle and process than the initial form directly.

Before running any type of simulation tests it is necessary to follow a few steps, to ensure best results.

3.5.2 Treatment, Solver & Results

There are some crucial issues to be considered in order to conduct tests, analyse and predict how the virtual artefact would behave as a physical object in possible scenarios of real world operating conditions, specifically: form and dimension of the model, mesh density, contacts and connections between component, material properties, the mechanics of human movement and of an artefact assembly (kinematics), type of medium, and physics. This stage comprises the following steps:

a) Treatment

After generating the 3D digital solid model (as above mentioned), it is time to define boundary conditions (i.e., connections, and fixtures), assign material properties, and other eventual key properties. All in accordance with the type of simulation one wishes to conduct.

b) Solver

Here is where we define the parameters for the simulation, assign values and settings; to calculate values for a certain set of functions at the nodes of the mesh, in order to solve a specific problem. Viz, to solve the equilibrium equations by running the real-time simulation tests, which can be (Solidworks 2012):

- **Static**: calculates displacements, reaction forces, strains, stresses, and factor of safety distribution;
- **Nonlinear**: calculates displacements, reaction forces, strains, and stresses at incrementally varying levels of loads and restraints;
- **Frequency**: calculates stresses caused by resonance;
- **Buckling**: calculates large displacements and failure due to axial loads;
- **Fatigue**: calculates the total lifetime, damage, and load factors due to cyclic loading;
- **Dynamic**: calculates the model's response due to loads that are applied suddenly or change with time or frequency;
- **Motion**: calculates the effects of motion components or assembly. It uses strong kinematic computational solvers, besides accounting for mass and inertia in the computations.

Running the adequate simulation, allows testing the accomplishment an object had in the past to effectively fulfil a specific action, that is, a task which has been previously formally described.

c) Results

Once the principle of controlled input and output data has been bestowed, the results of the simulation

calculations can then be analysed and compared within defined levels of certainty. These results may be illustrated by maps of displacements at the nodes of the mesh, maps of stress and strain from the nodal results, numerical results, or other results, so as to analyse how each node, or the whole assembly, reacts to distinct forces and magnitudes, such as certain stress levels, while indicating the distribution of stress, displacement and potential body deformation.

If necessary, one can modify the mesh density and other FEA characteristics, redefine parameters, assign new values and settings or any other input data, select another simulation study or run a new simulation test, in order to troubleshoot problems or evaluate the validity of the model itself.

Simulation results may provide new insights into the complex dynamics of certain phenomena. Taking the example of an event-based motion of an artefact or an assembly, here the computer tries to determine its behaviour by incorporating the effects of force and friction – e.g., ballistic, where the parameters of possible trajectories, elements positions, velocity, acceleration, friction and distance can be successively changed and tested. Another example could be to understand how the mechanism of an archaeological artefact assembly could have performed – e.g., to study the needed force to activate a specific mechanism or to exert mechanical forces to study phenomena and processes such as wear resistance.

Suffice is to recall that the accuracy of the input data is a key factor to determine the accuracy of the simulation results (Curtis 2010). A validated model has many applications in functional analysis. Furthermore, if the results are valid through a battery of tests, they can then be used as reference data to similar archaeological objects. However, without validation such analysis cannot be carried out with confidence. Of course, one should keep in mind that depending on the intended purpose and artefacts to be studied, some of these simulations might be more or less suitable, not suitable at all, or should even be used in conjunction with each others. Ideally, these data should be confirmed by also measuring the action, interaction, and reaction of real objects.

References

3D-COFORM (2009). *D.2.1 – Initial version of "User Requirement analysis and Functional Specifications" (version 8)*. 3DCOFORM Consortium. http://www.3d-coform.eu/downloads/D_2_1_User_Req_and_Fnctl_Specs_online.pdf

Adán, A., Adán, M., Salamanca, S., Merchán, P. (2008). Using Non Local Features for 3D Shape Grouping. In *Structural, Syntactic, and Statistical Pattern Recognition*. N. da Vitora Lobo, T. Kasparis, F. Roli, J.T. Kwok, M. Georgiopoulos, G.C. Anagnostopoulos, M. Loog (eds.). Springer-Verlag, Berlin-Heidelberg. *Lecture Notes in Computer Science* 5342:644-653.

Alkin, C., Imrak, C.E., Kocabas, H. (2005). Solid Modeling and Finite Element Analysis of an Overhead Crane Bridge. *Acta Polytechnica* 45(3):61-67. Czech Technical University in Prague.

Amendas, G., McConnachie, G., Pournou, A. (2013). Selective Reburial: a potential approach for the *in situ* preservation of waterlogged archaeological wood in wetland excavations. *Journal of Archaeological Science* 40:99-108.

Anderson, P.C., Georges, J.-E., Vargiolu, R., Zahouani, H. (2006). Insights from a Tribological Analysis of the Tribulum. *Journal of Archaeological Science* 33:1559-1568.

André, M.-F. (2011). Detecting and Predicting Climate Effects on Cultural Stone Deterioration. Invited key talk at the *Scientific Computing & Cultural Heritage Conference* - SCCH'11, Heidelberg.

Ankerst, M., Kastenmueller, G., Kriegel, H.-P., Seidl, T. (1999) 3D Shape Histograms for Similarity Search and Classification in Spatial Databases. *Proceedings of the 6th International Symposium on Large Spatial Databases* (SSD`99), Hong Kong.

Arnold, D., Guntram, G. (2008). *EPOCH Research Agenda for the Applications of ICT to Cultural Heritage*. Full report. D. Arnold, F. Niccolucci, D. Pletinckx, L. van Gool (eds.). Archaeolingua, Budapest.

Asahina, D., Taylor, M.A. (2011). Geometry of Irregular Particles: Direct surface measurements by 3-D laser scanner. *Powder Technology* 213:70-78.

Askeland, D.R. (1998). *The Science and Engineering of Materials*. (SI edition) Nelson Thornes, London.

ASME (2010). *ASME-B46.1-2009 - Surface Texture (Surface Roughness, Waviness, and Lay)*. American Society of Mechanical Engineers (ASME), New York (NY).

Astruc, L., Vargiolu, R., Ben Tkaya, M., Balkan-Atli, N., Özbaşaran, M., Zahouani, H. (2011). Multiscale tribological analysis of the technique of manufacture of an obsidian bracelet from Aşıklı Höyük (Aceramic Neolithic, Central Anatolia). *Journal of Archaeological Science* 38:3415-3424.

Astruc, L., Vargiolu, R., Zahouani, H. (2003). Wear Assessments of Prehistoric Instruments. *Wear* 255:341-347.

Baker, T. (2000). *Digital Crabtree: Computer Simulation of Folsom Fluting*. http://www.ele.net/algor/crabtree/crabtree.htm

Baker, T., Pelcin, A. (1998). *Applications of Finite Element Analysis to the Understanding of Flake Formation*. (modified 1999) http://www.ele.net/algor/ff_intro.htm

Baracchini, C., Callieri, M., Corsini, M., Dellepiane, M., Dercks, U., Keultjes, D., Montani, C., Scognamiglio, M., Scopigno, R., Sigismondi, R., Wolf, G. (2006). Starting the CENOBIUM Project: the cloister of Monreale (Sicily) revealed. In *The e-volution of Information Communication Technology in Cultural*

Heritage. M. Ioannides, D. Arnold, F. Niccolucci, K. Mania (eds.). Short papers from the joint event CIPA/VAST/EG/EuroMed, EPOCH Publication, pp.239-244.

Barthelmy, D. (2010). Mineralogy Database. http://webmineral.com

Bathow, C., Wachowiak, M. (2008). 3D Scanning in Truly Remote Areas. Paper presented at the Coordinate Metrology Systems Conference - CMSC, Charlotte (NC). http://www.accurexmeasure.com/applicationpages/3d%20scanning%20in%20remote%20areas.pdf

Bentkowska-Kafel, A., Denard, H., Baker, D. (eds.) (2012). *Paradata and Transparency in Virtual Heritage*. Ashgate

Beraldin, J.-A., Blais, F., Cournoyer, L., Godin, G., Rioux, M., Taylor, J. (2004). Active 3D Sensing for Heritage Applications. Proceedings of the Computer Applications and Quantitative Methods in Archaeology Conference (CAA'03), Vienna. K. Fischer-Ausserer, W. Börner, M. Goriany, L. Karlhuber-Vöckl (eds.). Archaeopress, Oxford. *BAR International Series* 1227.

Beraldin, J.-A. (2004). Integration of Laser Scanning and Close-range Photogrammetry – The last Decade and Beyond. http://www.isprs.org/proceedings/XXXV/congress/comm5/papers/188.pdf

Berger, H.P. (ed.) (2010). *Computational Mechanics Research Trends*. Nova Science Publishers, N.Y.

Bianco, G., Bruno, F., Muzzupappa, M., Luchi, M.L. (2010). Underwater 3D Shape Reconstruction by Fringe Projection. Proceedings of the Computer Applications and Quantitative Methods in Archaeology Conference (CAA'10), Granada. F. Contreras, M. Farjas, F.J. Melero (eds.). Archaeopress, Oxford. *BAR International Series* 249:19-22.

Blais, F. (2004). A Review of 20 Years of Range Sensor Development. *Journal of Electronic Imaging* 13(1):231-243.

Blanc, J., Grime, D., Blateyron, F. (2011). Surface characterization based upon significant topographic features. *Journal of Physics: Conference Series* 311-012014:1-6.

Blateyron, F. (2006). New 3D Parameters and Filtration Techniques for Surface Metrology. *Quality Magazine* (featured white paper). http://www.qualitymag.com/ext/resources/files/white_papers/New3DParametersandFiltrationTechniquesforSurfaceMetrology-DigitalSurf.pdf

Blateyron, F. (2013). The Areal Feature Parameters. In *Characterisation of Areal Surface Texture*. Leach, R. (ed.), Springer.

Blunt, L., Jiang, X. (eds.) (2003). *Advanced Techniques for Assessment Surface Topography*. Elsevier, London.

Bober, M., Preteux, F., Kim, W.-Y. (2001). *MPEG-7 Visual Shape Descriptors*. Mitsubishi Electric ITE-VII, VIL01-D112 Report. Mitsubishi Electric.

Boehler, W., Bordas Vicent, M., Marbs, A. (2003). Investigating Laser Scanner Accuracy. *Proceedings of the 19th CIPA Symposium*, Antalya.

Bonet, J., Wood, R.D. (1997). *Nonlinear Continuum Mechanics for Finite Element Analysis*. Cambridge University Press.

Breukmann (2013). *Breukmann 3D Scanner*. Breukmann. http://www.breuckmann.com

Bribiesca, E. (2000). A Measure of Compactness for 3D Shapes. *Computers & Mathematics with Applications* 40(10-11):1275-1284.

Bright, J.A., Rayfield, E.J. (2011). The Response of Cranial Biomechanical Finite Element Models to Variations in Mesh Density. *The Anatomical Report* 294:610-620.

Briscoe, B.J., Sinha, S.K. (2002). Wear of Polymers. Proceedings of the Institution of Mechanical Engineers, Part J. *Journal of Engineering Tribology* 216(6):401-413.

Brown, C.T., Witschey, W.R.T., Liebovitch, L.S. (2005). The Broken Past: fractals in archaeology. *Journal of Archaeological Method and Theory* 12:37-78.

Callister, W.D.,Jr. (2007). *Materials Science and Engineering. An introduction*. John Wiley & Sons, New York (NY).

CARARE (2012). *CARARE Metadata schema*. CARARE. http://www.carare.eu/eng/Resources/CARARE-Documentation/CARARE-metadata-schema

Carcagni, P., Daffara, C., Fontana, R., Gambino, M.C., Mastroianni, M., Mazzota, C., Pampaloni, E., Pezzati, L. (2005). Optical Micro-profilometry for Archaeology. In *Optical Methods for Arts and Archaeology*. R. Salimbeni, L. Pezzati (eds.). *Proceedings of the SPIE* 5857:118-128.

Chaouch, M., Verroust-Blondet, A. (2006). Enhanced 2D/3D Approaches Based on Relevance Index for 3D-Shape Retrieval. *Proceedings of the IEEE International Conference on Shape Modeling and Applications* (SMI'06).

Chaouch, M., Verroust-Blondet, A. (2007). Enhanced 2D/3D Approaches Based on Relevance Index for 3D-Shape Retrieval. *Proceedings of the International Conference on Shape Modeling and Applications - SMI*, pp.1-6.

Chen, S., Li, Y., Zhang, J., Wang, W. (2008). *Active Sensor Planning for Multiview Vision Tasks*. Springer-Verlag, Berlin-Heidelberg.

Chen, D.-Y., Tian, X.-P., Shen, Y.-T., Ouhyoung, M. (2003). On Visual Similarity Based 3D Model Retrieval. P. Brunet, D. Fellner (eds.). *Eurographics* 22(3):1-10.

Cheng, Y.Y. Cheung, W.L., Chow, T.W. (2010). Strain Analysis of Maxillary Complete Denture with Three-dimensional finite Element Method. *The Journal of Prosthetic Dentistry* 103(5):309-318.

Cheng, N. Takla, M., Subic, A. (2011). Development of an FE Model of a Cricket Ball. 5th Asia-Pacific Congress on Sports Technology (APCST). *Procedia Engineering* 13:238-245.

CIDOC-CRM (2006). *The CIDOC Conceptual Reference Model*. ICOM-CIDOC. http://www.cidoc-crm.org/index.html

Clough, R.W. (1960). The Finite Element Method in Plane Stress Analysis. *Proceedings of American Society of Civil Engineers - 2nd Conference on Electronic Computation*, Pittsburgh (PA), pp.345-378.

Corney, J., Rea, H., Clark, D., Pritchard, J., Breaks, M., Macleod, R. (2002). Coarse filters for shape matching. *IEEE Computer Graphics and Applications* 22(3):65-74.

Cook, R.D., Malkus, D.S., Plesha, M.E. (1989). *Concepts and Applications of Finite Element Analysis*. John Wiley & Sons.

Cotterell, B., Kamminga, J. (1990). *Mechanics of Pre-Industrial Technology. An introduction to the mechanics of ancient and traditional material culture*. Cambridge University Press.

Couper, M. (1998). Measuring Survey Quality in a CASIC Environment. *Proceedings of the Section on Survey Research Methods of the American Statistical Association.*

Cretté, S.A., Näsänen, L.M., González-Pereyra, N.G., Rennison, B. (2013). Conservation of Waterlogged Archaeological Corks using Supercritical CO_2 and Treatment Monitoring using Structured-light 3D Scanning. *The Journal of Supercritical Fluids* 79:299-313.

Crossman, A. (1997). Mineral Identification Chart. http://geology.com

Curtis, N., Jones, M.E.H., Lappin, A.K., O'Higgins, P., Evans, S.E., Fagan, M.J. (2010). Comparison between *in vivo* and theoretical bite performance: Using multi-body modelling to predict muscle and bite forces in a reptile skull. *Journal of Biomechanics* 43:2804-2809.

Czichos, H. (1987). *Tribology: a system approach to the science and technology of friction, lubrication and*

wear. Elsevier, Amsterdam.

Czichos, H., Saito, T., Smith, L. (eds.) (2006). *Springer Handbook of Materials Measurement Methods*. Springer Science+Business Media.

DCMI (1995). *Dublin Core Metadata Initiative*. ASIS&T. http://dublincore.org/

Degrange, F.J., Tambussi, C.P., Moreno, K., Witmer, L.M., Wroe, S. (2010). Mechanical Analysis of Feeding Behavior in the Extinct ''Terror Bird'' *Andalgalornis steulleti* (Gruiformes: Phorusrhacidae). PLoS ONE 5(8): e11856.

Deleanu, L., Georgescu, C., Suciu, C. (2012). A Comparison between 2D and 3D Surface Parameters for Evaluating the Quality of Surfaces. *The Annals of "Dunărea de Jos" University of Galati* 5:5-12. Technologies in Machine Building. http://freepdfdb.com/pdf/a-comparison-between-2d-and-3d-surface-parameters-for-57799261.html

Dennett, D.C. (1991). Cognitive Science as Reverse Engineering: Several Meanings of 'Top-Down' and 'Bottom-Up'. *Proceedings of the 9th International Congress of Logic, Methodology and Philosophy of Science*. D. Prawitz, B. Skyrms, D. Westerstahl (eds.).

Diaz-Andreu, M., Hobbs, R., Rosser, N., Sharpe, K., Trinks, I. (2005). Long Meg: rock art recording using 3D laser scanning. *Past: the newsletter of the Prehistoric Society* 50:2-6.

Dinwoodie, J.M. (2000). *Timber: Its Nature and Behaviour*. (2nd ed.) Taylor & Francis, Oxon.

Dorai, C., Jain, A.K. (1997). COSMOS: A Representation Scheme for 3D Free-Form Objects. *IEEE Trans. Pattern Analysis and Machine Intelligent* 19(10):1115-1130.

Dorai, C., Jain, A.K. (1997a). Shape Spectrum-Based View Grouping and Matching of 3D Free-Form Objects. *IEEE Trans. Pattern Analysis and Machine Intelligent* 19(10):1139-1145.

Dumont, E.R., Grosse, I.R., Slater, G.J. (2009). Requirements for comparing the performance of finite element models of biological structures. *Journal of Theoretical Biology* 256:96-103.

Dwyer, J.W. (1972). *Finite Element Modeling and Optimization of Aerospace Structures*. Technical Report AFFDL-TR-72-59. Air Force Flight Dynamics Laboratory, Air Force Systems Command, Wright-Patterson Air Force Base (OH); National Technical Information service, U.S. Department of Commerce, Springfield (VA).

EH - English Heritage (2010). *Waterlogged Wood. Guidelines on the recording, sampling, conservation and curation of waterlogged wood*. English Heritage, Swindon.

Eilam, E. (2005). *Reversing: Secrets of Reverse Engineering*. Wiley Publishing, Indianapolis (IN).

El Zaatari, S. (2010). Occlusal microwear texture analysis and the diets of historical/prehistoric hunter-gatherers. *Journal of Osteoarchaeology* 20:67-87.

El Zaatari, S., Grine, F.E., Ungar, P.S., Hublin, J.-J. (2011). Ecogeographic variation in Neandertal dietary habits: Evidence from occlusal molar microwear texture analysis. *Journal of Human Evolution* 61:411-424.

d'Errico, F., Backwell, L. (2009). Assessing the Function of Early Hominin Bone Tools. *Journal of Archaeological Science* 36(8):1764-1773.

Evans, T., Daly, P. (ed.) (2006). *Digital Archaeology: Bridging Method and Theory*. Routledge, London.

Faresin, E., Baschiera, A., Salemi, G., Asolati, M., Crisafulli, C. (2012). Micrometer MultiResolution Laser Scanning of a Renaissance Medallion. In *Progress in Cultural Heritage Preservation*. M. Ioannides, D. Fritsch, J. Leissner, R. Davies, F. Remondino, R. Caffo (eds.). Springer-Verlag. *Proceedings of the 4th International Conference EuroMed 2012*, Limassol, pp.525-532.

Farjas, M., García-Lázaro, F.J. (2008). *Modelización Tridimensional y Sistemas Laser Escáner 3D Aplica-*

dos al Patrimonio Histórico. Ediciones de La Ergástula, Madrid.

Farjas, M., García-Lázaro, F.J., Zancajo, J., Mostaza, T. (2010). Automatic Point-cloud Surveys in Prehistoric Site Documentation and Modelling. Proceedings of the Computer Applications and Quantitative Methods in Archaeology Conference (CAA'09), Williamsburg. B. Frischer, J. Webb Crawford, D. Koller (eds.). Archaeopress, Oxford. *BAR International Series* S2079.

Farjas, M., Quesada, N., Alonso, M., Diez, A. (2013). New Technologies Applied to Artefacts: seeking the representation of a column's capital. Proceedings of the Computer Applications and Quantitative Methods in Archaeology Conference (CAA'10), Granada. F. Contreras, M. Farjas, F.J. Melero (eds.). Archaeopress, Oxford. *BAR International Series* 2494.

Fletcher, T.M., Janis, C.M., Rayfield, E.J. (2010). Finite Element analysis of Ungulated Jaws: can mode of digestive phisiology be determined? *Paleontologia Electronica* 13(3-21A):15p.

Forte, M., Pietroni, E. (2009). 3D Collaborative Environments in Archaeology: experiencing the reconstruction of the past. *International Journal of Architectural Computing* 1(7):57-76.

Fortuny, J., Marcé-Nogué, J., Esteban-Trivigno, S. de, Gil, L., Galobart, À. (2011). Temnospondyli bite club: ecomorphological patterns of the most diverse group of early tetrapods. *Journal of Evolutionary Biology* 24(9):2040-2054.

Fortuny, J., Marcé-Nogué, J., Gil, L., Galobart, À. (2012). Skull Mechanics and the Evolutionary Patterns of the Otic Notch Closure in Capitosaurs (Amphibia: Temnospondyli). *The Anatomical Record* 295(7):1134-1146.

Fowles, P.S. (2000). The Garden Temple at Ince Blundell: a case study in the recording and non-contact replication of decayed sculpture. *Journal of Cultural Heritage* 1(1):89-91.

FPL - Forest Products Laboratory (2010). *Wood Handbook - Wood as an Engineering Material*. General Technical Report FPL-GTR-190. U.S. Department of Agriculture, Forest Service, Madison (WI).

Friess, M., Marcus, L.F., Reddy, D.P., Delson, E. (2002). The use of 3D laser scanning techniques for the morphometric analysis of human facial shape variation. In *Three-Dimensional Imaging in Paleoanthropology and Prehistoric Archaeology*. Proceedings of the 14th UISPP Congress, Liége (2001). B. Mafart, H. Delingette (eds.). Archaeopress, Oxford. *BAR International Series* 1049:31-35.

Frischer, B., Dakouri-Hild, A. (eds.) (2008). Beyond Illustration: 2D and 3D digital technologies as tools for discoveries in archaeology. Archaeopress, Oxford. *BAR International Series* 1805.

Gentilini, I., Shimada, K. (2011). Predicting and evaluating the post-assembly shape of thin-walled components via 3D laser digitization and FEA simulation of the assembly process. *Computer-Aided Design* 43:316-328.

Georgopoulos, A., Ioannidis, Ch., Valanis, A. (2010). Assessing the Performance of a Structured Light Scanner. Commission V Symposium, Newcastle upon Tyne. *International Archives of Photogrammetry, Remote Sensing and Spatial Information Sciences* 38(5):250-255.

Gernat, T., McPherron, S.J.P., Dibble, H.L., Hublin, J.-J. (2007). An Application of Structured Light Scanning to Documenting Excavated Surfaces and in situ Finds: examples from the Middle Paleolithic sites of Jonzac and Roc de Marsal, France. Proceedings of the Computer Applications and Quantitative Methods in Archaeology Conference (CAA'07), Berlin. A. Posluschny, K. Lambers, I. Herzog (eds.). Dr. Rudolf Habelt GmbH, Bonn. *Kolloquien zur Vor- und Frühgeschichte* 10:51-57.

Gilboa, A., Karasik, A., Sharon, I., Smilansky, U. (2004). Towards Computerized Typology and Classification of Ceramics. *Journal of Archaeological Science* 31:681-694.

Gluchy, A., Vargiolu, R., Mordant, C., Zahouani, H. (2008). Tribology's Contribution to Archaeology.

Surface Engineering 24(2):154-161.

Gorthi, S.S., Rastogi, P. (2010). Fringe Projection Techniques: Whither we are? *Optics and Lasers in Engineering* 48(2):133-140.

Green jr, R.J., Djordjevic, B.B, Hentschel, M.P. (eds.) (2003). *Non-destructive Characterization of Materials XI*. Springer-Verlag, Berlin-Heidelberg.

Griffiths, B. (2001). *Manufacturing Surface Technology: surface integrity & functional performance*. Manufacturing Engineering Modular Series. Penton Press, London.

Grieser, B., Bray, J. (2007). Identification of Production Potential in Unconventional Reservoirs. *Paper presented at the SPE Production Operations Symposium*, Oklahoma City (OK).

Guidazzoli, A., Liguori, M.C., Felicori, M.. (2012). Collecting, Sharing, Reusing Geo and Time-variant 3D Models of the City of Bologna: an open project. Proceedings of the 18th International Conference on Virtual System and Multimedia (VSMM). *IEEE*, pp.611-614.

Guidi, G., Frischer, B., De Simone, M., Cioci, A., Spinetti, A., Carosso, L., Loredana Micoli, L., Russo, M., Grasso, T. (2004). Virtualizing Ancient Rome: 3D acquisition and modeling of a large plaster-of-Paris model of imperial Rome. In *Videometrics VIII*. J.-A. Beraldin, S.F. El-Hakim, A. Gruen, J.S. Walton (eds.). *Proceedings of the SPIE* 5665:119-133.

Guidi, G., Remondino, F. (2012). 3D Modelling from Real Data. In *Modeling and Simulation in Engineering*. C. Alexandru (ed.). InTech, pp.69-102.

Guipert, G., Subsol, G., Jessel, J.P., Delingette, H., Mafart, B. (2003). The FOVEA Project: a New Look at Human Past. *Proceedings of the 9th International Conference on Virtual Systems and Multimedia*, Montreal.

Havemann, S. (2012). Intricacies and Potentials of Gathering Paradata in the 3D Modelling Workflow. In *Paradata and Transparency in Virtual Heritage*. A. Bentkowska-Kafel, H. Denard, D. Baker (eds.). Ashgate.

Hermon, S., Niccolucci, F., D'Andrea, A. (2005). Some Evaluations of the potential Impact of Virtual Reality on the Archaeological Scientific Research. *Proceedings of the 11th International Conference on Virtual Systems and Multimedia, VSMM2005*, Ghent. Archaeolingua, Budapest.

Hoadling, R.B. (2000). *Understanding Wood: a craftsman's guide to wood technology*. The Taunton Press, Newtown (CT).

Hopkins, H.J. (2008). Creep of Lead Dyeing Vessels in Pompeii: the use of Finite Element Analysis to answer 'unanswerable' questions. *Archaeometry* 53(6):1231-1248.

Image Metrology (n.a.). *SPIP - Scanning Probe Image Processor tutorial*. Image Metrology. http://www.imagemet.com/WebHelp/spip.htm#roughness_parameters.htm

d'Incau, E., Couture, C., Maureille, B. (2012). Human Tooth Wear in the Past and the Present: Tribological mechanisms, scoring systems, dental and skeletal compensations. *Archives of Oral Biology* 57:214-229.

Inokushi, S., Sato, K., Matsuda, F. (1984). Range Imaging System for 3-D Object Recognition. *ICPR*, pp.806-808.

ISO 13565-2 (1996). *ISO 13565-2:1996 - Geometrical Product Specifications (GPS) - Surface texture: Profile method; Surfaces having stratified functional properties - Part 2: Height characterization using the linear material ratio curve*. ISO.

ISO 14460-1 (1996). *ISO 14460-1:1996 - Geometrical Product Specifications (GPS) - Geometric Features - Part 1: General terms and definitions*. ISO.

ISO 25178-2 (2012). *25178-2:2012 - Geometrical Product Specifications (GPS) - Surface texture: Areal -*

Part 2: Terms, definitions and surface texture parameters. ISO.

ISO/IEC (2007). *ISO/IEC Guide 99:2007. International Vocabulary of Metrology - Basic and general concepts and associated terms (VIM)*. ISO.

Jayanti, S., Kalyanaraman, Y., Ramani, K. (2009). Shape-based clustering for 3D CAD objects: A comparative study of effectiveness. *Computer-Aided Design* 41:999-1007.

JCGM (2008a). *JCGM 100:2008. Evaluation of measurement data - Guide to the expression of uncertainty in measurement (GUM)*. Joint Committee for Guides in Metrology (JCGM).

JCGM (2008b). *JCGM 200:2008. International vocabulary of metrology - Basic and general concepts and associated terms (VIM)*. JCGM.

Kamat, V. R., Martinez, J. C. (2007). Variable-speed object motion in 3D visualizations of discrete-event construction simulation models. *ITcon* 12:293-303.

Kampel, M., Sablatnig, R. (2006). 3D Data Retrieval of Archaeological Pottery. Proceedings of the 12th International Conference, VSMM2006, Xi'an. Springer. *Lecture Notes in Computer Science* 4270:387-395.

Karasik, A., Mara, H., Sablatnig, R., Sharon, I., Smilansky, U., Israel, R. (2005). Measuring Deformations of Wheel-produced Ceramics Using High Resolution 3D Reconstructions. *Proceedings of the Computers Applications and Quantitative Methods in Archaeology* (CAA'05), Tomar. A. Figueiredo, G.L. Velho (eds.).

Karasik, A., Smilansky, U. (2008). 3D Scanning technology as a standard archaeological tool for pottery analysis: practice and theory. *Journal of Archaeological Science* 35:1148-1168.

Kazhdan, M., Funkhouser, T., Rusinkiewicz, S. (2003). Rotation Invariant Spherical Harmonic Representation of 3D Shape Descriptors. *Proceedings of the Eurographics Symposium on Geometry Processing*. L. Kobbelt, P. Schröder, H. Hoppe (eds.). The Europgraphics Association.

Kilikoglou, V. (2002). Failure Prediction and Function Determination of Archaeological Pottery by Finite Element Analysis. *Journal of Archaeological Science* 29:1317-1325.

Koenderink, J. (1990). *Solid Shape*. The MIT Press, Cambridge, Massachusetts.

Koenderink, J., van Doorn, A. (1992). Surface Shape and Curvature Scales. *Image and Vision Computing* 10(8):557-564.

Kooi, B.W. (1991). Archery and Mathematical Modeling. *Journal of the Society of Archer-Antiquaries* 34:21-29.

Kreuter, F., Couper, M., Lyberg, L. (2010). The use of paradata to monitor and manage survey data collection. *Proceedings of the Survey Research Methods Section, American Statistical Association*, pp.282-296.

Kuo, C.Y., Freeman, R.B. (2000). Imaging Indices for Quantification of Shape, Angularity and Surface Texture of Aggregates. *Transport Res Rec* 1727:57-65.

Kurowski, P. (2011). Engineering Analysis with Solidworks Simulation 2011. SDC Publications, Kansas.

La Pensée, A.A., Cooper, M.I., Parsons, J.B. (2006). Applications in the Field of Cultural Heritage Using "Off-the-shelf" 3D Laser Scanning Technology in Novel Ways. In *The e-volution of Information Communication Technology in Cultural Heritage*. M. Ioannides, D. Arnold, F. Niccolucci, K. Mania (eds.), Project papers from the joint event CIPA/VAST/EG/EuroMed, EPOCH Publication, 215-220.

Lacanette, D., Malaurent, P. (2010). La 3D au service de la conservation des grottes ornées, l'exemple de Lascaux et du simulateur Lascaux. *In Situ, Revue des Patrimoines* 13. http://insitu.revues.org/6793

Lanman, D., Taubin, G. (2009). *Build Your Own 3D Scanner: 3D photography for beginners*. SIGGRAPH2009

Courses. http://mesh.brown.edu/byo3d/

Larson, M.G., Bengzon, F. (2010). *The Finite Element Method: Theory, Implementation, and Practice*. Springer.

Levy, R., Dawson, P. (2009). Using finite element methods to analyse ancient architecture: an example from the North American Arctic. *Journal of archaeological Science* 36:2298-2307.

Li, T. (2011). *Softgauges for Surface Texture*. Ph.D. Thesis. School of Computing & Engineering, University of Huddersfield.

Lian, Z., Rosin, P.L., Sun, X. (2010). Rectilinearity of 3D Meshes. *International Journal of Computer Vision - IJCV* 89(2-3):130-151.

Lin, S.C.H., Douglass, M.J., Holdaway, S.J., Floyd, B. (2010). The Application of 3D Laser Scanning Technology to the Assessment of Ordinal and Mechanical Cortex Quantification in Lithic Analysis. *Journal of Archaeological Science* 37:694-702.

Lock, G. (ed.) (2003). *Using Computers in Archaeology: Towards Virtual Pasts*. Routledge, London.

London Charter (2009). *London Charter: for the computer-based visualization of Cultural Heritage*. London Charter. http://www.londoncharter.org

Mademlis, A., daras, P., Tzovaras, D., Strintzis, M.G. (2009). Ellipsoidal Harmonics for 3-D Shape Description and Retrieval. *IEEE Transactions on Multimedia - TMM* 11(8):1422-1433.

Mandelbrot, B.B. (1977). *Fractals, Forms, Chance and Dimension*. W.H. Freeman, San Francisco (CA).

Mandelbrot, B.B. (1982). *The Fractal Geometry of Nature*. W.H. Freeman, San Francisco (CA).

Mara, H., Sablatnig, R., Karasik, A., Smilansky, U. (2004). The Uniformity of Wheel Produced Pottery Deduced from 3D Image Processing and Scanning. Proceedings of the 28th Workshop of the Austrian Association for Pattern Recognition - OAGM/AAPR, Digital Imaging in Media and Education. Burger, W. & Scharinger, J. (eds.). *Schriftenreihe der OCG* 179:197-204.

Martinez-Ortiz, C., Žunić, J. (2009). Measuring Cubeness of 3D Shapes. In *Progress in Pattern Recognition, Image Analysis, Computer Vision, and Applications*. E. Bayro-Corrochano, J.-O. Eklundh (eds.). Springer-Verlag, Berlin-Heidelberg. *Lecture Notes in Computer Science* 5856:716-723.

Marwan, N., Saparin, P., Gowin, W., Kurths, J. (2004). *3D measures of complexity for the assessment of complex trabecular bone structures*. http://www.pik-potsdam.de/members/kurths/publikationen/2004/3d-measures-of-complexity-for-the-assessment-of-complex-trabecular-bone-structures

Masad, E. (2001). Review of Imaging Techniques for Characterizing the Shape of Aggregates Used in Asphalt Mixes. *Proceedings of the 9th Annual Symposium of the International centre for Aggregate Research* (ICAR), Austin (TX).

Masad, E., Al-Rousan, T., Little, D. (2007). *Test Methods for Characterizing Aggregate Shape, Texture, and Angularity*. NCHRP Report 555, National Cooperative Highway Research Program. Transportation Research Board of the National Academies, Washington D.C. (WA).

Mase, G.T., Mase, G.E. (1999). *Continuum Mechanics for Engineers*. CRC Press, Boca Ratón (FL).

MatWeb (2013). *MatWeb: Material Property Data*. MatWeb, LLC. http://www.matweb.com/index.aspx

Mélard, N. (2010). L'étude microtopographique et la visualisation 3D dans l'analyse de gravures préhistoriques – L'exemple des pierres gravées de La Marche. *In Situ, Revue des Patrimoines* 13. http://insitu.revues.org/6837

Moazen, M., Curtis, N., O'Higgins, P., Jones, M.E.H., Evans, S., Fagan, M.J. (2008). Assessment of the Role of Sutures in a Lizard Skull: a computer modelling study. *Proceedings of The Royal Society B* 276:39-46.

Moitinho, V. (2007). Virtual Archaeology: work in progress. Proceedings of the Computer Applications and Quantitative Methods in Archaeology Conference (CAA'07), Berlin. A. Posluschny, K. Lambers, I. Herzog (eds.). Dr. Rudolf Habelt GmbH, Bonn. *Kolloquien zur Vor- und Frühgeschichte* 10.

Moitinho, V., Barceló, J.A. (2011). Towards an Understanding of Archaeological Artefacts through Reverse Engineering. *Proceedings of the Scientific Computing & Cultural Heritage Conference* (SCCH2011), Heidelberg.

Moitinho, V., Barceló, J.A. (2012). Understanding Virtual Objects through Reverse Engineering. Proceedings of the III Congreso Internacional de Arqueología e Informática Gráfica, Patrimonio e Innovación, Arqueológica 2.0 (2011), Sevilla. *Virtual Archaeology Review - special issue on Virtual Museums* 3(7):14-17.

Moitinho de Almeida, V. (2007). *Espaços Museológicos Virtuais. A Villa Romana do Rabaçal, estudo de caso*. M.Sc. Thesis. Departament of Electrotechnic and Computers Engineering (DEEC-FEUP), University of Oporto.

Moitinho de Almeida, V. (2010). *Digitalização 3D de Artefactos Arqueológicos: para um estudo da relação forma-função*. M.Sc. Thesis. Department of Prehistory, Universitat Autònoma de Barcelona.

Moitinho de Almeida, V., Barceló, J.A. (2012). 3D Scanning and Computer Simulation of Archaeological Artefacts. *Proceedings of the 1st International Conference on Best Practices in World Heritage: Archaeology*, Menorca, 384-399. A. Castillo (ed.), Editorial Complutense, Madrid.

Moitinho de Almeida, V., Barceló, J.A., Rosillo, R., Palomo, A. (2013). Linking 3D Digital Surface Texture Data with Ancient Manufacturing Procedures. *IEEE Digital Heritage International Congress*, Marseille. A.C. Addison, G. Guidi, L. De Luca, S. Pescarin (eds.). pp.735-738.

Moreo, P., Pérez, M.A., García-Aznar, J.M., Doblaré, M. (2007). Modelling the Mechanical Behaviour of Living Bony Interfaces. *Computer Methods in Applied Mechanics and Engineering* 196(35-36):3300-3314.

Morris, A. (2008). *A Practical Guide to Reliable Finite Element Modelling*. John Wiley & Sons.

Muralikrishnan, B., Raja, J. (2008). *Computational Surface and Roundness Metrology*. Springer.

Musker, D.C. (1998). Protecting & Exploiting Intellectual Property in Electronics. *IBC Conferences*.

Niklas, K.J. (1999). Research Review: A mechanical perspective on foliage leaf form and function. *New Phytologist* 143:19-31.

Novotni, M., Klein, R. (2003). 3D Zernike Descriptors for Content Based Shape Retrieval. *Proceedings of the 8th ACM Symposium on Solid Modeling and Applications* (SM'03), ACM, New York (NY), pp.216-225.

Oden, J.T., Belytschko, T., Babuska, I., Hughes, T.J.R. (2003). Research Directions in Computational Mechanics. *Computer Methods in Applied Mechanics and Engineering* 192:913-922.

Osada, R., Funkhouser, T., Chazelle, B., Dobkin, D. (2002). Shape Distributions. *ACM Transactions on Graphics* 21(4):807-832.

OUP (n.a.). *Obsidian Use Project*. CNRS/IFEA/TCIU/LTDS/ANR. http://www.obsidianuseproject.org/OUP/?cat=71

Pagès, P., Salvi, J., Garcia, R., Matabosch, C. (2003). Overview of coded light projection techniques for automatic 3D profiling. *Proceedings of the 1003 IEEE Internatiooal Conference on Robotics & Automation*, pp.133-138.

Panagiotopoulou, O. (2003). Finite Element Analysis (FEA): applying an engineering method to functional morphology in anthropology and human biology. *Annals of Human Biology* 36(5):609-623.

Paquet, E., Rioux, M., Murching, A., Naveen, T., Tabatabai, A. (2000). Description of shape information for

2-D and 3-D objects. *Signal Process: Image Communication* 16(1-2):103-122. Elsevier.

Pereira, T., Moitinho, V. (2006). 3D Analysis on Quartzite Industries. Proceedings of the 15th UISPP Congress, Lisbon. A. Figueiredo, H. Kamermans (eds.). Archaeopress, Oxford. *BAR International Series* S2029 2009 37(C04):1-7.

Perros, H. (2009). *Computer Simulation Techniques: The definitive introduction!* Computer Science Department, NC State University (NC).

Perucchio, R., Brune, P. (2010). *I Mercati di Traiano Restituiti. Studi e restauri 2005-2007*. Palombi Editori, Roma.

Pescarin, S. (2007). Reconstructing archaeological landscape. Interpretation and integration in spatial and real-time open system. In *Space - Archaeology's Final Frontier? An intercontinental approach*. D. Keeler, R. Salisbury (eds.). Cambridge Scholars Publishing, pp.69-93.

Pieraccini, M., Guidi, G., Atzeni, C. (2001). 3D Digitizing of Cultural Heritage. *Journal of Cultural Heritage* 2:63-70.

Pieraccini, M., Noferini, L., Mecatti, D., Atzeni, C., Teza, G., Galgaro, A., Zaltron, N. (2006). Integration of Radar Interferometry and Laser Scanning for Remote Monitoring of an Urban Site Built on a Sliding Slope. *IEEE Transactions on Geoscience and Remote Sensing* 44(9):2335-2342.

Pressley, A. (2001). *Elementary Differential Geometry*. Springer, London.

Qi, Q., Jiang, X., Scott, P.J. (2012). Knowledge Modeling for Specifications and Verification in Areal Surface Texture. *Precision Engineering* 36(2):322-333.

Raja, V., Fernandes, K.J. (eds.) (2008). *Reverse Engineering: An Industrial Perspective*. Springer-Verlag, London.

Rao, S.S. (2011). *The Finite Element Method in Engineering*. Butterworth-Heinemann, Elsevier.

Record, S.J. (1914). *The Mechanical Properties of Wood*. John Wiley & Sons, New York (NY).

Reddy, J.N. (2004). *An Introduction to Nonlinear Finite Element Analysis*. Oxford University Press.

Reichenbach, T., Kovačić, Z. (2003). Derivation of Kinematic Parameters from a 3D Robot Model Used for Collision-free Path Planning. *Proceedings of the 11th Mediterranean Conference on Control and Automation*, MED '03.

Reilly, P., Rahtz, S. (ed.) (1992). *Archaeology and the Information Age. A Global Perspective*. Routledge, London.

Remondino, F. (2011). Heritage Recording and 3D Modeling with Photogrammetry and 3D Scanning. *Remote Sensing* 3(6):1104-1138.

Richmond, B.G., Wright, B.W., Grosse, I., Dechow, P.C., Ross, C.F., Spencer, M.A., Strait, D.S. (2005). Finite Element Analysis in Functional Morphology. *The Anatomical Report, part A - Discoveries in molecular, cellular, and evolutionary biology* 283(2):259-74.

Rickman, R., Mullen, M., Petre, E., Grieser, B., Kundert, D. (2008). A Practical Use of Shale Petrophysics for Stimulation Design Optimization: All Shale Plays Are Not Clones of the Barnett Shale. *Paper presented at the SPE Annual Technical Conference and Exhibition*, Denver (CO).

Ronzino, P., Hermon, S., Niccolucci, F. (2012). A Metadata Schema for Cultural Heritage Documentation. *Draft of the paper published at the Electronic Imaging & the Visual Arts Conference* (EVA 2012), Florence. V. Capellini (ed.). Firenze University Press. http://www.academia.edu/1227094/A_Metadata_Schema_for_Cultural_Heritage_Documentation

Rousan, T.M. (2004). *Characterization of Aggregate Shape Properties Using a Computed Automated System*. Ph.D. Thesis. Texas A&M University.

Russ, J.C. (1990). *Computer-assisted microscopy: The measurement and analysis of images*. Plenum Press, New York (NY).

Russ, J.C. (2011). *The Image Processing Handbook*. (6th ed.) CRC Press, Boca Ratón (FL).

Salvi, J., Pagès, J., Batlle, J. (2004). Pattern codification strategies in structured light systems. *Pattern Recognition* 37(4):827-849.

Sansoni, G., Trebeschi, M., Docchio, F. (2009). State-of-the-Art and Applications of 3D Imaging Sensors in Industry, Cultural Heritage, Medicine, and Criminal Investigation. *Sensors* 9:568-601.

Schulz, E., Calandra, I., Kaiser, T.M. (2010). Applying Tribology to Teeth of Hoofed Mammals. *Scanning* 32:162-182.

Schulz, E., Kaiser, T.M. (2007). Feeding Strategy of the Urus 'Bos primigenius' BOJANUS 1827 from the Holocene of Denmark. *Courier Forschungsinstitut Senckenberg* 259:155-164.

Scopigno, R., Cignoni, P., Callieri, M., Ganovelli, F., Impoco, G., Pingi, P., Ponchio, F. (2003). Using optically scanned 3D data in the restoration of Michelangelo's David. R. Salimbeni (ed.). *Proceedings SPIE - International Symposium on Optical Metrology for Arts and Multimedia* 5146:44-53.

Scott, P.J. (1988). Developments in Surface Texture Measurement. *Surface Topography* 1:153-163.

Serra, O. (1990). *Element, Mineral, Rock Catalog*. Schlumberger, Paris.

Sessen, R. van, Schmidt, C., Sheridan, S., Ullinger, J., Grohovsky, M. (2013). Dental Microwear Texture Analysis of Tell Dothan. Poster presented at *The 82nd Annual Meeting of the American Association of Physical Anthropologists*, Knoxville, Tenessee. http://www.academia.edu/3301349/Dental_Microwear_Texture_Analysis_at_Tell_Dothan

Sitnik, R., Krzesłowski, J., Mączkowski, G. (2012). Processing Paths from Integrating Multimodal 3D Measurement of Shape, Color and BRDF. *International Journal of Heritage in the Digital Era* 1(1):25-44.

Skar, B., Solstad, J., Risan, T., Haugen, A., Bakkestuen, V., Erikstad, L., Guttormsen, T. (2006). DEMOTEC - Development of a Monitoring System for Cultural Heritage through European Co-operation. In *The e-volution of Information Communication Technology in Cultural Heritage*. M. Ioannides, D. Arnold, F. Niccolucci, K. Mania (eds.). Short papers from the joint event CIPA/VAST/EG/EuroMed, EPOCH Publication, pp.80-84.

Slizewski, A., Friess, M., Semal, P. (2010). Surface Scanning of Anthropological Specimens: nominal-actual comparison with low-cost laser scanner and high end fringe light projection surface scanning systems. *Quartär* 57:179-187.

Smevik, T. (2009). *The Impedance of Brass Instruments, with special attention to numerical simulations analyzing the possible influence of wall vibrations*. Ph.D. Thesis. Department of Electronics and Telecommunications, Faculty of Information Technology, Mathematics and Electrical Engineering, Norwegian University of Science and Technology.

Stemp, W.J., Chung, S. (2011). Discrimination of Surface Wear on Obsidian Tools Using LSCM and RelA: Pilot Study Results (Area-Scale Analysis of Obsidian Tool Surfaces). *Scanning* 33:279-293.

Stemp, W.J., Lerner, H.J., Kristant, E.H. (2013). Quantifying Microwear on Experimental Mistassini Quartzite Scrapers: Preliminary Results of Exploratory Research Using LSCM and Scale-Sensitive Fractal Analysis. *Scanning* 35:28-39.

Stemp, W.J., Stemp, M. (2003). Documenting stages of polish development on experimental stone tools: surface characterization by fractal geometry using UBM laser profilometry. *Journal of Archaeological Science* 30(3):287-296.

Strang, G., Fix, G.J. (2008). *An Analysis of the Finite Element Method*. Wellesley-Cambridge Press.

Subic, A., Takla, M., Kovacs, J. (2005). Modelling and Analysis of Alternative Face Guard Designs for Cricket using Finite Element Modelling. *Sports Engineering* 8(4):209-222.

Sundar, H., Silver, D., Gagvani, N., Dickinson, S. (2003). Skeleton based shape matching and retrieval. *Proceedings of the IEEE Shape Modeling International* 130-139.

Tapete, D., Casagli, N., Luzi, G., Fanti, R., Gigli, G., Leva, D. (2013). Integrating Radar and Laser-based Remote Sensing Techniques for Monitoring Structural Deformation of Archaeological Monuments. *Journal of Archaeological Science* 40:176-189.

tDAR (2009). *tDAR: The Digital Archaeological Record*. Digital Antiquity. http://www.tdar.org/

USAITA - U.S. Army Information Technology Agency (n.a.). *Glossary*. U.S. Army Information Technology Agency. http://ita.army.mil/CatalogService.aspx?service_Id=122&serviceGroup_Id=9

USNCTAM - U.S. National Committee on Theoretical and Applied Mechanics, Manufacturing Studies Board, Commission on Engineering and Technical Systems, National Research Council (U.S.) (1991). *Research Directions in Computational Mechanics*. National Academy Press, Washington D.C. (WA).

Varaday, T., Martin, R.R., Coxt, J. (1997). Reverse Engineering of Geometric Models. An introduction. *Computer Aided Design* 29(4):255-268.

Váradi, K., Palásti-Kovács, B., Czifra, A., Néder, Á., Kovács, K. (2004). 3D Characterization of Engineering Surfaces. *Budapest Tech Jubilee Conference*.

Vargiolu, R., Morero, E., Boleti, A., Procopiou, H., Pailler-Mattei, C., Zahouani, H. (2007). Effects of Abrasion During Stone Vase Drilling in Bronze Age Crete. *Wear* 263:48-56.

Vila, L., Hein, A., Kilikoglou, V., Buxeda, J. (2007). Disseny Amforal i Canvi Tecnològic al Voltant del Canvi d'Era: l'aportació de l'Anàlisi d'Elements Finits. *Empúries* 55:27-38.

Wadell, H. (1935). Volume, Shape, and Roundness of Quartz Particles. *Journal of Geology* 43(3):250-280.

Wang, L. D., Park, J., Mohammad, L. (2003). Quantification of Morphology Characteristics of Aggregate from Profile Images. *Transportation Research Board 82nd Annual Meeting*, Washington, D.C. (WA).

Wang, W. (2011). *Reverse Engineering: Technology of Reinvention*. CRC Press, Boca Ratón (FL).

Whitehouse, D.J. (2002). *Handbook of Surface Metrology*. Institute of Physics, Bristol.

Wilson, J.D., Klotz, L.D., Nagaraj, C. (1997). Automated measurement of aggregate indices of shape. *Particulate Science and Technology* 15:13-35.

Winsberg, E.B. (2009). Computer Simulation and the Philosophy of Science. *Philosophy Compass* 4(5):835-845.

Winsberg, E.B. (2010). *Science in the Age of Computer Simulation*. The University of Chicago Press, Chicago.

Winsberg, E. (2013). Computer Simulations in Science. *The Stanford Encyclopedia of Philosophy* (Summer ed.). Edward N. Zalta (ed.). http://plato.stanford.edu/archives/sum2013/entries/simulations-science/

Wroe, S., Ferrara, T.L., McHenry, C.R., Curnoe, D., Chamoli, U. (2010). The craniomandibular mechanics of being human. *Proceedings of The Royal Society B* 277(1700):3579-3586.

Zaharia, T.B., Prêteux, F.J. (2003). Descripteurs de forme pour l'indexation de maillages 3D. *Technique et Science Informatiques* 22(9):1077-1105.

Zapassky, E., Finkelstein, I., Benenson, I. (2006). Ancient standards of volume: negevite Iron Age pottery (Israel) as a case study in 3D modeling. *Journal of Archaeological Science* 33:1734-1743.

Zhang, C., Chen, T. (2001). Efficient feature extraction for 2D/3D objects in mesh representation. *Proceedings of the IEEE International Conference on Image Processing* 3(3):935-938.

Zhang, C., Cao, C., Gu, F., Si, J. (2002). A Domain-Specific Formal Ontology for Archaeological Knowledge

Sharing and Reusing. In *Practical Aspects of Knowledge Management*. Proceedings of the 4th International Conference (PAKM'02). D. Karagiannis, U. Reimer (eds.). Springer-Verlag, Berlin-Heidelberg. *Lecture Notes in Computer Science* 2569:213-225.

Zhang, L., Yang, K.H., King, A.I. (2001). Comparison of Brain Responses Between Frontal and Lateral Impacts by Finite Element Modeling. *Journal of Neurotrauma* 18(1):21-34.

Zhang, S. (2010). Recent progresses on real-time 3D shape measurement using digital fringe projection techniques. *Optics and Lasers in Engineerings* 48(1):149-158.

Zienkiewicz, O.C., Cheung, I.K. (1967). *The Finite Element Method in Structural and Continuum Mechanics: numerical solution of problems in structural and continuum mechanics*. McGraw-Hill, London.

Zienkiewicz, O.C. (2005). *The Finite Element Method: it's basis and fundamentals*. (6th ed.) Elsevier.

Ø4
Case Studies

> *Meanwhile my life was under a cloud. All pleasures palled upon me; all sights tantalized and tempted me to outspoken treason, because I could not but compare what I saw in Two Dimensions with what it really was if seen in Three, and could hardly refrain from making my comparisons aloud. I neglected my clients and my own business to give myself to the contemplation of the mysteries which I had once beheld, yet which I could impart to no one, and found daily more difficult to reproduce even before my own mental vision.*

Edwin A. Abbot (1838-1926), in Flatland. A Romance of Many Dimensions (1884)

Continuing in the same trend presented in the previous chapters, the current chapter describes the implementation of the framework through the presentation of three case studies. These case studies span a broad diachrony ranging from the Palaeolithic in Cantabria to the Neolithic in Catalonia, Spain, whereas the archaeological objects of study encompass rock art, sculptures, lithics, and bows, as well as a variety of raw-materials. Since each case study has its own archaeological questions and aims, and is strongly limited by time, different parts of the framework are tackled and therefore implemented. The following case studies

thereof described are neither intended to be exhaustive nor to be limiting in scope, but to be exemplary and illustrative of the potentialities and effectiveness of the proposed framework. Results are presented throughout each case study, and conclusions are given at the end of each one.

The **1st Case Study** is focused on the engraving block of El Mirón Cave (Ramales de La Victoria, Cantabria, Spain), where the ultimate goal of this ongoing work is to provide new information and a better knowledge about the engravings in such archaeological context. Different strategies for capturing geometric data are tested, to understand to what extent distinct technical choices determine the detection, characterization, and interpretation of the carvings. A preliminary geometric analysis of the signatures of engraving mechanisms is presented. The final objective is twofold: to isolate the motifs of the palimpsest; and towards the understanding of possible types of engraving techniques and tools

In the **2nd Case Study** is focused on the Neolithic stelae with horns from the Serra del Mas Bonet (Vilafant, Catalonia, Spain), and in a set of lithic tools that have been associated with them. This investigation is directed toward a better comprehension of the manufacturing procedures used mainly in the production of one of these stelae. Different strategies for the geometric analysis, description and comparison of the objects are presented.

The **3rd Case Study** is focused on a small selection of wooden artefacts from the Neolithic lakeside site of La Draga (Banyoles, Catalonia, Spain). More specifically, on three likely bows (if so, the oldest Neolithic bows in Europe, dated between 5.324 and 4.960 cal. BCE). This investigation is directed toward the understanding of possible relationships between form, texture, material, and function(s) of these archaeological artefacts.

Every equipment and software mentioned in this research was used as a means (tools) for attaining very specific objectives. Their use does not imply that they are the 'best' available for all purposes within this framework, but that they enable to achieve the objectives set for each stage of the framework, were made available for this research, and in a few cases I was prior acquainted with – the latter exempting me from spending time learning how to use even more software, therefore allowing to focus on further issues. There are indeed other free, proprietary/commercial and non-comercial software which can be utilized to achieve similar purposes.

I explicitly did not intend to rewrite a step-by-step manual on how to use each equipment or software. If doing so, both chapters 3 and 4 would most certainly be obsolete even before being finished, since new technologies, equipment, software, models and versions appear in the market every year. Those interested in more detailed technical procedures should consult the corresponding user´s manuals.

Ø4-A
El Mirón Cave, Cantabria

A.1 Problem Statement & Objectives

The palimpsest nature of some rupestral engravings is a drawback to the analysis of their motifs. The aging of engraving grooves makes them appear uniform, erasing diachronic information, and conserving only geometry. Graphic solutions based on light/shadow relationships are insufficient for relative chronology. A more efficient way to characterize "engraving groove families" is by distinguishing morphologies of strokes. A set of engravings from El Mirón Cave was chosen as an optimal test case for 3D scanning. There is an accumulation of linear engravings on a block, fallen from the cave ceiling atop a Lower Magdalenian layer, which was covered by later Magdalenian deposits. Radiocarbon assays of levels pre- and post-dating them place the engravings around 16.000-13.000 BP. 3D data were collected with a structured light scanner with different fields of view (FOV) at resolutions ranging from 50 µm to 280 µm. Strategies based on geometric features extraction are here presented.

In the short term, the objectives of this study are:

- To test and analyse to what extent different scanner's FOV and resolutions determine the detection of grooves and subsequent characterization of individual signatures, ergo the interpretation of the carvings;
- To distinguish morphologies of strokes;

- To proceed with the analysis and characterization among the grooves on a quantitative and objective basis.

The ultimate goal in documenting rock art at El Mirón Cave is to provide new information and a better understanding about the engravings in such archaeological context.

This first case study is organized as follows. It begins with an archaeological contextualization of the engraved block of El Mirón Cave. Next, the issue of the insufficiency of graphic solutions based on light/shadow relationships for resolving the problem of palimpsests of engravings is addressed. Then, I describe the approach based on the 3D scanning of the grooves with different resolutions and subsequent morphological feature extraction. As part of an ongoing work, preliminary results are presented to demonstrate the potentialities of the used methods, tools, and techniques. Finally, a conclusion is given.

The case study here presented is an extension of the co-authored article "(Re)seeing the Engraved Block of El Mirón Cave" (Moitinho de Almeida et al. 2012), where section *A.2 Archaeological Contextualization* is fully authored and updated by Lawrence G. Straus (IIIPC-UC: Instituto Internacional de Investigaciones Prehistóricas de Cantabria, Universidad de Cantabria, UNM: University of New Mexico); and section *A.2.1 The Question of Rock Engravings* is a reduced version of the one authored by Luis Teira (IIIPC-UC). Both sections are presented herein with the kind permission of the respective co-authors. All photographs in this chapter appear here by courtesy of Luis Teira.

A.2 Archaeological Contextualization

El Mirón Cave is located in Ramales de la Victoria – (ETRS89) 43º 14' 42.76" N / 3º 27' 9.16" W – in the upper valley of the Asón River in eastern Cantabria province, close to the border with Vizcaya, Spain (Figure 4A.1). It is on the northern edge of the Cantabrian Cordillera, some 20 km from the present shore of the Bay of Biscay at an elevation of 260 m asl. It is surrounded by peaks that reach and even exceed 1.000 m asl and is below los Tornos pass (920 m) that connects the Cantabrian Coast with the *meseta* of Old Castile in Burgos Province.

The cave faces due west from a steep cliff on Mt. Pando and has a large mouth (20 m high x 16 m wide) (Figure 4A.2 and 4A.3). The vestibule is 30 m deep x 8-10 m wide x 13 m high. This leads back to an inner cave that is accessible for another 100 m. The archaeological site is mainly located in the vestibule. It was discovered in 1903 but largely ignored since then, despite being adjacent to the well-known cave art sites of Covalanas and La Haza. Straus and González-Morales have been conducting systematic excavations since 1996, uncovering a long, rich cultural sequence extending from the late Middle Palaeolithic through the early Bronze Age, plus evidence of human visits in the Middle Ages, dated by 83 radiocarbon assays between 41.000 BP and 1.400 AD. The most important part of the sequence is the series of levels pertaining to the Magdalenian-Azilian cultural complex, Late Last Glacial. It is to this period that the engraved block relates.

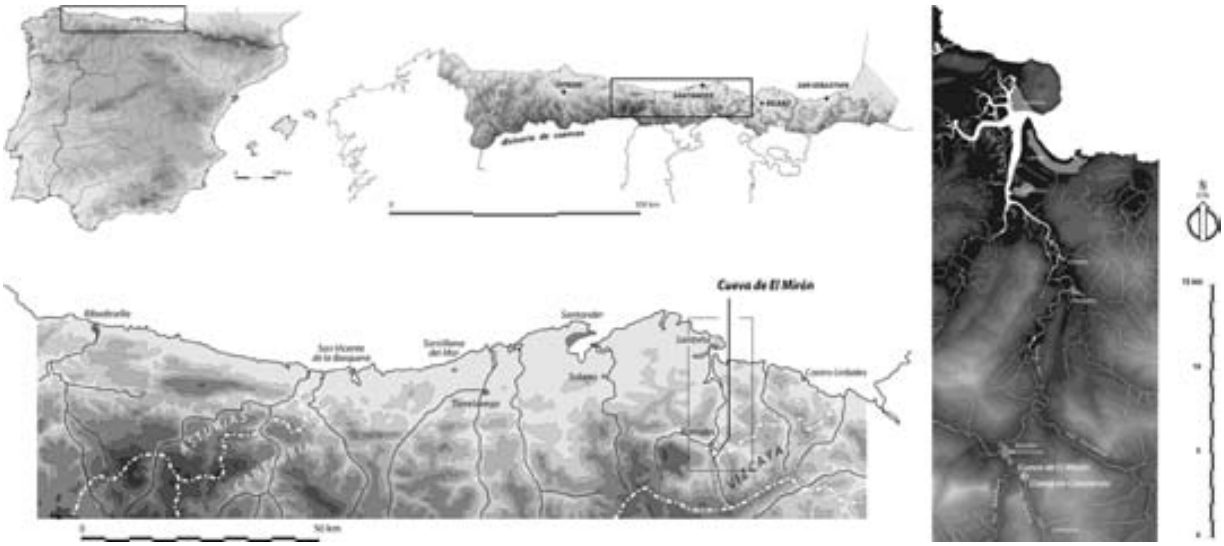

Fig. 4A.1 Geographical location of El Mirón Cave in the Iberian Peninsula (top left. Enlarged detail order: top centre, bottom, and right) (maps by IIIPC).

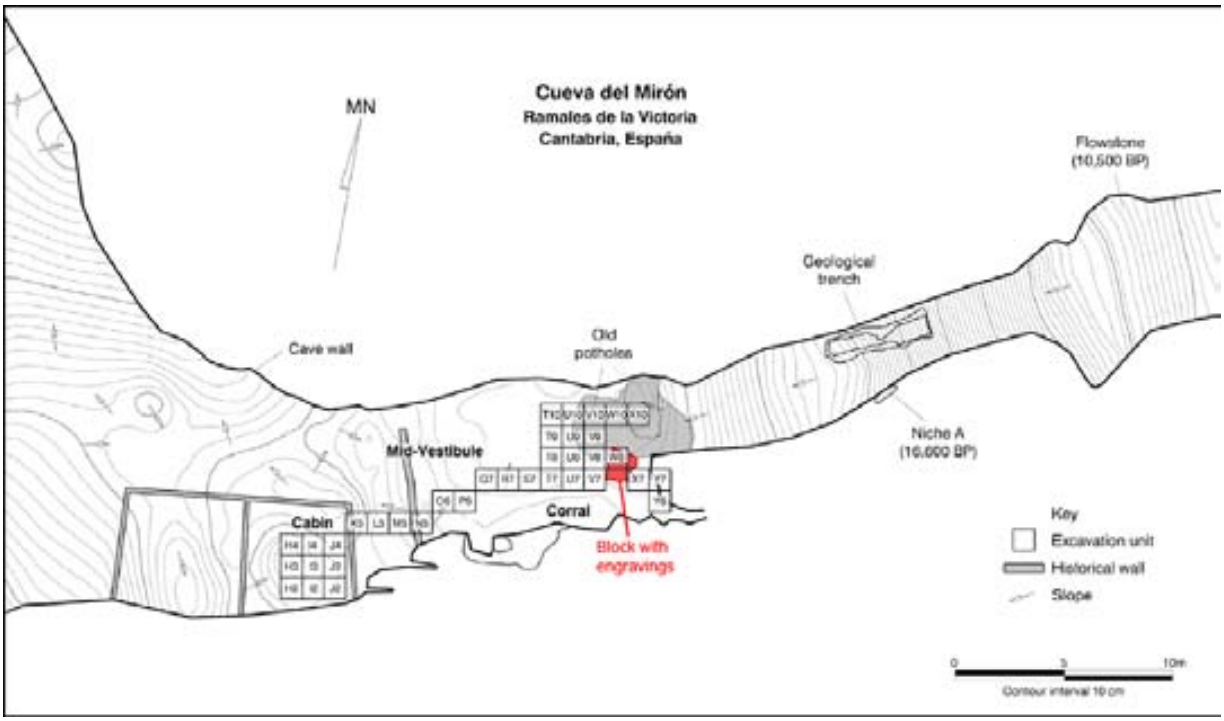

Fig. 4A.2 Topographical map of El Mirón Cave vestibule showing excavation trenches and location of the human burial in square X7, behind the engraved block (Straus et al. 2011).

Fig. 4A.3 Entrance mouth of the cave views: from outside (left), and from inside (right). The red circle indicates the location of the engraved block (photos by Luis Teira).

One of the few large limestone blocks and by far the largest one found during the excavations is the object of the present study, as its western face is decorated with engraved lines and its eastern face is stained with red ochre. The top of this block was visible at the start of the research, though largely buried in goat excrement and mixed sediments. Subsequent excavation revealed it to measure over 1,7 m long on a North-South axis about 1 m wide East-West and about 1 m thick. The northern end of the block had been undercut and possibly damaged by the clandestine digging of a ca. 25 cubic meter pit prior to 1996. Controlled excavation of the sediments immediately to the west of the block (squares V7, V8) revealed that the block had fallen atop Level 110 (as also shown by the southern face of the treasure hunters' pit under the block overhang) and that it has subsequently been covered over by Levels 109-101. This means that the *terminus post quem* for the engravings on the block is the formation of Level 110 which is radiocarbon dated directly under or in the immediate vicinity of the base of the block to 16.520±40 and 16.130±250 (uncal.) BP, respectively, and corresponds to the end of the Initial Cantabrian Magdalenian.

The block had fallen from the cave ceiling at the angle it forms with the rear wall of the vestibule. Its weathered "outer" face (the former ceiling) landed atop Level 110 and the flat inner face that had sheared off along a plane of weakness in the bedrock landed in a position tilted at an angle oriented toward the cave mouth, such that sunlight reaches it at the end of the afternoon in summertime. It was this flat face that was engraved and subsequently covered over by Lower, Middle and Upper Magdalenian layers dated between about 15.000-12.000 (uncal.) BP, and finally by sediments of Holocene age. The Middle and Upper Magdalenian levels provide the *terminus ante quem* dating for the engravings. The eastern face of the block was painted red, apparently in relationship to the secondary burial of ca.100 ochre-stained bones of a young adult human in sediments also impregnated with red ochre rich in hematite crystals during the Cantabrian Lower Magdalenian around 15.600 (uncal.) BP (Straus and González-Morales 2011, 2012). The block predates the deposition of Levels 505 and 504 (the overlying layer with red ochre and most of the human remains). The formation of Levels 505 and then 504 must have been very fast and in the time period between ca. 15.700-15.500 (uncal.) BP, with Level 503.1 being about 15.100 BP.

Fig. 4A.4 Excavation in progress, with the fallen block marked in red (Straus et al. 2011).

The engravings on the smooth, west-facing side of the block are all linear and do not seem to be representative of anything recognizable at the present time. There are two generations of lines: shallow+thin, and deep+wide. By extrapolating the slope of the relevant archaeological levels, it has been deduced that similar linear engravings, as well as a fine engraving of a horse on the rear wall of the vestibule close to the engraved block were probably also executed during the Lower-Middle Magdalenian (García Díez, González-Morales and Straus 2012). Although non-figurative, the engravings on the block are among the most precisely dated yet known for the European Upper Palaeolithic, rivaled only by such sites as Le Placard in west-central France and Ambrosio in southern Spain. The Lower Magdalenian levels in El Mirón (as in other sites of the region) are extremely rich in lithic and bone artefacts, remains of red deer, ibex and salmon, hearths with fire-cracked rocks, personal ornaments such as perforated shells and teeth, and works of portable art, notably red deer scapulae engraved with images of red deer and other ungulates, typical of this period in the central Cantabrian region (González-Morales and Straus 2009, Straus and González-Morales 2012).

Excavations has been authorized (and partially financed) by the Regional Government of Cantabria, and funded by U.S. National Science Foundation, Fundación M. Botín, L.S.B.Leakey Foundation, Ministerio de Educación y Ciencia, National Geographic Society, University of New Mexico, Stone Age Research Fund (Jean and Ray Auel, principal donors), and with material support by the Universidad de Cantabria and the Town of Ramales de la Victoria.

A.2.1 The Question of Rock Engravings

The difficulty in reading and interpreting surfaces with high densities of superimposed engravings – so-called palimpsests (Ripoll 1972) – is that we only have their geometric traces, the form of the lines (Mélard 2010). What gave sense to the act of repeatedly engraving the same space, overlapping marks and, apparently, the annulling of previously drawn motifs, was the fact that the grooves also displayed colour as they were originally made. The trace of each design cut through the surficial patina of the rock being engraved, acting like a coloured pencil. With the passage of time, the grooves would take on a patina like the rest of the rock and

they would become camouflaged. In this sense, the surface once again would become attractive and practical for the engraving of new designs. It is also possible to think that the surface was consciously smeared to wipe out the contrast of different patinas.

With reference to rock engravings, in the best of cases one applied renderings of solar studies or the play of lights and shadows within a geometric digital model (Cassen and Robin 2010). This doesn't mean that it is an inadequate technique. On the contrary, the recreation of the visual experience by means of virtual maps of lights and shadows is a natural means for the understanding of engraved designs. Nevertheless, this strategy is insufficient for resolving the problem of palimpsests of engravings. However, aided by the vast calculation capacities of computers, we can organize new modes of documentation oriented toward the characterization of engraved grooves based on their specific geometry. Of course, we cannot recuperate the original colour, but can help obtain hierarchical images of engraving styles, working processes, evidence of manual habits. This was our goal in doing the experiment with the Magdalenian engravings on the block in El Mirón Cave.

A.3 Framework Implementation

A.3.1 3D Digital Surface Model Generating

Because of the specificities of these engravings, it was important for us to document them with as much detail as possible, in order to detect and analyse details not otherwise possible with conventional tools or with the human eye; for cyclic monitoring and preservation; and for other future researches. Therefore, we decided to use the shortest FOV available for this scanner, the 90 mm set of lenses, which has the highest resolution and gives the maximum level of detail (x,y resolution: 50 µm). However, we also decided to use two other FOV (150 mm and 450 mm) with lower resolution to test their efficiency in this very same context.

There are several technical reasons that can explain the complexity of 3D scanning, namely: general logistics; the relative location, distribution, and type of engravings; ambient light conditions; and hardware-software issues.

A.3.1.1 Workspace, 3D Scanner and Calibration

The access to the cave was not very complicated. We took the national main road to arrive at Mt. Pando. Then, we drove up the all-terrain car through a dirt track for about 300 m. From here, we carried all the equipment – relatively numerous, weighty, and bulky – to the cave along a narrow footpath on the steep cliff for another 125 m.

Regarding power supply, we took a portable electric generator. It was important to place it far away from our workspace, because it easily caused the soil to vibrate and this would consequently affect the reliability of the measurements. As to the scanning ambient light conditions, for better results, capturing data with structured

light scanners should be done in a dark environment – when outdoors, preferably during the night – because the more contrasted the projected and reflected patterns are, the more consistent data we get. In this respect, fabric curtains were provided to prevent the entrance of indirect sunlight on the engraved block's area (Figure 4A.5).

Fig. 4A.5 Preparation of the 3D scanning workspace (photos by Luis Teira).

The entire surface with the engravings was scanned with a 3D structured light scanner: SmartSCAN3D Duo System, Breukmann. Three interchangeable stereo FOV were used: the 90 mm, the 150 mm, and the 450 mm sets of lens. The system's characteristics – according to the manufacturer – have been compiled into Table 4A.1.

Table 4A.1 System characteristics, according to the manufacturer.

	Parameters	FOV 90	FOV 150	FOV 450
Camera	camera type	Basler 102fc		
	camera #	20616138/20616239		
	digitization (x,y) [pixel]	1388x1038		
	camera connection	IEEE 1394		
	pixel size [mm]	0,05	0,09	0,28
	x,y -resolution (interpol.) [µm]	50	90	280
	camera shutter [ms]	1 … 82 (default 10)		
	camera gain [dB]	1 … 10 (default 2,92)		
	camera offset [GV]	0,7 … 15,4 (default 0,7)		
	camera angle [degree]	right: -10º / left: +20º		
	camera aperture [f/number]	(5.6-)8/8(-11)	5.6/5.6	2.8-4/2.8-4
	camera focal distance [mm]	75	50	16
Projector	projector #	1046		
	light source	100 W halogen lamp		
	pattern	SV 25 (25-M15-F3)		
	angle [degree]	0º		
	apperture [f/number]	2-2.8	(2)-2.8	2
	focal distance [mm]	35	25	n.a.
general	weight [kg]	3,8		
	operating distance [mm]	730		
	maximum FOV [mm²]	75x55	116x84	404x296
	depth of measurement volume [mm]	50	70	240

The scanner was connected to a laptop: HP Mobile Workstation - EliteBook 8730w; Intel(R) Core(TM)2 Duo CPU, P8800 @2.66GHz (instead of 2,33 GHz), 3,96 GB RAM (instead of 2 GB RAM), 160 GB hard disk; graphic card NVIDIA 512 MB (instead of Open GL like GeForce 8600GT 256MB); Microsoft Windows XP Professional x64bit Edition, version 2003. The technical procedures for using this 3D scanner model and calibrating the sets of lens are further explained by Breukmann (2009).

In the matter of hardware-software and Operating Systems (OS) issues, at the time the scanner used in this research was acquired Microsoft had already released its Windows 7 OS. However, the scanner's software could only run on Microsoft's Windows XP Professional, i.e. an older OS with all its inherent limitations. Even though finding a laptop (more practical to take to field work) with the minimum requirements, including OS, was not an easy task, we finally managed one with a few superior characteristics.

Calibrating the scanner with the selected set of lenses was necessary, in order to guarantee a sufficient sharpness in the complete measurement volume (Breukmann 2009) and to further process the output data. Thus, this stage was performed prior to scan acquisition. The calibration of each set of lens was executed using the scanner's proprietary software Optocat 2009R1 v.8.00.28-1520, x64 Bit Edition (Breukmann). It took place in the cave's vestibule between squares Q7 and T10, while the 3D scanning workspace was being prepared for timesaving. To proceed with the calibration, the scanners' chest was used to put both controller and laptop, while the calibration cards were placed on a folding table (Figure 4A.6).

Fig. 4A.6 Preparation of the calibration workspace (left), and during calibration work (right) (photos by Luis Teira).

After calibration, only the necessary equipment was moved near to the engraved block, though the number and diversity of cables and individual components connected to the scanner were to some extent a drawback in such a delicate archaeological environment. The already existing scaffold structure and toeboards were now used to place only the strictly necessary equipment.

A.3.1.2 3D Data Acquisition and Post-processing

Due to logistic matters, tight schedule, and hardware constraints, after calibrating the scanner we proceeded only with the point cloud capture and scans pre-alignment in El Mirón Cave to ensure that there weren't any

relevant parts of the engraved block missing, as well as to assess the general quality of the recorded data. The same proprietary software, Optocat, continued to be used. All raw acquisition data was saved at a specified repository, for potential future re-processing (3D-COFORM 2009). The 3D scanning survey was completed in one and a half workday.

It is crucial to have a thorough understanding of the sequential steps, because the final outcome depends intrinsically on all of them. Consequently, each step's parameters must be specifically tailored according to clear objectives previously set.

The overall accuracy of the mesh heavily depends on the 3D data acquisition flow, overlapping areas between patches, number and positions of the single views (Breukmann 2009). The scanning flow consisted in alternating between rows going from left to right and from right to left, and from bottom to top (Figure 4A.7), but it could as well have been done the other way round. The orientation of the 3D model's coordinate system was automatically defined by the view of the first scan of the project. To facilitate the matching procedure and minimize measurement error, the amount of overlapping area between scans was set to approximately one third. Each scan was immediately pre-aligned with the previous point cloud, by selecting at least 3 pairs of corresponding points – $[p_1, p_2, p_3, p_N]$ $[q_1, q_2, q_3, q_N]$; where ideally $N>3$ – and using the Iterative Closest Point algorithm (ICP) (Figure 4A.8). To overcome most of the self-occlusion problems, we used multiple viewing angles during scans, by changing the scanner's position in respect to the engraved surface of the block, and whenever needed by rearranging the toeboards' position (Figure 4A.9). Likewise, it is important to remember that either missing data, noise data, filling holes, filtering and certain parameter's settings during scanning or post-processing may conceal or distort relevant data (Moitinho de Almeida and Barceló 2012), such as engraving grooves. Inasmuch we were only concerned with the geometric data (based on *x*,*y*,*z* coordinates) of the engravings, and the scanner has a low resolution camera (1,4 Megapixel), we decided not to capture any image texture during scanning.

Fig. 4A.7 3D Data acquisition flow: alternation between left-right and right-left rows, and from bottom to top.

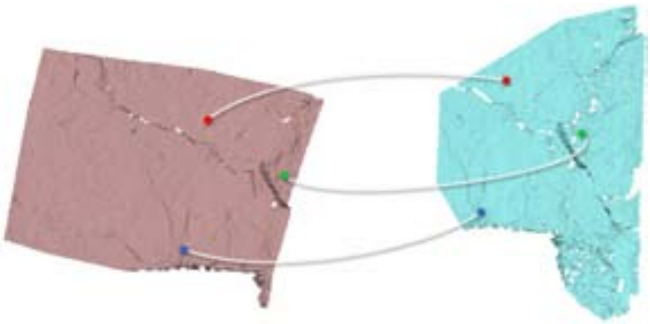

Fig. 4A.8 Pre-alignment of pairwise 3D patches: selection of 3 pairs of corresponding points.

Fig. 4A.9 Using multiple viewing angles during scanning (left and right) (photos by Luis Teira).

Although some of the characteristics of the laptop were above the minimum requirements indicated by the scanner manufacturer, this did not always guarantee a sufficient performance throughout the 3D data acquisition and post-processing stages. The fact that we were often dealing with large amounts of data turned even more difficult for the system to manage and very much time consuming. Therefore, we decided to scan the engraved block with the 90 mm FOV in three separated parts. This set of lenses – which, according to the manufacturer, has a resolution of 50 µm – required a total number of 77 scans. Throughout this process, in view of the fact that the provided fabric curtains didn´t entirely prevent the entrance of indirect sunlight, and the intensity of light entering the cave varied dramatically during the day – sunny to cloudy and rainy day –, the parameters of the scans had to be constantly readjusted and frequently repeated. This problem was only overcome before scanning with the 150 mm and the 450 mm sets of lenses, by darkening the scanning area homogeneously with more curtains. Unfortunately, due to the tight schedule, we were not able to repeat the shortest FOV scans in the 2011 surveying. This work was successfully repeated in the summer of 2012 during the night.

An important factor to take into account is that the higher the FOV, the lower the number of scans needed to cover the entire area (Figure 4A.10). However, the resolution also tends to diminish leading to less fine density 3D meshes. Therefore, as to the 150 mm FOV, it required 26 scans at a resolution of 90 µm, whereas the 450 mm FOV required only 18 scans at a resolution of 280 µm.

Fig. 4A.10 3D Scanning of the engraved surface with FOV: 90 mm (left), and 450 mm (right) (photos by Luis Teira).

After completely capturing the unordered point clouds, it was necessary to post-process the scanned data. This stage was executed later at the Institución Milá y Fontanals, Consejo Superior de Investigaciones Científicas (IMF-CSIC), Barcelona, using the same software. It comprised:

a) Data Cleaning

All evident extraneous and undesired points were manually removed, in particular scanned dust in the air and other surfaces that did not clearly make part of the engraved block.

b) Point Clouds Final Alignment

A concluding semi-automatic fine alignment was performed (ICP; points subsampling: 1/1; convergence: 0). This step took from one minute to half an hour long, depending mainly on the density of the point clouds and the number of scans.

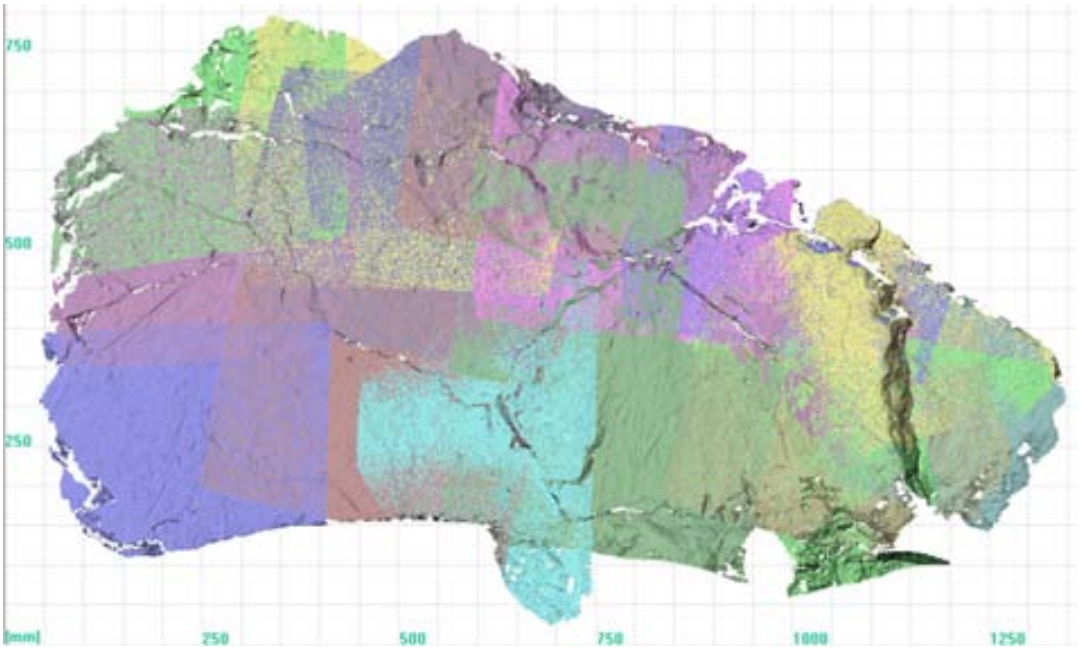

Fig. 4A.11 Point clouds final alignment (450 mm FOV). Each colour represents an individual scan.

c) Scans Merging

The scans were merged using 'maximum reliability' options, and avoiding any type of smooth filtering. At the end of the merging process overlapping areas and similar vertices were semi-automatically removed, data structure was automatically optimized, and vertex normals were automatically calculated. This step took from eight minutes to more than five hours long (after a few failed attempts with the system crashing), depending again mainly on the complexity and number of scans.

All files were completely merged, except for the three individual parts scanned with the 90 mm set of lens which could not be merged together because of insufficient computer resources.

d) Polygonal Mesh Generating

The polygonal mesh was generated without applying any decimation, compression, or filling holes, in order to avoid further data manipulation and keep its authenticity as close as possible to both captured RAW data and real surface of the block.

The 3D digital surface models were then exported in STL file format, in order to carry out geometric feature extraction. Table 4A.2 shows the number of scans captured, and weight (KB) of the aligned (CTR: Optocat's scanning file extension) and merged scans files. The difference between the total number of scans of 2011 and 2012 – 77 and 83, respectively – was due to changes in the scaffold structure and toeboards, which were used to place the scanner in different viewing angle positions.

Table 4A.2 3D digital surface of the engraved block, scanned with stereo FOV: 90 mm, 150 mm, and 450 mm.

FOV stereo		**Number of scans**	**Aligned scans** (*.ctr) (KB)	**Merged scans** (*.stl) (KB)
90 mm (2011)	part1	29	1253809	813933
	part2	31	1310809	848647
	part3	17	656614	415992
90 mm (2012)	part1	30	1239225	768853
	part2	31	1362638	862086
	part3	22	988490	634805
150 mm		26	1126090	769858
450 mm		18	585418	411617

A.3.2 Geometric Information Extraction from 3D Digital Surface Model

As a work in progress, this stage has been carried out at LAQU-UAB and at IMF-CSIC, Barcelona. It consists in using different approaches to extract meaningful data from the 3D surface model, in a way that it can be decoded and understood by the archaeologist. Up to now I have used MeshLab v1.3.0 (Visual Computing Lab, ISTI-CNR) and Rapidform XO Scan 2010 (formerly INUS Technology, now 3D Systems), to take the opportunity to compare as end user some of the tools efficiency and output data. The former is a free-ware and open-source software widely used in 3D digital cultural heritage context, among others, whereas the latter – which had already been acquired – is a proprietary software mainly used in the various fields of engineering. This section focuses on a small area of the engraved block, because of the large concentration and visible variety of grooves herein (Figure 4A.12).

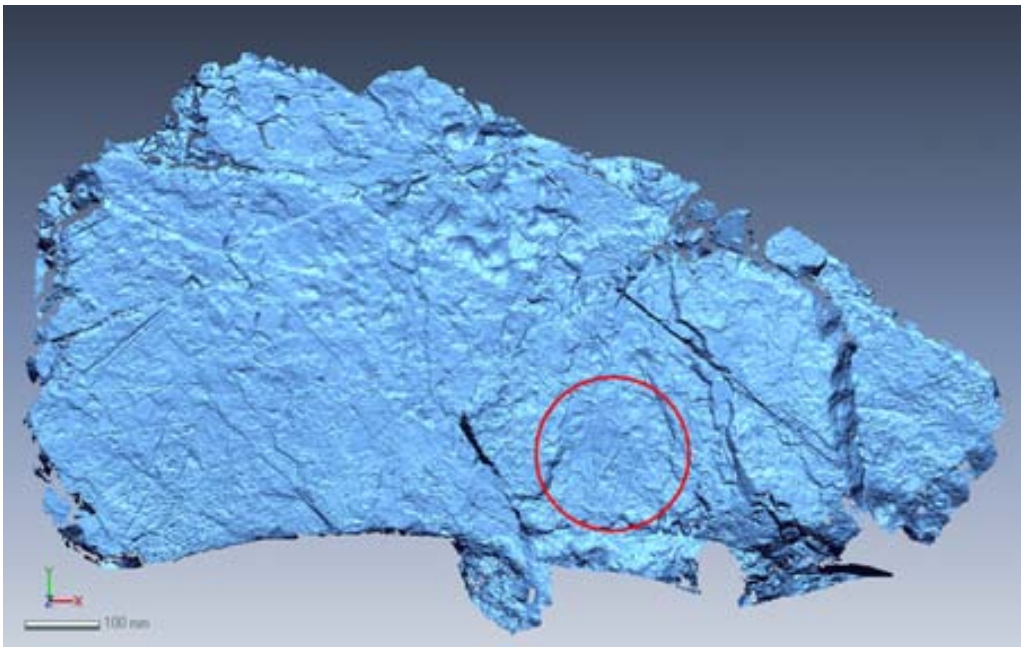

Fig. 4A.12 3D Digital surface model of the engraved block, scanned with the 450 mm FOV. Studied area [1] marked in red.

A visual inspection on the data set was conducted. As expected, the instability of ambient light in 2011 during 3D data acquisition (90 mm FOV) had inevitably caused noise data (Figure 4A.13) – which lead to erroneous data, causing lack of data consistency in some areas of the engraved surface. As earlier mentioned, in 2012 we returned to El Mirón to repeat the scanning of the engraved block with the 90 mm FOV, these are the good data that I am now working with.

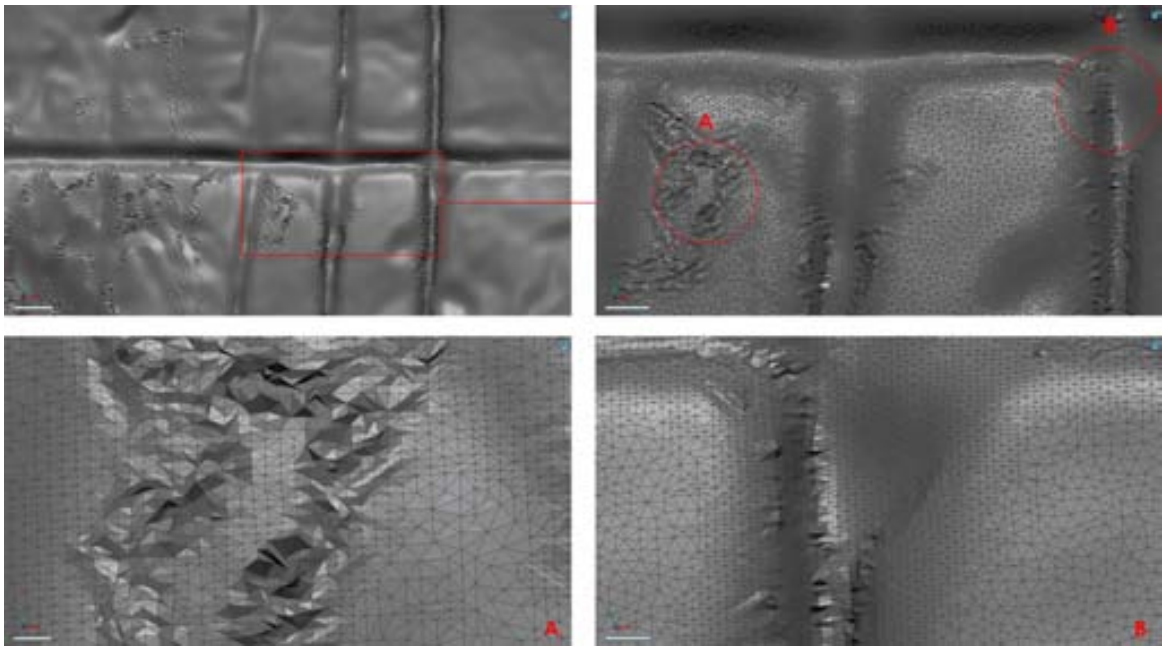

Fig. 4A.13 3D Digital surface model of the engraved block (90 mm FOV, 2011): noise data due to instability in light conditions during 3D scanning.

A.3.2.1 FOV Comparison

This stage consisted in comparing the overall performance between the 90 mm, 150 mm, and 450 mm field of view, to thereafter be able to assess their range of applicability, i.e., the required level of detail to be used in other similar engravings. It comprised the analysis of curvature, mesh deviation, and profiles.

Curvature analysis enabled to semi-automatically enhance subtle grooves and detect small features by using comparisons (i.e., bending energy measure) to the surrounding surface. Although MeshLab also permits to analyse curvature angles of the surface in a semi-automatic way, I chose to use Rapidform only because its tool seemed more efficient. Since each FOV determines the resolution of the captured geometries of the micro topography, I had to change the parameters of the maximum curvature (with allowable value hidden) until I got best results for an efficient analysis – 90 mm FOV: maximum curvature -0,1/0,1; 150 mm FOV: -0,3/0,3; 450 mm FOV: maximum curvature -0,1/0,1 – (Figure 4A.14). The colourmap is from red (convex) to blue (concave), corresponding to high to low values of the curvedness, whereas grey colour indicates planar patches.

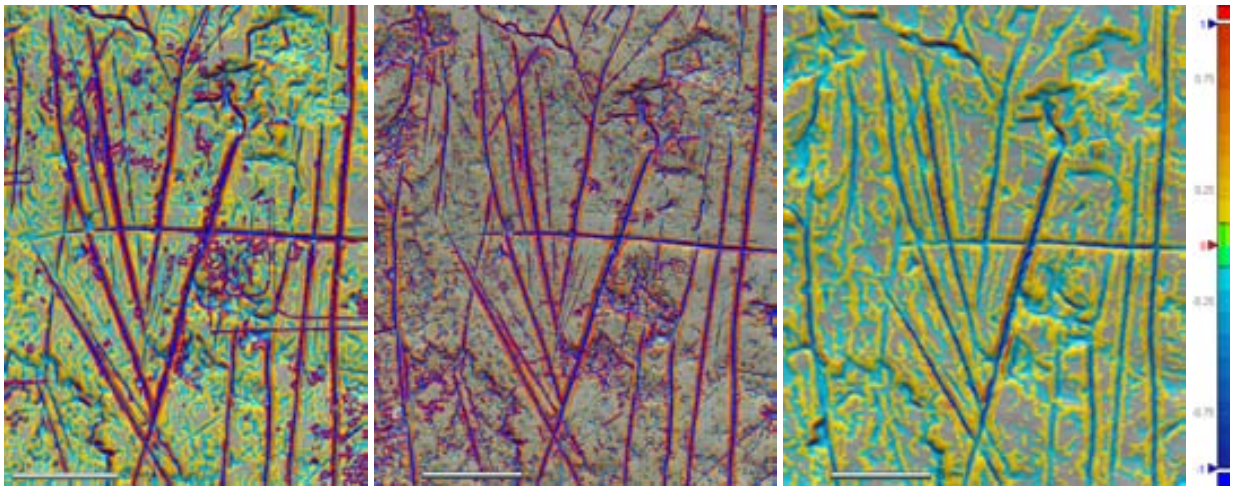

Fig. 4A.14 Curvature analysis of studied area [1] of the 3D digital surface model's micro topography. 90 mm FOV (2011): maximum curvature -0,1/0,1 with allowable value hidden (left). 150 mm FOV: maximum curvature -0,3/0,3 with allowable value hidden (centre). 450 mm FOV: maximum curvature -0,1/0,1 with allowable value hidden (right).

Figure 4A.15 shows the area used to proceed with the analysis of mesh deviation between the three FOV. The surface area scanned with the 90 mm FOV was used as reference model to semi-automatically align the other two models – the sampling ratio was set to 1/1, and the maximum average deviation allowed is 0,001 mm. The colourmaps in Figure 4A.16 (left) display the maximum deviation between meshes – the allowable tolerance was set between -0,001 mm and 0,001 mm with allowable value hidden. The histograms in Figure 4A.16 (right) indicate: average deviation between the 90 mm and 150 mm FOV meshes is 0,0005 mm, where 76,3% of the total deviation stands between -0,0287 mm and 0,0296 mm; average deviation between 90-450 mm FOV meshes is 0,0084 mm, where 78,79% of the total mesh deviation stands between -0,0624 mm and 0,0791 mm; average deviation between 150-450 mm FOV meshes is 0,0086 mm, where 76,23% of the total mesh deviation stands between -0,0483 mm and 0,0654 mm. This is to say, as expected the 90-150 mm FOV meshes showed to have the lowest deviation, followed by the 90-450 mm and 150-450 mm FOV meshes.

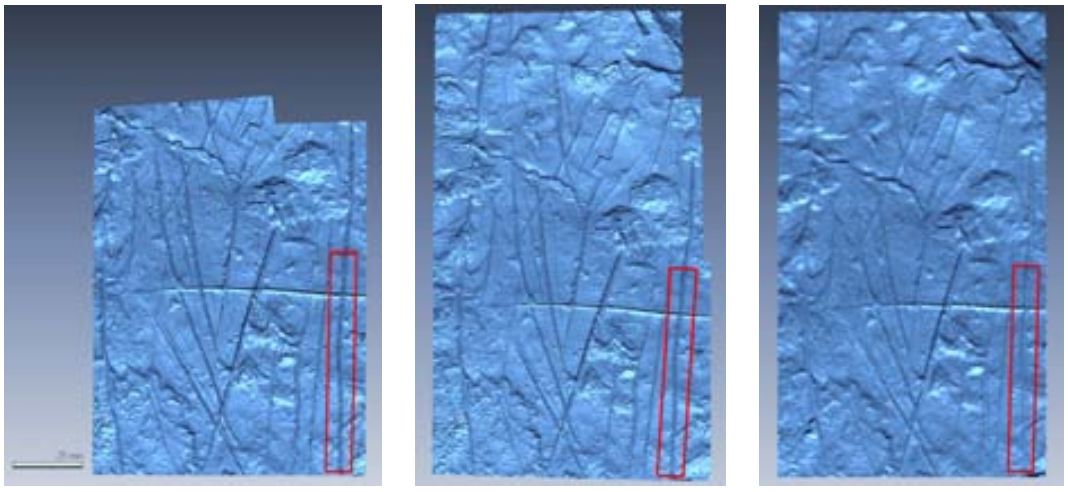

Fig. 4A.15 Detail of the surface area, scanned with the 90 mm (left), 150 mm (centre), and 450 mm (right) FOV. Studied area [2] marked in red.

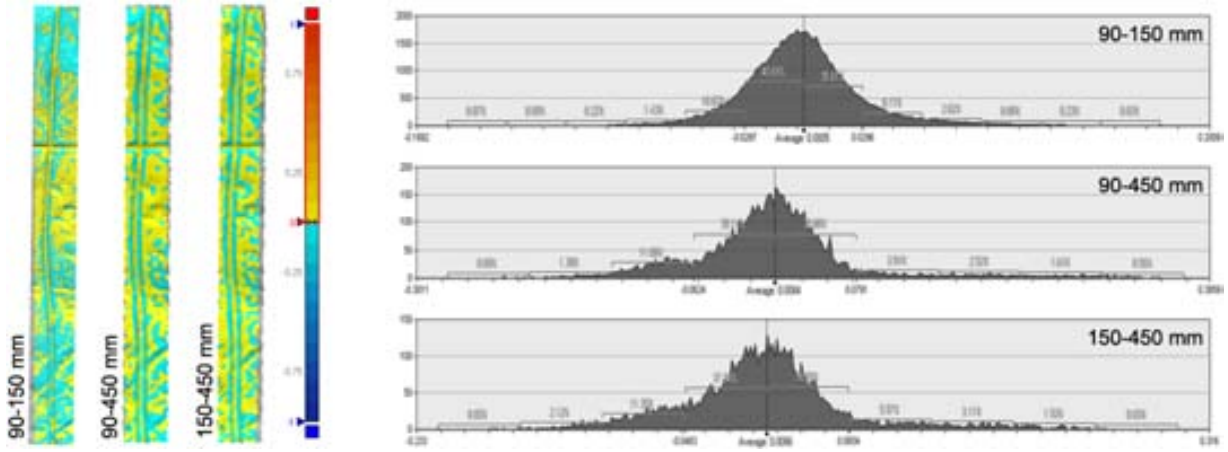

Fig. 4A.16 Colourmaps (left) and histograms (right) of the mesh deviation between the 3D digital surface models of study area [2], scanned with the 90 mm, 150 mm, and 450 mm FOV.

The vertical groove from studied area [2] was selected in order to proceed with a comparison between groove profiles. The extraction of profiles was made by means of automatic multi-slice technique (Figure 4A.17) – five parallel equal cross-sections, perpendicular to a plane tangent to the upper surface and starting from the same aligned position. The sampled profiles of each FOV were then overlapped and positioned (Figure 4A.18), in order to be able to proceed with further analysis of the morphological data, as well as typological classification and quantitative comparisons (Karasik and Smilansky 2008).

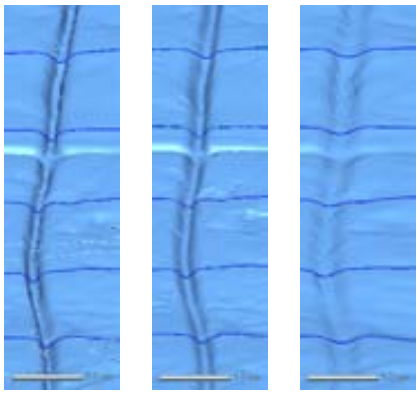

Fig. 4A.17 3D Digital surface models of the selected engraved groove. Five equal cross-section analysis was performed for each selected groove, in order to compute the average section. In dark blue: 90 mm (left), 150 mm (centre), and 450 mm (right).

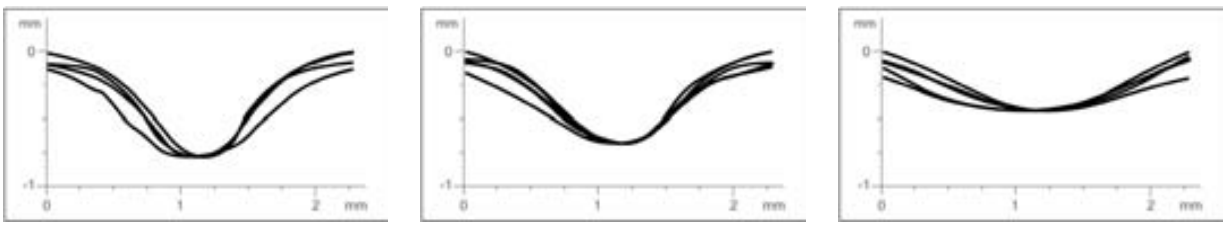

Fig. 4A.18 Groove engraving morphology. Overlap of the positioned five profiles: 90 mm (left), 150 mm (centre), and 450 mm (right) (Moitinho de Almeida et al. 2012d). The topographic information is represented as a height function Z(x,y) of two independent variables (x, y). The height function is developed by juxtaposing a set of parallel profiles.

When comparing the 90 mm FOV scans with both 150 mm and 450 mm FOV it seems clear that this set of lenses permits the capture of engraved stroke morphology more efficiently, accurately (sub-milimetric), and objectively, in a way that suits best our purposes.

The 150 mm set of lenses appears to have captured efficiently most of the surface irregularities that were also acquired with the 90 mm one. Nevertheless, it is possible to perceive that the groove's morphology becomes wider, smoother, shallower and less sharp. This can be a problem when characterizing and analysing engraving groove families at certain scales, especially if the differences between some of the stroke morphologies are subtle.

The 450 mm set of lenses proved to be not suitable at all for this specific study, when compared with both 90 mm and 150 mm sets of lenses. On one hand, it is obvious the inefficiency in capturing the overall irregularities of the surface – some of the strokes were not even captured. On the other hand, the inaccuracy of a groove's morphology is evident, as it becomes even wider, smoother, shallower and less sharp, in a way that it becomes almost impossible to distinguish one stroke from another, and thus proceed with further geometric comparisons.

A.3.2.2 Further analysis of the grooves

A full morphological analysis of study area [1] has not yet been accomplished, because it is very much time consuming and beyond the scope of this thesis. Notwithstanding, preliminary results are herein presented.

During the visual inspection aforementioned I used a basic approach based on moveable virtual light sources to reveal the grooves and highlights details in greater relief (Figure 4A.19), for an initial understanding of the overall design, engraving techniques and tool signatures (EH 2010).

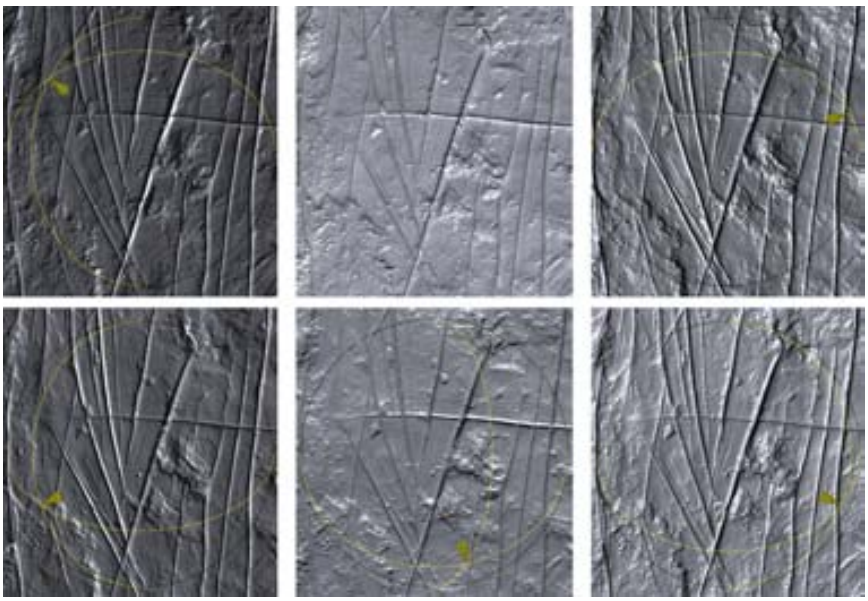

Fig. 4A.19 Maps of light and shadow of study area [1] (150 mm FOV).

Besides the visual information available from the front view of the model, the reverse side may sometimes provide further qualitative information, making possible to observe details not otherwise possible with the real engraving surface. Another basic approach which revealed to be useful when drawing a strategy for extracting groove profiles (to thereafter be able to measure and quantify them), in the sense that it also allowed me to perceive some strokes' discontinuities or irregularities. By way of illustration, Figure 4A.20 shows front and back views of a detail from the selected area where the overlapping of carvings is well visible. The strokes appear here randomly numbered from 1 to 5, and the intersection areas labelled from A to C.

- Strokes 1 and 2: appear to be nearly parallel and have discontinuous paths. The depth of these two strokes is markedly less pronounced than that of stroke 5 in intersection area A. This area shows slight changes in the trajectories of both strokes after they intersect the transversal one, which is a common technical occurrence when carving or etching. The lower part of stroke 2 (i.e., below stroke 5) is shorter and shallower than the upper part. On the contrary, the upper part of stroke 2 (i.e., above stroke 5) is shorter and shallower than the lower part. Could this possibly indicate an intent on giving continuity to what would have been an 'unfinished stroke'? The visual comparison between these two strokes raised the working hypothesis of a conceptual frame in the engraving planning. Yet, two strokes are definitely not enough and this hypothesis will have to be properly tested and grounded.
- Stroke 3: appears to have a continuous path. This stroke is less deep than stroke 5 in B. It is interesting to note that the upper part of this groove is more irregular than the lower part. This could be explained by: although the path is continuous, its intersection with stroke 5 caused an abrupt alteration in the carving tool (e.g., slight fragmentation), or a change in gesture or force. Or none of these, it was just caused by natural irregularities of the stone's surface or material composition, among other possibilities.
- Stroke 4: appears to have a deep and discontinuous path. C shows a slight change in trajectory of stroke 4 after it intersects the transversal stroke.
- Stroke 5: appears to have a deep and continuous path. The visual comparison between the five strokes suggests that this transversal stroke was carved before the other four strokes, and in a single movement.

However, the fact that an intersecting groove is deeper than others does not necessarily mean that the former was carved first, instead it may for instance indicate that a higher pressure was applied while carving or another tool was used. Likewise, the diversity in groove profiles may not necessarily indicate distinct tools or toolpoints, instead it may suggest the blunting or sharpening (or any other altering procedure) of the tool point, using another face of a toolpoint that has an irregular form, variation in force applied, change in position of the body/arm, different 'artist'/skills, variation in stone composition, or erosion, among other possibilities – as I will demonstrate next. Again, these are merely working hypothesis. As such, they must be interpreted with much caution since they rely exclusively on visual observation.

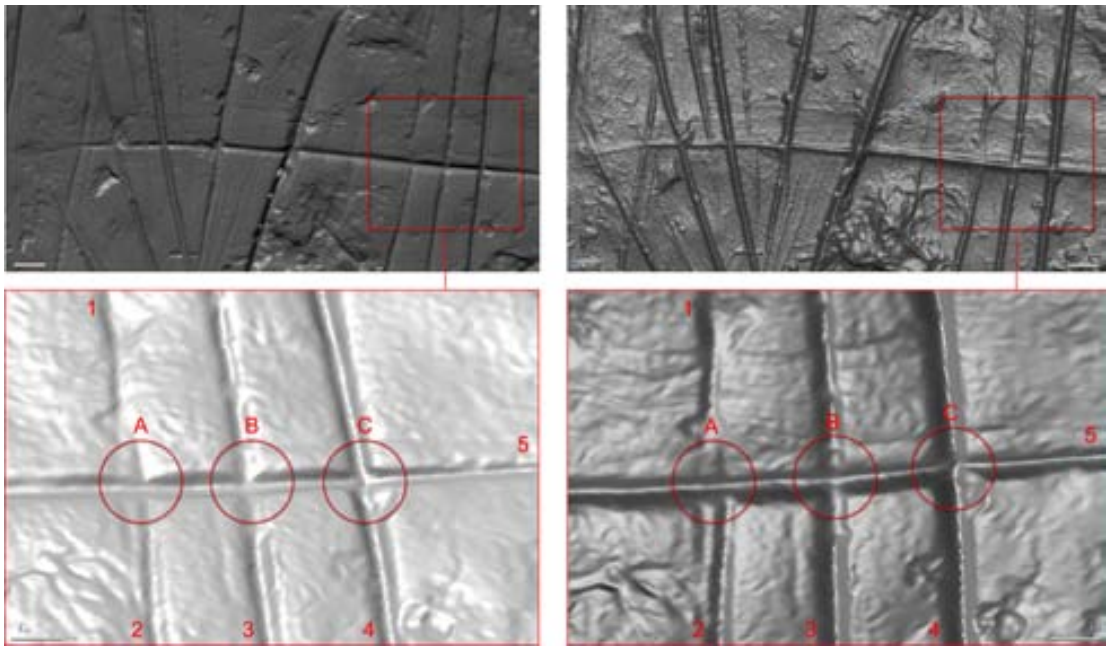

Fig. 4A.20 Front (top and bottom left) and back (top and bottom right) views (150 mm FOV) of the 3D digital surface model with visible overlapping grooves. Detail of strokes overlapping (bottom) – the models are reoriented for higher readability.

The following approach is based on the 2D profile surface texture standard ISO 25178-2:2012, using the 3D digital surface model captured in 2012 with the 90 mm FOV.

Figure 4A.21 displays a selected sequence of profiles from a set of grooves along carved paths, showing a pattern on the shapes of most profiles, yet a clear variability in their depths. This may suggest that different forces were applied with the tool.

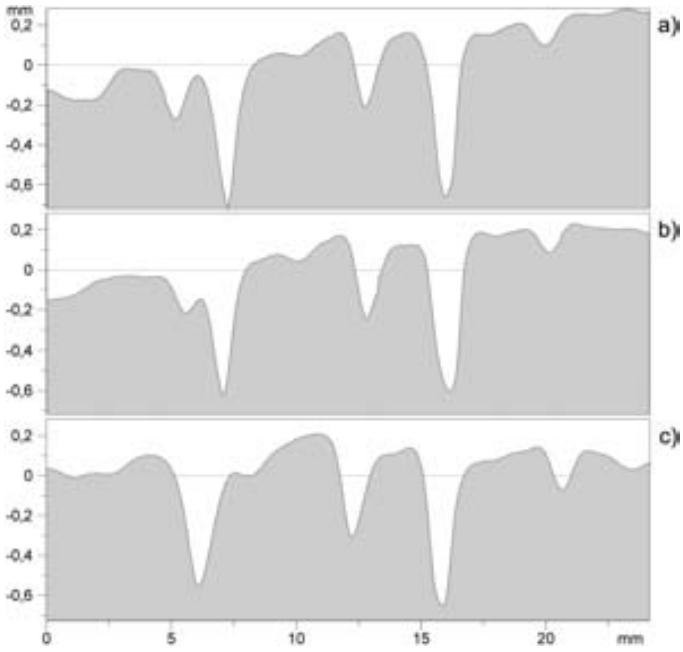

Fig. 4A.21 Profile sequence from a set of grooves showing geometric variability along the carved paths (90 mm FOV).

Whereas Figure 4A.22 displays a higher scale of analysis (μm) with a profile sequence from one single groove – from near one of it extremities (a) towards the centre (f) –, where the individual variability is much more evident, despite the natural irregularities of the engraved block surface. The extremity's profile (a) is wider, smoother, shallower and less sharp. Then, as the profile moves towards the centre of the groove it tends to become narrower, deeper and sharper, until it reaches a 'stable' level, which suggests some stability on the force applied with the tool. However, variations in the profile's shape continue to take place (e), which in turn may for instance suggest variations in orientation of working movement, faces of the toolpoint now being used for carving, surface irregularities or variation in stone composition, or even skills issues.

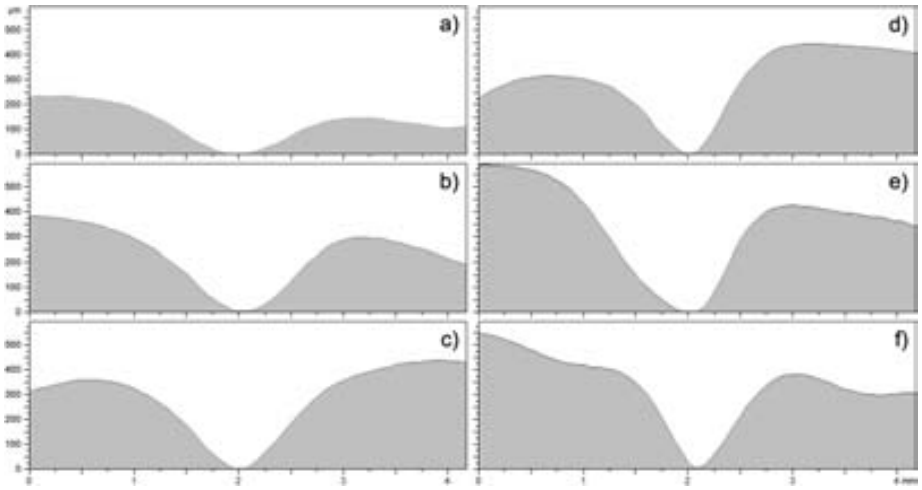

Fig. 4A.22 Profile sequence from a same groove showing geometric variability along the carved path (90 mm FOV).

A.4 Conclusions

The study of the engravings's morphology through 3D scanning is primarily dependent on the level of detail of the captured 3D data. The 450 mm FOV proved to be not suitable at all for this specific study. Even though both recordings with 90 mm and the 150 mm FOV allowed to identify previously unknown carvings, as expected the former showed even more details. Therefore, the results of the 90 mm FOV clearly demonstrated that this set of lenses permits the capture of engraved stroke morphology more efficiently, with a higher level of detail, and objectively, in a way that suits best our purposes.

Visual inspection, and specially semi-automatic curvature analysis and profiles extraction of the 3D digital surface models have permitted to detect many more grooves and start to analyse subtle features not otherwise possible with the real engraving surface, conventional tools, or with the human eye. Hitherto these preliminary results seem promising, in that they are contributing to the geometric characterization of the signatures of engraving mechanisms, therefore allowing the development of a series of working hypotheses on possible types of engraving tools and techniques. Nevertheless – as I have demonstrated – it all starts with good quality high resolution scan data, otherwise these digital tools will not be of any help for this kind of analysis.

The scanning procedures used in El Mirón had the potential to stand alone in the provision of reference values for the type of study in question (BAM 2001). Hence, they were used as reference procedures in the next two case studies, as well as in other subsequent projects, which allowed me to validate routine procedures for the same type of tasks. For several different reasons, the most challenging 3D scanning projects – besides the ones presented in this thesis – took place in Peña Lostroso (Bronze Age) and in La Garma Cave (both in Cantabria, Spain), where I was fortunate to work again with Luis Teira and now also with Marian Cueto (IIIPC-UC). It is worth mentioning that La Garma Cave is registered by UNESCO on the same World Heritage List of Cave of Altamira and Paleolithic Cave Art of Northern Spain.

As a work in progress, there is still much work ahead. A full morphological analysis of the engraving block has not been yet accomplished, because it is time consuming and labour intensive, and clearly beyond the scope of this thesis. Hence, currently I am continuing to isolate the strokes and to extract the profiles for equal sections of each of the engraved groove of the selected area – from the 3D digital surface model captured in 2012 with 90 mm FOV. Later, I will extend this to the entire engraved block. As part of the procedure, profile measurements are continuing to be taken following the surface texture standards ASME B46.1-2009 (ASME 2010) and ISO 25178 (ISO 2012). Additional volume and areal texture measurements are also being taken, namely to detect and analyse possible internal micro-striations along the grooves, which may allow to determine the direction of the carving movement and the evolution of tool wear. The next step will consist in statistically try to group the strokes into clusters. In the end, I aim to distinguish different types of strokes, determine carving sequences, attempt to isolate the motifs, and suggest possible types of engraving tools.

In order to delve further into such complex and challenging issues through three-dimensional digital surface analysis, future work may include: comparing 3D data of the grooves within the engraved block and between other rupestral engravings from the same cave; and correlate them with possible types of engraving tools (e.g., sharp flakes, blades, and burins) discovered at El Mirón.

Ø4-B
Serra del Mas Bonet, Catalonia

B.1 Problem Statement & Objectives

The construction of a large railway infrastructure in 2008 led to the discovery of a prehistoric settlement in the Serra del Mas Bonet, in the Catalan region of Alt Empordà. During the fieldworks numerous negative structures of various functions and types were documented, as well as a broad diachrony ranging from the 5th to the 2nd millennium cal BC. The best represented occupation phase is the late Neolithic (late 4th millennium cal BC), characterized by different negative structures, as well as a good preservation of its deposits. The most unique and unparalleled known finds of such deposits are a set of stelae with carved horns on blocks of sandstone.

The aim of this case study is to be able to provide meaningful information towards a better comprehension of the manufacturing procedures used by the craftsperson on this set of stelae, by:

- Describing quantitatively different types of geometrical features of the stelae and lithic tools;
- Differentiating morphologies within stelae and lithic tools;
- Associating the observed macro traces with possible gestures, carving techniques and used tools. This approach is based both on formal (experimental replicas) and 3D digital analysis. The objective is to test hypothesis concerning the manufacturing procedures used by a craftsperson to sculpt a stelae, by experimentally replicating tools and archaeological surfaces. The best-preserved stela

(SMB/08 E-17/5/958) was chosen as an optimal test case, because it retains a large amount of macro-traces, and its finding is associated to fragments resulting from the configuration of is preform as well as to some lithic tools.

This second case study is organized as follows. It starts with an archaeological contextualization of the Neolithic stelae with horns from the Serra del Mas Bonet. Then, an experimental physical work was performed, consisting in the replication of part of stela SMB/08 E-17/5/958 by applying possible manufacturing procedures. Next, the framework is set up, in which the experimental objects and surfaces are included. After that, results are presented to demonstrate the practical interest of the used methods, tools, and techniques. Finally, a conclusion is given.

B.2 Archaeological Contextualization

The construction of a large railway infrastructure in 2008 led to the discovery of a prehistoric settlement in the Serra del Mas Bonet, Vilafant (Alt Empordà), province of Girona, autonomous community of Catalonia, Spain. This open-air settlement is located along the western and southern slopes of a small hill (±75 m altitude) which gives its name, and enjoys a privileged view over the fertile plain of Empordà. About 500 meters west, the river Manol, the largest tributary of the Muga, waters the Serra del Mas Bonet. The local geology lies on a Pliocene NPg formation made up of alternating layers of gravel, arkosic sands, silts and clays. The Serra del Mas Bonet is near the megalithic area of Albera, Rodes Sierra, and Cape Creus (Rosillo et al. 2010).

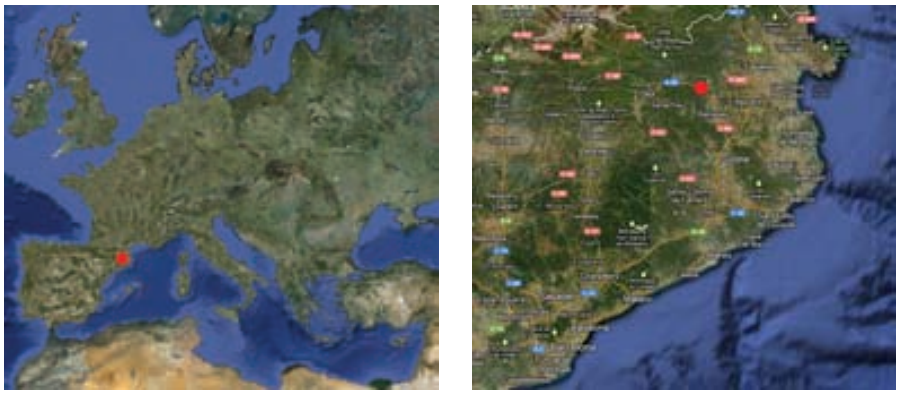

Fig. 4B.1 Geographical location of the Serra del Mas Bonet in Europe (left), and in the autonomous community of Catalonia (right) (maps by Google).

During archaeological fieldwork, 141 negative structures of various functions and types - cabins, silos, post holes, ditches, combustion, among others - were excavated in an extension of 2,5 ha, and documented. These structures span a broad diachrony ranging from the 5th to the 2nd millennium cal BC.

Fig. 4B.2 Panoramic photograph, facing north, of the site during the construction works of the railway infrastructure (photo by Rafel Rosillo, Arqueolític).

The best represented occupation phase corresponds to the late Neolithic Veraza culture – dating from late 4th to early 3rd millennium cal BC –, characterized by different negative structures, as well as a good preservation of its deposits, namely: pottery, fauna, malacological ornaments, bone punches, and lithics (flint blades, mortars and pestles, etc); one menhir (SMB/08 E-17/8/943), 2 complete stelae (SMB/08 E-17/5/958, SMB/08 E-52/1/22), and 4 fragments of stelae (SMB/08 E-1/3/956, SMB/08 E-48/1/45, SMB-08 E-185/2/5, SMB/08 E-1/3/957). But the most unique and unparalleled known finds of such deposits are the set of stelae with carved horns on blocks of fine or medium-grained sandstone – an unprecedented element of megalithic art within the Empordà, where the zoomorphic figures were hitherto unknown (Rosillo et al. 2010).

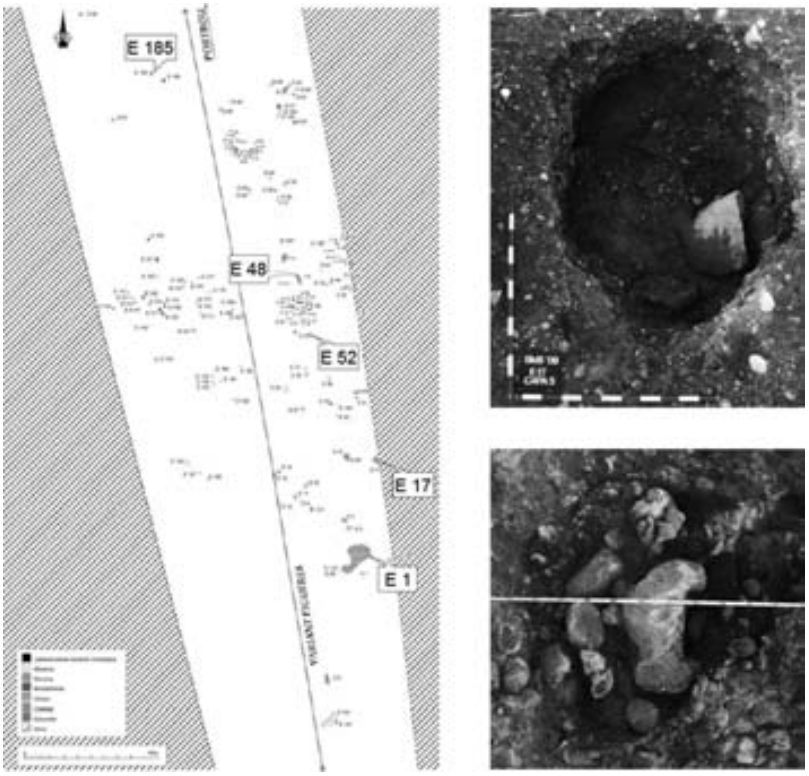

Fig. 4B.3 Plan of the Serra del Mas Bonet excavation showing location of the negative structures where the menhir and the stelae were deposited (left). Photographs of structures E17 (top right) and E52 (bottom right), with fragments of stela SMB/08 E-17/5/958 and stela SMB/08 E-52/1/22 deposited, respectively (Rosillo et al. 2010).

Fig. 4B.4 Menhir SMB/08 E-17/8/943 (left), fragments 'b' and 'a' of stela SMB/08 E-17/5/958 (top left), stela SMB/08 E-52/1/22 (top centre), fragment SMB/08 E-1/3/956 (top right), fragment SMB/08 E-48/1/45 (bottom left), fragment SMB-08 E-185/2/5 (bottom centre), fragment SMB/08 E-1/3/957 (bottom right) (Rosillo et al. 2013).

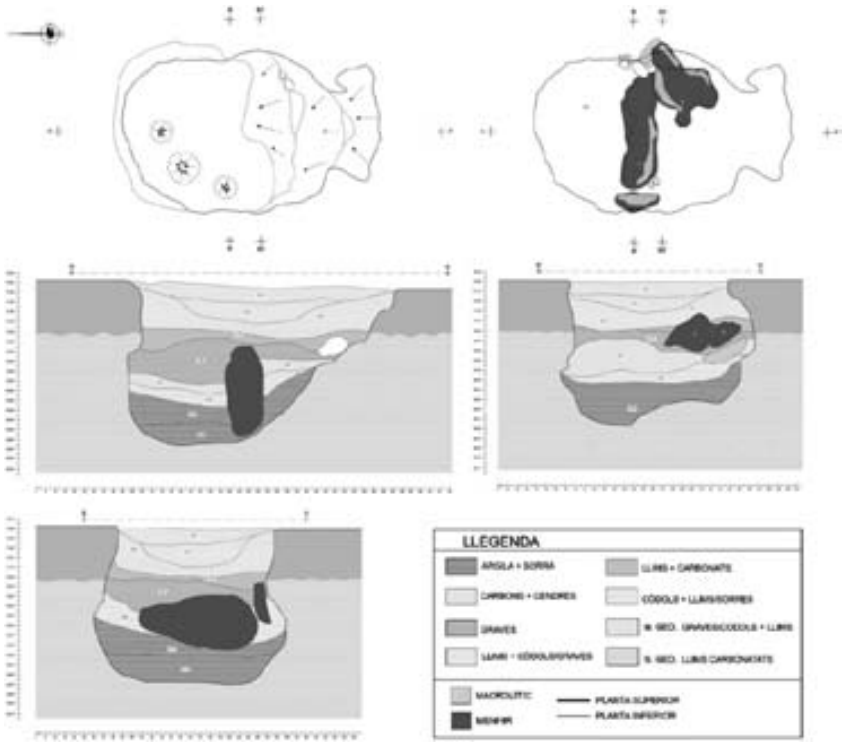

Fig. 4B.5 Plan and profiles of structure E17 (Rosillo et al. 2010).

These stelae display several technological marks, which have enabled to generate hypotheses about used tools and manufacturing procedures. Moreover, a number of lithic tools associated with the stelae have been recovered that could produce evidence to different manufacturing stages (Rosillo et al. 2013).

B.3 Framework Implementation

B.3.1 Experimental Replication of Archaeological Surfaces

The experimental work (Ingersoll et al. 1997, Terradas and Clemente 2001, Baena and Terradas 2005, Baena 2010, Palomo 2012) described in this section was entirely conducted by Antoni Palomo (UAB, Arqueolític) and Rafel Rosillo. The objective was to test hypothesis concerning the manufacturing procedures used by a craftsperson to sculpt the stelae, by experimentally replicating tools and archaeological surfaces.

Stela SMB/08 E-17/5/958 (hereinafter referred to as "stela E17") was carved from a solid block of fine-grained sandstone and whitish colour. It appeared broken in two pieces (E17a and E17b) and associated with another large fragment (E17c), product of an early stage of the block's reduction sequence. The stela shows a pair of protuberances, each one shaped at each end of the upper and wider areas, and partially separated from the body by a deep carved plane and two grooves (Rosillo et al. 2013).

After performing a visual inspection on stela E17, selected blocks of sandstone coming from the same bedrock were used to manufacture experimental replicas (Figure 4B.6, Table 4B.1) of:

- Six surface textures present in the stela, which were labelled from E_s1 to E_s6;
- Approximately half a stela, which included half body and one protuberance. In this case, the objective was twofold: (i) to continue testing different processes, tools, and gestures; (ii) to perceive the amount of effort a craftsperson could have put into making one of these medium-sized sculptures.

As for the experimental lithic tools – labelled from L1 to L4 –, these were replicated from limestone and quartz pebbles coming from the river Manol, which is very close to this prehistoric settlement. Even though copper is not present in the archaeological record, the stelae's chronological context allowed this possibility. Therefore, copper punches were also included as tools in this experimental work.

Fig. 4B.6 Experimental replication of archaeological surface textures. From left to right: original block of sandstone, experimental lithics L1 and L2, manufacture of surface textures 1, 2, and 3 (top); Original block of sandstone, experimental copper punches, manufacture of surface texture 4 (centre); Original block of sandstone, experimental lithic, manufacture of surface textures 5, and 6 (bottom) (photos by Rafel Rosillo and Antoni Palomo).

Table 4B.1 Qualitative description of the experimental replication of archaeological surface textures: identification of experimental surfaces and tools, type of tool used and applied technique; visual inspection of approximate movement direction of both hand and tool towards the experimental surface, amount of removed surface area, and type of produced surface. Comparisons made between surfaces: (*) E_s1, E_s2, E_s3, and E_s4; (**) E_s5 and E_s6.

Exp. surface	Exp. tool	Tool type and technique	Direction of movement (approximate angle)	Removed surface area	Produced type of surface
E_s1	lithics L1, L2	chopper used as hammerstone, and hammerstone; pitting	perpendicular (90º)	small and precise; efficient for details (*)	coarse (*)
E_s2	lithics L1, L2	chopper used as hammerstone, and hammerstone; pitting	tangential (20º-45º)	larger and less precise; efficient for general reduction (*)	coarser (*)
E_s3	lithics L1, L2	chopper used as hammerstone, and hammerstone; pitting	perpendicular (90º) + tangential (20º, superficially)	intermediate (with respect to E_s1 and E_s2)	intermediate (with respect to E_s1 and E_s2)
E_s4	copper	punches; pitting	perpendicular (90º) + tangential (20º, dragged movement)	smaller, more precise and quick; more efficient for details (*)	coarsest (*)
E_s5	lithic L2	hammerstone; incision through pitting	perpendicular (90º)	small and precise (**)	coarser (similar to E_s1) (**)
E_s6	lithic L2	hammerstone; incision through pitting and abrasion	perpendicular (90º) + longitudinal abrasion in both directions	small and precise + small (**)	coarse with longitudinal smoothness (groove) (**)

Lithics L3 and L4 were used as hammerstones on a fine block of sandstone, which got fragmented into pieces immediately after the first hammerings.

The work of replication of approximately half a stela comprised the following sequence:

1. Trapezoidal shaping of the volume using direct percussion tools (hammerstone and chopper used as hammerstone) harder than sandstone (limestone, basalt and quartz), by making major withdrawals. The rectangular morphology of the initial block of sandstone made this trapezoidal configuration easier.
3. Reduction through pitting. The coarse surface was produced by using a uniface (L1), which proved to be much more efficient (i.e., more precise, removed larger areas, the work required less effort and less time) than the hammerstone without configured edges.
4. Configuration of the protuberance and cutout through pitting. The incisions were made by using a uniface.
5. Attainment of the volume's longitudinal groove through pitting and bushhamering with a hammerstone. Finish produced by abrasion (i.e., longitudinal motion with friction) with the same tool.

At this stage, the possibility of using indirect percussion with copper punches was ruled out. On the one hand, the resulting traces seemed to be much deeper than the archaeological ones. On the other hand, the efficiency was lower when compared with the chopper's edges. The combination of the described techniques and stone tools would allow a craftsperson to manufacture a stela similar to the one analysed in approximately one working day.

Hitherto, both surface texture and finishing were controlled by the naked eye. Yet, there are certain limitations involved in such a visual evaluation in that the eye can be at times 'fooled' (Uddeholm 2004) – as I will demonstrate in section *B.3.3.2.2.2 3D Digital Areal Surface Texture Parameters: ISO 25178-2*, when measuring the directions of the surface textures with 3D digital surface metrology software.

B.3.2 3D Digital Surface Model Generating

The archaeological objects of this research initially included: one menhir, two stelae, four fragments of possible stelae, and a total of twenty-four lithics that were contained in the same structures of the stelae. Regarding to the lithics, eleven were not scanned, therefore could not be included in the current study. As to the experimental objects referred in the previous section, all were scanned and included.

All measurement procedures were the same within each stage and step of the framework: from 3D data acquisition, to geometric features extraction.

B.3.2.1 Workspace, 3D Scanner and Calibration

All archaeological objects were 3D scanned indoors at Arqueolític, in a large passage room where the light was controlled most of the time. The experimental objects were all 3D scanned indoors at IMF-CSIC, in a fully controlled dark environment.

The same non-contact close-range 3D structured light scanner, computer, and software, described in the previous case study, were used to capture the 3D digital surfaces of both archaeological and experimental objects. The scanner was calibrated at Arqueolític and again at IMF-CSIC, with the below mentioned set of lens.

As already stated, there are several technical reasons that can explain the complexity of 3D scanning. In the present case study, factors such as dimensions, overall geometry, surface's microtopography, and type of raw-material of the object to be scanned; amount of time available to scan; required level of detail (LOD); and hardware-software issues, determined the set of lenses to be used in each case. According to the manufacturer, the 450 mm stereo field of view (FOV) has a lower resolution (280 μm) and LOD, but a wider scanning window (404x296x240 mm), when compared with the 150 mm stereo set of lens which has 90 μm resolution and a 116x84x70 mm scanning window. That is to say, the higher the FOV, the lower the number of scans needed to cover the entire area. However, the resolution also tends to diminish, leading to less fine density 3D meshes. The opposite is also true.

Therefore, the archaeological and experimental lithics were scanned with 90 mm stereo FOV. Given the characteristics of the stelae and menhir, these were digitized with 450 mm stereo FOV. Because of the amount of time available to scan, and the computer did not have enough processing capacity to deal with very heavy files, it was not possible to scan them then with a higher LOD. So as to enable a first analysis and comparative study, I chose to use the same scanner, FOV, and overall 3D data capturing and processing strategies on the remaining experimental surfaces. Inasmuch I was only concerned with the geometric data (based on *x*,*y*,*z* coordinates) of the objects, and the scanner has a low resolution camera (1,4 Megapixel), I decided not to capture any image texture during scanning.

B.3.2.2 3D Data Acquisition and Post-processing

As aforementioned, it is crucial to have a thorough understanding of the sequential steps, because the final outcome depends intrinsically on all of them. Consequently, each step's parameters must be specifically tailored according to clear objectives previously set. To minimize measurement error, a sufficient amount of overlapping area between scans is needed (>30%). Once again, I used multiple viewing angles during scans to overcome most of the self-occlusion problems, by changing the scanner's position in respect to the objects, and vice-versa. Because it was not always possible to fully control the stability of light, some scans had to be repeated to avoid either missing data or noise data. It is important to realise that either missing data, noise data, filling holes, filtering, and certain parameter's settings during the scanning or post-processing stages

may conceal, distort, or even delete, relevant data, such as use-wear traces and working surfaces (Moitinho de Almeida, and Barceló 2012). The orientation of each 3D model's coordinate system is automatically defined by the view of the first scan of the project. All raw acquisition data was saved at a specified repository, for potential future re-processing (3D-COFORM 2009).

The same general post-processing procedures described in the previous case study were here used. After capturing the unordered point clouds, it was necessary to post-process the scanned data – i.e., from data cleaning, to point clouds final alignment, scans merging, and polygonal mesh generating – to thereafter export the 3D models of each object in STL file format, and carry out geometric feature extraction.

Up to now I have not been able to post-process the point cloud data of the menhir, which was scanned in four individual parts, because the available computer lacks of processing capacity to deal with such heavy files.

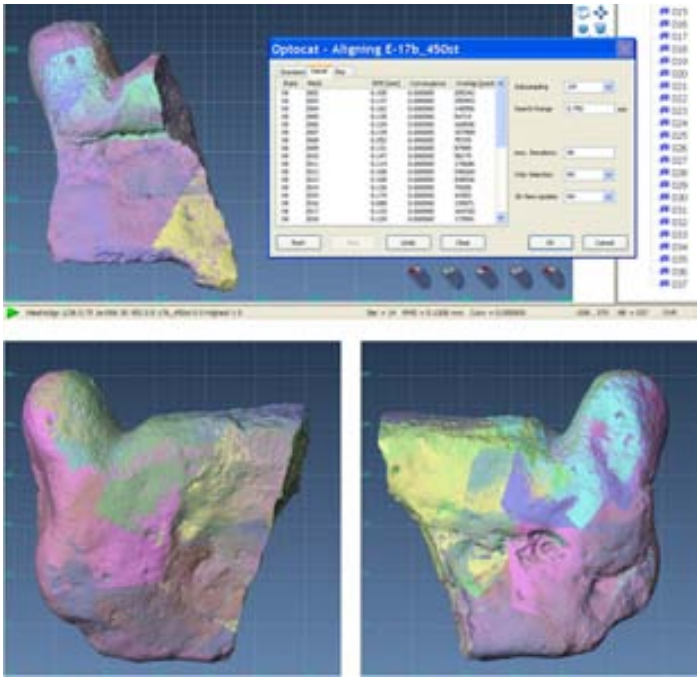

Fig. 4B.7 Scans final alignment: front view of fragment E17b (top); back view (bottom left) and front view (bottom right) of fragment E17a. Each colour represents an individual scan.

Tables 4B.2 to 4B.4 show the number of scans captured, weight (KB) of the aligned and merged scans files, and computed topological measures (number of mesh vertices and faces) of the final STL 3D surface models, of archaeological lithics and stelae and experimental lithics. Since only the areas of interest of the experimental surfaces and stela were scanned, they are not here displayed.

Table 4B.2 3D digital models of the archaeological lithics, scanned with 150 mm stereo FOV.

Arch. Lithic	Number of scans	Aligned scans (*.ctr) (KB)	Merged scans (*.stl) (KB)	Poly-vertices	Poly-faces
17.1.117	21	500533	174531	1787467	3574387
17.2.311	14	321598	149160	1527540	3054790
17.2.312	16	312503	169203	1732813	3465260
17.4.578	27	572294	188506	1930628	3860586
17.4.580	11	178423	100178	1026067	2051641
17.6.754	20	375322	109420	1120649	2240913
17.7.793	16	300435	137269	1406447	2811223
17.7.798	18	403554	136017	1393036	2785607
48.1.40	16	431200	118131	1209805	2419320
52.1.26	17	169453	56451	578163	1156104
52.1.27	22	376338	159368	1636967	3263687
52.1.28	35	1169405	374984	3840699	7679657
52.1.29	22	792773	368475	3786326	7545723

Table 4B.3 3D digital models of the experimental lithics, scanned with 150 mm stereo FOV.

Exp. Lithic	Number of scans	Aligned scans (*.ctr) (KB)	Merged scans (*.stl) (KB)	Poly-vertices	Poly-faces
L1	12	233319	75969	778048	1555840
L2	11	178586	51884	1046576	2089408
L3	13	314409	135677	1389525	2778648
L4	12	306686	159595	1634671	3268489

Table 4B.4 3D digital models of the archaeological stelae, scanned with 450 mm stereo FOV.

Stelae	Number of scans	Aligned scans (*.ctr) (KB)	Merged scans (*.stl) (KB)	Poly-vertices	Poly-faces
E1a	38	646695	199632	2047914	4088307
E1b	43	1174447	445915	4574356	9132098
E17a	29	756560	449945	4615489	9214445
E17b	37	730708	328757	3368877	6732802
E17c	21	445342	227116	2326740	4651204
E48	32	721802	365804	3823875	7488579
E52	32	585340	207942	2161105	4257508
E185	34	619692	247497	2673316	5062466

The process of final scans alignment, scans merging, plus polygonal mesh generating can be much time consuming – the former could take from just 2 minutes to approximately half an hour, whereas the latter from 15 minutes to 5 hours.

B.3.3 Geometric Information Extraction from 3D Digital Surface Model

The following stage consisted in extracting geometric information from the three-dimensional surface models of both archaeological and experimental objects.

B.3.3.1 Lithics Description

After reorienting the 3D models, the origin of the Cartesian coordinate system was aligned with the centre of geometry of each model. The orthographic views of the lithics are shown in Annex B (Figures 4B.28 - 4B.34). I used MeshLab v1.3.0 and Rapidform XO Scan 2010 software to generate automatically orthographic views in accordance to first angle projection, meaning that the object is located in quadrant I. The former is an open-source software, and the latter had already been acquired.

Tables 4B.5 and 4B.6 display the automatically computed geometric results for the scanned archaeological and experimental lithics, respectively. For the most part, MeshLab was able to compute the geometric data and topological measurements necessary for this study. As this software was not able to open any STL files larger than 400 MB in MeshLab, I overcame this problem by using only Rapidform for the heavier files. There is a sizeable amount of several other variables and control measurements compiled from the 3D digital models collected that are not here displayed, because it is my view that these are sufficient to achieve the current goal.

Table 4B.5 Computed geometric measures of the 3D digital models of the archaeological lithics.

Arch. Lithic	Width (mm)	Height (mm)	Depth (mm)	Area (mm^2)	Volume (mm^3)	Centre of mass (mm) x	y	z
17.1.117	89,3244	86,6787	92,5996	27074,951	358679,2622	-3,7938	0,9366	-1,059
17.2.311	108,7045	130,6764	44,0883	28653,1754	330260,8194	-3,1283	-0,0841	-5,1971
17.2.312	137,4701	127,2122	51,177	34424,9343	414903,7481	-3,8563	13,1472	1,8355
17.4.578	106,7123	141,2644	23,437	29208,4519	205564,6427	0,6249	1,9875	-1,6179
17.4.580	73,6631	72,5982	60,5058	14740,3932	155363,6898	0,2409	2,712	-1,9315
17.6.754	109,2885	101,9271	35,199	22987,9239	210232,2064	1,3476	1,0955	1,8675
17.7.793	69,8673	78,2859	77,8953	20482,0329	202940,4267	1,1903	-9,5211	-6,0381
17.7.798	109,7889	106,4177	42,6546	24868,1554	285779,5271	-3,0721	-1,4204	0,7013
48.1.40	81,4756	107,9523	62,4444	22979,7339	266834,5797	-5,3302	1,1781	-5,9244
52.1.26	54,0569	74,306	35,8131	9353,6636	63933,5599	-0,9069	2,1587	-4,3115
52.1.27	78,6937	64,0883	78,9669	18220,9327	196155,9349	0,1227	-1,6962	-1,1818
52.1.28	136,6529	140,3562	89,9466	51250,9444	904473,6586	-0,7131	0,428	-3,7033
52.1.29	137,1498	127,0151	86,9769	47737,1341	844905,3999	0,0407	1,1025	-2,9744

Table 4B.6 Computed geometric measures of the 3D digital models of the experimental lithics.

Exp. Lithic	Width (mm)	Height (mm)	Depth (mm)	Area (mm^2)	Volume (mm^3)	Centre of mass (mm) x	y	z
L1	90,8369	80,9103	55,6656	19055,3632	214228,65	-0,5664	9,6012	-0,3757
L2	68,5776	102,2681	49,8968	16602,2962	168700,2454	0,7294	0,3029	0,2923
L3	112,1856	136,5284	60,5846	31181,5482	403154,8986	-0,7085	12,97	1,1157
L4	98,3624	100,1452	80,0248	28684,8868	389490,8662	-0,1975	0,795	2,347

Subsequent statistical analysis was carried out using JMP v.10 software. The overlay plot displayed in Fig. 4B.8 (left) expresses the relation between width, height, and depth parameter's values for the bounding box of each of the archaeological lithics. In the case of lithics 17.1.117, 17.4.580, 17.7.793, and 52.1.27, the plot indicates that these measurements have similar values. Thus, their forms are close to either uniform polyhedral (i.e., cube, dodecahedron, icosahedron, octahedron, tetrahedron) or ideal round forms (i.e., cone, cylinder, hemisphere, sphere). The problem is that it does not indicate neither how much close, nor to which form.

The centre of mass (i.e., the centre of gravity) is an important parameter to understand the motion of an object and the forces acting on it (Newton 1687, Feynman et al. 1963, Gordon 1978, Cotterell, and Kamminga 1990, Goldstein 2001). It is interesting to notice in the graph displayed in Fig. 4B.8 (right) that the centre of mass of each model never coincides with its centre of geometry. Approximately half of the values of the centres of mass of the archaeological lithics appear to the left of the axial plane Y (i.e., where X has negative coordinates). As to the experimental lithics, all four fall along the axial plane Y and were made by the same person, Antoni Palomo. Likewise, we can observe that they are more numerous in the top octants (i.e., where Y has positive coordinates).

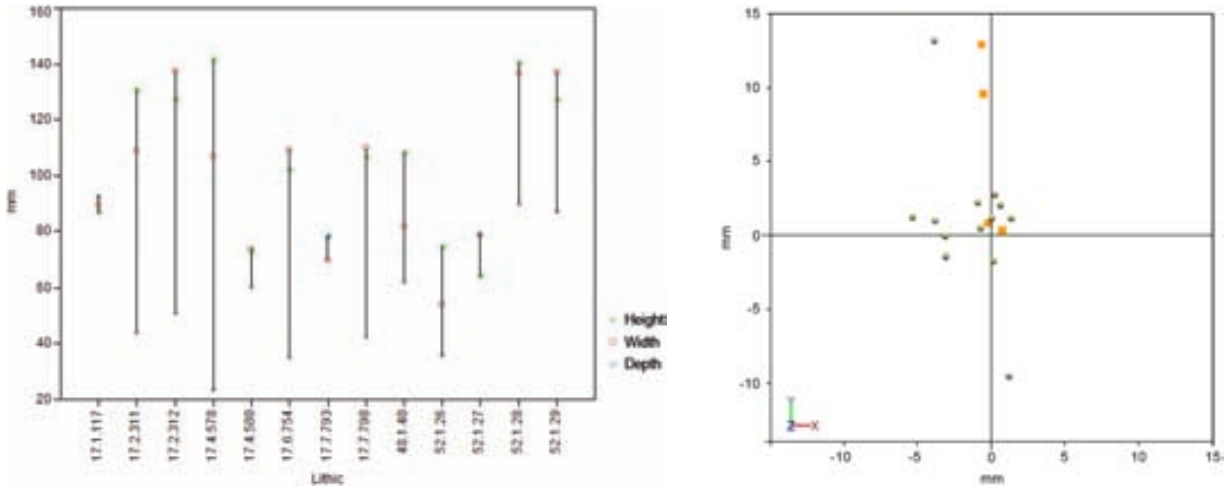

Fig. 4B.8 Width, height, and depth overlay plot, of the archaeological lithics (left). Cartesian coordinate system with centres of mass of the archaeological (circles), and experimental (squares) lithics (right).

It will require larger samples than those used in this study to enable to infer possible relationships between their spatial distribution in the eight octants and laterality, authorship, or hafting issues, if there exists any. These issues should be thereby clarified by further research in this field.

B.3.3.1.1 Archaeological Lithics Description through Form Index

Knowing that the scanned lithics include several irregular and complex forms, I followed an approach based on global 3D form indexes to characterize quantitatively the overall form of each individual archaeological lithic (Whitehouse 2002, Varadi et al. 2004, Masad et al. 2007, ASME 2010, Asahina 2011, Barceló et al. 2012).

Form indexes must be invariant to scaling and Euclidean transformations. Since each form index measures a different aspect of the model, it is often required a combination of a few indexes for identifying different properties, and provide new information. Nonetheless, only one form index parameter was here experimentally considered, the Sphericity Index (Waddell 1932, Asahina 2011):

$$\Psi = [\pi^{1/3} (6V_p)^{2/3}] / A_p$$

where V_p is a measure of the volume and A_p the surface area of the object. The mathematical derivation of this index requires both volume and surface area parameters values of an object. The latter is extremely difficult to measure by manual methods, but the generated 3D digital models enabled to efficiently compute this robust measurements in less than a second (Tables 4B.4 and 4B.5).

As previously mentioned, the sphericity of a sphere is 1 and, by the isoperimetric inequality, any object which is not a sphere will have sphericity less than 1 (Table 4B.7; Figure 4B.9, left vertical scale). The vertical scale of the right side of the graph indicates the sphericity index of an icosahedron (0,939), dodecahedron (0,91), cylinder (0,874), hemisphere (0,84), and tetrahedron (0,671) as reference values, in order to enable a cross comparison with other form factors.

Table 4B.7 Sphericity index of the 3D digital models of archaeological lithics.

Arch. Lithic	Sphericity Index
17.1.117	0,9017
17.2.311	0,8064
17.2.312	0,7815
17.4.578	0,5767
17.4.580	0,9481
17.6.754	0,7438
17.7.793	0,8154
17.7.798	0,8437
48.1.40	0,8722
52.1.26	0,8266
52.1.27	0,896
52.1.28	0,8825
52.1.29	0,9054

The highest factor of sphericity was obtained from lithic 17.4.580 (0,9481), whilst lithic 17.4.578 (0,5767) exhibit the lowest sphericity factor, followed by lithics 17.6.754 (0,7438) and 17.2.312 (0,7815). 76,9% of the lithics ranged between 0,8064 (17.2.311) and 0,9054 (52.1.29). The accuracy of the measurements was $1*10^{-9}$, but the values herein presented were rounded to four decimal points.

From the distribution of sphericity index and volume features of the archaeological lithics, it was possible to infer two major groups of lithics with distinct volume values, where small lithics (11 lithics ranging between 63933,5599 mm^3 and 414903,7481 mm^3) are more numerous than large ones (2 lithics – 52.1.29: 844905,3999 mm^3; and 52.1.28: 904473,6586 mm^3). The former group contains lithics having any possible sphericity distribution, ranging from the lowest to the highest computed values, while the latter group contains only two lithics with high sphericity values (52.1.28: 0,882; 52.1.29: 0,905).

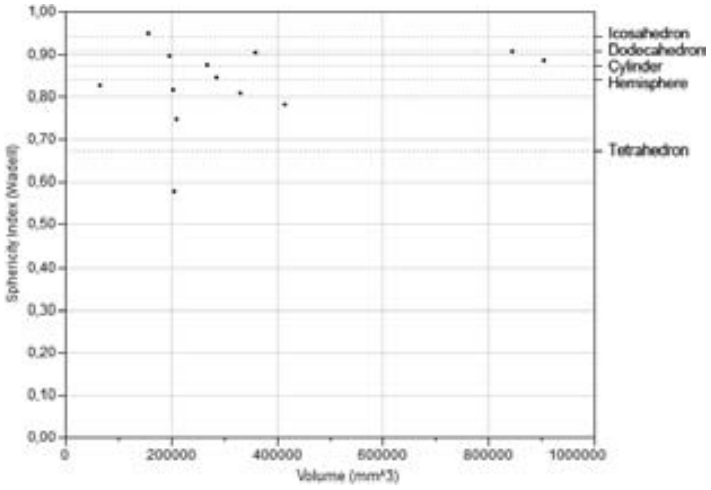

Fig. 4B.9 Distribution of sphericity index and volume of the archaeological lithics.

Considering the distribution of these values, it is not possible to infer any clear relationship between sphericity index and volume parameters within such a small sample of lithics.

Notwithstanding, the data displayed up until now show that the measurements which have been herein undertaken are representative, in order to characterize morphologically the artefacts considered and differentiate from one another.

B.3.3.1.2 Lithics Surface Texture Description through Curvature Analysis

So far, I have used curvature analysis technique on archaeological and experimental lithics to semi-automatically detect and differentiate surface regions, as well as the curvedness of local geometric features. These comprise working surfaces and edges, along with significant use-wear macro traces and other more shallow traces.

Although MeshLab v1.3.0 also permits to analyse the amount of curvature at a surface point in a semi-automatic way, I chose to use Rapidform XO Scan 2010 only because its tool seemed more efficient. The colourmap plotted in the latter software ranges from values 1 (top of the scale: red, convex) to -1 (bottom of

the scale: blue, concave), corresponding to high to low values of the curvedness, whereas 0 (green, or grey if the allowable values are hidden) indicates planar patches (Figure 4B.10). Hence, curvature is not only a given value, but also a sign that indicates the direction of deviation.

Knowing that each FOV determines the resolution of the captured geometries of the 3D digital microtopography of the surface, it was necessary to adjust the parameters of the maximal curvature to -0,1/0,1, which gave best results for an efficient detection of dynamic surfaces.

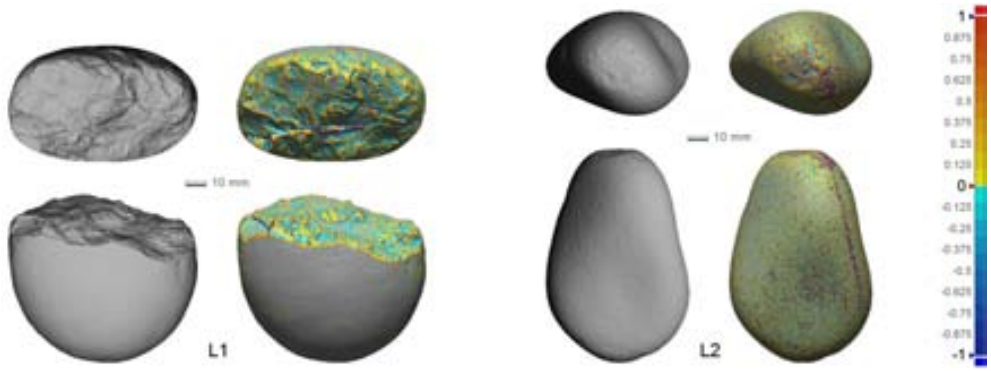

Fig. 4B.10 3D Digital surface models: differentiation of surface regions through curvature analysis of experimental lithics L1 (left), and L2 (right).

Next step will comprise: (i) quantifying this new geometric information extracted from the lithics; (ii) statistically analysing all features' data (clustering and classification); (iii) correlating these local geometric features with both carved form and surface textures of the stela. However, due to time constraints, this study on the functional analysis of lithics will definitely have to be carried out in future works.

B.3.3.2 Stelae Description

After orienting the 3D model, the origin of the Cartesian coordinate system was aligned with the centre of geometry of each model. The orthographic views of the stelae are shown in Annex B (Figures 4B.20 - 4B.27).

Table 4B.8 shows the results of automatically computed geometric and topological measures of the scanned archaeological stelae. Again, there is a sizeable amount of several other variables and control measurements compiled from the 3D digital models collected that are not here displayed, because it is my view that these are sufficient to achieve the current goal.

Table 4B.8 Computed geometric measures of the 3D digital models of the archaeological stelae.

Stelae	Width (mm)	Height (mm)	Depth (mm)	Area (mm2)	Volume (mm3)	Centre of mass (mm) x	y	z
E1a	301,659	319,1183	172,9865	243226,1438	7659261,025	-11,4893	0,2801	-3,6158
E1b	383,406	464,961	310,109	603627,052	29205686,42	-0,087	-9,516	-1,855
E17a	575,972	590,961	229,643	713817,178	33169521,78	13,058	23,683	9,795
E17b	422,49	607,2	221,252	509046,329	17974404,47	-14,598	11,696	-9,207
E17c	328,118	496,703	197,977	382038,717	14785779,87	22,669	40,286	-8,19
E48	638,401	312,697	147,153	528928,019	17103021,32	-9,298	15,919	-0,615
E52	514,223	313,489	139,481	356813,201	9710253,336	-24,497	-4,643	-4,643
E185	499,325	216,36	166,449	370708,408	9971360,14	-18,585	14,38	-0,095

B.3.3.2.1 Stelae Protuberances' Description through Shape Index

Knowing that the scanned protuberances include several irregular shapes, this time I followed an approach based on global 2D shape indexes to characterize quantitatively the shape of each individual archaeological protuberance (Whitehouse 2002, Varadi et al. 2004, Masad et al. 2007, ASME 2010, Asahina 2011, Barceló et al. 2012). Again, only one shape index parameter is here experimentally considered, the Shape Factor.

Like form indexes, shape indexes must also be invariant to scaling and Euclidean transformations. Since each shape index measures a different feature of the model, it is often required a combination of a few indexes for identifying different properties, and provide new information. Nonetheless, only one shape index parameter was here experimentally considered, the Shape Factor, sometimes called "circularity".

Compactness is an intrinsic property of objects. As aforementioned, Shape Factor is a compactness measure of shape, which can be used to quantify the degree to which an object resembles a circle. The shape factor of a circle is 1, and by the isoperimetric inequality any object which is not a circle will have a value less than 1. Squares are around 0.78, and a thin thread-like artefact would have the lowest shape factor tending towards 0. This shape descriptor is similar to Roundness, yet emphasizes the configuration of the perimeter by reflecting the smoothness of contour, rather than the length relative to object area. Shape Factor is defined as such:

$$Shape\ Factor = (4\pi A) / p^2$$

where A is a measure of the surface area of the object and p is the perimeter of the contour. The accuracy of the measurements was $1*10^{-9}$, but the values herein presented were rounded to four decimal points.

To proceed with this approach, cross-sections in parallel planes of the pair of protuberances of stela E17 were first carried out. Each plane distances 15 mm from the next, starting from the top (Figure 4B.11). Thus, eleven cross-sections were extracted. Then, both area and perimeter measurements of each intersection were automatically computed, to thereafter calculate the Shape Factor eigenvalue for every cross-sections (Table 4B.9, Figure 4B.12). This procedure was adjusted in E1a, E1b, E52a, E52b, and E185, where cross-section planes

were defined in accordance with the longitudinal central axis of each protuberance. The width and depth of each cross-section of the pairs of protuberances from stelae E17 and E52 were also measured to support the data (Table 4B.10, Figure 4B.13).

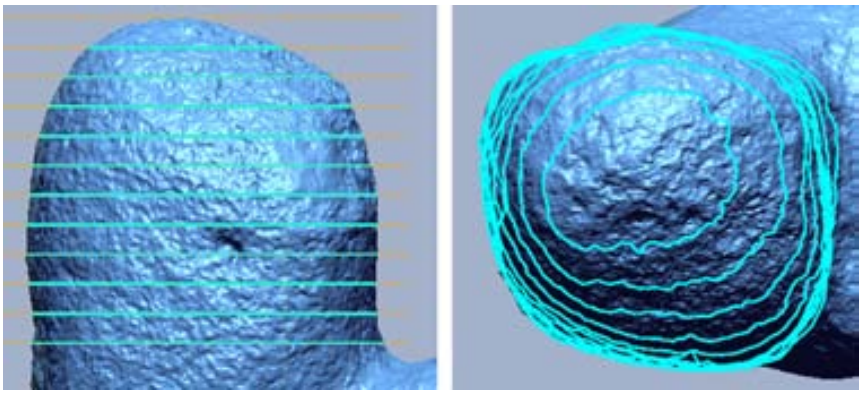

Fig. 4B.11 3D Digital surface model of fragment E17b: planar cross-sections, front view (left), and top view (right).

Table 4B.9 Archaeological protuberances: Shape factor of the extracted planar cross-sections.

Cross-section	Shape Factor						
	E1a	E1b	E17a	E17b	E52a	E52b	E185
1	0,7078	0,7943	0,8238	0,7689	0,9074	0,6829	0,6935
2	0,7865	0,5875	0,911	0,8712	0,8478	0,7696	0,7786
3	0,8074	0,6899	0,9268	0,9205	0,8178	0,8284	0,7833
4	0,7984	0,729	0,9177	0,9335	0,8293	0,845	0,8294
5	0,7645	0,8221	0,9308	0,9388	-	-	0,8398
6	0,8025	0,7915	0,9186	0,9397	-	-	0,8159
7	0,8169	0,7435	0,9104	0,9378	-	-	0,8051
8	0,7653	0,7623	0,9026	0,9222	-	-	0,814
9	0,7752	0,8019	0,913	0,9328	-	-	0,8548
10	0,7796	0,8246	0,9189	0,933	-	-	0,8367
11	0,7026	-	0,9254	0,9268	-	-	0,8488

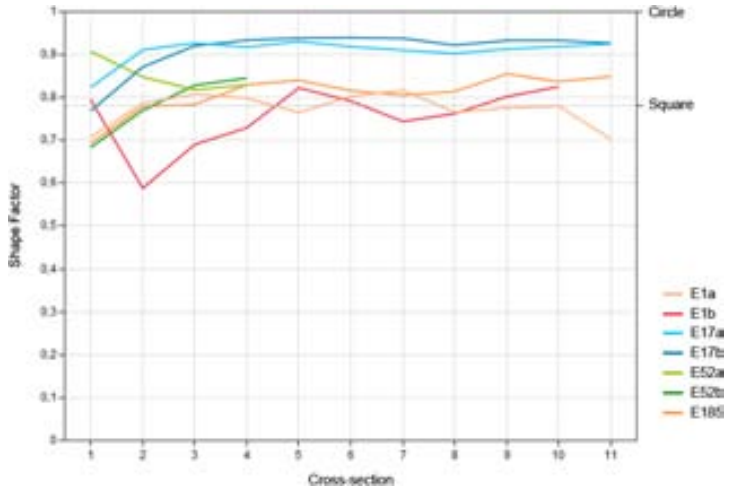

Fig. 4B.12 Protuberances of stelae E17, E52, E185, and fragments E1a and E1b: shape factor of the extracted planar cross-sections. The vertical scale on the right side of the graph also indicates the Shape Factor of a square (0,78) as reference value, in order to enable a cross comparison with another shape index.

From the distribution of the shape factor values (Figure 4B.12), it is possible to distinguish the pair of protuberances of stela E17 from the others. The former shows close values across most sections, specially the Shape Factor in sections 3 (deviation: 0,0063), 5 (deviation: 0,008), and 11 (deviation: 0,0014). Even though the top of the protuberances shows higher deviations (section 1: 0,0549; and section 2: 0,0398), these deviations may become rather insignificant in this scale of analysis. In respect to stela E52, one of its protuberances is partially fragmented on the top, which explains the initial divergence of both Shape Factor and width values.

Table 4B.10 Archaeological pairs of protuberances: width and depth of the extracted planar cross-sections.

Cross-section	Width				Depth			
	E17a	E17b	E52a	E52b	E17a	E17b	E52a	E52b
1	90,8995	99,0653	54,817	81,1955	89,5478	83,0904	48,2552	42,9841
2	126,3884	136,0202	86,0012	106,9315	118,7131	116,8417	60,8585	62,6808
3	150,8883	154,5769	110,5841	117,9499	138,7544	142,0106	69,6996	72,1794
4	162,8278	163,7787	124,6944	128,5735	154,512	159,4176	78,9815	80,609
5	171,4282	170,4588	-	-	161,7911	168,5553	-	-
6	178,4912	175,1316	-	-	166,3234	173,645	-	-
7	181,8668	177,0884	-	-	171,7553	173,6199	-	-
8	184,4128	177,6041	-	-	175,8916	172,2299	-	-
9	188,3539	172,062	-	-	176,2088	171,2387	-	-
10	192,1779	173,6609	-	-	178,4029	171,395	-	-
11	199,9314	178,2732	-	-	182,8612	172,2951	-	-

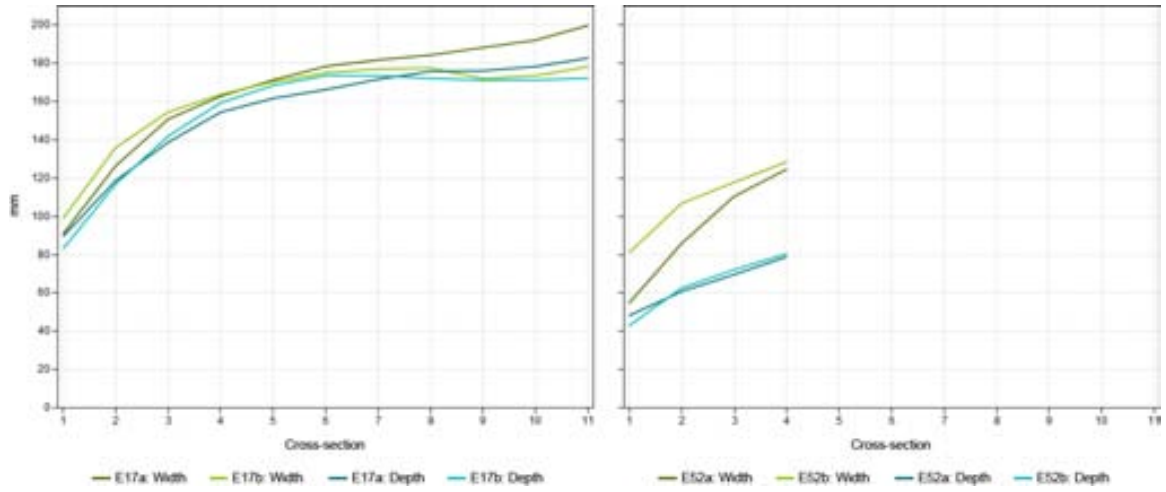

Fig. 4B.13 Protuberances of stelae E17 and E52: width and depth of the extracted planar cross-sections.

The resulting data suggests a conceptual frame in the manufacturing planning and shaping of both protuberances of stela E17, as well of both protuberances of stela E52. The measured values from the remaining protuberances do not show converging paths, thus suggesting the manufacture of further independent stelae.

B.3.3.2.2 Surface Texture Description of Stela E17b and Experimental Surfaces

Surface textures usually consist of a series of peaks and valleys that have characteristic form size and spacing, and normally of a periodic nature (Blunt and Jiang 2003). Surface texture is a key parameter in archaeological materials, where its study has been central to use-wear research, as well as in the understanding of manufacturing processes. Every manufacturing technique leaves a micro-scale 'fingerprint', or signature, on the surface which is unique to the manufacturing process. It is the surface that interacts with its working environment through some form of mechanical contact (Blunt and Jiang 2003, Demkin and Izmailov 2010) – i.e., the mechanical surface – that is of interest here.

In this section, I describe the 3D digital geometric surface texture – i.e., the microtopography – of stela E17b and experimental surfaces, in order to associate them with possible gestures, carving techniques, and used tools. The method included: (i) using curvature analysis technique; (ii) applying surface roughness areal parameters, regulated by international standards, to describe and compare 3D digital surface texture patterns of a set of sampled areas, bringing further quantitative analysis to ancient manufacturing processes.

B.3.3.2.2.1 Curvature analysis

This technique was here applied to detect and describe semi-automatically the amount of curvature and distribution on surface texture patterns, from stela E17b and the experimental surfaces.

Knowing that each FOV determines the resolution of the captured geometries of the 3D digital microtopography of the surface, I had to adjust the parameters of the maximal curvature to -0,1/0,1, which gave best results for an efficient detection. Figure 4B.14 (top-centre) indicates eight contiguous non-segmented regions

revealed by E17b's colourmap, which I named with letters from A to H. The remaining images show the results of the computation of the curvatures. The images on the bottom refer to the experimental surfaces numbered from 1 to 6, whereas the ones above pertain to the archaeological surfaces.

The results of the plotted colourmaps visually suggested the following correlations between: the experimental surface texture 2, and archaeological regions A and F (2-A,F); 4-B; 5-C; and 6-D. E is a small region which stands out from the surrounding. Its surface microtopography resembles to 5, but within the limitations of this technique it can be confounded with surface 1, or even 3. It was not possible to infer from this technique if this region could eventually be the result of either an intentional or an unintentional action (namely, if the path of the tool used for carving region C can easily intersect region E, causing some abrasion of the latter; depositional or post-depositional process) of the manufacturing process. Although region H is not correlated with any of the experimental surfaces, the fact that this surface of E17b matches perfectly with E17a, the opposite surface matches with E17c, and all present the same type of macro traces, indicated a fractured region. Albeit there is an intense correlation between regions G and H, the former also revealed slight correlations with surface 2. This suggested that the surface of region G was initially fractured, and subsequently the same technique of surface 2 was used, but without the same precision and finishing of region F.

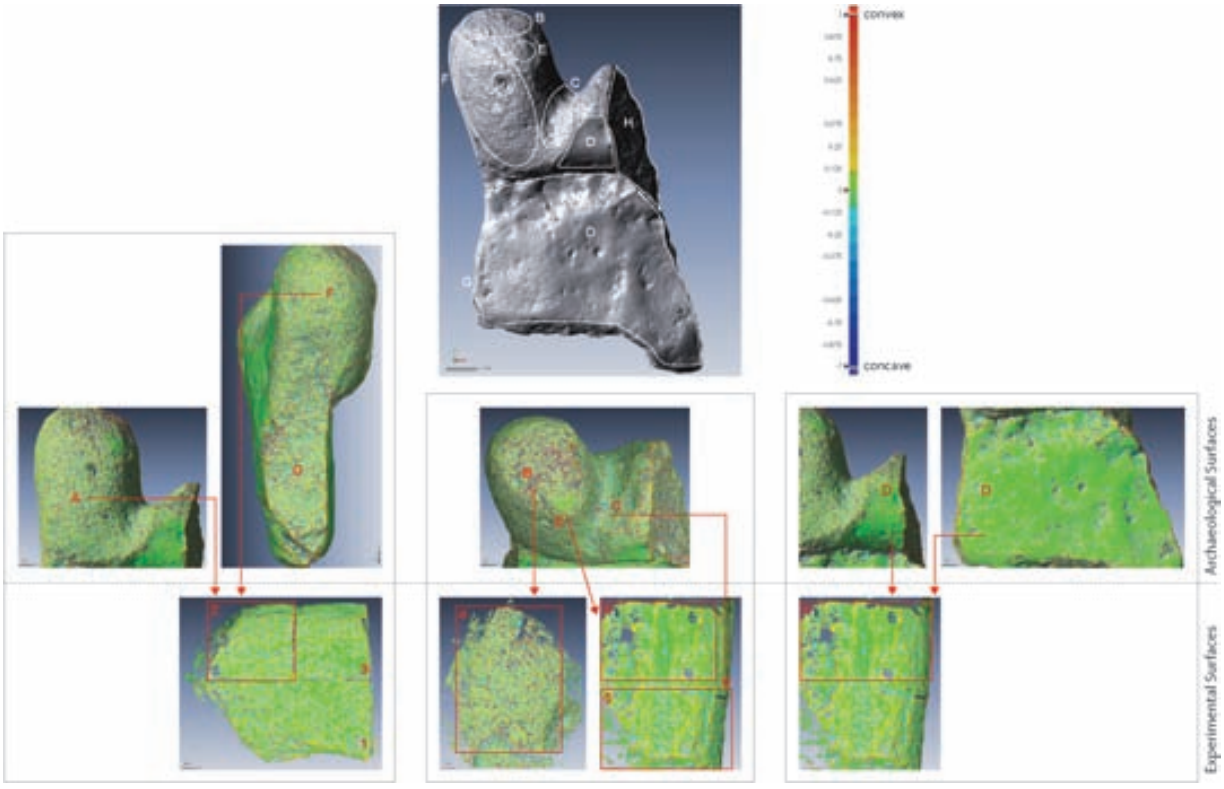

Fig. 4B.14 3D Digital surface models: Analysed non-segmented surface regions of stela E17b (top-centre), curvature analyser scale (top-right), curvature analyser colourmaps of both archaeological (horizontal centre images) and experimental surfaces (bottom images).

B.3.3.2.2.2 3D Digital Areal Surface Texture Parameters: ISO 25178-2

The aim of this section is to describe and compare archaeological and experimental 3D digital surface texture patterns. To this end, the following method was applied:

a) Choice of metrological solution

This step consisted of choosing the measurement instrument.

As described above, the same 3D scanner, FOV, and overall 3D data capturing and processing procedures used on the archaeological stelae and menhir were chosen for the experimental surfaces, so as to make comparisons more consistent.

b) Digital data acquisition / Sampling

It consisted in making use of the 3D digital models of the archaeological objects previously scanned, and further scan the experimental surfaces with the same procedures. Next, in selecting a set of texture samples from both archaeological and experimental surfaces (Figure 4B.15). The samples were either contiguous or separated (Blateyron 2013), each measuring 50*50 mm.

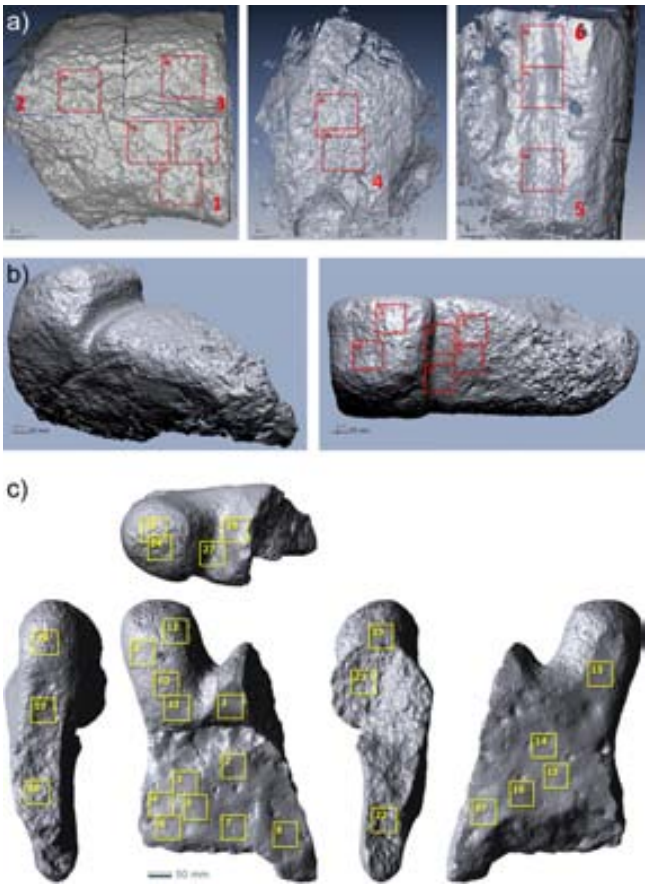

Fig. 4B.15 3D Digital surface models of : (a) 6 experimental surface textures (labelled E_s1a, s1b, s1c, s2a, s3a, s4a, s4b, s5a, s6a, s6b); (b) experimental stela, halfway sculpted (from Est_s01 to Est_s06); (c) Fragments A of Stela SMB/08 E-17/5/958 (from Ast_s01 to Ast_s27), five orthographic views (top, left, front, right, back) in accordance to first angle projection, meaning that the object is located in Quadrant I. Squares indicate the areas sampled (50*50 mm).

I initially selected 10 samples from the experimental surfaces (labelled E_s1a, s1b, s1c, s2a, s3a, s4a, s4b, s5a, s6a, s6b), 6 samples from the experimental stela (labelled from Est_s01 to Est_s06), and 27 samples from the archaeological stela (labelled from Ast_s01 to Ast_s27). The squares in Figure 4B.14 indicate the areas sampled. The small extension of the experimental surfaces did not permit to obtain a larger number of samples per region, more representatives of the applied gestures and techniques.

Samples E_s5a, E_s6a, E_s6b, Est_s2, Est_s5, Ast_s12, Ast_s26, and Ast_s27, were excluded from the present analysis, because they visibly contained two different types of textures. Hence, smaller samples will be required, at least on these regions.

c) Digital surface pre-processing

It consisted on 3D digital surface levelling and form removal.

Before proceeding with the surface's waviness, roughness, and microroughness measurements, it was necessary to: level the surfaces by removing the slope using the least squares plane method; and remove the surface's general form by polynomial approximation (Figure 4B.16). I have explored the use of Mountainsmap 7 software trial version (Digital Surf) not only to pre-process the samples, but also to perform the 3D areal surface texture measurements.

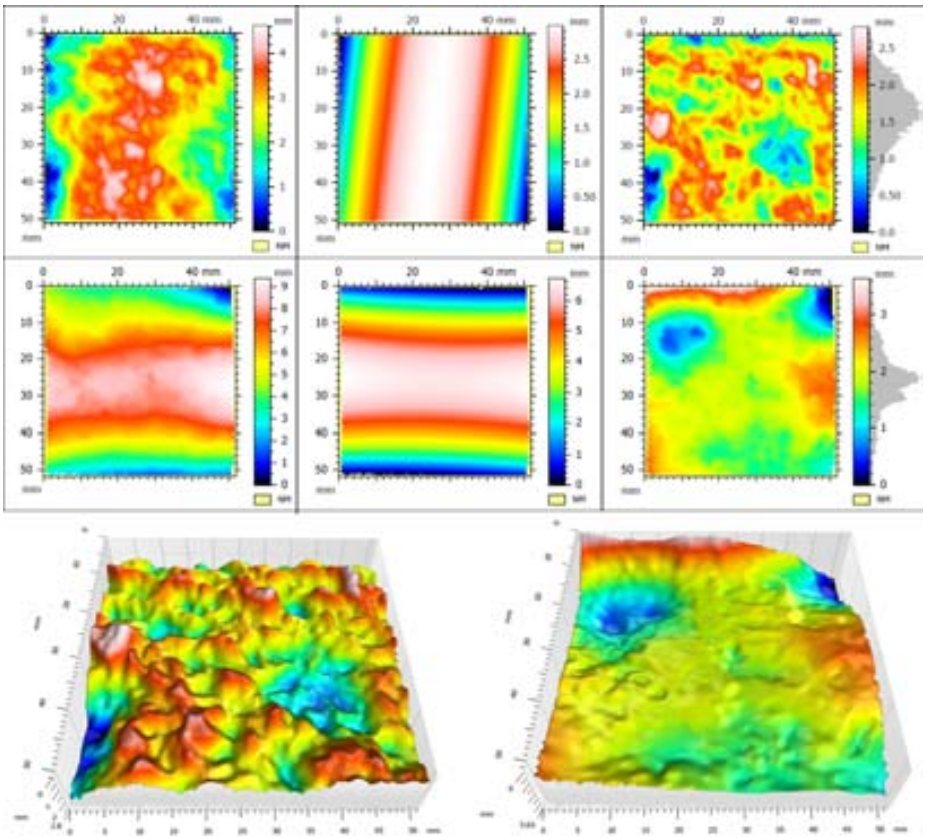

Fig. 4B.16 Pseudo-colour view of samples Ast_s09 (top) and Ast_s01 (centre): surface (left), subtracted form, polynomial of degree 2 (middle), surface texture after form subtraction (right). 3D view of the surface with form removed: samples Ast_s09 (bottom left), and Ast_s01 (bottom right).

d) Digital surface description, comparison, and analysis

It consisted in quantitatively describing and analysing archaeological 3D digital areal surface texture patterns and features and compare with the experimental ones.

The natural scale of the data was used, and the origin of the z axis (depth) was set at the highest value of the sampled data.

The following set of ISO 25178-2 parameters (ISO 2012) were used as metric variables to describe each sample: *Sa* (average roughness, mm), *Sk* (core roughness depth, mm), *Smr* (areal material ratio, %), *Spd* (density of peaks, 1/mm^2), *Vmc* (core material volume, mm^3/mm^2), *Vvc* (core void volume, mm^3/mm^2). Additionally, the texture's isotropy (%), as well as the first, second, and third main directions (º) were taken into account. An isotropic surface has values near 100 % and presents identical characteristics regardless of the direction of the measurement. Conversely, an anisotropic surface has values near 0 % and presents either oriented or periodic structure. The calculation of the isotropy value is similar to the ISO 25178 *Str* (texture aspect ratio) parameter, with the difference that in the first form is removed automatically before the autocorrelation function is applied (Blateyron 2006, MountainsMap 2013).

Variability and similarities between sampled textures and their constitutive features were statistically analysed in JMP® 10 software (SAS Institute). The results of the *Sa*, *Sk* (Gaussian filter: 0,8 mm), *Smr* (c=0,001 mm under the highest peak), *Spd* (pruning=5%), *Vmc* (p=10%, q=80%), *Vvc* (p=10%, q=80%) parameters (Table 4B.11), plus the isotropy (0,2 threshold) and the three main directions (Table 4B.12) of the sampled surfaces textures, enabled to distinguish three major groups of all sampled surface areas (Figure 4B.17, left):

1) Fine – only natural polished (in the present case, due to erosion) archaeological samples (Ast_s01-Ast_s08, Ast_s13-Ast_s17). No experimental surfaces were associated with, which makes sense, as we did not introduce in this analysis any polished or other fine experimental surfaces. However, it was possible to record inter-individual variations among them. Even though all samples from this group showed a wide range of texture directions (Figure 4B.18), samples Ast_s01 to Ast_s08, located on the front surface of the stela, indicated a predominance of oblique directions, and low isotropy; whereas samples Ast_s13 to Ast_s17, located on the back surface of the stela, indicated a predominance of perpendicular and near to perpendicular directions, and medium isotropy (Figure 4B.19). These differences between front and back surfaces may suggest evidence on depositional (e.g. pressure of the sandy soil towards the stela) or post depositional processes affecting the natural eroded texture (e.g. wide range of directions, with a preponderance of oblique directions).

2) Coarse and regular – most of the remaining manufactured archaeological samples were here directly associated with the texture signatures of the experimental stela (Est_s03, Est_s06), thus suggesting that they may share similar manufacturing strategies. The latter was manufactured only with the gestures (perpendicular and tangential to the surface) and lithic tools used in the experimental surfaces 1, 2, and 3 (Figure 4B.6). Even though experimental surface 4 (copper tools used) was included in this group, at this stage I believe this may be indicating that these sampled textures are just coarse and regular, and

not that they are associated with the manufacturing of the archaeological stela.

3) Coarse and irregular - this group included samples from fragmented surfaces not manufactured (Ast_ s21, s22), as well as surfaces slightly manufactured (Ast_s19, s20, s23-25). The latter were to some extent associated with Est_s01 and Est_s04.

Table 4B.11 ISO 25178-2 3D digital areal surface texture parameters data (*Sa*, *Sk*, *Smr*, *Spd*, *Vmc*, *Vvc*) of the analysed archaeological (Ast) and experimental (E, Est) samples.

Sample	*Sa*	*Sk*	*Smr*	*Spd*	*Vmc*	*Vvc*
Ast_s01	0,354	0,0042	0,0069	0	0,3605	0,5647
Ast_s02	0,4131	0,0046	0,0181	0,0004	0,4648	0,5949
Ast_s03	0,1705	0,0034	0,0244	0,0015	0,1838	0,2505
Ast_s04	0,2455	0,0025	0,0076	0,0019	0,283	0,3259
Ast_s05	0,1183	0,0039	0,0092	0,0049	0,1206	0,1671
Ast_s06	0,161	0,0028	0,0155	0,0049	0,1744	0,2378
Ast_s07	0,2253	0,0037	0,0073	0,0064	0,2629	0,2886
Ast_s08	0,3162	0,0049	0,0085	0,0023	0,3459	0,4145
Ast_s09	0,3491	0,0112	0,0106	0,0133	0,3991	0,4954
Ast_s10	0,3031	0,0099	0,0103	0,0111	0,3521	0,4639
Ast_s11	0,3568	0,0085	0,0056	0,0059	0,403	0,5528
Ast_s13	0,1267	0,0031	0,0077	0,0061	0,1358	0,1668
Ast_s14	0,2971	0,003	0,0092	0,0011	0,3527	0,432
Ast_s15	0,2322	0,003	0,0076	0,0022	0,2796	0,347
Ast_s16	0,2771	0,0035	0,0095	0,0011	0,311	0,3923
Ast_s17	0,2624	0,0033	0,007	0,0026	0,3129	0,3631
Ast_s18	0,506	0,0098	0,0054	0,0049	0,6193	0,722
Ast_s19	0,6206	0,0104	0,0061	0,0038	0,6716	0,9786
Ast_s20	0,6131	0,0107	0,0053	0,0046	0,6693	0,9722
Ast_s21	1,0232	0,0129	0,0052	0,0027	1,2391	1,4778
Ast_s22	0,8583	0,0128	0,0048	0,0038	1,0412	1,1609
Ast_s23	0,5368	0,0118	0,0053	0,0068	0,6463	0,8459
Ast_s24	0,7611	0,0183	0,0098	0,0061	0,8681	1,122
Ast_s25	0,5634	0,01	0,0073	0,0046	0,682	0,7428
E_s1a	0,2661	0,0177	0,0181	0,0072	0,2866	0,4339
E_s1b	0,4351	0,0196	0,0177	0,0023	0,4706	0,6317
E_s1c	0,305	0,0186	0,0177	0,0057	0,3337	0,4716
E_s2a	0,5457	0,0212	0,0183	0,0011	0,6297	0,8347
E_s3a	0,2469	0,0151	0,0189	0,0042	0,2665	0,4055
E_s4a	0,4179	0,0109	0,0058	0,0065	0,4572	0,6194
E_s4b	0,4717	0,0109	0,0051	0,0072	0,5199	0,6848
Est_s01	0,6175	0,0099	0,0073	0,0038	0,7408	0,9617
Est_s03	0,3895	0,0102	0,006	0,0094	0,4365	0,613
Est_s04	0,6153	0,0102	0,0046	0,0053	0,6853	0,8418
Est_s06	0,3697	0,0099	0,0048	0,0061	0,414	0,5341

Even though the K Means NCluster analysis clearly distinguished sub-groups of archaeological texture patterns (Figure 4B.17, right), the small number of experimental surface samples did not enable further conclusions on linking experimental to archaeological 3D digital textures.

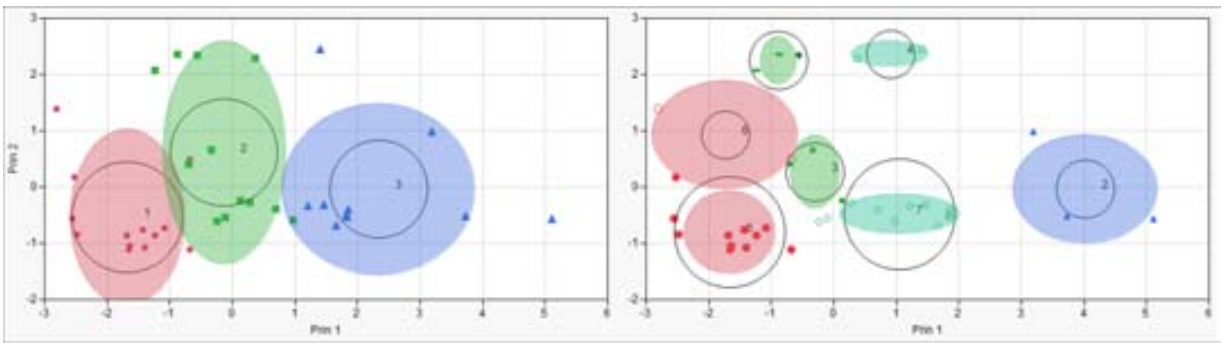

Fig. 4B.17 K Means NCluster=3, ellipse 90% coverage (left): fine texture in red, coarse and regular texture in green, coarse and irregular texture in blue; and K Means NCluster=7, ellipse 90% coverage (right) analysis of the sampled surface textures, using the *Sa*, *Sk*, *Smr*, *Spd*, *Vmc*, and *Vvc*, ISO 25178-2 parameters.

In some cases, variability in the surfaces' signatures may not express different types of manufacturing technique (namely, gestures, working position, tools, abrasion and lubrication materials, number of manufacturers). Instead, it may express varying degrees of wear (namely, due to time, applied force, or stela-tool interfacial bonds and real contact area). In addition, some wear traces/patterns may also result from shearing and rupture of rubbing materials inside and around the contact region of the stela (Myshkyn et al. 2005). Consequently, the association of these measurements must be interpreted with some caution, since it is determined by several technical issues and the skills of the craftsperson (Baena and Cuartero 2009).

Table 4B.12 Isotropy and three main directions of the of the analysed archaeological (Ast) and experimental (E, Est) surface textures. The accuracy of the measurements was $1*10^{-8}$ for isotropy, and $1*10^{-10}$ for the main directions, but the values displayed here were rounded to one decimal point.

Sample	Isotropy (%)	1st direction (°)	2nd direction (°)	3rd direction (°)
Ast_s01	24,3	153,5	0,2	26,5
Ast_s02	21	0,2	17,1	39,2
Ast_s03	22,6	135,3	63,2	153,5
Ast_s04	24,1	116,8	0,2	153,5
Ast_s05	41,3	153,5	0,2	26,5
Ast_s06	30,5	153,5	26,5	17
Ast_s07	44	26,8	45,3	0,2
Ast_s08	40,1	63,5	26,8	56,5
Ast_s09	67,2	90,1	116,8	141,4
Ast_s10	54,5	135,1	90	116,5
Ast_s11	54,6	0,1	135	45
Ast_s13	48,4	90,1	71,5	26,5
Ast_s14	21,1	90,1	153,5	63,2
Ast_s15	80,9	44,3	90	62,7
Ast_s16	52,9	45	116,5	63,5
Ast_s17	53,2	45,6	26,8	71,8
Ast_s18	72,2	63,5	128,5	0,2
Ast_s19	65,3	63,5	90,1	116,5
Ast_s20	58,5	63,3	147,8	26,5
Ast_s21	28,2	116,8	90,1	63,3
Ast_s22	46,3	90,1	153,5	44,8
Ast_s23	40,8	0,2	153,3	26,8
Ast_s24	45	0,2	63,5	116,5
Ast_s25	41,7	90	116,5	153,5
E_s1a	61	63,5	123,5	57,8
E_s1b	52,9	90,1	45	141,2
E_s1c	72	90	153,5	132,5
E_s2a	24,1	116,5	94,2	8,7
E_s3a	55	171,4	90,1	11,9
E_s4a	75,4	90,1	153,2	146,4
E_s4b	74,3	116,5	0,2	90
Est_s01	85,9	0,2	45	26,8
Est_s03	32,1	0,1	45	63,5
Est_s04	56,2	0,2	45,1	26,5
Est_s06	31,5	157,2	128,5	0,2

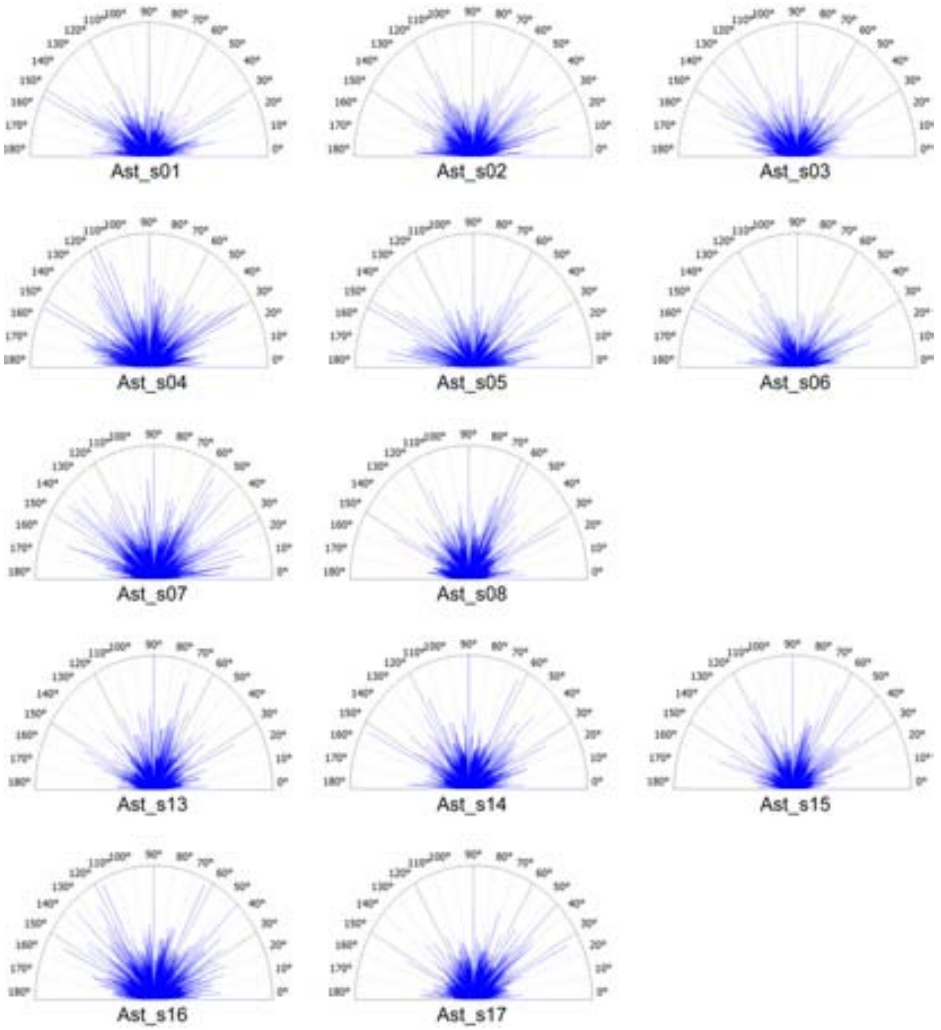

Fig. 4B.18 Texture direction and intensity graphics of the archaeological sampled surfaces: Ast_s01 to Ast_08, located on the front view surface of the stela; and Ast_s13 to Ast_17, located on the back view surface of the stela.

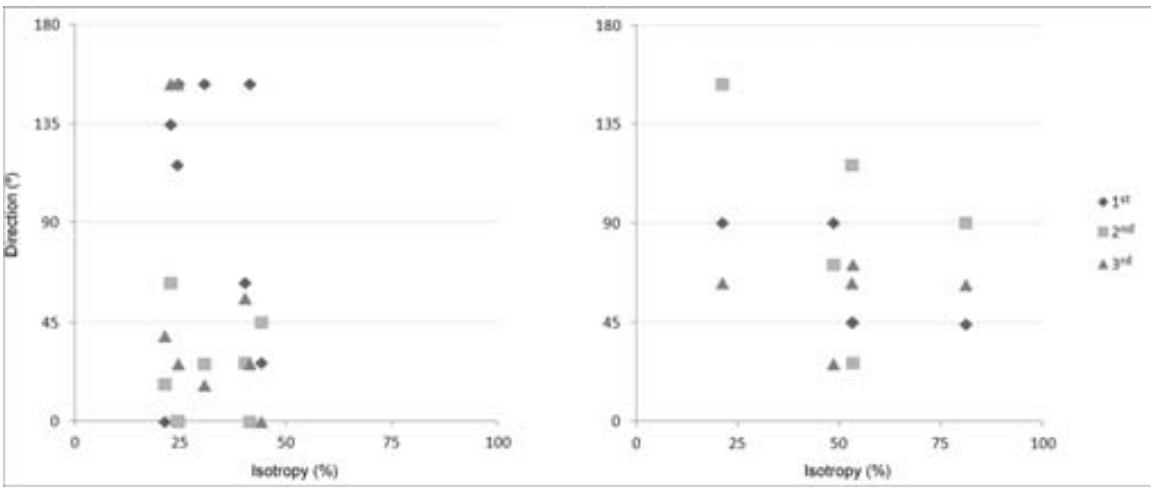

Fig. 4B.19 Isotropy and three main directions scattered plot of the sampled surface textures: Ast_s01 to Ast_08 (left), located on the front view surface; and Ast_s13 to Ast_17 (right), located on the back view surface.

Table 4B.13 displays a selection of data from Tables 4B.1 and 4B.12, in order to enable a brief comparison between: visual evaluation of the movement direction of both hand and tool towards the experimental surfaces; and the three main directions of the 3D digital sampled surface textures measured by Mountainsmap 7 software. E_s5a, E_s6a, E_s6b were excluded from the present analysis, because they visibly contained two different texture patterns.

Table 4B.13 Visual evaluation of direction of movement on experimental surface textures E_s1, E_s2, E_s3, E_s4, E_s5, E_s6; and metrology software measurement of the three main directions on the corresponding 3D digital samples. Samples E_s5a, E_s6a, and E-s6b were excluded, because they visibly contained two different texture patterns.

	Visual evaluation		**Metrology software evaluation**		
Exp. surface	**Direction of movement** (approximate angle)	**Sample**	**1st direction** (º)	**2nd direction** (º)	**3rd direction** (º)
E_s1	perpendicular (90º)	E_s1a	63,5	123,5	57,8
		E_s1b	90,1	45,0	141,2
		E_s1c	90,0	153,5	132,5
E_s2	tangential (20º-45º)	E_s2a	116,5	94,2	8,7
E_s3	perpendicular (90º) + tangential (20º, superficially)	E_s3a	171,4	90,1	11,9
E_s4	perpendicular (90º) + tangential (20º, dragged movement)	E_s4a	90,1	153,2	146,4
		E_s4b	116,5	0,2	90,0
E_s5	perpendicular (90º)	E_s5a	-	-	-
E_s6	perpendicular (90º) + longitudinal abrasion in both directions	E_s6a	-	-	-
		E_s6b	-	-	-

None of the three main directions of sample E_s1a indicates 90º. However, if we allow for an increase of 30º to either side – which would enable to reflect small variations on human movement direction –, then 90º could be extended to a 60º-120º range. Only in this case would the 1st and 2nd direction values sustain the visual evaluation. As to the remaining two samples of experimental surface E_1, both 1st direction values concur with the visual evaluation. According to the visual evaluation, a tangential movement was applied on sample E_s2a, yet the 1st and 2nd main directions indicate near to perpendicular or perpendicular movements, respectively. The tangential movement is not revealed until the 3rd main direction. Concerning sample E_s3a, both 1st and 3rd main directions indicate tangential movement, where the first shows a clear superimposition (thus, not so superficial as it seemed) with respect to the perpendicular direction, i.e., the 2nd main direction. Regarding sample E_s4a, the 1st main direction corroborates the perpendicular movement, and so does the 2nd if we again allow for an increase of 30º to either side. Though, this sample does not indicate any tangential movement within its three main directions. Finally, in sample E_s4b both 3rd and 1st directions confirm the perpendicular to near perpendicular movements, respectively. Whereas the 2nd direction's value is close to zero, thus indicating a tangential movement almost coincident with the experimental surface plane.

B.4 Conclusions

The approach herein presented demonstrates the interest of the proposed framework towards the understanding of ancient manufacturing procedures, by bringing quantitative 3D digital methods and techniques to ancient manufacturing processes analysis.

The possibility to include physical experimental work in this study permitted to raise and test interesting hypothesis, which undoubtedly enriched this investigation by yielding valuable information.

The ability of 3D scanners – as the type of one used here – to document geometric surfaces is well known. Although the 450 mm FOV has a lower resolution (280 μm) and LOD when compared with the other set of lens available on this scanner, it demonstrated sufficiently capable to acquire meaningful shape, form, and texture data from sandstone objects. Henceforward, it was of paramount importance to ensure data consistency and best results, by applying the same methods, techniques, and measurement schemes within each stage and step of the framework.

The 3D models allowed achieving stimulating results, as they enabled to characterize morphologically the artefacts considered and differentiate from one another. In respect to the lithics geometric description, due to the scope of the present thesis, time constraints, and the complexity of use-wear analysis of lithic tools, it was definitely not feasible to undertake further studies on functional issues. As to the stela's protuberances, it was surprising to verify how a single and quite simple shape index – in this case, Shape Factor – allowed to infer a conceptual frame in the manufacturing planning and shaping of both fragments of stela E17.

Curvature analysis enabled to semi-automatically detect use-wear macro traces on the lithics, and to visually differentiate surface texture regions mainly on the archaeological stela and experimental surfaces. Although the interest of this 3D analytical technique, it has revealed insufficient in the context of the current study, in that it did not allow to quantitatively describe and compare between surface texture patterns.

This prompted me to delve deeper into 3D areal parameters and specialized metrology software, which provided a new insight into the quantitative description and analysis of the three-dimensional digital surface textures of stela E17b and experimental surfaces. On this subject, I understand that:

- The surfaces of the blocks of sandstone should have been previously scanned, to understand to what extent did the experimental work alter the original surface of the block. It was not always straightforward to determine – namely, from the three main directions of movement – which features corresponded either to the original surface or to experimental work.
- The experimental replication of surface textures can be wider in terms of the prior mentioned technical issues, as well as in the extension of the surfaces. In addition, the variables and data should be fully controlled and truly quantified during this type of experimental work.
- If there is no other interest besides studying 3D digital surface textures, samples can be individually 3D scanned. This will, on the one hand, avoid the need to digitize the entire object, besides the prior

mentioned hardware-software and time issues. On the other hand, permit more efficiently to scan samples with a higher level of detail. As aforementioned, in this case the archaeological objects had been earlier fully scanned, in order to generate 3D digital replicas for multiple uses.

- Surface metrology applications have the potential to greatly contribute to our understanding of ancient manufacturing procedures, among other archaeological issues.
- The power of the ISO 25178-2 surface texture parameters and measurement of texture direction is vast, and can undoubtedly shed light on distinct archaeological issues.
- On the basis of these analyses, I identified a set of 3D texture parameters which enabled discrimination of the current working surfaces with the best probability: *Sa*, *Sk*, *Smr*, *Spd*, *Vmc*, *Vvc*. Every selection of parameters and variables should always depend on the archaeological question behind and be adequate to describe the texture features of the objects of study.
- The analysis of the data should be done with caution as its interpretation depends on many factors, which include, but are not limited to, all steps of the method, measurement parameters/variables scheme, and performed type of analysis.

*

In order to pursue further the investigation towards the understanding of archaeological manufacturing procedures through three-dimensional digital surface texture analysis, future work may include:

- Comparing 3D surface texture data between all stelae and menhir from the Serra del Mas Bonet, and correlate them with the lithics' use-wear traces.
- Investigating 3D digital sampling issues, in order to allow a better representativeness of the surface textures. This would comprise 3D scanning the sampling areas with higher resolution and testing smaller sample sizes, so as to analyse to what extent different levels of detail and sample size determine the identification of combined texture signatures, ergo the interpretation of used gestures and tools. If smaller samples do not give satisfactory results, then produce larger experimental surfaces.
- Creating a 3D digital reference collection of quantified material surface textures, towards the understanding of mechanisms of texture formation, as well as the identification of wear patterns.
  Using a simplified approach, each wear model would: (i) describe specific variables; (ii) be digitized at regular time intervals, using for instance the same gestures, force, and tool (these variables can be controlled by mechanical/electronic devices). Each new 3D wear model would then be measured with surface metrology software:

  Wear = (set of texture parameters before test 'n') - (set of texture parameters after test 'n')

  These resulting wear gradients may then enable further correlations between surfaces, gestures, tools, among others.
- Applying computer simulation (FEA) to a tribological system, hence extending the potentialities of the 3D digital reference collection.

Annex 4B

3D Digital Surface Models of Archaeological Objects: orthographic views

(in accordance to first angle projection, meaning that the object is located in quadrant I).

Fig. 4B.20 Archaeological fragment SMB/08 E-1/3/956 (E1b).

Fig. 4B.21 Archaeological fragment SMB/08 E-1/3/957 (E1a).

Fig. 4B.22 Archaeological stela SMB/08 E-17/5/958, fragment A (E17a).

Fig. 4B.23 Archaeological stela SMB/08 E-17/5/958, fragment B (E17b).

Fig. 4B.24 Archaeological fragment associated with stela SMB/08 E-17/5/958, fragment C (E17c).

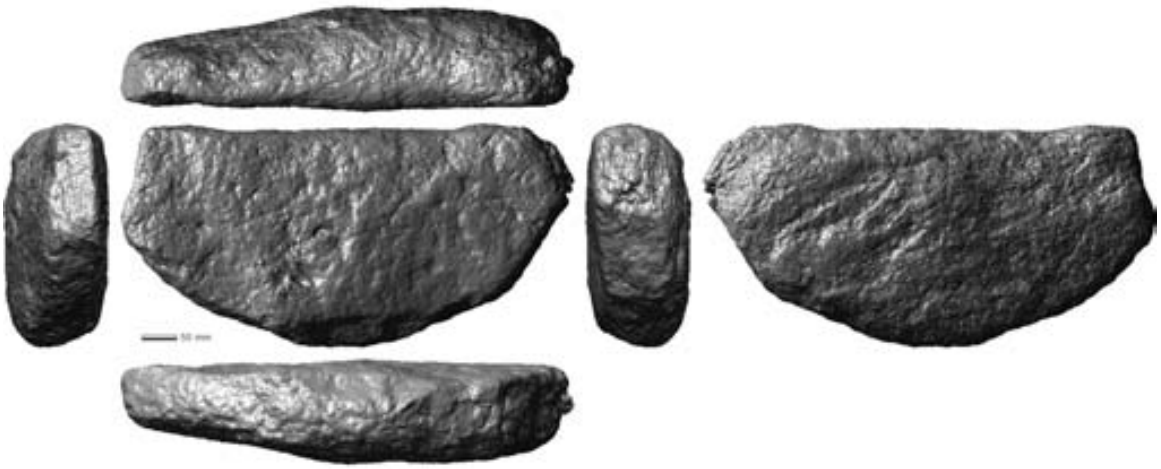

Fig. 4B.25 Archaeological fragment SMB/08 E-48/1/45 (E48).

Fig. 4B.26 Archaeological stela SMB/08 E-52/1/22 (E52).

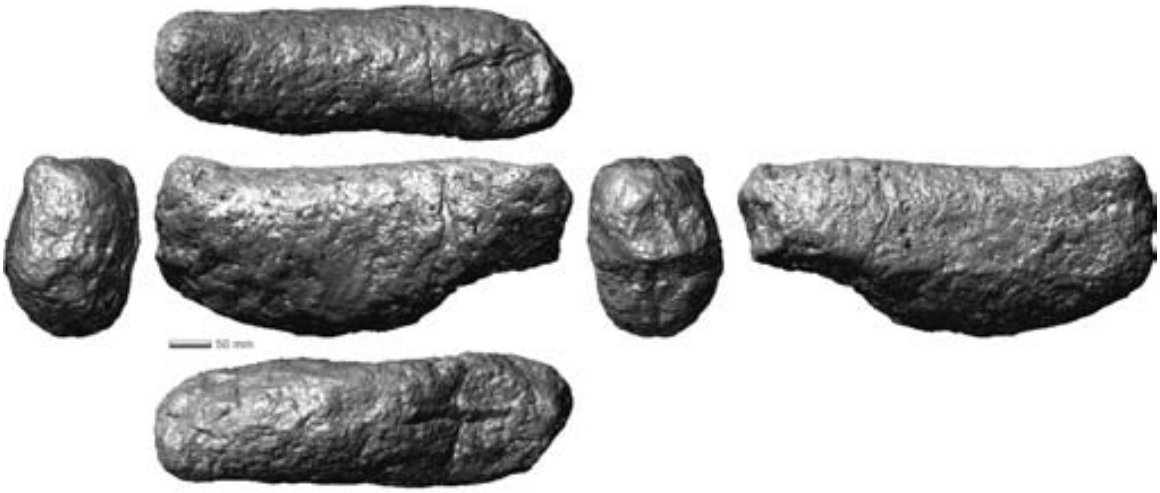

Fig. 4B.27 Archaeological fragment SMB-08 E-185/2/5 (E185).

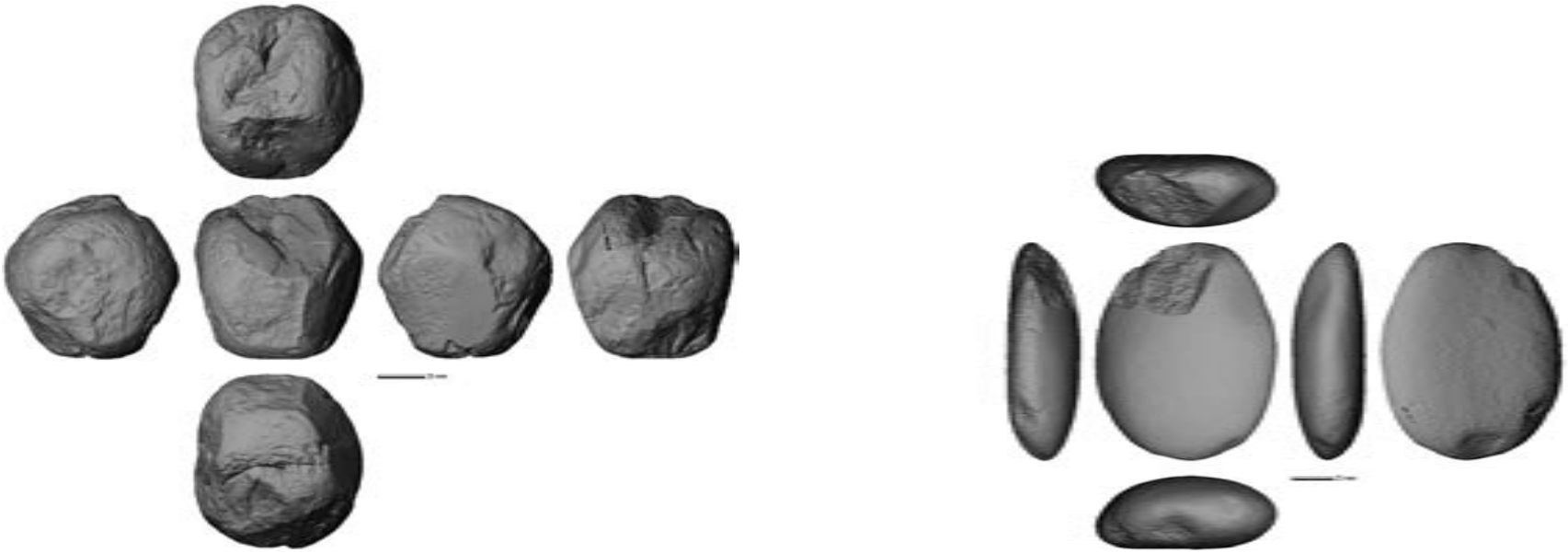

Fig. 4B.28 Archaeological lithics E17-C1-C117 (left) and E17-C2-C311 (right).

Fig. 4B.29 Archaeological lithics E17-C2-C312 (left) and E17-C4-C578 (right).

Fig. 4B.30 Archaeological lithics E17-C4-C580 (left) and E17-C6-C754 (right).

Fig. 4B.31 Archaeological lithics E17-C7-C793 (left) and E17-C7-C798 (right).

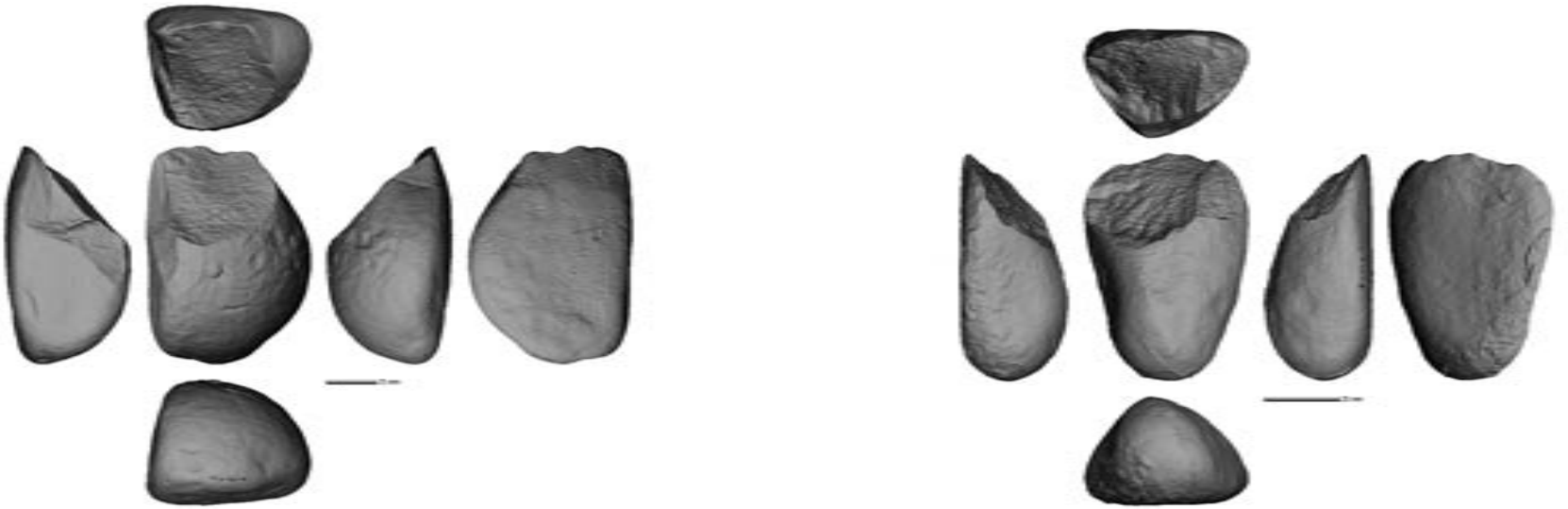

Fig. 4B.32 Archaeological lithics E48-C1-C40 (left) and E52-C1-C26 (right).

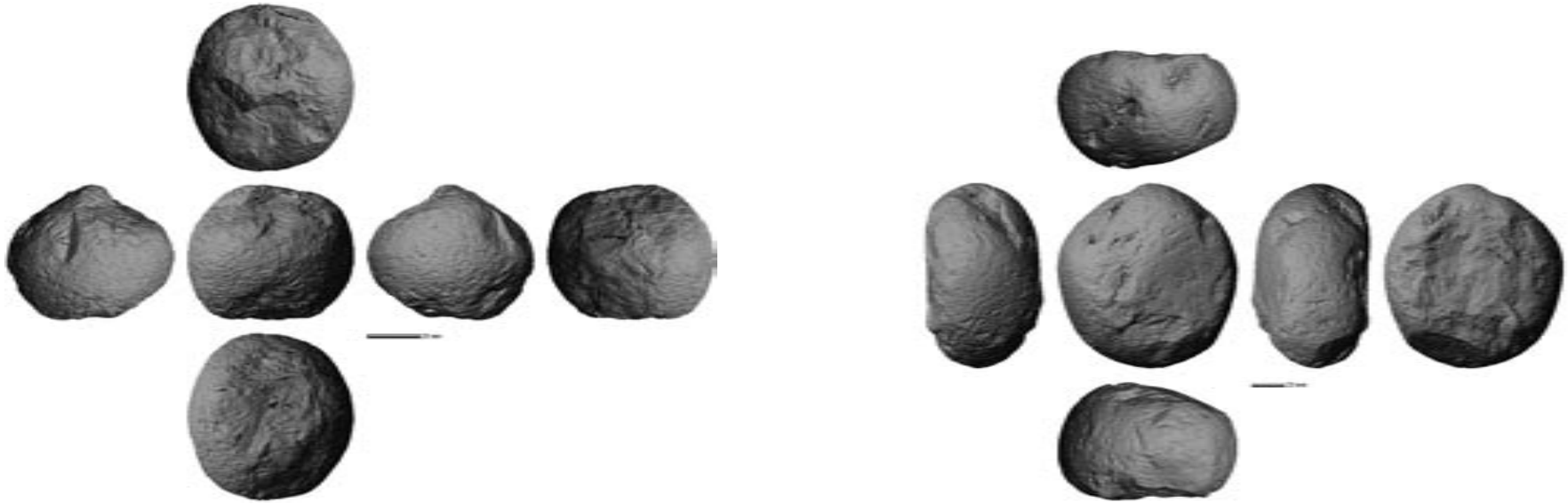

Fig. 4B.33 Archaeological lithics E52-C1-C27 (left) and E52-C1-C28 (right).

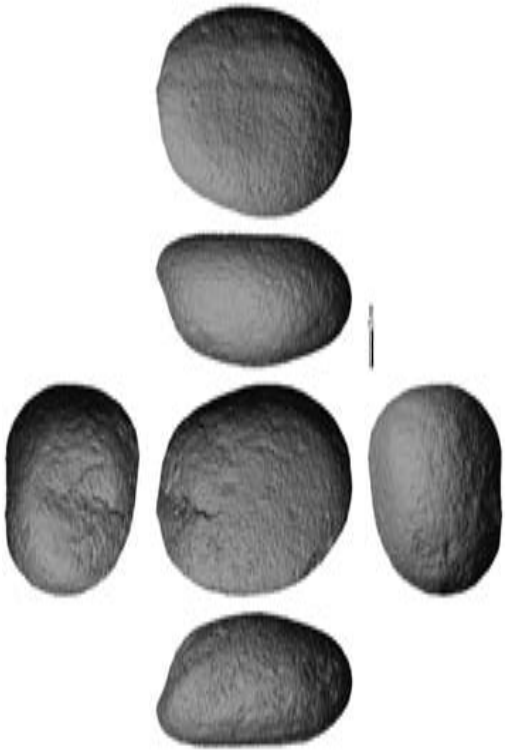

Fig. 4B.34 Archaeological lithic E52-C1-C29.

ø4-C
La Draga, Catalonia

C.1 Problem Statement & Objectives

The Neolithic lakeside settlement of La Draga is located on the eastern shore of the Banyoles Lake (Girona, Catalonia). It was discovered in 1990 during the construction works of the Olympic channel. This site is the only prehistoric site in an open-air lakeside environment found in the Iberian Peninsula, and one of the three found in the Mediterranean region. One of the other aspects that make this settlement so unique is the vast number and variety of wooden and other vegetable fibres objects found. Among them is an especially noteworthy wooden item referred to as a bow. Up to now, two fragments and one complete bow have been recovered. These are the most ancient bows found in Europe from the Neolithic period, dated between 5.324 and 4.960 cal. BCE. This settlement is a very rich source of information on the use of wood resources, woodworking technology for the production of tools, and their functions, and contributes substantially to our knowledge of how the first farming communities which settled in the Iberian Peninsula lived and organised themselves.

The objective of this case study is to be able to provide meaningful information towards a better comprehension of the relationships between form, texture, material, and function(s) of a set of wooden artefacts, by:

- Measuring and describing quantitatively their geometrical features and material properties;
- Testing hypothesis concerning the form, material, and mechanics of the only complete bow (D12_JF-JG-81), which was chosen as an optimal test case.

Furthermore, and given the specificities of these fragile and perishable artefacts, it aims to document them with as much detail as possible, to avoid manipulating them further, for conservation monitoring and preservation, as well as for future researches.

This third case study is organized as follows. It starts with an archaeological contextualization of the Neolithic lakeside site of La Draga. Then, in order to confirm the effectiveness of the proposed framework for archaeological interpretations, real artefacts from this site were selected for scanning. This selection comprised several wooden artefacts with hunting and defence actions as functional hypotheses, including possible spears, darts, arrows, arrowheads, and bows. However, the work herein presented focuses mainly on the bows, in view of the great complexity of the research topic and the objects of study themselves. Next, a general geometrical characterization from the 3D digital surface models is provided. After that, a description of real-world tests conducted to obtain the material properties of several wood species is given. Then, an experimental approach based on the use of FEA and computer simulation was performed, to gain new insight into the behaviour of bows. Results are presented throughout this chapter's sections to demonstrate the practical interest of the proposed framework. Finally, conclusions are given.

C.2 Archaeological Contextualization

The archaeological lakeside settlement of La Draga is located on the eastern shore of the Banyoles Lake, 172 m asl, in the province of Girona, north-eastern Catalonia, Spain (Figure 4C.1). It was discovered in 1990 during the construction works of the Olympic channel. This site is the only prehistoric site in an open-air lakeside environment found in the Iberian Peninsula, and one of the three found in the Mediterranean region (together with La Marmota in lake Bracciano, near Rome, Italy; and Dispilio in lake Orestiada, northern Greece). It is an early Neolithic village (Cardial-ware phase) dating from 5.324-4.960 cal. BCE, which makes it one of the oldest of the Neolithic period in the Iberian Peninsula (Bosch et al. 2000, 2006, 2011, 2012).

Fig. 4C.1 Geographical location of: the autonomous region of Catalonia in Europe (left), the city of Banyoles in Catalonia (centre), the archaeological site of La Draga in Banyoles (left) (maps by Google).

Since 1990, three different areas have been excavated: Sector A, the upper area (water table approximately

70 cm below the archaeological level); Sectors B and D (Figure 4C.2), the lower area, beside the Lake (water table approximately 40 cm above the archaeological level); Sector C, the Neolithic lakeshore, which is now under water. These variations in the groundwater level have affected the conservation of the Neolithic objects herein found.

Fig. 4C.2 Excavation of sector D: 2011 campaign (left), and 2012 campaign (right) (photos by J. Casanova and Equipo Draga, respectively).

One of the other aspects that make this settlement so unique is the vast number and variety of wooden and other vegetable fibres objects found. The overlap between the archaeological level and the water table in sectors B and C enabled the preservation of the most important collection of bioarchaeological remains in subfossil state from this period, such as a large amount of posts and planks from the wooden structures (more than one thousand), numerous and various wooden and basketry objects (up to 18 taxa and 305 items encompassing functional proposals, such as: construction, domestic and personal items, hunting, defence, agricultural tools) and large quantities of cereal grains and animal bones. Furthermore, numerous remains of wooden structures (housing) and others (fireplaces, septic tanks, pavements), as well as domestic areas have been well documented.

According to Burjachs and Piqué (Bosch et al. 2000, Terradas et al. 2012), the environmental data reveals that well constituted lakeshore woods (e.g., *Corylus avellana, Fraxinus sp., Alnus glutinosa, Populus sp., Ulmus, Salix sp., Laurus nobilis*, *Prunus spinosa* and *Sambucus sp*.) and hinterland forests (e.g., *Quercus sp deciduous*, *Buxus sempervirens, Taxus baccata*, and wild fruit-bearing trees) grew round about the village.

The subsistence of the communities herein settled was primarily based on fully consolidated agriculture and livestock, leaving hunting and gathering as secondary activities. These secondary activities permitted to obtain a wide range and variety of foodstuffs from the Lake, the Mediterranean Sea, the woods of the immediate hinterland and the highlands which formed the border of their supply area (Tarrús 2008, Antolin and Buxó 2011, Saña 2011, Bosch et al. 2011, 2012, Terradas et al. 2012, Piqué et al. in press).

The topographical location of La Draga – a small peninsula with the appearance of an island – made it easy to defend. The causes for the abandonment of this site, after more than a century of settlement, are still being investigated.

Hence, this settlement is a very rich source of information on the use of wood resources, woodworking

technology for the production of tools, and their functions, and contributes substantially to our knowledge of early Neolithic settlements in the Iberian Peninsula, as well as in the Mediterranean area (Bosch et al. 2000, 2006, 2011, Tarrús 2008, Terradas et al. 2012)

The research carried out at the La Draga site has been financed by the Department of Culture of the Government of Catalonia and the Spanish Ministry for Economy and Competitiveness. This project has been conducted under the coordination of the County Archaeological Museum of Banyoles, with the participation of the UAB Department of Prehistory, the Department of Archaeology and Anthropology of the CSIC – Institute Milà i Fontanals (IMF-CSIC), the Archaeological Museum of Catalonia and the Centre for Underwater Archaeology of Catalonia (CASC).

C.2.1 Selected Artefacts

In order to confirm the effectiveness of the proposed framework for archaeological interpretation, real artefacts from the Neolithic lakeside site of La Draga were selected. In a first stage, several wooden artefacts with hunting and defence actions as functional hypotheses, were selected.

Among the selected items are many possible arrows, darts, spearheads, and a spear (Bosch et al. 2000, 2006, 2011, Tarrús 2008), though these hypothesis are being investigated. But one of the noteworthy wooden items is an object referred to as a bow. Up to now, two fragments (D02_KA89-11, D05_KE90-7) and one complete (D12_JF-JG-81) have been found. D02_KA89-11 was excavated in sector B, in 2002; D05_KE90-7 in sector B, in 2005; and D12_JF-JG-81 in sector D, in 2012 (Figures 4C.3-4C.5) (to simplify matters, also referred to as “D02”, “D05”, and “D12”, respectively, in the following). Each of these self-bows is made from a segment of trunk or stave longitudinally sectioned. One of the faces of the bow has not been modified in relation to the original morphology of the timber, corresponding to the cortical surface of the last ring of growth, of which just the bark is removed (Piqué et al. in press). All three artefacts are made out of yew wood (*Taxus baccata*), as were the majority of Neolithic bows in Europe (Clark 1963, Bergman et al. 1988, Junkmanns 2001).

It is worth mentioning that so far these are the most ancient bows found in Europe from the Neolithic period, dated between 5.324 and 5.000 cal. BCE (Piqué et al. in press). Most of the Neolithic bows in Europe have been recovered in central and northern Europe. Some fragments from central Europe are dated between 5.200-5.000 BCE, but the majority is from later periods than La Draga, often more than a thousand years younger (Piqué et al. in press).

Bow and arrow making was a skilled occupation involving many activities, from the perception (Henderson 2000) and selection of adequate raw-materials for each component, to the manufacturing processes, techniques, and tools. All requiring expertise to ensure the production of efficient and enduring artefacts, which may have also determined the relative value of each bow (Tarrús 2008, Piqué et al. in press). These bows could have served different purposes, such as hunting, warfare, playing, training, or even represented elements of prestige.

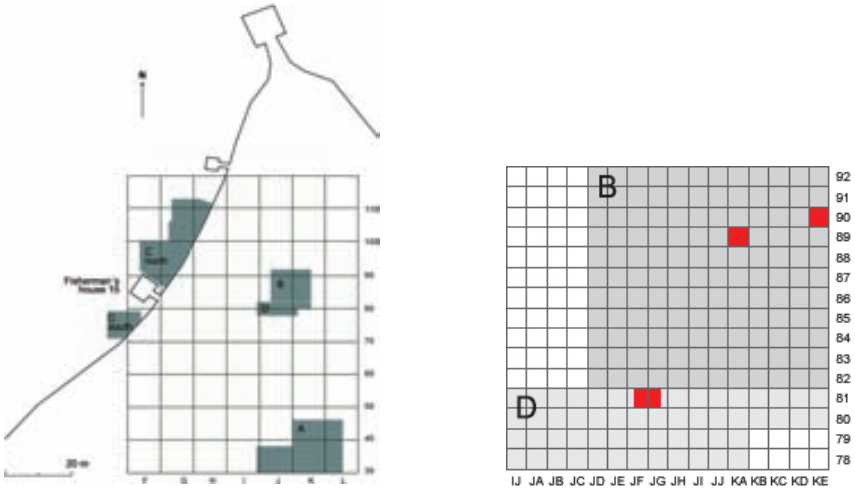

Fig. 4C.3 Plan of La Draga showing excavated areas and sectors (adapted from Bosch et al. 2006) (left), and detail of sectors B and D with the location (in red) of artefacts D02_KA89-11, D05_KE90-7, and D12_JF-JG-81 (right). The site occupies approximately 8.000 m^2.

Fig. 4C.4 Artefact D12_JF-JG-81, excavated during the 2012 campaign (photo by Equipo Draga).

Research carried out by Saña (Tarrús 2008, Saña 2011, Terradas et al. 2012) documented 51 animal species, 5 domestic and 46 wild. Thus, a clear presence of wild mammals exploited for food consumption, among them: aurochs (*Bos primigenius*), wild boar (*Sus scropha*), red deer (*Cervus elaphus*), roe-deer (*Capreolus capreolus*), wild goats (*Capra pyrenaica*), and some lagomorphs (*Oryctolagus cunniculus*) and small carnivores (*Vulpes vulpes*, *Meles meles*, *Martes marte*, *Felis silvestris*). Although there are other animal species – i.e., fish, birds, reptiles, and molluscs – from the lake and its surroundings that also appear in the archaeological record, their contribution to human subsistence is not representative. The hunting grounds extended beyond the nearby forests into the mountains (indicated by relics of roe-deer and wild goats). Some species might have been hunted specially because of their nutritional and calorific value, among other issues, while other species were hunted to obtain raw-material, namely skins for winter clothing (indicated by remains of a few foxes and a small musteline).

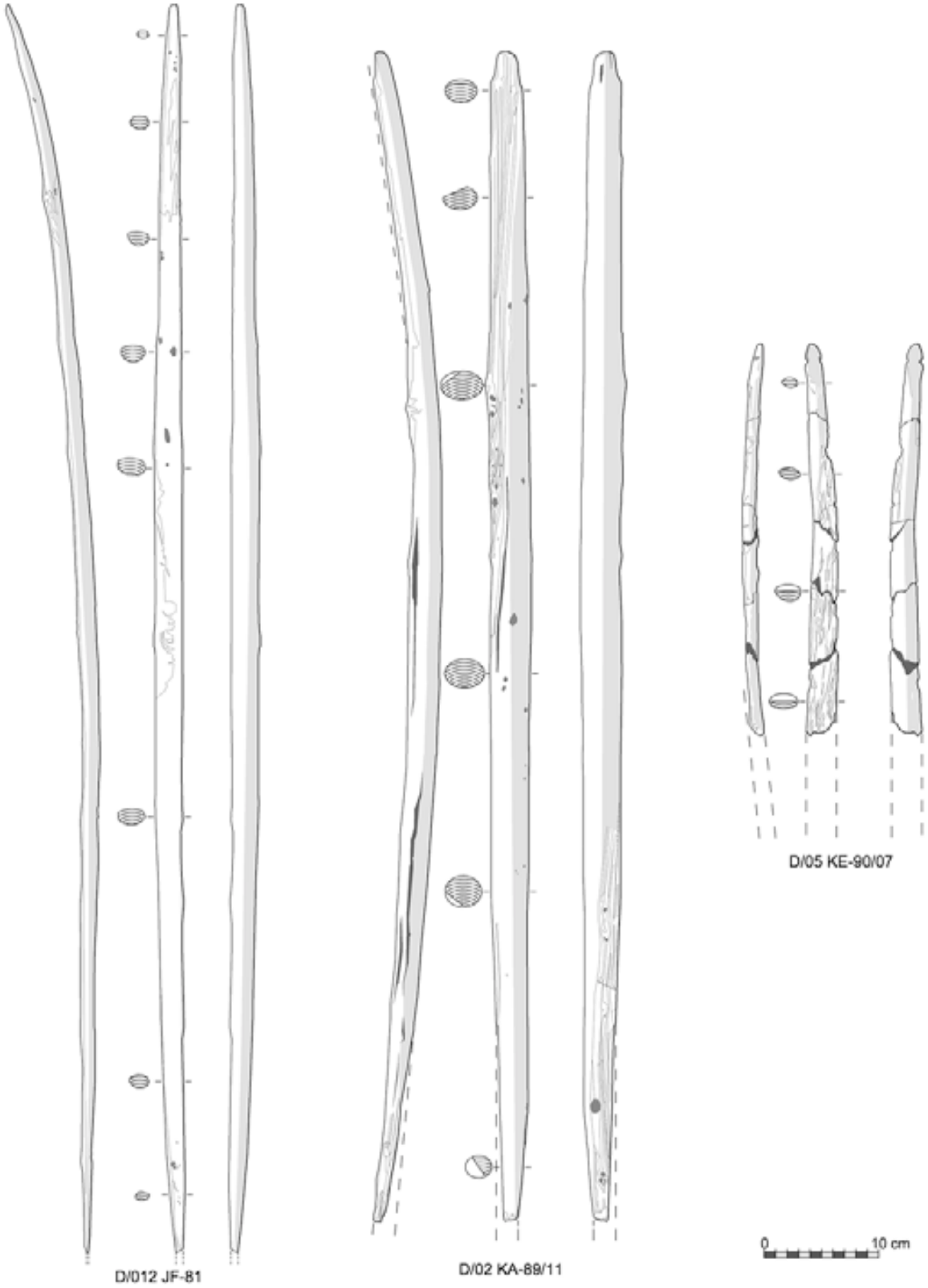

Fig. 4C.5 The bows of La Draga: D12 JF-JG-81 (left), D02 KA-89-11 (centre), D05 KE-90-7 (right) (illustration by Xavier Cardus; Piqué et al. in press).

In spite of the low-level exploitation of the hunted wild animals (only 3% of the total faunal remains analysed, 14,6% if potentially supplied biomass is considered), there is a remarkable and varied body of sig-

nificant archaeological objects which can be related to cynegetic or defensive/offensive activities of the Neolithic inhabitants of this lacustrine site (Bosch et al. 2000, 2006, 2011, Palomo et al. 2005). So far there is no archaeological evidence of conflict or violence in La Draga or other contemporary sites in this geographic area. The first signs of violence don't appear in this area until the fourth millennium cal BCE (Agustí, Mercadal 2006, Piqué et al. in press).

The discovery of this body of archaeological materials opens new perspectives in the understanding of how these first farming communities which settled in the Iberian Peninsula lived and organised themselves.

C.3 Framework Implementation

C.3.1 3D Digital Surface Model Generating

The archaeological objects of this work initially comprised twenty-one wooden artefacts with hunting and defence actions as functional hypotheses, including possible spears, darts, arrows, arrowheads, and bows. However, the work herein presented focuses mainly on the three bows, in view of the great complexity of the research topic and the objects of study themselves.

Most of these wooden artefacts have been restored – from 1995 to 1997, they were sent to the laboratory of restoration at Laténium, Parc et Musée d'Archéologie de Neuchâtel (Switzerland), to be lyophilizated; since 1998, they have been sent to the CASC´s restoration laboratory – and are now deposited at the MACB (Bosch et al. 2000, 2006, 2011, Tarrús 2008).

The only artefact which has not yet been restored is D12_JF-JG-81. Like all the other wooden artefacts recovered in La Draga, D12 was kept preserved in a humid soil and an anaerobic environment until it was finally discovered, in 2012. After excavated, it was immediately and carefully stored in a proper container, where it was submerged in water. Next, the artefact was cleaned by the conservation team (Júlia Chinchilla and Irene García) – which basically consisted in removing the sediment – and then kept in a proper container where it remained submerged in another solution of water and borax (3ºC) before being sent to CASC for restoration. It was exactly during this short time, right after the conservation team finished their work, that this artefact was made available for scanning. One of the interests of digitizing this artefact right after being excavated has to do with conservation monitoring purposes (Amendas 2013, Cretté 2013) – during restoration process its basic specific gravity is likely to decrease along with the progress of deterioration, which may cause alterations in form and texture, and consequently eliminate or distort use-wear traces.

All twenty-one artefacts were scanned in two phases, during the 2011 and 2012 excavation campaigns. The measurement procedures were the same within each stage and step of the framework.

C.3.1.1 Workspace, 3D Scanner and Calibration

The artefacts were scanned indoors at MACB, in two separate rooms. One of the rooms had two large windows with curtains that did not entirely block the entering of sun light, whereas the other had a controlled dark environment. Exception was made for artefact D12 which was scanned indoors at Arqueolític, Banyoles, in a closed room with a fully controlled dark environment.

The same 3D structured light scanner, computer, and software – described in the first case study – , were used to capture the 3D digital surfaces of the selected wooden artefacts.

Given the specificities of these artefacts – overall dimensions, type of raw-material, surface/texture (macro-topography generally smooth, but with visible use-wear traces), highly fragile and perishable nature – it was important to document them with as much detail as possible, to minimize handling them further, for conservation monitoring and preservation, as well as for future researches. Therefore, the scanner was calibrated at MACB with the 90 mm and 150 mm stereo FOVs, and at Arqueolític with the 150 mm stereo FOV, as I will explain next.

C.3.1.2 3D Data Acquisition and Post-processing

Due to logistic matters and to the short opening hours of the museum's research facilities, after calibrating the scanner with the selected set of lenses I decided to continue only with the point cloud data acquisition and interactive pre-alignment at MACB (Figure 4C.6) – to ensure that there weren´t any relevant parts of the form missing, as well as the quality of the recorded data –, using the scanner's proprietary capturing software Optocat 2009. Inasmuch I was only concerned with the artefact's geometric data and the scanner has a low resolution camera, I did not capture any image texture during scanning. All raw acquisition data was saved at a specified repository, for potential future re-processing (3D-COFORM 2009). The scan data cleaning, merging and polygonal mesh generating were done later at IMF-CSIC, Barcelona, using the same software.

During the first scanning phase I used the shortest FOV available for this scanner, the 90 mm set of lenses, which has the highest resolution and gives the maximum level of detail. However, the 3D scans of the larger artefacts could not be post-processed due to insufficient computer resources to deal with such heavy files. Consequently, several artefacts were rescanned in 2012 with the immediate lower FOV, the 150 mm set of lenses, so as to enable post-processing the data.

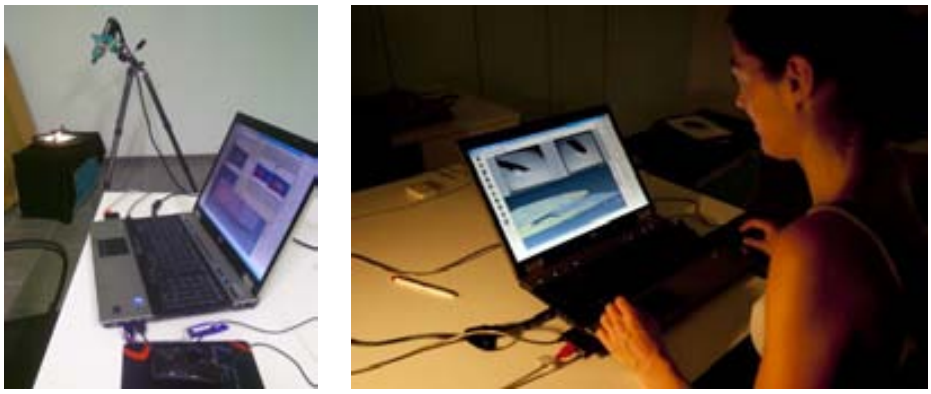

Fig. 4C.6 3D Data acquisition (left), and pre-alignment process (right; photo by Marco Ansaloni).

The same general 3D data acquisition and post-processing procedures described in the previous case studies were here used. As mentioned in the previous case studies, due to the fact that each stage of the process depends on the outcome of the previous ones and determines the following ones, here again all parameters must be tailored accordingly.

The overall accuracy of the mesh heavily depends on the 3D data acquisition flow, overlapping areas between patches, number and positions of the single views (Breukmann 2009). The scanning flow described in case study 4A was now adapted to the geometry of each wooden artefact. The orientation of the 3D model's coordinate system was automatically defined by the view of the first scan of the project. To minimize measurement error, and improve the quality of the alignment, a sufficient amount of overlapping area (>30%) between scans was ensured. To overcome most of the self-occlusion problems, I used multiple viewing angles during scans, by changing the scanner's position in respect to the artefact. For the smaller artefacts a manual turntable was used to avoid handling them further – ideally an automated turntable would have been used, since it reduces the amount of time and work during scanning and post-processing. However, the entangled geometry of some wood knots invariably led to some small holes in the mesh.

Further factors may limit the precision and even reliability of the 3D geometrical data: alterations of the original artefact in form, size, texture and colour, due to taphonomic or post-excavation factors; the present and overall geometry of the artefact (i.e. the topography of the object); the type of raw material and archaeological surface finishing; the presence of several distinct characteristics on a specific surface area (e.g. wood hardened with fire, plus restoring product, plus natural wood surface; wet wood). In view of the exceptional nature of archaeological wooden artefacts, Figures 4C.7 and 4C.8 illustrate some of the difficulties encountered during 3D data acquisition of some of these artefacts. Although the remaining scanned artefacts with hunting and defence actions as functional hypotheses are not included in the current work, they did permit to continue testing, comparing, and studying several technical issues, which also enabled me to undertake more efficient and quicker decisions.

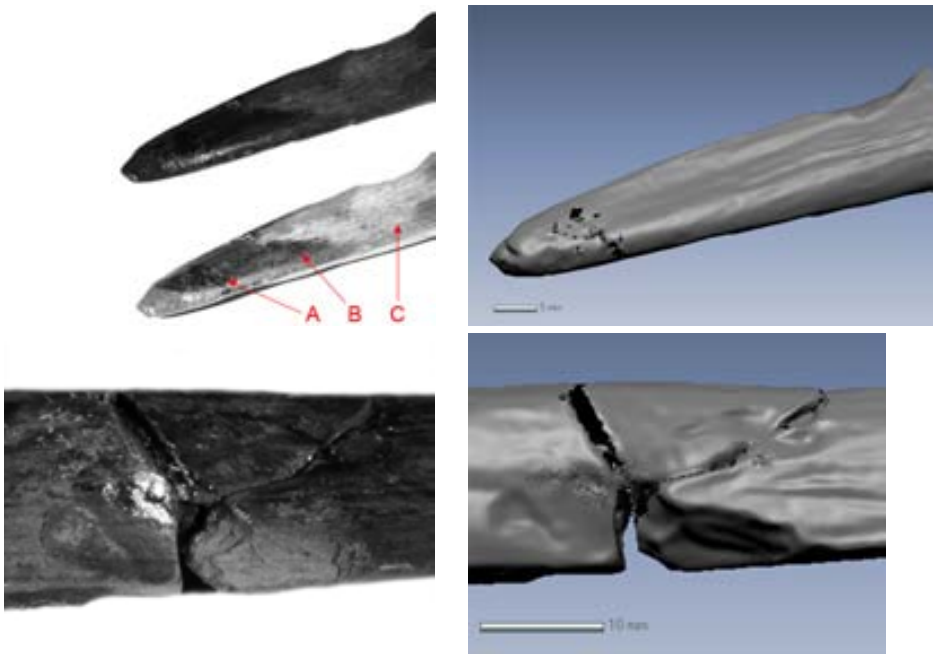

Fig. 4C.7 Scanning captured images with different exposures of detail of artefact D98-JH86-50 (top left), and 3D digital surface model (top right). Problems during scanning: presence of several distinct characteristics on a specific surface area - restoration product (A), wood hardened with fire (B), and natural wood (C). Scanning captured image of another detail of artefact D98-JH86-50 (bottom left) and 3D digital surface model (bottom right). Problems during scanning: fragmentation, and restoration techniques, i.e., surface finishing. This wooden artefact is made of *Buxus sempervirens*, and is referred as a dart (Bosch et al. 2006).

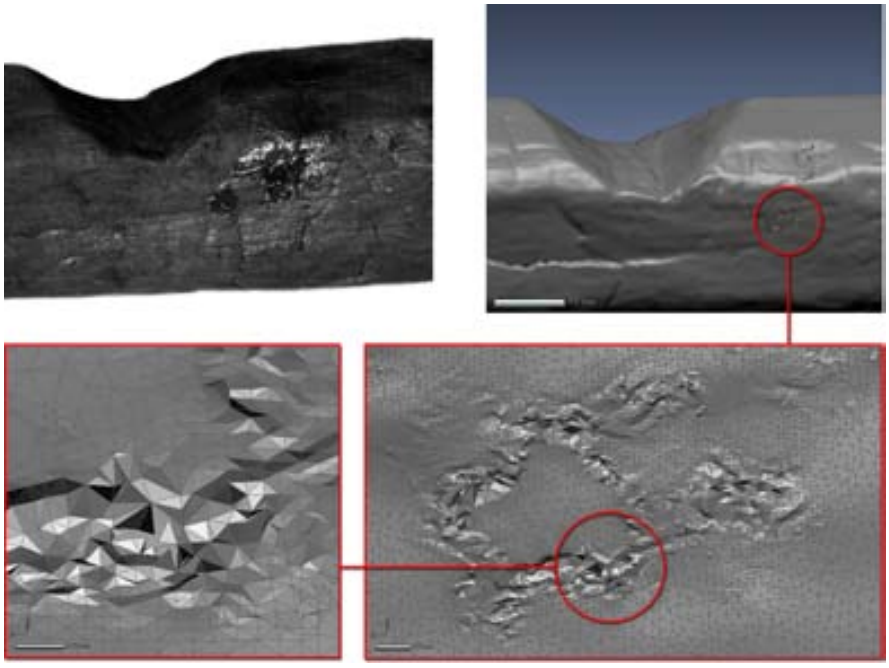

Fig. 4C.8 Scanning captured image of detail of artefact D98-FI98-1 (top left), 3D digital surface model (top right), surface mesh details (bottom left and right). Problems during 3D data capture: noise data due to the presence of glue. This wooden artefact is made of *Buxus sempervirens*, and is referred as a possible digging stick used for agriculture and/or to hunt (Bosch et al. 2006).

As above mentioned, artefact D12 was kept submerged in a proper container before being sent to CASC for restoration. It was exactly during this short time, right after the conservation team finished their work, that this artefact was made available for scanning. It was scanned inside the container in order not to jeopardise its integrity. During this process the parts that were not being scanned stood submerged, leaving only the surface area that was being scanned wet but momentarily not soaked.

Regarding to the scanning ambient light conditions, the intensity of light entering one of the rooms varied dramatically during the day, also due to clouds. The parameters of the scans had to be constantly readjusted and often repeated to avoid either missing data or noise data. In view of the fact that the other room consisted in a controlled dark environment, the scanning process was faster and the software's quality data inspector showed best results – these are the good data that I am now working with. It is important to realise that either missing data, noise data, filling holes, filtering, and certain parameter's settings during the scanning or post-processing stages may conceal, distort, or even delete, relevant data, such as use-wear traces (Moitinho de Almeida, and Barceló 2012).

The final alignment of the scans lasted from 1 to 40 minutes to process, depending on the dimension and complexity of each artefact. As for the merging process, in general it lasted from just a couple of minutes to half an hour long; though in the worst cases from 3 to 6 hours long, after several failed attempts with the system crashing. Of course this is also due to the aforementioned 3D surface model requirements and inherent technical constraints, resulting in heavy files difficult for the system to manage.

One of the extremities of artefact D12 was partially cracked and slightly moved during scanning, leading to a mismatch of this area's scan files. Therefore, it was necessary to implement a corrective action by digitally matching this part of the 3D model. The 3D surface models (Figure 4C.9) were then exported in STL format in order to proceed with geometric features extraction.

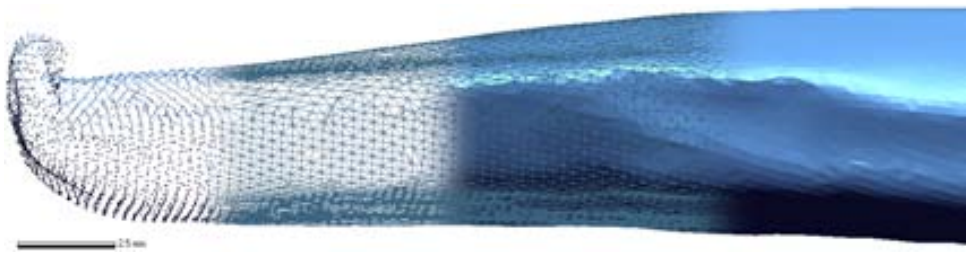

Fig. 4C.9 Detail of 3D digital surface model of wooden artefact D12_JF-JG-81. From left to right: point cloud, polygonal mesh, polygonal mesh and surface, surface.

Table 4C.1 shows the number of scans captured, weight (KB) of the aligned and merged scans files, and computed topological measures (number of mesh vertices and faces) of the final STL 3D digital surface models of the bows.

Table 4C.1 3D digital models of D02_KA89-11, D05_KE90-7, and D12_JF-JG-81, scanned with 150 mm stereo FOV.

Artefacts	Number of scans	Aligned scans (*.ctr) (KB)	Merged scans (*.stl) (KB)	Poly-vertices	Poly-faces
D02_KA89-11	110	294922	144345	1482320	2956065
D05_KE90-7	50	85668	40442	414657	828236
D12_JF-JG-81	97	188536	112669	1151777	2302775

C.3.2 Geometric Information Extraction from 3D Digital Surface Model

The purpose of this section is to provide a general geometrical characterization from the 3D digital surface models of artefacts D02_KA89-11, D05_KE90-7, and D12_JF-JG-81 (Figure 4C.10), in order to be able to differentiate one from another. In spite of an exhaustive description of each artefact being beyond the scope of this thesis, a brief but representative geometric analysis is here given.

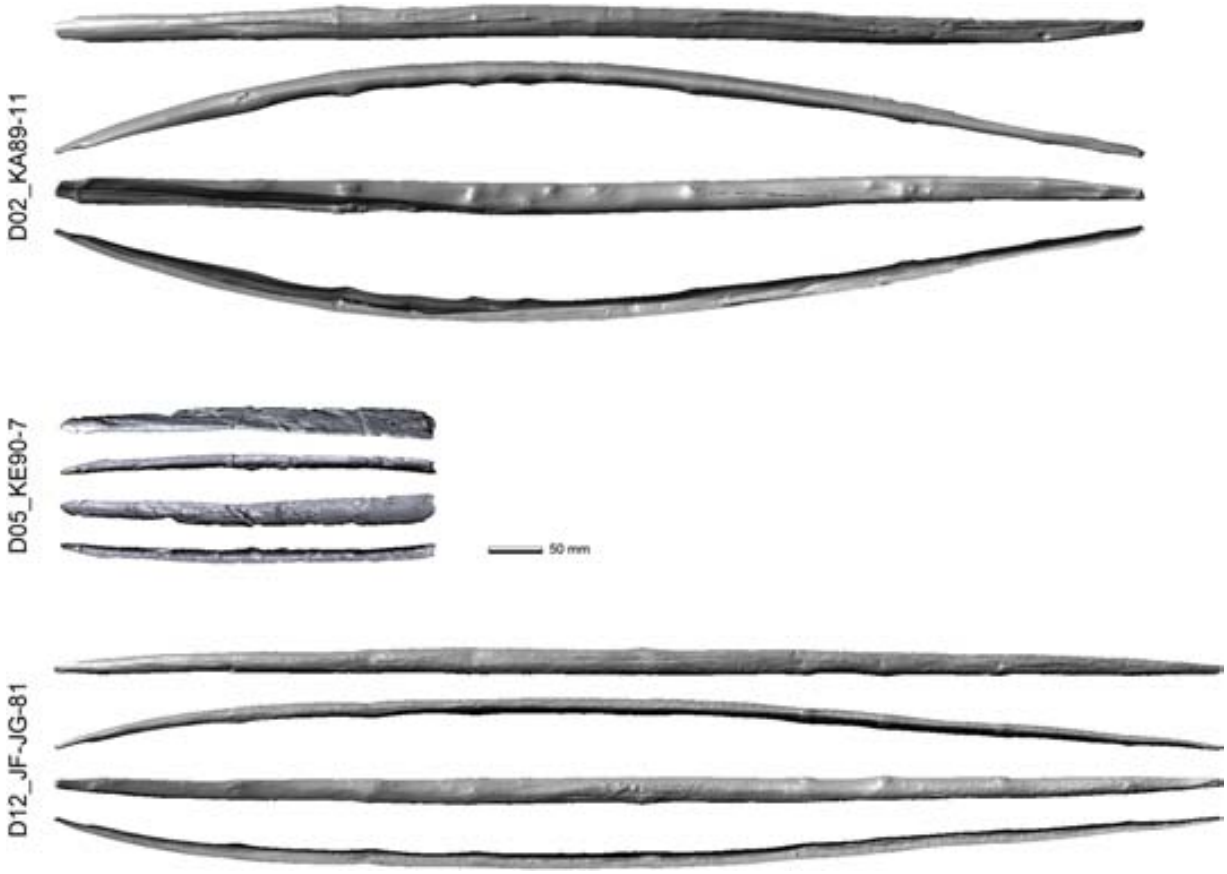

Fig. 4C.10 3D Digital surface models of wooden artefacts D02_KA89-11 (top), D05_KE90-7 (centre), D12_JF-JG-81 (bottom), scanned with 150 mm FOV. Back, left side, belly, and right side views (from top to bottom).

This stage took place at LAQU-UAB, Bellaterra, and at IMF-CSIC, Barcelona. Once again, both MeshLab v1.3.0 and Rapidform XO Scan 2010 software were used.

Before continuing and in order to give clarity to some of the technical terms and basic concepts related to bows, Figure 4C.11 shows the anatomy of a simple non-recurve bow – as those recovered in La Draga – (left), and the bow in three situations (right): unbraced, braced, and fully drawn. In essence, a bow consists of two elastic limbs separated by a grip – also known as 'handle' or 'handgrip'. The bow is braced by fastening a string between both nocks. Then, an arrow is set on the string and the archer pulls the bow from braced situation into full draw (Kooi 1991). Ancient bows would have had their strings made of vegetable fibres, sinew, or rawhide. No strings were found attached to the bows from La Draga, though some fragments of strings made of vegetable fibres were found and have been recently spatially associated with the bows.

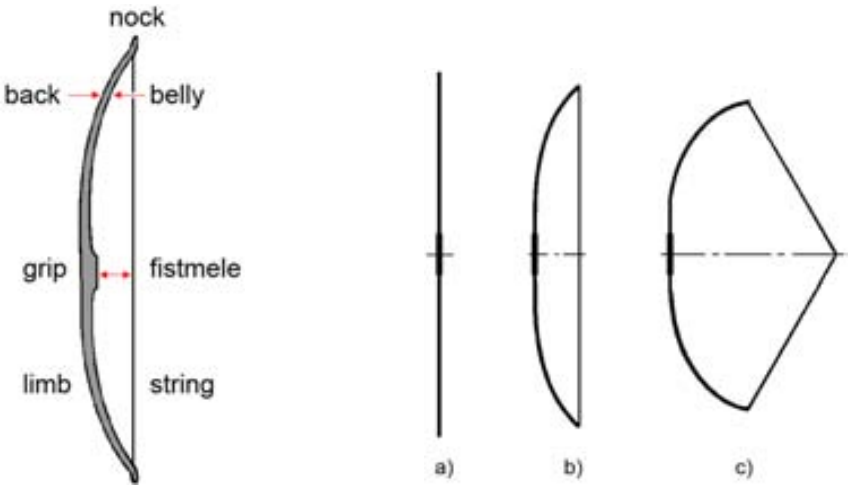

Fig. 4C.11 Non-recurve bow anatomy (left), and in three situations (right): a) unbraced, b) braced, c) fully drawn (adapted from Kooi 1983). In essence, a bow consists of two elastic limbs separated by a grip. The bow is braced by fastening a string between both nocks. Then, an arrow is set on the string and the archer pulls the bow from braced situation into full draw (Kooi 1991).

C.3.2.1 Shape and Form

The data collected from basic measurements was the starting point to describe the 3D models (Table 4C.2).

As mentioned above, artefact D12 was scanned still wet and before being restored. According to Kohdzuma (2005, p.2), even though the wood substance is reduced the outward size is unchanged, "the reason that the size of the cell walls does not change is that the new voids opened up by the decomposition and disappearance of constituent of the cell walls are immediately filled by water". Therefore, I will assume that the measurements taken from this artefact now closely reflect the original artefact by the time it was covered with the organic sediment of the archaeological level and the chalk of the lake.

Table 4C.2 Computed geometric measures of the 3D digital models of D02_KA89-11, D05_KE90-7, and D12_JF-JG-81. Width, height, and depth refer to the model's bounding box.

3D model (*.stl)	Length (mm)	Height (mm)	Width (mm)	Area (mm^2)	Volume (mm^3)
D02_KA89-11	992,6	87	35,9	69166,6	296135,8
D05_KE90-7	343,6	18,3	30,7	18093,5	53692,1
D12_JF-JG-81	1073,6	48	26,5	54673	198544,4

Next step consisted in sampling sections at small intervals in order to highly represent differences in shape among each of the artefacts, and correlate the data. The fact that the generated mesh had a few holes – i.e., data missing due to the entangled geometry of the artefact and water reflection – hindered some sections of being fully measured. To overcome this obstacle, only where necessary the holes were filled in a derivative 3D model. Cross-sections in parallel planes were then recorded at 10 mm intervals (Figure 4C.12; measured values are listed in Annex C, Tables 4C.8 and 4C.9). Subsequent statistical analysis was carried out using JMP v.10 software. Width, height (i.e. thickness), area, perimeter, and Shape Factor measurements of every planar cross-section are shown in Figure 4C.13, while height-width and area-perimeter ratios are displayed in Figure 4C.14.

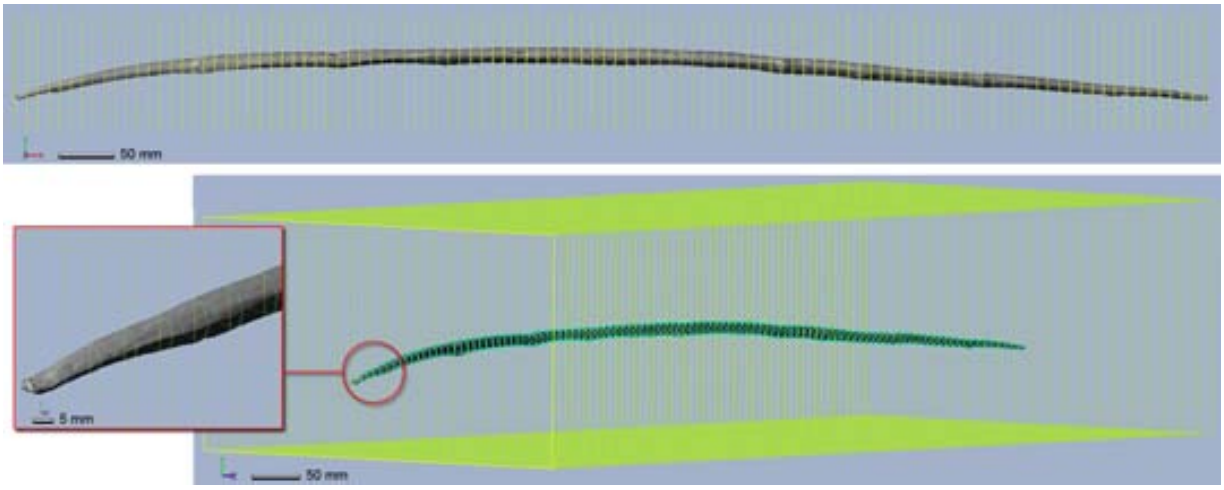

Fig. 4C.12 3D Digital surface model of artefact D12_JF-JG-81 sectioned every 10 millimetres: side view with parallel planes intersecting the model (top), sections along the model and detail (bottom).

The variability within the measured values of D02 is evident. It is possible to observe a general trend with the limbs becoming narrower toward the tips, despite not being symmetrical. However, the irregularity of the curves (Figure 4C.13) together with the dispersion of the data in the scatter plots (Figure 4C.14) reflect well the variations in the form of this artefact. These variations can, for instance, be due to localised natural protrusions and depressions (e.g., wood knots, chrysals), functional, fragmentation, post-depositional, or even restoration factors, which can occur in either surface and in different degree of irregularity. Significant differences are observed at D02, with most of its cross-sections exhibiting higher perimeter, area, height and width values. This artefact has a constant Shape Factor in the middle portion (and slightly higher than D12),

whereas each limb has its own irregular shape. In addition, the decrease of Shape Factor values towards the ends also indicates a high curvature of the bow's profile.

Because D05 consists on a small fragment, the 3D digital model was also inverted in order to see if it was possible to infer if this end pertained either to the upper limb or to the lower limb of the bow. However, the graphics do not indicate a clear and distinct answer. As expected, the irregularity of the curves (Figure 4C.13) together with Shape Factor decreasing towards the middle part, reflect well the state of preservation of this artefact.

D12 is the only bow that is complete, perhaps because of this it is the longest – "the length of a bow should be in proportion to the length of the arrow to be used with it, and also to its own weight" (Longman 1894, chapter XVII, p.5). There is a great consistency of the measurements along this artefact. In the main, the values of the measurements are much regular, slightly increasing from the ends to the middle part. The limbs gradually become narrower toward the tips. The high symmetry between both limbs is noteworthy. The near linear area-perimeter ratio together with width and height, and the constancy of Shape Factor values indicate similar and generally smooth cross-section shapes.

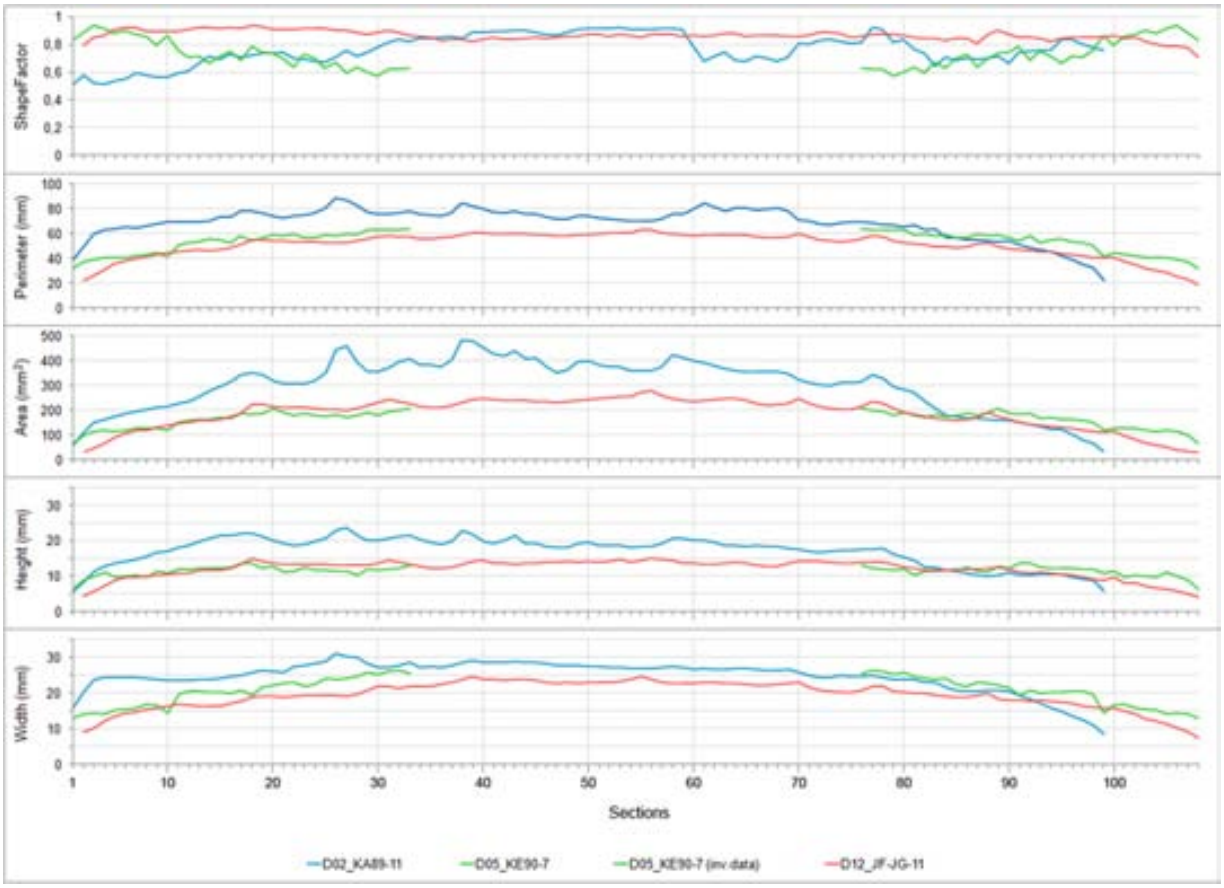

Fig. 4C.13 3D Digital models of artefacts D02_KA89-11, D05_KE90-7, and D12_JF-JG-81, sectioned every 10 millimetres. The graphics show separately the distribution of five different measurements along each section: Shape Factor, perimeter, area, height (i.e., thickness), and width (from top to bottom).

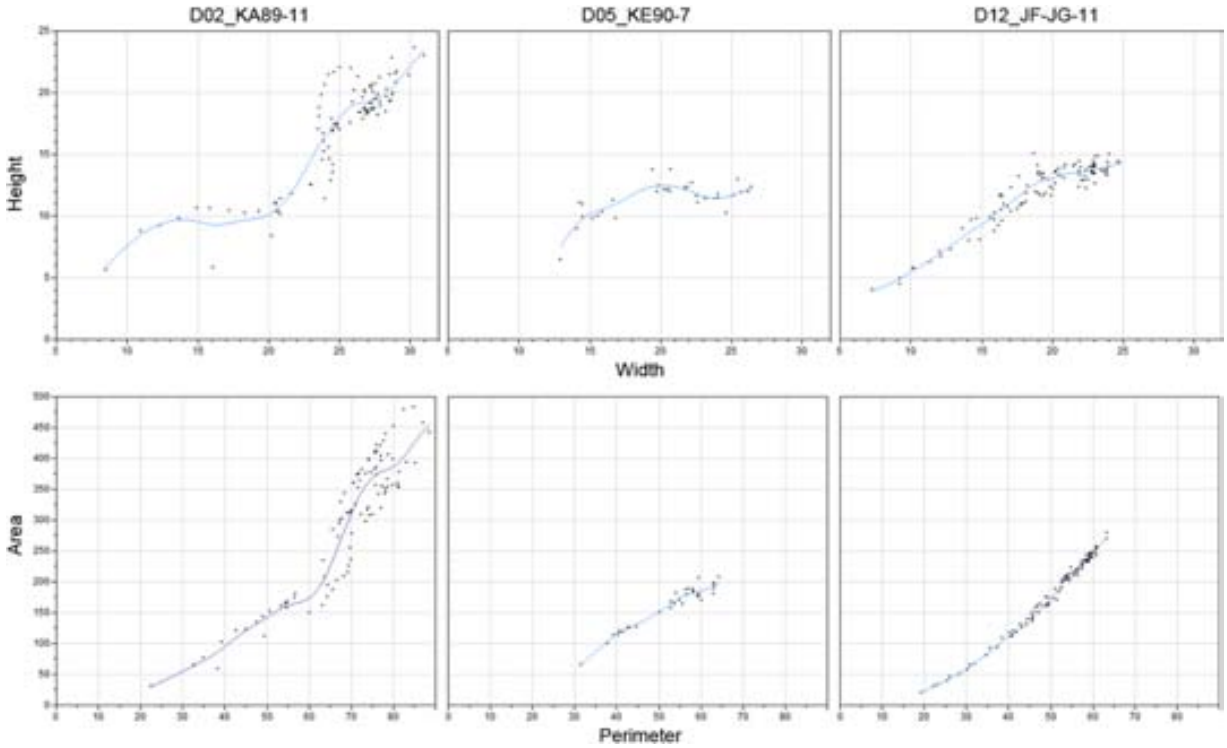

Fig. 4C.14 3D Digital models of artefacts D02_KA89-11, D05_KE90-7, and D12_JF-JG-81, sectioned every 10 millimetres: height-width ratio (top), and area-perimeter ratio (bottom) of the extracted planar cross-sections.

The length of the complete bow D12 (1073,6 mm) is within the expected range of short bows, this is to say, between 1000 and 1500 mm (Dias-Meirinho 2011). The maximum width of all three bows is within the expected range of short bows – between 20 and 60 mm (Dias-Meirinho 2011): D02 is 30,96 mm, D05 is 26,39 mm, and D12 is 24,73 mm. Likewise, the maximum height is within the expected range of short bows: D02 is 23,63 mm, D05 is 13,76 mm, and D12 is 15,07 mm. The width-height ratio of D12 falls clearly in the range of other short bows, while the ratio of D02 can be considered to be either at the very limit of short bows or in the range of long bows. However, the fragmented end of D05 is wider than D12 and seems to converge with the width of D02, and both width-height ratio curve show similarities. If these considerations are to be true, then D05 could fall either in the shortbow or longbow category. Although the total length of D02 is presently 992,6 mm (i.e., the length of the bounding box indicates a very shortbow, or just a shortbow if we consider a slight downsizing caused by taphonomic and restoration processes, or measure the bow along its curvature), it is important to take into account that this artefact is fragmented. In fact, the results of the cross-sections measurements and ratios suggest it is either a shortbow or a longbow. Yet, to be considered a longbow it would have to be at least 1500 mm length, which in practice would mean that more than 500 mm is missing from the current fragment. According to Longman and Walrond (1894), bows were sometimes strengthened by intentionally shortening them, and provided the bow was originally long enough to allow of this being done. Though, it cannot be ruled out that this bow may have been modified after being (un)intentionally fragmented in order to enable it to be used by younger and/or smaller members of the group, as part of a recycling system. As to D12, it is definitely a short bow.

When compared to longbows, shortbows require less raw-material and effort to manufacture, are physically lighter in weight (of the same material), easier to carry and to manoeuvre through brush or dense woodlands, and are easier to swing on flying or running game (Hamm 2007).

When analysing the complete bow of La Draga in the context of the European Neolithic bows, Figure 4C.15 suggests that most very shortbows and shortbows were manufactured upon what could have been an empirical scale factor about their size and proportions.

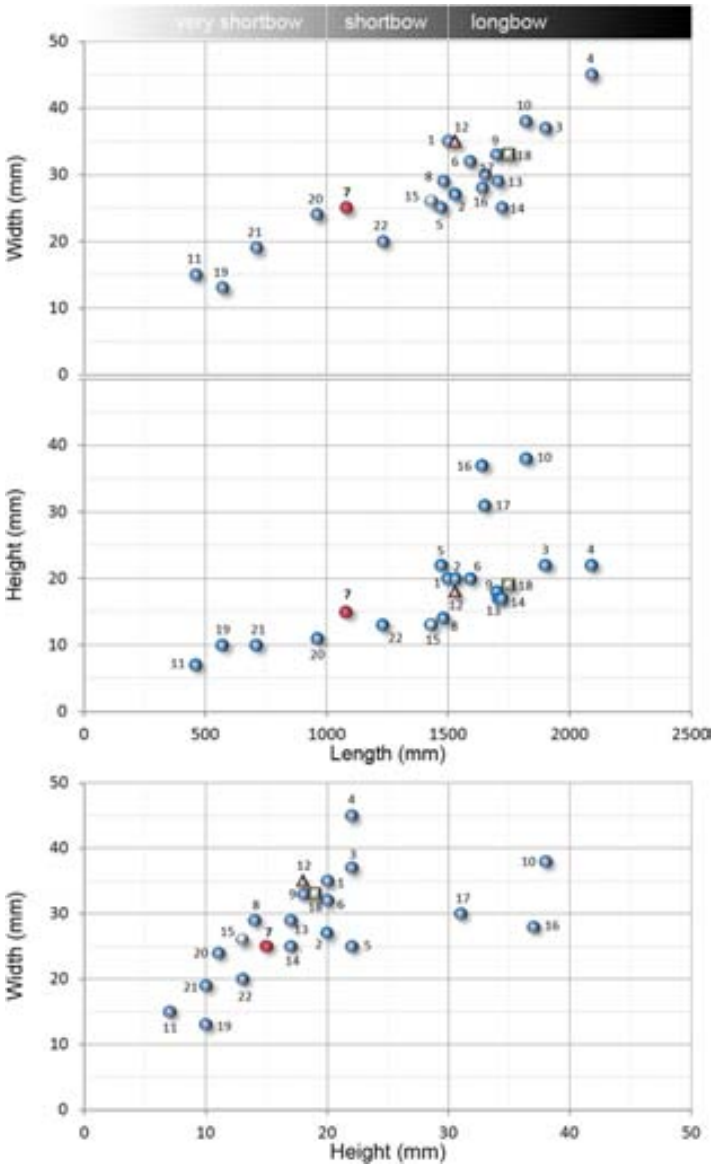

Fig. 4C.15 The complete bow of La Draga in the context of the European Neolithic bows. Width-length ratio (top, adapted from Piqué et al 2013), height-length ratio (centre), and width-height ratio (bottom). 1 Bodman (Clarke 1963); 2 Cambridge (Clarke 1963); 3 and 4 Chalain (Baudais 1985, Dias-Meirinho 2011); 5 and 6 Chalain (Baudais 1985); 7 Draga JF/JG-81 (Piqué et al. in press); 8 Edington Burtle (Clark 1963); 9 Egolzwill 4 (Junkmans 2006); 10 Hauslabjoch (Ötzi) (Egg and Spindler 1993); 11 Horgen-Scheller (Junkmans 2006); 12 Muldbjerg (Dias-Meirinho, M.H. 2012); 13 Niederwill (Junkmans 2006); 14 Onstwedde (Clarke 1963); 15 and 16 Robenhausen (Junkmans 2006); 17 Sutz (Junkmans 2006); 18 Thayngen "Weier" (Guyan 1990); 19 and 20 Zürich-Mozartstrasse (Junkmans 2006); 21 and 22 Zürich-Seefeld (Junkmans 2006).

As to the longbows, the data is not clear enough to infer if their size and proportions were corrected taking into account a series of further scaling factors (Bardi 2000a), or any other type of factor. All bows are made from *Taxus baccata*, except for 12 and 18 which are made from *Ulmus* and *Fraxinus excelsior*, respectively. In respect to bows 2 and 12, it was not possible to ensure from the selected literature if both are in fact Neolithic, in spite of their chronologies (radiocarbon dated). As to bow 15, it was not possible to completely verify in the selected literature if one of its ends is either complete or fragmented.

Chrysals consist in small zones of crushed wood on the belly of a bow (Figure 4C.16). They are caused by the compression of the grain of the wood in the act of drawing the bow, and the sudden release of the string in loosing, which does not give the grain time to recover its original position. Chrysals can appear in new bows, in consequence of wood seasoning process; and in older ones, from the bow being shot in a different way from that to which it was accustomed – for instance, by a person with few technical skills – (Ascham 1545, Longman and Walrond 1894, Stemmler 1942, Elmer 1952, Miller et al. 1986). If so, along with the overall dimensions of bow D12, could be the case of a bow used by an apprentice still with few technical skills. Yet, in spite of the fact that the bows recovered in La Draga may not be longbows, "in an effort to get the most out of a longbow it was usually stressed somewhat past its elastic limit, until small compression ridges were formed on the bow's belly" (Hardy 1976, Blyth 1976, Gordon 1978: cited by Cotterell and Kamminga 1990, p.182), which would result in a non-recoverable elongation (i.e., plasticity behaviour) (Dias-Meirinho 2011). Furthermore, "although a loss in energy would occur during initial use of the bow, there would be very little further permanent deformation as hardening would take place and allow the bow to deform elastically at the higher stresses" (Blyth 1976: cited by Cotterell and Kamminga 1990, p.182). Notwithstanding, one should also consider that these deformations on the wood fibres can firstly occur because of the existence of knots on the opposite face and later increased by one or more of the aforementioned factors. Suffice is to recall that a 3D surface model alone does not provide a full record of the stave. As such, it does not exempt the examination of the original artefact by a wood specialist.

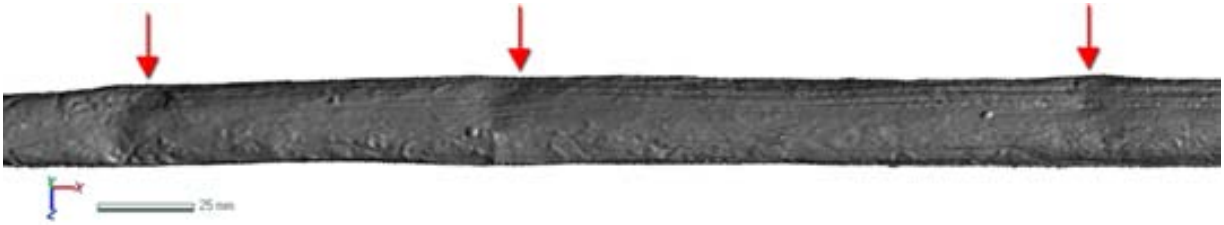

Fig. 4C.16 Detail of 3D digital surface model of artefact D12_JF-JG-81 exhibiting chrysals on the belly.

The curvature of a bow can occur because of the natural or functional deformations mentioned, as well as if it has for instance taken a set from much shooting, or the duration and/or condition of being left braced. The curvature can increase or decrease the draw weight and length of a bow. Besides differential preservation issues, it is possible to observe that neither bow displays an even curve. Both artefacts are asymmetrically curved – D02 exhibits a greater curve, when compared to D12 –, caused by depositional factors or suggest that they bent through non-centered handles. On this subject, neither bow exhibits especially narrow handgrips – "a narrow handle means a narrow arrow pass, which means the bow will shoot a large variety of

spined arrows without having to deal with the dreaded archer's paradox" (Hamm 2007). According to Longman and Walrond (1894, chapter XVII, p.14) "it is important that the handle should fit the hand, as unless this is the case it will not be possible to grasp the bow in the proper manner". The measurements taken from the middle portions of D02_KA89-11 and D12 indicate that both handles would be too large to fit the hand of a child. The former could eventually fit the hand of a teenager (but definitely the hand of an adult), while the latter would fit his hand (at least those of several today's 11 year old adolescents).

Figure 4C.17 shows the 3D digital models of the nock-ends. Nock A and fragmented end B belong to artefact D02, nock C is from artefact D05, Nocks D and E are from artefact D12. Fifty cross-sections in parallel planes of every nock were recorded at 1 mm intervals (measured values are listed in Annex C, Tables 4C.10 - 4C.12), starting from each extremity. Width, height (i.e. thickness), area, perimeter, and Shape Factor measurements of each section are shown in Figure 4C.18. The relationships between area, perimeter, height, and width are shown in Figure 4C.19.

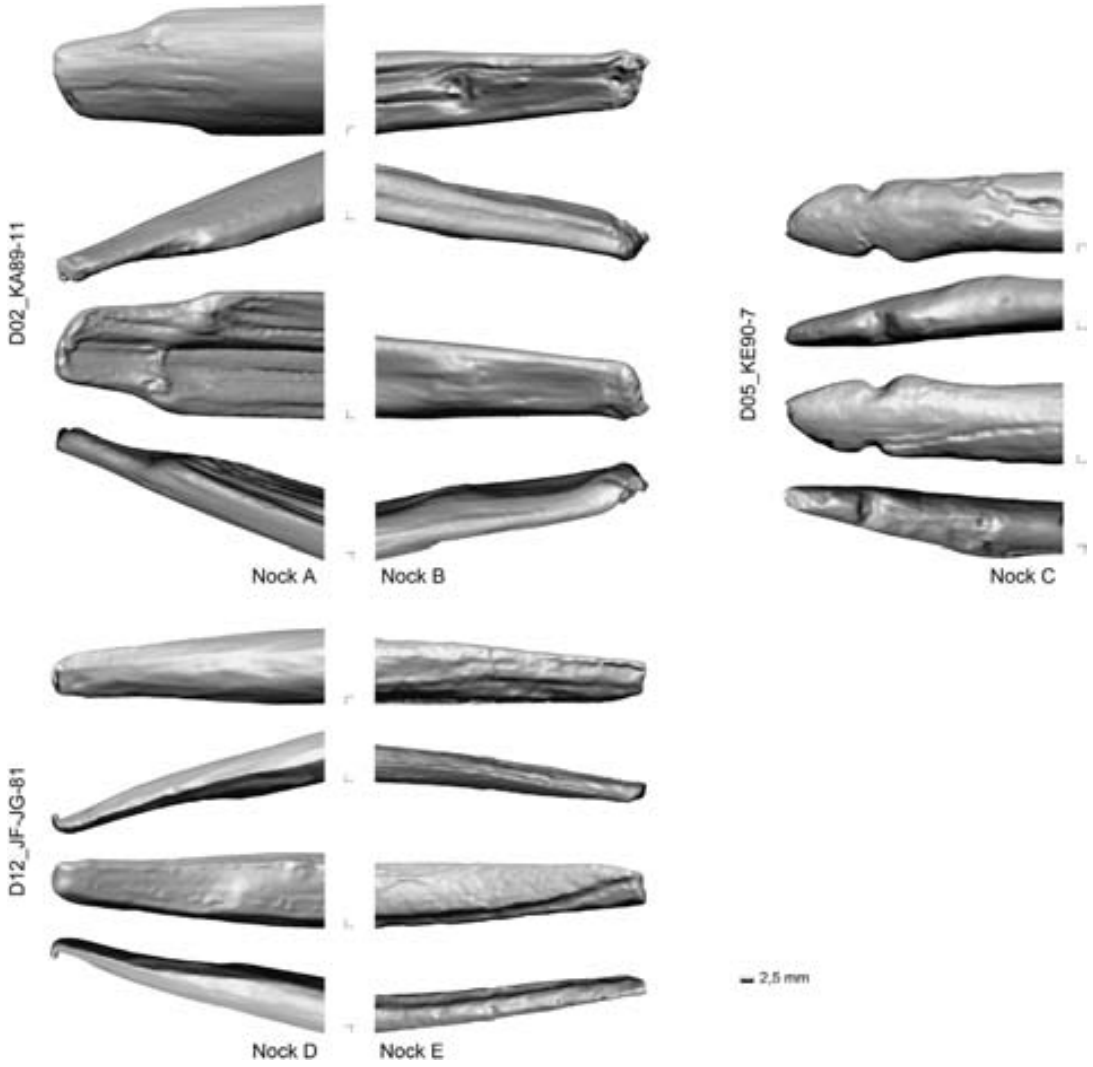

Fig. 4C.17 3D Digital surface models of nock A (top left) and fragmented end B (top centre) from artefact D02_KA89-11, nock C (top right) from artefact D05_KE90-7, and nocks D (bottom left) and E (bottom right) from artefact D12_JF-JG-81. Back, left side, belly, and right side views (from top to bottom).

Nock A has been modified for holding the bowstring, while nock B just ends in a point and shows no special shaping to fix the bowstring. Both ends exhibit longitudinal fractures. Nock A is the widest nock of all five, in contrast has the lowest Shape Factor. Approximately after section 10 there is a resemblance between nock B and nocks D and E, despite knowing that the sections of the former are wider, thicker, have larger areas and perimeters.

General differences between the morphology of nock C and the others are evident, even by naked eye examination. This nock has been modified to engage the bowstring. It is shouldered (i.e., has two parallel notches) and has a head ending in a point. The height values fall in the other nocks' range. The nock's 'neck' is characterized by a rapid change in width (with direct repercussion in both area and perimeter values), a slight increase in height, and the highest circularity value (section 17) – remember that Shape Factor emphasizes the configuration of the perimeter by reflecting the smoothness of contour. The absence of the other nock (and more than half of the bow) precludes any comparisons between its nocks.

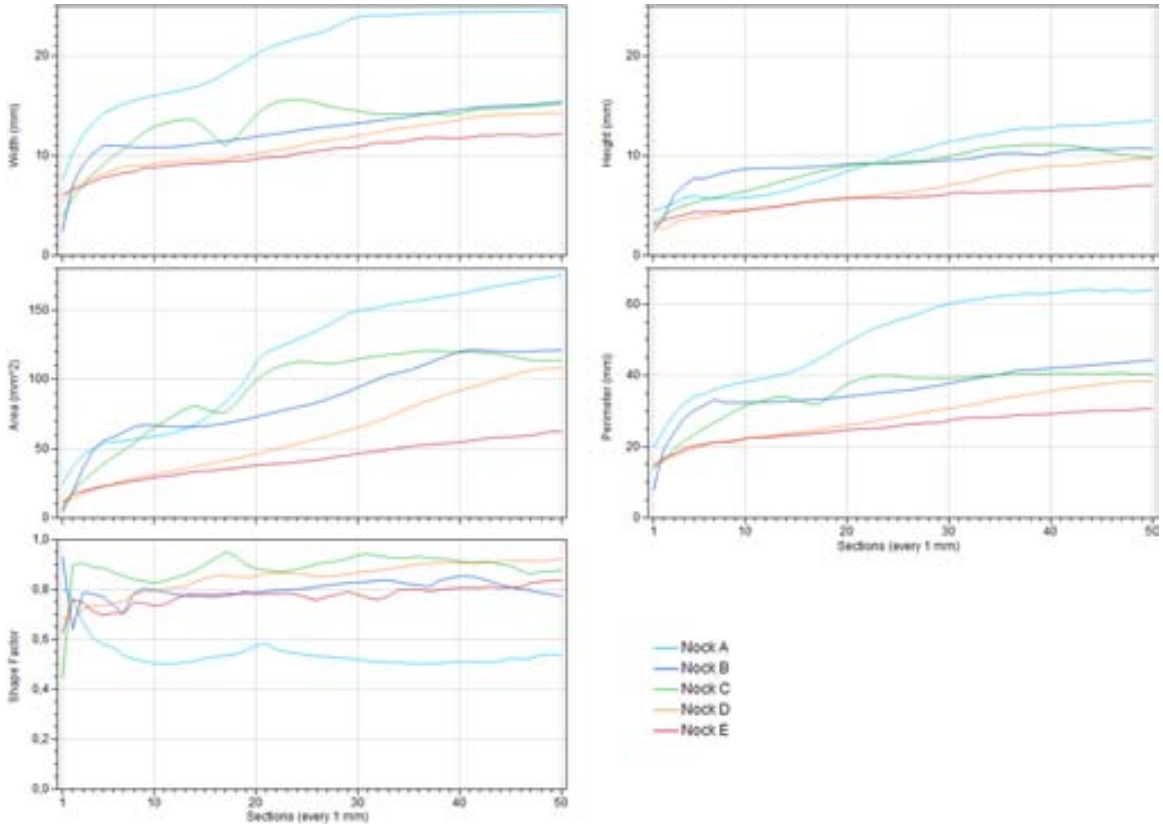

Fig. 4C.18 Artefact D02_KA89-11: nock A and fragmented end B; artefact D05_KE90-7: nock C; artefact D12_JFJG-81: nocks D and E. 3D digital models sectioned every 1 millimetre: width (top left), height (top right), area (centre left), perimeter (centre right), and Shape Factor (bottom left) of the extracted planar cross-sections.

Both nocks D and E end in a point and show no special shaping for holding the bowstring. The extremity of nock D is slightly crushed (Piqué et al. in press), whereas nock E shows two fractures: a longitudinal one, and a transversal one due to post depositional processes. The relationship between both nocks is most evident. They start by being almost perfectly balanced with respect to width, height, perimeter, and area. Then, around

section 20 they slightly begin to diverge – nock D becomes wider, thicker, and more circular. The Shape Factor curves confirm that nock D has a more regular and circular shape than nock E. Nevertheless, taking into account the scale of measurements, the consistency of their overall size and morphology is still quite remarkable, which reinforces a conceptual frame in the manufacturing planning and shaping of both nocks.

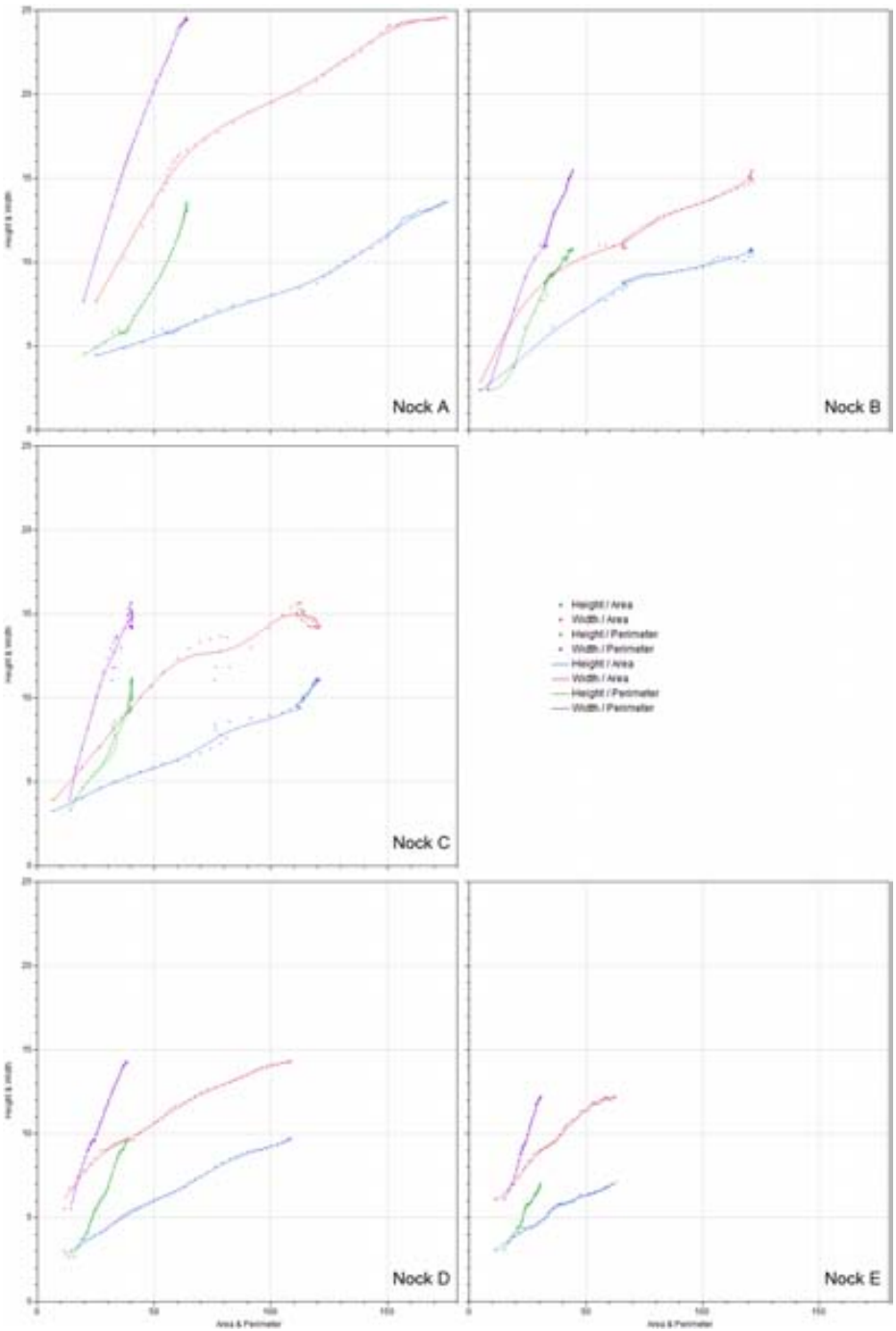

Fig. 4C.19 Artefact D02_KA89-11: nock A (top left) and fragmented end B (top right); artefact D05_KE90-7: nock C (centre left); artefact D12_JF-JG-81: nocks D (bottom left) and E (bottom right). 3D digital models sectioned every 1 millimetre: height-area, width-area, height-perimeter, and width-perimeter ratios of the extracted planar cross-sections.

These measurements confirm the large variability in the form of the nock-ends recovered in La Draga.

It is interesting to notice the variability of dimensions, shapes and forms within the two fragmented and one complete bows recovered in La Draga. According to Junkmanns (2006), small bows were made to be used by children or adolescents for games and learning. Notwithstanding, this diversity could also have been determined by traditions (Dias-Meirinho 2011), the objectives of hunting, the characteristics of the prey, hunting strategies and forms of organization of these activities (Lupo et al. 2005, Piqué et al. in press), as also suggested by the number of distinct types of projectiles recorded (e.g., microliths of flint, spears of bone, wooden pointed shafts and arrowheads).

C.3.2.2 Texture Description through Curvature Analysis

As earlier mentioned, surfaces may be created by a wide range of manufacturing processes, where each manufacturing technique leaves its own 'fingerprint' on the surface produced. These can either enhance the capacities of the resulting surface or deleteriously affect the ability of the resulting surface to perform its intended function. "It is therefore important that the 'fingerprint' which is produced as a result of any surface manufacturing method be understood in terms on the function for which the surface is intended" (Blunt and Jiang 2003, p.4).

Curvature analysis technique was here applied to detect and describe semi-automatically the amount of curvature and distribution on surface texture patterns. Knowing that each FOV determines the resolution of the captured geometries of the 3D digital microtopography of the surface, it was necessary to adjust the parameters of the maximal curvature to -0,2/0,2, which gave best results for an efficient detection of tool marks.

General differences between surface textures of back and belly sides of artefact D02 (Figures 4C.20 - 4C.22) are evident, even by naked eye examination. The back side has not been much modified in relation to the original morphology of the timber, corresponding to the cortical surface of the last ring of the tree, of which just the bark (Bosch et al. 2006, Piqué et al. in press) and small branches have been removed. According to McEwen et al. (1991, p.78) "a rounded back disturbs the layers of wood beneath the bark as little as possible, making it less likely for the bowyer to weaken the structure inadvertently by, for example, cutting across the grain". The back surface is rougher than the surface of the belly, which shows clear evidences of have being polished. As aforementioned, all this contributes to a uniform distribution of stress along the length of the bow, reducing the chance of breakage and improving performance – meaning that the bowyer must have had an understanding of the effects of surface production methods on the functional capacities of the bow. These techniques were generally applied in the manufacture of bows, during the Neolithic (Junkmanns 2001). It is not possible to determine whether the handgrip has been wrapped in leather, cord or similar, since such procedure does not necessarily leaves marks on the wood (Junkmanns 2001, Cattelain 2006, Dias-Meirinho 2011). Both ends exhibit longitudinal fractures, however the work traces present especially on end B indicate it was subsequently modified, thus suggesting that this artefact was later reused (Piqué et al. in press). Returning to the subject of shortbows and longbows, it could then be the case of D02_KA89-11 being initially a large shortbow or eventually a longbow, and after fragmentation occurring being 'recycled' into a small shortbow.

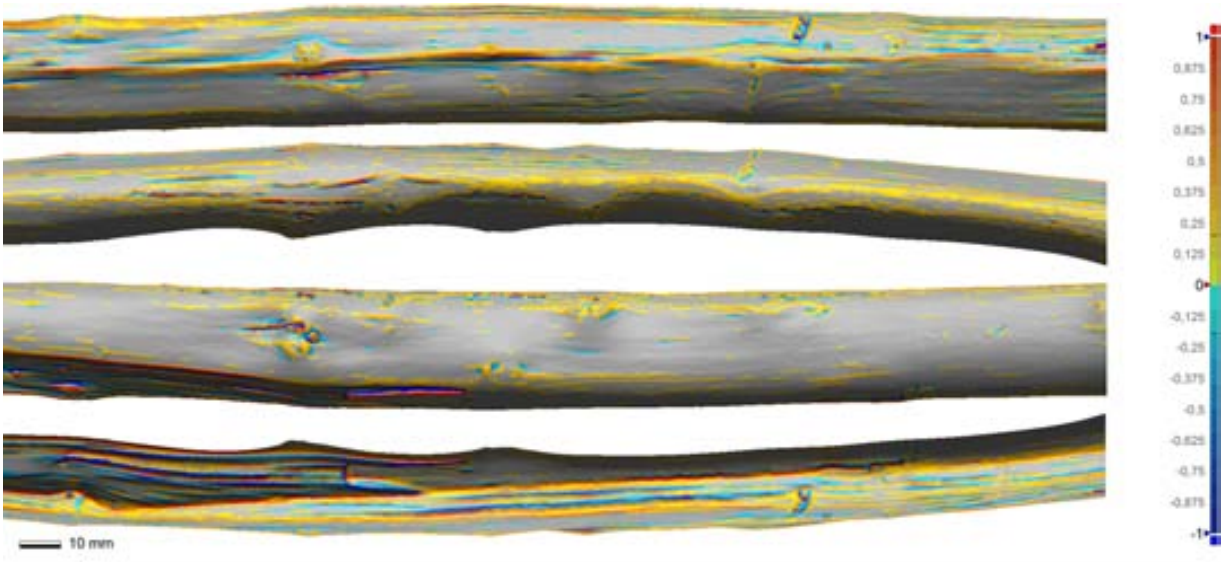

Fig. 4C.20 Curvature analyser colourmap of artefact D02_KA89-11: detail of middle portion. Back, left side, belly, and right side views (from top to bottom). 150 mm FOV: maximum curvature -0,2/0,2 with allowable value hidden.

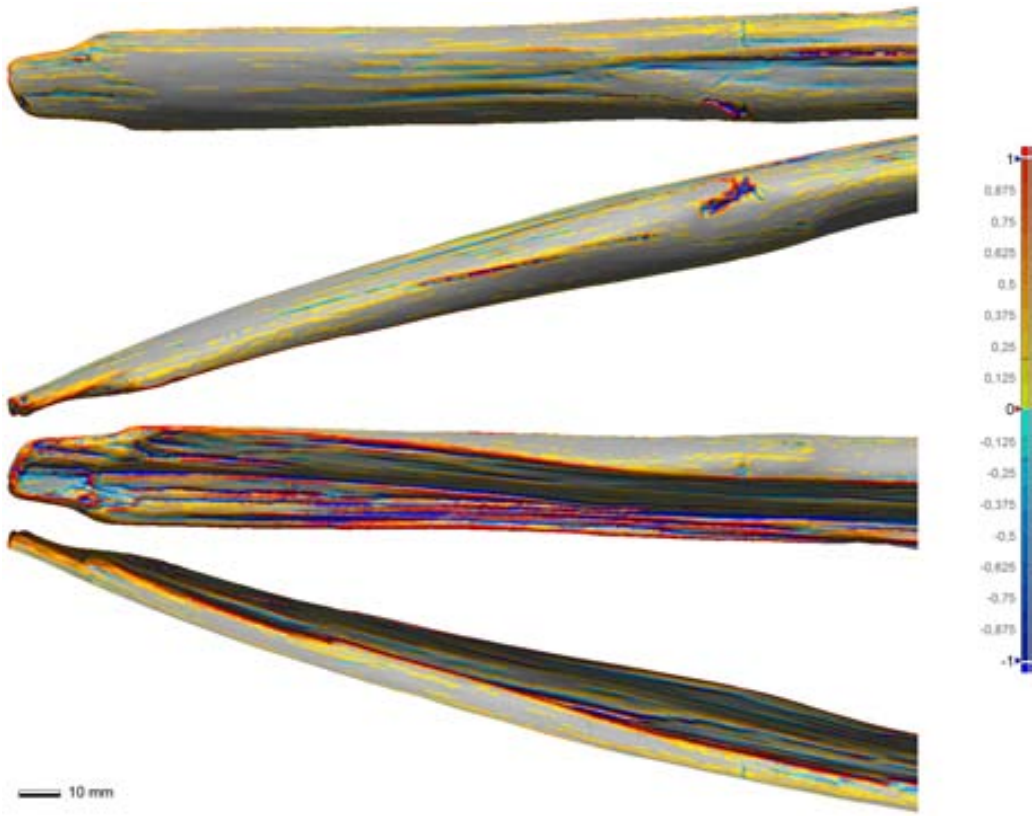

Fig. 4C.21 Curvature analyser colourmap of artefact D02_KA89-11: detail of end A. Back, left side, belly, and right side views (from top to bottom). 150 mm FOV: maximum curvature -0,2/0,2 with allowable value hidden.

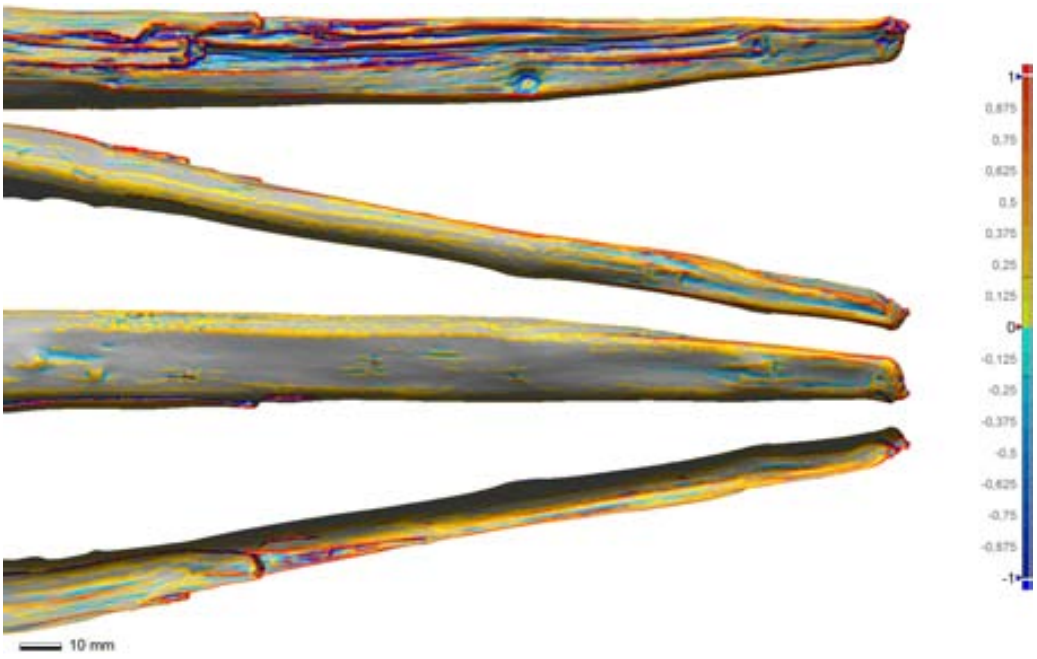

Fig. 4C.22 Curvature analyser colourmap of artefact D02_KA89-11: detail of end B. Back, left side, belly, and right side views (from top to bottom). 150 mm FOV: maximum curvature -0,2/0,2 with allowable value hidden.

The surface of fragment D05 (Figure 4C.23) is generally much deteriorated. One of its faces has not been much modified in relation to the original morphology of the timber, corresponding to the cortical surface of the last ring of the tree (Bosch et al. 2006, Piqué et al. in press) – except for the nock –, while the other has been polished. There is clear evidence of regular tool marks, especially on the sides of the limbs and nock.

Fig. 4C.23 Curvature analyser colourmap of artefact D05_KE90-7: detail of end C. Back, left side, belly, and right side views (from top to bottom). 150 mm FOV: maximum curvature -0,2/0,2 with allowable value hidden.

Once again, the back side of artefact D12 (Figures 4C.24 - 4C.26) has not been much modified in relation to the original morphology of the timber, corresponding to the cortical surface of the last ring of the tree, of which just the bark and small branches have been removed (Bosch et al. 2006, Piqué et al. in press). According to Ascham (1545, p.115) "every bow is made either of a bough, of a plant, or of the bole of the tree. The bough commonly is very knotty, and full of pins, weak, of small pith, and soon will follow the string, and seldom weareth to any fair color; yet for children and young beginners it may serve well enough". There is clear evidence of regular tool marks on the sides of the limbs, as well as on the back of both ends – end D in particular, which is well preserved because it was in contact with the chalk of the lake (Piqué et al. in press). The surface finishing of the belly shows uneven signs of polishment: end D is more polished than end E, and the middle portion shows a discontinuity of both limbs' polishment. It is not possible to determine whether the handgrip has been wrapped in leather, cord or similar, since such procedure does not necessarily leave marks on the wood (Junkmanns 2001, Cattelain 2006, Dias-Meirinho 2011). However, I draw the attention to the peculiar marks on the belly of the middle portion, particularly on one of its sides, which may eventually indicate the contact area between bow and arrow, i.e., the location of the grip. If so, these marks could occur either as a result of few technical skills of the archer to nock the arrow (i.e., to set an arrow in a bow), or as a consequence of the phenomenon known by the archer's paradox (Rendtroff 1913, Kooi and Sparenberg 1997, Kooi 1998a, 1998b), where an incorrect dynamic spine (i.e., the arrow's stiffness) would result in an unpredictable contact between the arrow and the bow.

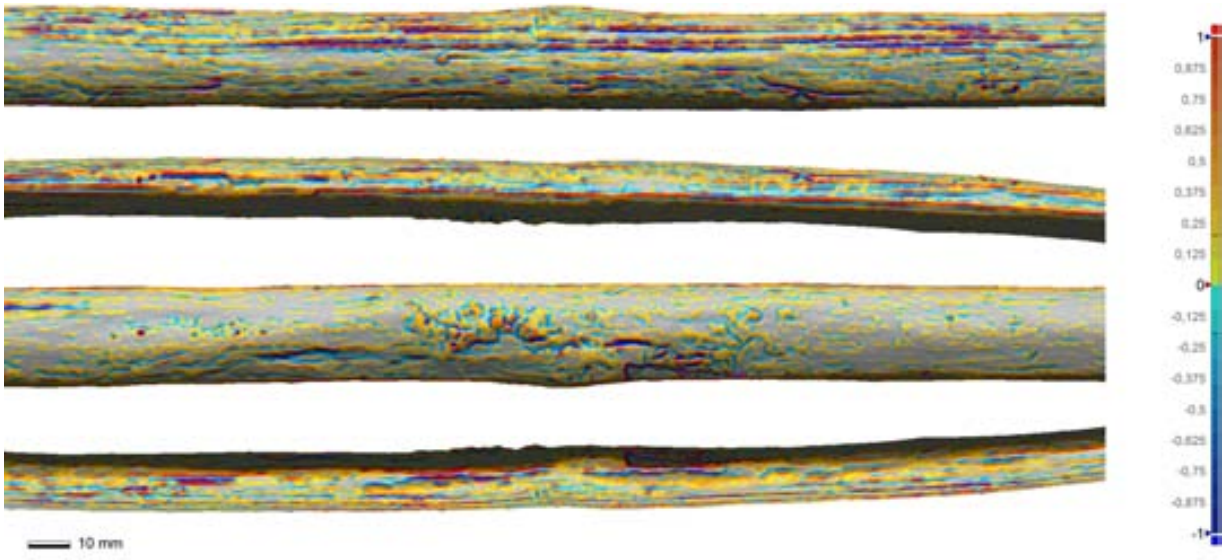

Fig. 4C.24 Curvature analyser colourmap of artefact D12_JF-JG-81: detail of middle portion. Back, left side, belly, and right side views (from top to bottom). 150 mm FOV: maximum curvature -0,2/0,2 with allowable value hidden.

Fig. 4C.25 Curvature analyser colourmap of artefact D12_JF-JG-81: detail of end D. Back, left side, belly, and right side views (from top to bottom). 150 mm FOV: maximum curvature -0,2/0,2 with allowable value hidden.

Fig. 4C.26 Curvature analyser colourmap of artefact D12_JF-JG-81: detail of end E. Back, left side, belly, and right side views (from top to bottom). 150 mm FOV: maximum curvature -0,2/0,2 with allowable value hidden.

C.3.3 Material – Wood

There are several analytical methods that have been widely used in the field of material science, for the estimation of fundamental material properties. As stated before, these methods can be applied to obtain important quantitative data on materials used in archaeological objects.

The material in the scope of this section is wood. I address mainly physical and mechanical properties in considerable detail for, in the one hand, their novelty in mainstream archaeological research. On the other hand, for their power in the testing and analysis of functional aspects of archaeological objects.

Initially I was driven to believe that it would be rather plain and simple to obtain all the required physical and mechanical properties' quantitative data of *Taxus baccata*, *Buxus sempervirens*, *Salix sp*, *Cornus* and *Corylus Avellana*. As previously mentioned, all three bows excavated in La Draga are made of *Taxus baccata*, while the latter wood species were identified in other possible related artefacts, such as arrows (shafts, arrowheads) and spears. But I couldn't be wronger. In spite of the relative easiness of finding the properties of woods used especially in the construction industry, refurbishment, wood composites, or for fuel, these have not been scientifically investigated yet as one would expect (Mackenzie-Helnwein et al. 2005). Moreover, the scarce information found in the available material libraries, and literature was often incomplete and contradictory. To overcome this obstacle, it would be necessary to conduct real-world tests to obtain the values in question. Therefore, the next challenge consisted in finding modern logs of these woods. A true epic, I must confess. Given the nature of *Taxus baccata* being a protected species in the Iberian Peninsula, and the fact that *Buxus sempervirens* appears nowadays as a shrub in open woods, it turned to be very difficult if not impossible to find stems with the minimum required dimensions for the tests. Finally, thanks to the interest and effort of many individual people and of several public institutions from Spain, France, and Portugal, I finally managed to arrange a few *Corylus avellana*, *Salix sp* and *Taxus baccata* logs that did meet all the mandatory requirements specified by the standards. A couple of *Buxus sempervirens* stems were also arranged, but unfortunately had to be excluded because they were too thin to extract any useful test specimen. *Cornus* was as well excluded from this study, due to the fact that no logs were arranged in good time for the tests. All logs used in this scientific research were kindly supplied free of charge.

C.3.3.1 Wood Specimens

Three wood species were chosen as the test subjects for this investigation:

- ***Corylus avellana***: *Betulaceae* family. The *common hazel*, is a deciduous hardwood (i.e., angiosperm) native to Europe and western Asia. It is a large, spreading shrub or small tree, usually growing 3 m to 8 m tall, but can reach 15 m.
  The test specimen were extracted from one air-dry log (labelled *CL1*) (Figure 4C.27) cut in February 2012 at the Park of the Castel of Montesquiu (Catalonia), approximately 70 km from La Draga, spe-

cific altitude not known (the Park's altitudes vary from 580 m to 875 m), and was supplied for the tests thanks to Jordi Jürgens, from the Oficina Tècnica de Parcs Naturals de la Diputació de Barcelona.

Fig. 4C.27 *Corylus avellana* log.

- ***Salix sp***: *Salicaceae* family. This genus is formed by *willows*, *sallows*, and *oisers*. It is a deciduous hardwood, found primarily on moist soils in cold and temperate regions of the Northern Hemisphere. It is a low-growing tree or shrub.

  The test specimens were extracted from two air-dry logs (Figure 4C.28), from two different sources. One log (labelled *S1-A*) was cut in February 2012 at the Park of the Castel of Montesquiu (Catalonia), and made available thanks to Jordi Jürgens. The other log (labelled *S2*) came from a tree growing for five years in a seedling nursery near Girona (Viveros Casa Paraire, Bordils, Catalonia), approximately 15 km from La Draga, at 46 m above sea level (asl), then purchased by the Council of Barcelona about ten years ago and planted in the streets of the Zona Franca, approximately 120 km from La Draga, at 5 m asl. This log was made available for the tests thanks to Juan Serrahimas (Parcs i Jardis de Barcelona, Ajuntament de Barcelona), and Raquel Piqué (UAB).

Fig. 4C.28 *Salix sp* logs: S1-A (top), and S2 (bottom).

- ***Taxus baccata***: *Taxaceae* family. Originally known as *yew*, is a softwood (i.e., gymnosperm) conifer native to western, central and southern Europe, northwest Africa, northern Iran and southwest Asia. It is an evergreen tree, growing 10 m to 20 m tall at a slow rate, with a trunk usually up to 1,5 m diameter, exceptionally 4 m. Yew trees grow relatively slowly, and can be very long-lived.

  The test specimens were extracted from air-dry logs (Figure 4C.29), from two different sources. One log (labelled *Tcat*) came from the Natural Park of the Volcanic Area of La Garrotxa (Mas El Prat, Serra del Corb, Les Preses, Catalonia), approximately 40 km from La Draga, at 600 m asl, thanks to Emili Bassols and Joan Montserrat (Department of Natural Heritage, from the Natural Park of the Volcanic Area of La Garrotxa), Maria Saña (UAB), and Ramon Buxó (Archaeological Museum of Catalonia). The other log (labelled *Tfr*) came from Montpellier (France; no record of the altitude is

available), approximately 230 km from La Draga, thanks to Jean Gerard (CIRAD), Jean Gaujoux (forest owner), and Mériem Fournier (AgroParisTech-LERFoB).

Fig. 4C.29 *Taxus baccata* logs from Catalonia (top), and France (bottom).

This step comprised cutting and visually analysing the wood test specimens in accordance to UNE 56-528-78 "Características físico-mecánicas de la madera. Preparación de probetas para ensayos", as well as to the corresponding test standards (see section *C.3.3.2.1. Physical and Mechanical Tests*) – these were cut by a professional carpenter, Hans Nottelmann. Given the nature of wood, it can be hard to obtain specimens completely free of defects and inclusions. The samples consisted mostly in clear, consistent growth rings patterns, knot-free, straight-grained test pieces. The size and grain orientation of the samples was determined by the type of physical and mechanical properties required, and according to the corresponding test standard. Since the Spanish standards required smaller test specimens than the equivalent international ones, and some of the wood logs were not big enough, the former standards were adopted most of the times. Full details of the materials and procedures are given in each of the referenced standards.

In order to widen the spectrum of analysis of wood species used in the manufacture of bows since the Mesolithic, four other species were later included in this research, but not here tested:

- ***Fraxinus excelsior***: *Oleaceae* family. The *european ash*, or *common ash*, is a deciduous hardwood, native to most of Europe, from northern Iberian Peninsula to southern Scandinavia, southwestern Asia and North Africa. It is a vigorous medium-sized to large tree, usually growing 15 m to 30 m tall and and 1 m to 2 m trunk diameter, but can reach heights of up to 43 m with a girth of 6 m.
- ***Pinus sylvestris***: *Pinaceae* family. The *european scots pine* is an evergreen softwood coniferous tree native to Europe and northern Asia. It is a medium-sized to large tree, usually growing 20 m to 35 m tall with 0,6 m to 1 m trunk diameter, exceptionally 45 m tall with a girth of 1,7 m.
- ***Quercus laurifolia***: *Fagaceae* family. The *laurel oak* is a deciduous hardwood tree, native to the USA (southeastern Virginia to southern Florida and Texas) and introduced in Europe in 1786. It is a

medium sized tree, usually growing 20 m to 25 m tall and 0,6 m to 1,2 m trunk diameter, exceptionally 43 m.

- ***Ulmus procera***: *Ulmaceae* family. The *atinian elm*, or *common elm*, is a deciduous hardwood tree, native to southern and western Europe. It is one of the largest and fastest-growing deciduous tree in the continent, growing to over 35 m by 15 m, and up to 2 m trunk diameter, but can reach heights of up to 46 m.

C.3.3.2 Wood Properties

Wood is a biological material, hygroscopic, orthotropic and highly heterogeneous. Its structure can be divided in three main levels: fibre structure, cell structure, and macrostructure (bark, cambium, sapwood, heartwood) (Figures 4C.30 and 4C.31). Wood consists not only of water but also of naturally occurring polymers such as cellulose (mainly comprised of carbon, hydrogen, and oxygen), hemicelluloses, and lignin, as well as several percent of ash and extractives. Heartwood cells are dead and physiologically inactive, and the content of moisture is reduced, whereas sapwood is active in water conduction and other physiological tasks. As Askeland (1998) refers, wood can be considered as a complex fibre-reinforced composite composed of long, unidirectionally aligned tubular polymer cells in a polymer matrix, where the polymer tubes are composed of bundles of partially crystalline cellulose fibres aligned at various angles to the axes of the tubes. Briefly speaking, the fundamental composition and structure of wood, from the molecular to the cellular or anatomical level, determines the properties and behaviour of wood in different axis (Gibson and Ashby 1988, Askeland 1998, Hoadling 2000, Alakangas 2005, Ashby 2005, Kohdzuma 2005, Callister 2007, Keunecke 2008a, FPL 2010, Schmulsky and Jones 2011, Casteren et al. 2012, Derome et al. 2013).

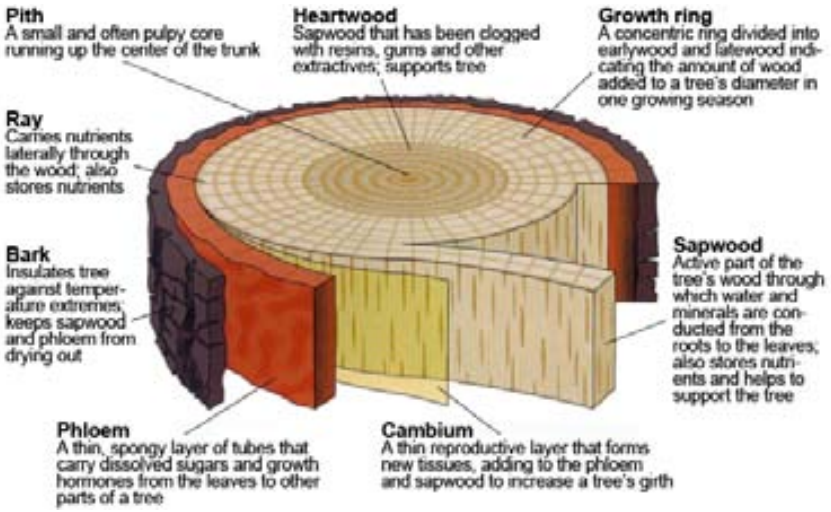

Fig. 4C.30 Anatomy of wood: tree trunk (adapted from Arno 1993).

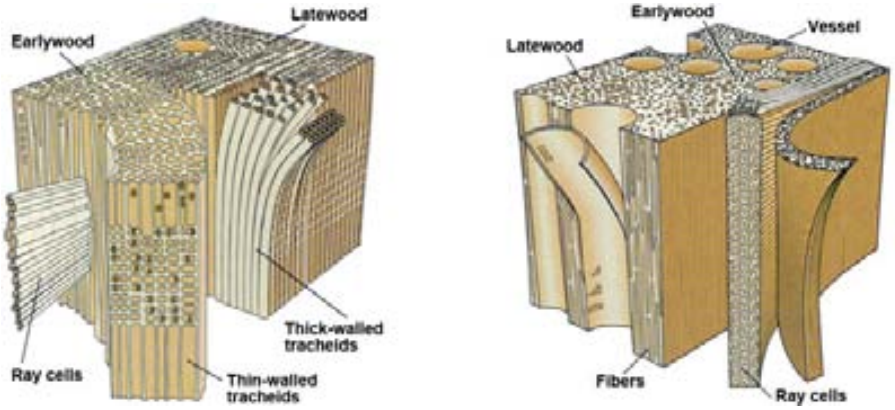

Fig. 4C.31 Anatomy of wood: softwood (bottom left) and heartwood (bottom right) (adapted from Arno 1993).

The microscopic photographs of the tested woods were captured at the Laboratorio de Arqueobotánica, from the Department of Prehistory, UAB (Figure 4C.32). The photographs show differences within the Catalan and French *Taxus baccata* microstructure. The fine-scale morphology of *Taxus baccata* differentiates from the other wood species for being more homogeneous and tighter.

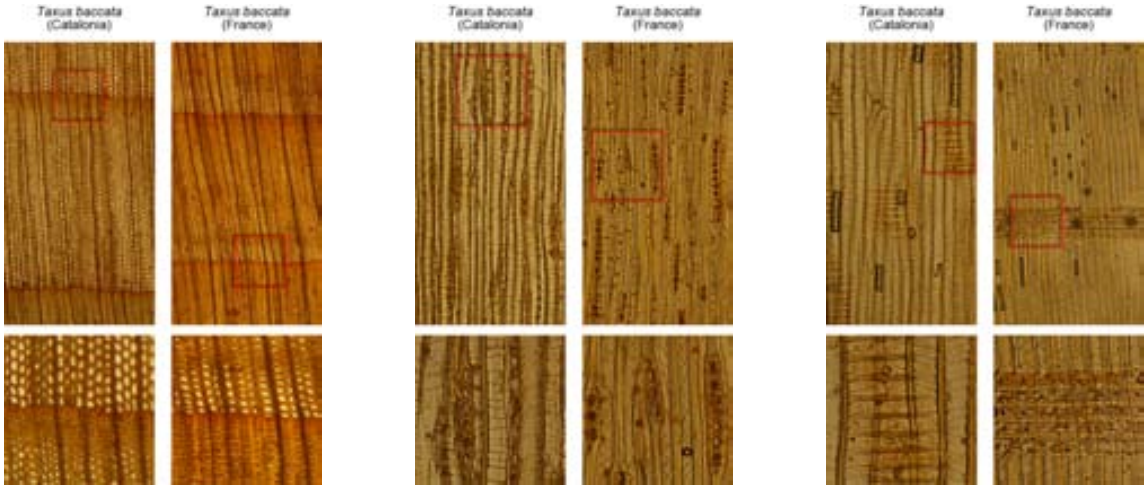

Fig. 4C.32 Transmitted light microscope (Olympus BX 40) images of *Taxus baccata* microstructure. General view (top) and detail (bottom). Transverse section showing transitions in earlywood and latewood (EW/LW) (left). Tangential section showing tracheids and ray cells (centre). Radial section showing tracheids and ray cells (right) (photos by Raquel Piqué, Laboratorio de Arqueobotánica, UAB).

C.3.3.2.1 Physical and Mechanical Tests

Both physical and mechanical tests were conducted at the Laboratory of Destructive Tests, Department of Mechanical and Materials Engineering, Alcoy Campus of the Polytechnic University of Valencia (Valencia Community), under the supervision of Antonio Nadal Gisbert, and with the technical assistance of Matías Monzó Pérez. The materials and procedures for testing the wood samples followed the specifications set in international and national standards. The general properties of materials have already been well described in the previous chapter.

From a mechanical point of view, wood is a highly complex material. The physical and mechanical behaviour of wood is intrinsically related with its basic composition and structure (Gibson and Ashby 1988, Askeland 1998, Hoadling 2000, Alakangas 2005, Kohdzuma 2005, Callister 2007, FPL 2010, Schmulsky and Jones 2011, Gunduz et al. 2013). Because of the fact that this material is heterogeneous and orthotropic (i.e., has different mechanical properties along three mutually perpendicular axes: longitudinal, radial, and tangential; it is a class of anisotropy), in both its hygroscopic and mechanical behaviours, it was necessary to perform some of the tests not only parallel but also perpendicular to the wood's grain. The longitudinal axis is parallel to the grain (fibre), i.e., to the cylindrical trunk of the tree; the radial axis is perpendicular to the grain in the radial direction (normal to the growth rings); and the tangential axis is perpendicular to the grain, but tangent to the growth rings. Wood is said to be a viscoelastic material (a rheologic phenomena), because it encounters a combination of viscous (Newton's law), and elastic (Hooke's law) behaviours.

As a standard procedure – American Standard ASTM D143-09 "Standard test methods for small clear specimens of timber", Spanish Standard UNE 56-528-78 "Características físico-mecánicas de la madera. Preparación de probetas para ensayos" – all wood samples were individually: labelled; measured with a calliper accurate to 0,1 mm; weighed on a digital balance accurate to 0,01 g, as the mass of the samples weighed less than 100 g in anhydrous form; and photographed before and after each test. Both moisture content and temperature were controlled to ensure comparable test results; samples were air dried until constant mass was achieved. For a generic knowledge on standard terminology relating to wood see the American standard ASTM D9-87 R99.

Density was determined in accordance with the UNE 56-531-77 "Características físico-mecánicas de la madera. Determinación del peso específico", and calculated for each test specimen. The specific weight was determined in accordance with the same standard, and its value refers to the mean (average) of the results of *n* samples tested. The values are here expressed in g/cm^3, at ω%.

The moisture content was determined in accordance with the Spanish version of the European Standard UNE-EN 13183-1, "Moisture content of a piece of sawn timber. Part 1: Determination by oven dry method". Samples were air dried at 24 ºC and 36%H (relative humidity in laboratory conditions), and oven dried at 103±2 ºC to constant weight. The moisture content (ω) of wood is expressed in percentage, and defined by

$$\omega = ((m_1 - m_2) / m_2) \times 100$$

where m_1 is the mass of the specimen before oven dry in grams, and m_2 is the mass of the specimen after oven dry in grams.

The compressive strength parallel to grain was determined mostly in accordance with the Spanish Standard UNE 56-535-77 "Características físico-mecánicas de la madera. Determinación de la resistencia a la Compresión Axial". Both Catalan and French *Taxus baccata* samples were tested on a Universal Testing Machine (UTM, Elib 40, Ibertest), nominal capacity up to 50KN, control and measuring computer interface (software Wintest 32, Ibertest) (Figure 4C.33). The samples of *Salix sp* and *Corylus avellana* were tested on another

UTM (Metrocom hydraulic), nominal capacity up to 20T (nearly 200KN), without computer interface. Because of the size and characteristics of the available logs, the dimensions of the wood samples were smaller than was required by the standard: instead of 50*50*150 mm, the Catalan and French *Taxus baccata* samples measured 25*25*100 mm, while the *Salix sp* and *Corylus avellana* samples measured 50*50*100 mm. We hoped that this modification affected little the test, since they may be representative of the woods tested. The compressive strength parallel to grain (C_{H}) at ω% of moisture content is expressed in kg/cm^2, and defined by

$$C_{\mathrm{H}} = C_r / S$$

where C_r is the failure due to axial load on wood; S is the compressed surface area. The compressive strength value refers to the mean of the results of n samples tested.

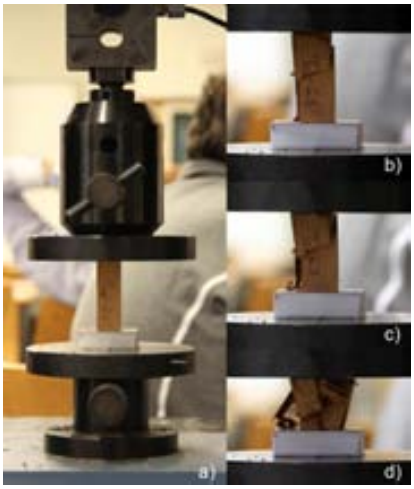

Fig. 4C.33 Compressive test parallel to grain: coarse of the deformation and fracture of specimen Tcat-63, *Taxus baccata*.

The compressive strength perpendicular to grain (radial and tangential) was determined in accordance with the Spanish Standard UNE 56-542-88 "Características físico-mecánicas de la madera. Determinación de la resistencia a la Compresión Perpendicular a las Fibras". All samples were tested on the UTM Elib 40 (Figure 4C.34). The compressive strength perpendicular to grain ($C_{\perp \mathrm{H}}$) at ω% of moisture content can be expressed in MPa, and is defined by

$$C_{\perp \mathrm{H}} = C_{LE} / S$$

where C_{LE} is the axial load on wood in yielding moment; S is the compressed lateral surface area in cm^2. The compressive strength perpendicular to grain value refers to the mean of the results of n samples tested in the radial axis, and in the tangential axis.

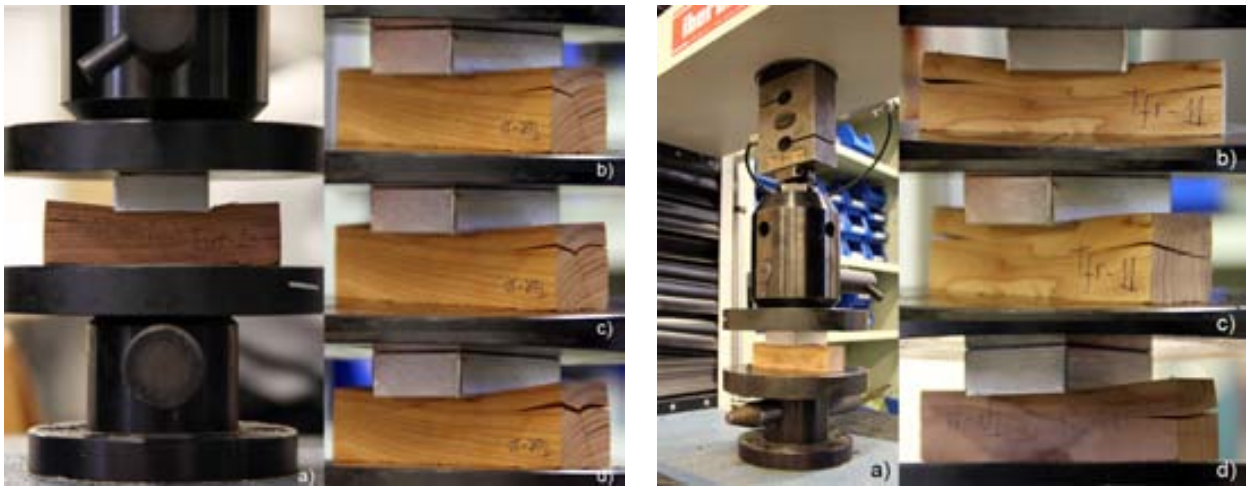

Fig. 4C.34 Compressive test perpendicular (radial) to grain: coarse of the deformation and fracture of specimen Tcat-13, *Taxus baccata* (left). Compressive test perpendicular (tangential) to grain: coarse of the deformation and fracture of specimen Tfr-11, *Taxus baccata*. b) tangential surface on failure; c) right cross-section on failure; d) left cross-section on failure (right).

The bending strength, or flexural strength, was determined in accordance with UNE 56-537-79 "Características físico-mecánicas de la madera. Determinación de la resistencia a la Flexión Estática", the British Standard BS 373:1957 "Methods for testing small clear specimens of timber", and ASTM D143-09. The samples were tested on the UTM Elib 40, with a three-point bending setup (Figure 4C.35). Bending is defined by

$$\sigma_H = 3Pl / 2bh^2$$

where σ_H is the resistance to static bending of wood at ω% of moisture content, in kg/cm^2; P is the axial load (force) in kg, l is the length of the specimen between supports in cm, b is the measure in cm of the specimen in the radial direction, and h is the measure in cm of the specimen in the tangential direction. The bending strength value refers to the mean of the results of n samples tested.

Fig. 4C.35 Static bending (flexural) test: coarse of the deformation and fracture of specimen Tfr-33, *Taxus baccata*.

The elastic modulus, i.e. Young's modulus, was determined in accordance with BS 373:1957. Although wood can be characterized by three different Young's moduli E_1, E_2, E_3, indicated by the direction of load, it was only considered for static bending tests where the orientation of the annual rings is parallel to the direction of loading.

The description of the static bending failures was done in accordance with ASTM D143-09 "Standard test methods for small clear specimens of timber", section 8.7 "Description of static bending failure". The fracture processes are related, on the one hand, to the charging system, on the other hand to the macro and microstructure of the material to be tested. The type of fracture is then classified in accordance with:

- Appearance of the fractured surface – which may be roughly divided into "brash" (i.e., abrupt failure) and "fibrous" (i.e., fracture showing splinters);
- Manner in which the failure develops - which may be divided into "simple tension" and "cross grain tension".

C.3.3.2.2 Results

The interpretation of the tests results was done in accordance to UNE 56-540-78 "Características físico-mecánicas de la madera. Interpretación de los resultados de los ensayos", and the determined values are listed in Table 4C.3 and Figure 4C.36. To a certain extent, the values *per se* are not at all that meaningful, but they become useful to use when compared with other woods or different materials.

As earlier mentioned, *Fraxinus excelsior*, *Pinus sylvestris*, *Quercus laurifolia*, and *Ulmus procera* were not included in these tests. For this reason, their values were imported from a well-known online engineering material database (MatWeb 2013), except for the ultimate tensile strength of compression parallel to grain of *Quercus laurifolia* (Biblis 2001) which had no available data there. The database does not present any further information, namely, description and number of tested specimens, standard deviation, and used standards. As such, this information should be analysed with further caution.

Even though there is a general disparity between the data from the woods tested in this investigation and the ones not tested, the data displayed confirms, on the one hand, that wood strength varies widely among and within species; on the other, when subjected to compression, it is considerably stronger parallel to its longitudinal axis. This degree of anisotropy demonstrates the importance of transverse forces when considering the bending and fracture of, for instance, a bow.

Because density – along with moisture content, temperature, and duration of loading – is known to be one of the main factors controlling the mechanical properties of wood, such as strength, stiffness, and performance in use (Gibson and Ashby 1988, Askeland 1998, Holmberg 1999, Hoadling 2000, Saranpaa 2003, Callister 2007, FPL 2010, Schmulsky and Jones 2011, Casteren et al. 2012), a strong correlation, at least within the tested woods, was expected. In addition, and of similar relevance, is the modulus of elasticity, which is another good overall indicator of a wood's strength.

Table 4C.3 Physical and mechanical properties of the selected wood species. *Taxus baccata*, *Salix sp*., and *Corylus avellana* show original data determined at UPV, where Yield strength values indicate the proportional limit stress. *Fraxinus excelsior*, *Pinus sylvestris*, *Quercus laurifolia*, *Ulmus procera* show data from Matweb whenever available. (*) Data not available in MatWeb, (**) Data from Biblis (2001). All data refer to mean values within species, and are in MPa (1 MPa = 1 N/mm^2; 1 MPa = 0.001 GPa), except for density which is in g/cm^3 (1 g/cm^3 = 1 Mg/m^3). The number of samples tested (*n*) and standard deviation (*st. dev.*) is indicated whenever known.

Physical and Mechanical properties			***Taxus baccata*** (Catalonia)	***Taxus baccata*** (France)	***Salix sp.***	***Corylus avellana***	***Fraxinus excelsior***	***Pinus sylvestris***	***Quercus laurifolia***	***Ulmus procera***
Compression parallel to grain		Yield strength	29,5	30,23	20,9	25,56	51	54	48,1	55
		(n) st.dev.	*(3) 5,07*	*(3) 2,8*	*(3) 0,86*	*(3) 3,34*	*	*	*	*
		Ultimate tensile strength	41	46,9	23,4	30,7	161	102	159,6 **	78
		(n) st.dev.	*(3) 6,04*	*(3) 5,06*	*(3) 1,66*	*(3) 3,62*	*	*	*	*
Compression perpendicular to grain	Radial	Yield strength	9,22	12,25	1,86	7,39	*	*	*	*
		(n) st.dev.	*(3) 0,2*	*(1) -*	*(1) -*	*(1) -*	*	*	*	*
	Tangential	Yield strength	7,31	8,25	2,8	8,99	*	*	*	*
		(n) st.dev.	*(3) 0,57*	*(1) -*	*(1) -*	*(1) -*	*	*	*	*
	R+T	Yield strength	8,26	10,25	2,33	8,19	10,8	7,5	7,31	9,8
Flexural		Ultimate tensile strength (MOR)	45,79	74,06	46,63	83,28	118	102	86,9	87
		(n) st.dev.	*(2) 21,36*	*(3) 12,15*	*(3) 3,1*	*(3) 13,24*	*	*	*	*
		Elastic modulus (Young's modulus)	5802,71	6466,56	3326,4	6334,64	13130	11760	11700	10780
		(n) st.dev.	*(2) 957,83*	*(3) 1651,2*	*(3) 127,04*	*(3) 1112,9*	*	*	*	*
Density			0,7242	0,7692	0,4360	0,6835	0,72	0,73	0,63	0,67
(n)			*(5)*	*(3)*	*(14)*	*(7)*	*	*	*	*

Taxus is well known for its extraordinary longitudinal elasticity and toughness. As Keunecke (2008a) points out, it is regarded as highly deformable in the longitudinal direction prior to and beyond the elastic limit, and is able to absorb a large amount of energy during deformation. *Taxus* showed to have the highest density among the tested samples. These showed a conspicuous relationship between density and the modulus of elasticity, with the French *Taxus* having slightly higher values than the Catalan one, though a much higher module of rupture (MOR). There is a significant variability between the Catalan and French *Taxus* samples, as the latter showed to be able to bow under higher stress without easily fracturing. The reason for the differences among these two *Taxus* is related to fine-scale differences in their wood anatomy and mechanics. In turn, *Salix* showed to be much easier to split and far easier to crush than the rest of the woods.

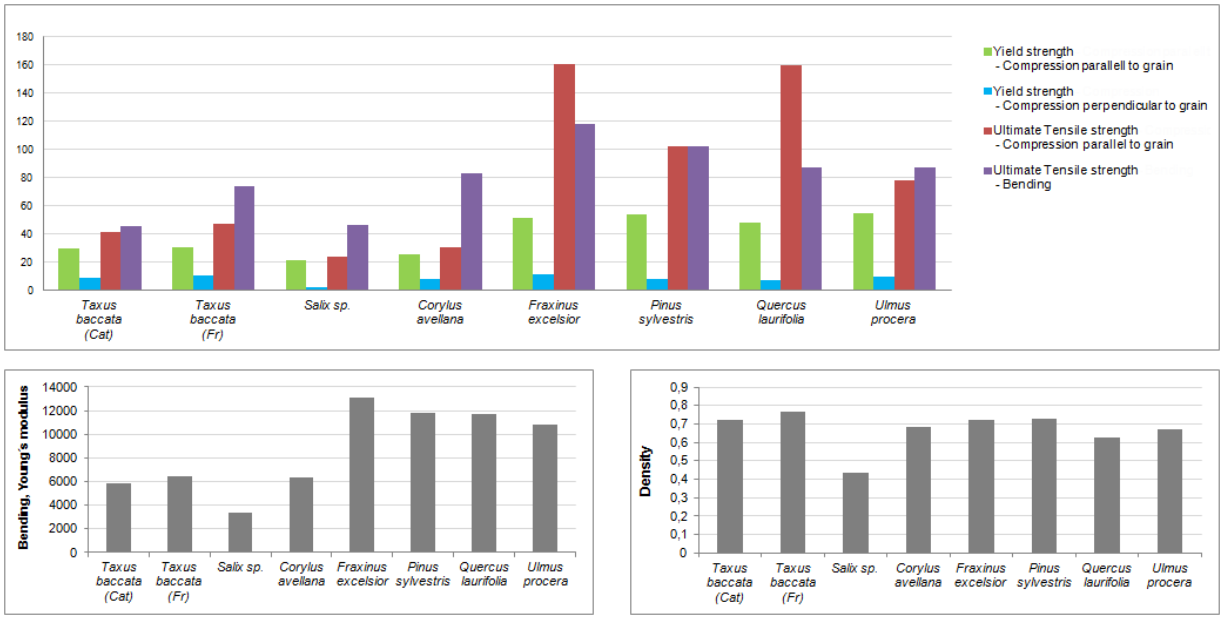

Fig. 4C.36 Selected woods column charts: strengths (top), stiffness (left), and density (right).

The modes of failure in wood can be explained by their different anatomy, density, and mechanical properties (Casteren 2012). Figure 4C.37 and Table 4C.4 show the contrasting behaviour for static bending failures between *Taxus*, which is a very dense softwood, and *Salix* and *Corylus*, which are lesser dense hardwoods.

Fig. 4C.37 Static bending failures: appearance of the manner in which the failure develops (left), and the fractured surface (right) of the tested specimens (photos by Antonio Nadal).

Table 4C.4 Static bending failures: classification of the appearance of the fractured surface, and the manner in which the failure develops of the tested specimens.

Static bending failure	***Taxus baccata*** (Catalonia)	***Taxus baccata*** (France)	***Salix sp.***	***Corylus avellana***
Failure develop	cross grain tension	cross grain tension	simple tension	simple tension
Fractured surface	brash	brash	fibrous	fibrous

There did not seem to be any data for *Corylus avellana*; Poisson's ratio data for *Fraxinus excelsior*, *Quercus laurifolia*, and *Ulmus procera*; or shear modulus data for *Salix sp*, *Fraxinus excelsior*, *Pinus sylvestris*, *Quercus laurifolia*, and *Ulmus procera*, readily available in the literature.

Table 4C.5 lists additional mechanical properties data collected from scattered literature (MatWeb, Carmichael 1950, cited in O'Brien 2003; Sekhar and Sharma 1959; Jakubczyk 1966, cited in Keunecke 2008a; Niemz 1993, cited in Danielsson 2013; Sell 1997; Subic and Cooke 2003, Keunecke et al. 2007, 2008b, FPL 2010, Baño et al. 2012). Unfortunately, no data was found for *Corylus avellana*. Likewise, the Poisson's ratio for *Fraxinus excelsior*, *Quercus laurifolia*, and *Ulmus procera* did not seem to be readily available in the literature. Therefore, whenever available, I decided to experimentally use data from other species but from the same genus. In the case of *Salix sp*, Subic and Cooke (2003) determined a unique value based on the average values for softwoods and hardwoods; whereas for *Ulmus*, O'Brien (2003) cites also only one value (Carmichael 1950). In neither case was it possible to confirm to which of the Poisson´s ratio were the authors referring to. As to *Quercus*, the data shows the mean values between *Quercus rubra* and *Quercus alba*.

Table 4C.5 Poisson's ratio, Tensile strength, and Shear modulus of the selected woods. Poisson's ratio of *Taxus baccata* (Keunecke 2008b), *Salix sp* (Subic and Cooke 2003), *Fraxinus americana* (FPL 2010), *Pinus sylvestris* (Niemz 1993, cited in Danielsson 2013), *Quercus* (mean value between *Q. rubra* and *alba*) (FPL 2010), and *Ulmus thomasii* (Carmichael 1950, cited in O'Brien 2003). Tensile strength of *Taxus baccata* (||: Sell 1997, ⊥: Sekhar and Sharma 1959, both references cited in Keunecke 2008a), *Salix sp*, *Fraxinus excelsior*, *Pinus sylvestris*, and *Ulmus procera* (MatWeb), *Quercus* (*laurifolia*, ⊥: MatWeb; *nigra*, ||: FPL 2010). Shear modulus of *Taxus baccata* (Keunecke et al. 2007), *Pinus sylvestris* (Baño et al. 2012). Shear strength of *Taxus baccata* (Jakubczyk 1966, cited in Keunecke 2008a), *Fraxinus excelsior*, *Pinus sylvestris*, *Quercus laurifolia*, and *Ulmus procera* (MatWeb). (L) longitudinal, (R) radial, (T) tangential, (||) parallel to grain, (⊥) perpendicular to grain. (*) Data not available.

Mechanical properties (additional data)		***Taxus baccata***	***Salix sp.***	***Fraxinus***	***Pinus sylvestris***	***Quercus***	***Ulmus***
Poisson's ratio (MPa)	μ_{LR}	0,041	*	0,371	0,46	0,36	*
	μ_{LT}	0,029	*	0,44	0,44	0,438	*
	μ_{RT}	0,2	*	0,684	0,61	0,589	*
	μ_{TR}	0,5	*	0,36	0,31	0,296	*
	μ_{RL}	0,46	*	0,059	0,03	0,069	*
	μ_{TL}	0,48	*	0,051	0,02	0,035	*
	(orientation unknown)	-	0,35	-	-	-	0,35
Tensile strength (MPa)	||	108	83	161	102	73,1	78
	⊥	3,3... 4,5	2,4	6,9	2,9	5,45	3,9
Shear modulus (MPa)	G_{LR}	1740	*	*	*	*	*
	G_{TR}	368	*	*	604,3	*	*
	G_{TL}	1650	*	*	*	*	*
Shear strength (MPa)	(orientation unknown)	14,6	6,7	12,5	9,8	12,6	6,9

As can be seen, the Poisson's ratio of *Taxus* stands out among the other wood species, because the deformations along the radial and tangential axis caused by stress along the longitudinal axis (μLR and μLT, respectively) are far lower than the deformations caused by stress along the radial and tangential axis (μRT, μRL, μTR, μTL). Yet, for the rest of the species it is the deformation along the longitudinal axis which shows the lowest values. In respect to the shear strength of yew, it clearly exceeds those of the other species. According to Keunecke et al. (2007), this results from the cellular structure of its tracheids.

The good correlation between these results indicates that these species can be fairly considered as orthotropic elasto-plastic material. Although the mean values of the selected woods do not fall exactly within Ashby's expected ranges (Figures 4C.38 and 4C.39) (Ashby 2005), I assume that these charts are only indicative and do not represent the true property averages for every wood species.

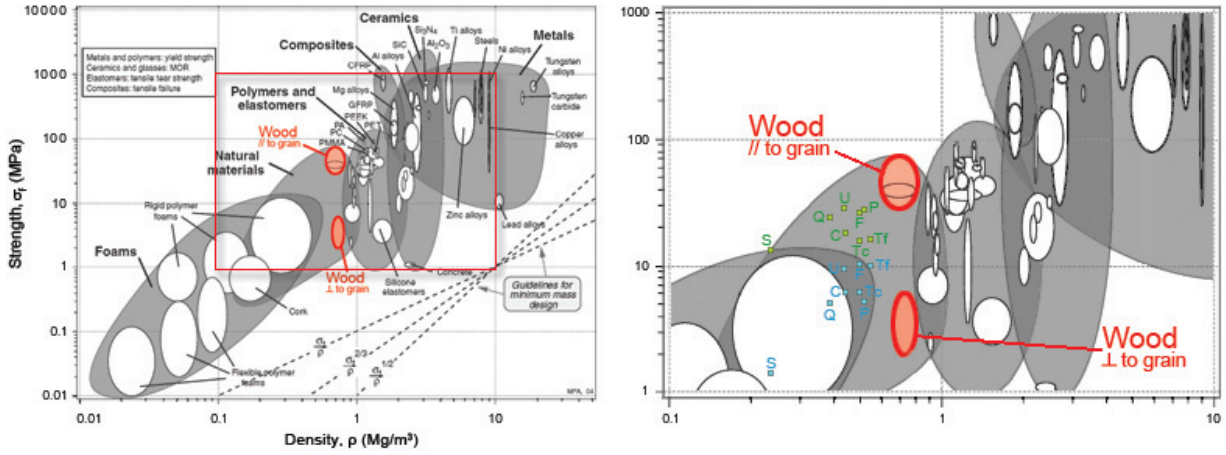

Fig. 4C.38 Strength versus density materials chart (left), and strength versus density of the selected woods (detail, right) (adapted from Ashby 2005). Compression parallel (green marks) and perpendicular to grain (blue marks).

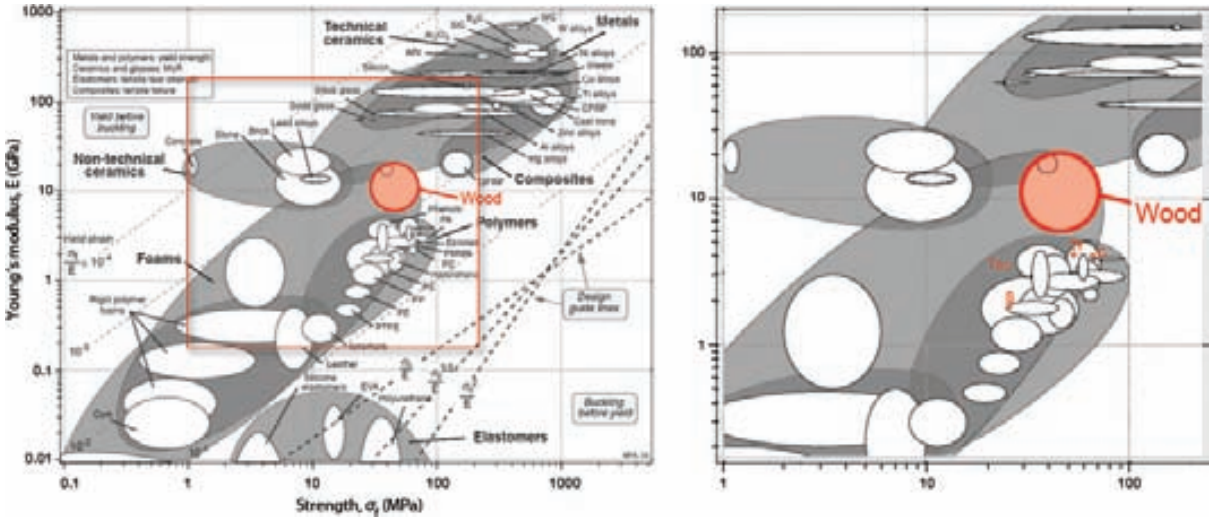

Fig. 4C.39 Young's modulus versus strength materials chart (left), and Young's modulus versus strength of the selected woods (detail, right; orange marks) (adapted from Ashby 2005).

As previously stated, the samples for this study were taken from a few logs which neither represent the whole tree with all its imperfections and individual morphology, nor eventually a group of trees from a specific region and/or climate, ultimately the place from which the wood to manufacture these archaeological artefacts might have come. Thus, it is possible that this sampling may have determined in some way the observed results reported here. Even though variation in properties is common to all materials – and definitely in wood – future research should incorporate a wide quantity of material, representative of a larger quantity for which the properties are to be determined, by including multiple samples from different parts of a given tree, as well from different trees from either the same region or other regions.

Likewise, it is important to take into account that the nature and the magnitude of variability in these wood properties can be due to several other factors, such as: tree height, maturity, and age; complex interaction with temperature and moisture; air drying process; discontinuity and distortion of wood fibres due to knots or holes; seasonality, soil conditions, fertilization, growing speed, growing space, and other climatic, provenance, ecological, biological, or genetic factors (Coffey 1962, Gerhards 1982, Plumb 1985, Gibson and Ashby 1988, Aicher et al. 1988, Beismann et al. 2000, Dinwoodie 2000, Haselein et al. 2002, Alakangas 2005, Eriksson 2005, Jönsson and Thelandersson 2005, Sjördin and Serrano 2006, Taskini 2006, 2007, Kretschmann 2008, Korkut and Hiziroglu 2009, FPL 2010, Kúdela and Lagaňa 2010, Kord 2011, Ozyhar et al. 2013).

C.3.4 Computer Simulation

As earlier mentioned, one way of studying archaeological bows consists in making replicas and using them for experiments (Miller 1986, Bergman et al. 1988, McEwan et al. 1991, Alrune 1992, Prior 2000, Junkmanns 2001, Bellintani et al. 2006, Rosendahl et al. 2006, Hamm 2007). Having a digital surrogate of a specific archaeological artefact makes it possible to compare, among other issues, different materials and forces in identical models without having to actually use it (!) or make a replica. The present approach emphasizes on the use of mathematical models and computer simulation, since they permit theoretical experiments on computers in order to gain new insight into the behaviour of bows.

Much research has been carried out on the kinematics and dynamics of bows (Pope 1923, Rheingans 1936, Hickman 1937, Klopsteg 1943, Hickman et al. 1947, Schuster 1969, Marlow 1979, Kooi and Sparenberg 1980, Kooi 1983, 1991; Miller 1986, Bergman et al. 1988, Cotterell and Kamminga 1990, McEwen et al. 1991, Baker 1992, Bardi 2000a, 2000b; Hoadling 2000, Tapley 2000, Denny 2003, French et al. 2006, Grayson 2007, Zaniewski 2009, Dias-Meirinho 2011), but in short:

1 – The bow is braced by fastening a string between both nocks.

2 – After an arrow is set on the string the archer pulls the bow from braced situation into full draw. As the bow is drawn, tensile stress increases along the back simultaneously with compressive forces developing on the belly, completing the static action in which the elastic parts of the bow store potential energy.

The weight of a bow refers to the maximum force (measured in Newtons or pounds) exerted to draw the string back to a specified distance, while the draw length refers to how far back the string is pulled. In general, the larger these two factors, the more energy created.

3 – After aiming, the arrow is then loosed or released. In a few milliseconds, the force in the string accelerates the arrow and transfers part of the stored potential energy of the bow limbs to both kinetic energy in the limbs and kinetic energy in the arrow, providing for its velocity in flight and target distance.

4 – At the same time the bow is held in its place and the archer feels a recoil force in the bow hand. After the arrow leaves the string, the bow returns to its initial position because of damping.

The behaviour of the bow-arrow-archer system (i.e., interior ballistics) and the arrow in flight (i.e., exterior ballistics) are of great complexity. The overall performance of a bow – as the one studied here – and arrow depends on several parameters: bow length, brace height, string length, draw, and mass of arrow. As well as on three functions: distributions of bending stiffness, mass along the bow, and form of the bow in its unstrung situation (Kooi 1983). Furthermore, the energy which an archer can put into a bow and the quality of the shooting are also limited by the characteristics of the archer's own body and skills (Gordon 1978, Greenland 2002, Dias-Meirinho 2011). Nonetheless, reduced to its simplest terms the usual prerequisite of a bow is that it is capable of shooting an arrow.

Assuming that:

- The design of a bow is characterized by the combination of form, material, and manufacturing procedures, among other constraints;
- The performance of the bow is determined by the overall design, among other constraints;

to what purview could form (and texture) and material properties control the performance of the bow – including consistency from shot to shot, and durability – , and simultaneously influence the choice of different manufacturing procedures and techniques? Or on the contrary, did they limit each other?

In this section, the main objective is to gain a preliminary insight into what would have made artefact D12_JF-JG-81 an efficient bow. This bow was chosen as an optimal test case because it is the only one which is complete. I describe an account of experiments which aimed to develop a FE model to comprehensively assess how the overall geometry of this artefact would react to distinct woods, forces and magnitudes, by (i) measuring the corresponding stress, strains, and displacements; and (ii) analysing the visual output of the software. More advanced aspects, beyond the scope of this research, are outlined at the end of this chapter as topics for further study.

The experiments presented below are the result of a developed work based on an early simulation test conducted with experimental data by Esteban Galindo Gali and Juan José Jiménez Iglesias at CimWorks, Barcelona.

Most of this stage took place at LAQU-UAB. I used a HP Compaq 8000 Elite CMT Business PC, with

an Intel(R) Core(TM)2 Duo CPU E8400 @3.000GHz processor, 3,50 GB RAM, 32 bits OS, graphic card NVIDIA GeForce 9500 GT.; and Solidworks Simulation Premium 2013 software (Dassault Systèmes).

C.3.4.1 FE Model

Before running any type of simulation tests it is necessary to follow a few steps to ensure best results. This stage consisted in converting the 3D digital surface model into a FE model. It should be noted that the objective here is to generate the simplest and reliable FE model, which should still represent deciding relationships with the accuracy and/or resolution required to answer the current questions (Biomesh 2010).

a) Prepare surface mesh

Because computational resources were a problem, the digital model was prior fixed and optimized in RapidForm and then simplified in Solidworks.

- **Fix mesh defects**: automatically find and fix all defects in the mesh: folded (<18º), dangling (2 or 3 side open), crossing, tangled, reversed, redundant, non-manifold, and small poly-faces (<0,0002 mm^2); small clusters (<15 poly-faces) and tunnels (<10 poly-faces). Defects were deleted, and whenever necessary holes were filled. This procedure was run twice, in order to iron out any remaining defects.
- **Global remesh**: in order to regenerate and clean the mesh structure using its curvature flow. Default settings were used in this procedure.
- **Decimate mesh**: in order to reduce the number of poly-faces. This procedure was run twice (2x80%), since sudden reduction can change important features on the original form.
- **Optimize mesh**: in order to create regular sized triangles, more triangles in the high curvature regions, and fewer triangles in the low curvature regions. Default settings were used in this procedure.
- **Mesh simplification**: a global simplification with 95% reduction amount was applied to the imported mesh size, resulting in a final mesh size with 20000 faces.

b) Create 3D continuous surface model

Surface shapes were controlled to increase the robustness of the overall topology, and a few surface errors fixed.

c) Convert continuous surface model into solid model

This solid mesh consists in parabolic tetrahedral solid elements, generated using the Voronoi-Delaunay meshing technique. The FE model has 22370 nodes, 12692 elements, and 65910 degrees of freedom (DOF). The element size is 5,72144 mm, with a tolerance of 0,286072 mm. The software determined the mesh quality as being high (Figure 4C.40).

Fig. 4C.40 Detail of the FE model of wooden artefact D12_JF-JG-81. From left to right: solid mesh and elements; solid mesh, elements, and surface of the solid model; elements and surface of the solid model; surface of the solid model. It is not a solid model with a mesh on it, the mesh of elements is now the model.

C.3.4.2 Simulation Studies

The simulation studies were based on the assumption that:

- The bow is made up of a short middle section and two limbs, which for all positions of the draw bend in arcs of circles (Hickman 1937);
- For this form of bending all sections of the bow are stressed equally (Hickman 1937), except for the grip which is restrained;
- Both geometry and mass change along the bow;
- The material properties of the selected wood species – and in the case of *Taxus baccata* of its origin – are constant throughout the entire FE model.

And comprised the following steps:

a) Treatment

The model was partially restrained to prevent free body motion. In this way, I have applied a more realistic constraint by fixing it in the centre of the artefact (Figure 4C.12), i.e., where the grip of the bow could eventually be. The reference temperature for the current restrained FE model was set at zero strain (24,85ºC), meaning that no strains exist in the model due to variations in temperature conditions.

The outcome values of the physical and mechanical properties of the selected woods where then imported into the software, so as to start creating a specific material library for all the wooden artefacts of the archaeological site of La Draga.

b) Solver

The type of study is static, requiring a geometrically non-linear analysis, and a large displacement formulation. I used the default FFEPlus iterative solver and the Newton-Raphson (NR) numerical technique to solve the set of FEA algebraic equations for nonlinear studies, and because of the current size of the problem (namely, DOF), speed and it is less demanding on computer memory. The FFEPlus solver uses approximate techniques to solve a problem. In each iteration it assumes a solution and then evaluates the associated errors. The iterations continue until the errors become acceptable. Concerning material classification, the software only had the linear elastic option for orthotropic materials.

To perform the simulation studies I have applied a range of static forces until material failure, each

defined by two uniformly distributed external loads on the extremities of the bow. The direction of the force vector applied has a strong impact on the proportion of the total draw force that is applied in a particular direction during the simulation (Curtis 2010). Hence, in this first experiment the directions of both force vectors – one on the upper knock (135º), and the other on the lower knock (225º) – were defined by an external reference geometry (Figure 4C.41), which simplified a bow in non-recurve fully drawn position generated by a hypothetical string, since it was not possible to include in this research the material properties for any possible vegetable fibre, rawhide, or sinew string. For each solution step, the original load direction is maintained on the deformed geometry, while the load location is updated through a function curve with an automatic stepping time increment of 13 steps in 1 second (step 1: 0,01s; step 2: 0,03s; step 3: 0,07s; step 4: 0,15s; step 5: 0,25s; step 6: 0,35s; step 7: 0,45s; step 8: 0,55s; step 9: 0,65s; step 10: 0,75s; step 11: 0,85s; step 12: 0,95s; step 13: 1s) (Figure 4C.42).

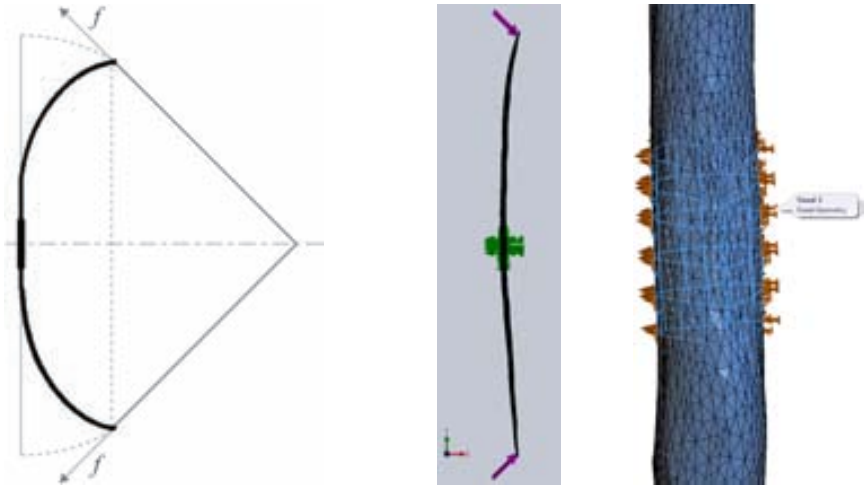

Fig. 4C.41 Support diagram for the simulation tests of a drawn bow, side view (left). FE model of artefact D12_JF-JG-81: location of initial applied loads (in violet), and fixed geometry (in green) (centre); detail of the area with fixed geometry (right).

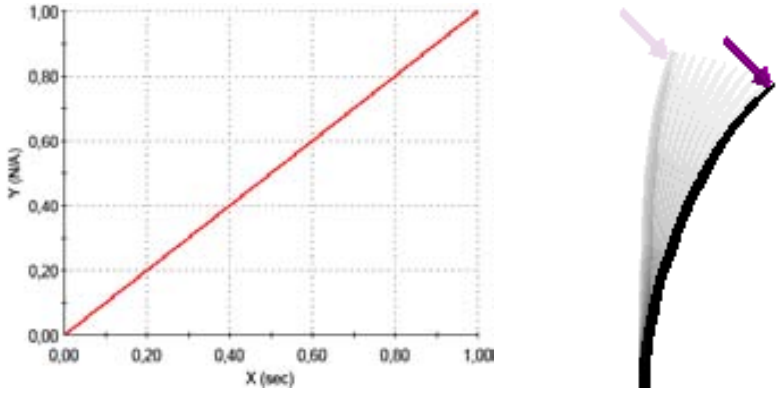

Fig. 4C.42 Applied time curve graphic (left), and detail of the upper limb of the FE model of artefact D12_JF-JG-81 subjected to various loads applied across 13 steps in 1 second to the back side of the knock (right).

c) Results

The stress, strain, and displacement on the same artefact FE model upon different woods and force magnitudes were computed. The results of the simulation calculations are quantitatively displayed below, as well as illustrated, and should be as accurate as the assumed values of the parameters used in the calculations (Baugh 2006).

In measuring fracture strength it is important to distinguish between the strength of the wood from which the bow is made, and the actual failure limit of the bow as a whole which is also dependent on both form and dimension. The ultimate tensile stress was used as the stress limit value to predict material failure. Because the Poisson ratio of *Corylus avellana* was not defined, the software used a default value (0.0).

Table 4C.6 displays the outcome values of the solver studies every 10N before material failure – at some point the stress becomes greater than the yield stress, the material behaves plastically and does not return to its previous state, and fracture is about to occur. Whereas Table 4C.7 displays the outcome values of the solver studies on material failure, meaning that lower action forces than those indicated on the table should be applied to avoid the fracture of the artefact: *Taxus baccata* (Cat) < 33,6N; *Taxus baccata* (Fr) < 52N; *Salix* < 36N; *Corylus avellana* < 58N; *Fraxinus* < 95N; *Pinus* < 84N; *Quercus* < 72,5N; *Ulmus* < 64,5N. Just to mention, one Newton corresponds to a force capable of giving a mass of 1 kg an acceleration of one meter per second.

Table 4C.6 Mechanical response (across 13 steps/1s) of the artefacts' FE model to variations in force and wood species: forces (action force; N), maximum stress (von Mises stress, N/m^2), maximum strain (equivalent strain: ESTRN), resultant maximum displacement (URES; mm).

Force (N)	Response	*Taxus baccata* (Catalonia)	*Taxus baccata* (France)	*Salix*	*Corylus avellana*	*Fraxinus*	*Pinus*	*Quercus*	*Ulmus*
10	Stress (max)	12399330	12433021	11442219	12345169	10624455	10467989	10522603	12015393
	Strain (max)	0,00137666	0,00124133	0,00256224	0,0009687	0,00058357	0,00065051	0,00065696	0,00057091
	Displacement	33,2624	29,7331	60,2400	30,1556	14,0190	15,7306	15,7963	17,2834
20	Stress (max)	25898190	25867748	24463934	25698032	21711172	21442956	21559436	24621400
	Strain (max)	0,00287669	0,00259700	0,00548575	0,00202906	0,00119153	0,00133147	0,00134465	0,00117438
	Displacement	70,6559	62,8618	130,6650	63,7883	28,8705	32,5004	32,6403	35,8092
30	Stress (max)	40410948	40247380	38512140	39996996	33258874	32925624	33107844	37812976
	Strain (max)	0,00450735	0,00405773	0,00863118	0,00317342	0,00182371	0,00204254	0,00206272	0,00181023
	Displacement	111,2650	98,8113	202,5130	100,2750	44,5341	50,2739	50,4956	55,5235
40	Stress (max)		55431100		55096700	45258580	44901420	45154008	51570428
	Strain (max)		0,00559853		0,00438193	0,00247947	0,00278271	0,00281009	0,00247701
	Displacement		136,4230		138,4020	60,9583	68,9662	69,2755	76,3056
50	Stress (max)		71208520		70774840	57697380	57350116	57677520	65856796
	Strain (max)		0,00718379		0,00562551	0,00315801	0,00355053	0,00358529	0,00317167

Force (N)	Response	*Taxus baccata* (Catalonia)	*Taxus baccata* (France)	*Salix*	*Corylus avellana*	*Fraxinus*	*Pinus*	*Quercus*	*Ulmus*
	Displacement		174,2080		176,6100	78,0779	88,4656	88,8672	97,9576
60	Stress (max)					70546056	70230504	70636112	80618296
	Strain (max)					0,00385759	0,00434329	0,00438550	0,00388972
	Displacement					95,7622	108,5670	109,0610	120,2150
70	Stress (max)					83771112	83494600	83980944	
	Strain (max)					0,00457630	0,00515788	0,00520753	
	Displacement					113,8720	129,0510	129,6350	
80	Stress (max)					97320856	97075880		
	Strain (max)					0,00531121	0,00599006		
	Displacement					132,2240	149,6650		
90	Stress (max)					111157376			
	Strain (max)					0,00606018			
	Displacement					150,6710			

Table 4C.7 Mechanical response (across 13 steps/1s) of artefact D12_JF-JG-81 FE model to wood species and force on material failure: forces (action force; N), resultant reaction force (N) on the entire model, maximum stress (von Mises stress across all steps; N/m^2), maximum strain (equivalent strain: ESTRN), resultant maximum displacement (URES; mm).

	Taxus baccata (Catalonia)	*Taxus baccata* (France)	*Salix*	*Corylus avellana*	*Fraxinus*	*Pinus*	*Quercus*	*Ulmus*
Response	33,6N	52N	36N	58N	95N	84N	72,5N	64,5N
Reaction force	47,501	73,479	50,85	81,999	134,28	118,75	102,5	91,205
Stress (max)	45848600	74410900	47078400	83552400	118164000	102585000	87365600	87397800
Strain (max)	0,00511755	0,0075026	0,0105384	0,00662434	0,00643887	0,0063271	0,00541568	0,00421898
Displacement	126,35	181,649	242,308	206,205	159,867	157,895	134,799	130,347

The reaction forces are directly opposite to the action forces; and the resultant force on the entire FE model is a single force which represents the vector sum of all three force vectors (x, y, z components), where the force component in the x axis (Fx) contributes the most to the overall resultant force (Figure 4C.43).

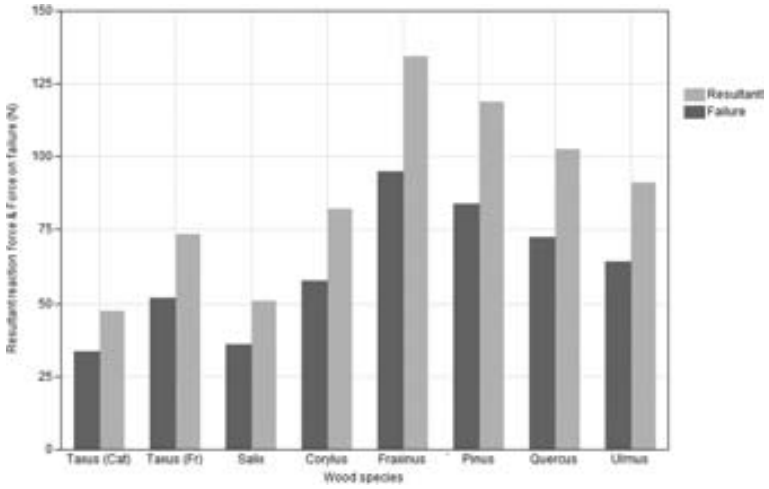

Fig. 4C.43 Column chart displaying force on material failure and resultant reaction force on the entire FE model.

Drawing the bow, or pulling the arrow back in the bowstring, places the back under tensile stress and the belly under compressive forces (McEwan et al. 1991, Miller 1986, Müllner et al. 2006). According to Bergman et al. (1988), McEwen et al. (1991), Junkmanns (2001), and Denny (2003) most bows break because tensile stress causes failure of the back. The tensor plot in Fig. 4C.44 is provided for visual reference, since it confirms both compression behaviour and tensile behaviour on the FE model – only a small portion is depicted for higher readability.

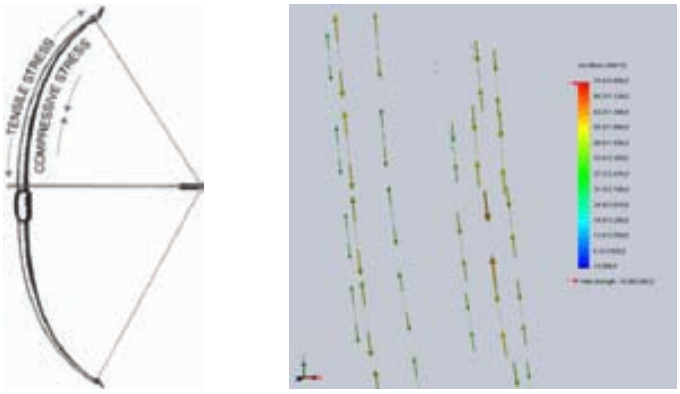

Fig. 4C.44 Drawing the bow, or pulling the arrow back in the bowstring, places the back under tensile stress and the belly under compressive forces (adapted from McEwan et al. 1991). Detail of the nonlinear nodal stress (von Mises) tensor plot of the lower limb FE model (French *Taxus baccata*, 52N), indicating the tensile stress on the back and the compressive stress on the belly.

As previously demonstrated, some woods are more prone to failure than others. It can be seen (Figures 4C.45, 4C.46, 4C.50, 4C.51) that by changing the material parameters of each wood species the FE model of the artefact responds accordingly. In the graphs below, the bow starts to draw from an initial condition of zero stress and strain. The total strain energy is the area under the load deflection curve. The fine-scale morphology of *Taxus baccata* seems to be peculiarly adapted for storing strain energy (Gordon 1978), when compared to the other species but *Salix*.

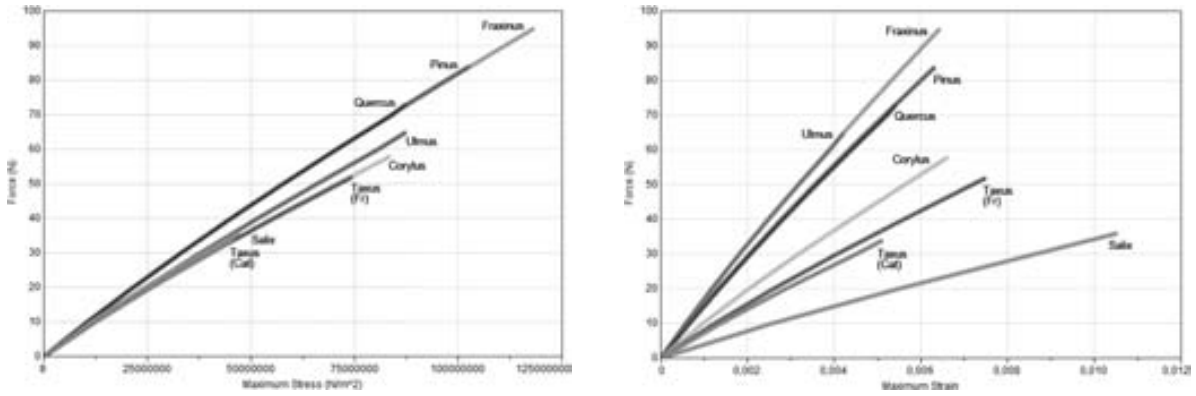

Fig. 4C.45 Maximum stress (left), and maximum strain (right) responses of artefact D12_JF-JG-81 FE model to variations in force and wood species.

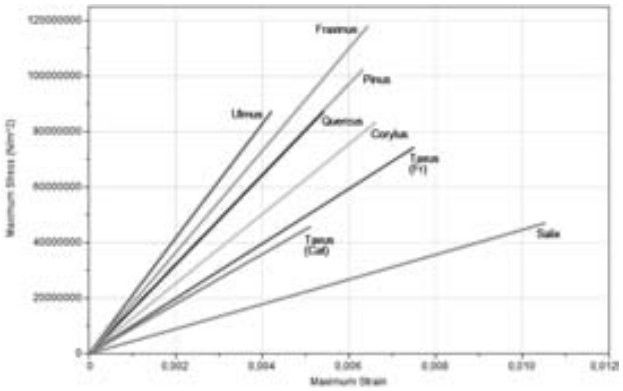

Fig. 4C.46 Maximum stress to maximum strain graphic of artefact D12_JF-JG-81 FE model to variations in force and wood species.

Colour plots are a very valuable visual indicator of how close to breaking the bow limbs are – red corresponds to high stress, strain, or displacement, while dark blue corresponds to algebraically lower magnitudes of stress, strain, or displacement. Figure 4C.447 displays the von Mises stress distribution throughout the belly, indicating the areas where material failure is predicted in the current simulation study (French *Taxus baccata*, 52N). Figures 4C.48 and 4C.49 show a detail of one of the areas where material failure is predicted. In the former, it is possible to verify both compression and tensile behaviours on the FE model (c), as well as the eigenvectors of the three principal stress tensors (d, e, f). While in the latter, it is possible to observe the strain distribution and the eigenvectors of the three principal strain tensors (from a to i).

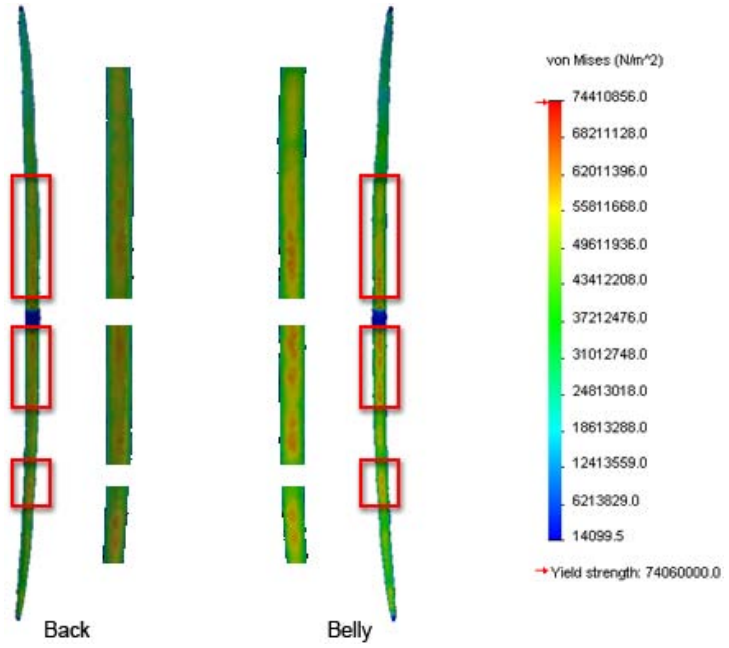

Fig. 4C.47 Nonlinear nodal stress distribution throughout the back (left) and belly (right) of artefact D12_JF-JG-81 FE model (French *Taxus baccata*, 52N). Red rectangles indicate areas (details displayed in the centre) where material failure is predicted in the current simulation study.

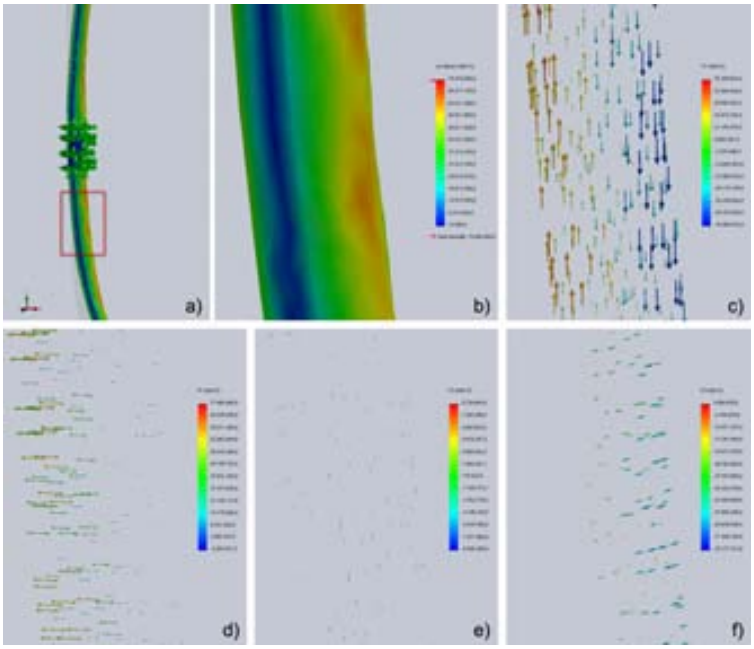

Fig. 4C.48 Nonlinear nodal stress distribution on artefact D12_JF-JG-81 FE model (French *Taxus baccata*, 52N): a) red rectangle indicating detail of studied area; b) von Mises stress colour plot, material failure is predicted in red for the current simulation study; c) SY tensor plot, normal stress in Y axis; d) P1 tensor plot, 1st principal stress; e) P2 tensor plot, 2nd principal stress; f) P3 tensor plot, 3rd principal stress.

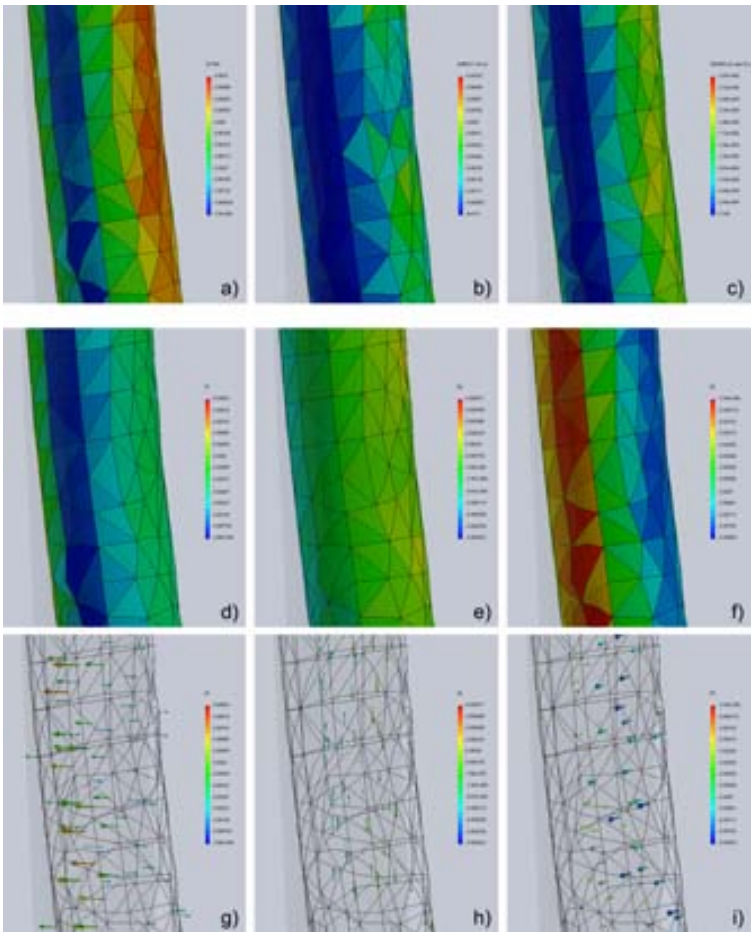

Fig. 4C.49 Total strain distribution on artefact D12_JF-JG-81 FE model (French *Taxus baccata*, 52N), detail of studied area with superimposed mesh: a) ESTRN colour plot, equivalent strain; b) ENERGY colour plot, total strain energy; c) SEDENS colour plot, strain energy density; d) E1 colour plot, 1st principal strain; e) E2 colour plot, 2nd principal strain; f) E3 colour plot, 3rd principal strain; g) E1 tensor plot, 1st principal strain; h) E2 tensor plot, 2nd principal strain; i) E3 tensor plot, 3rd principal strain.

Besides the draw weight of the bow, a force-draw plot indicates its actual draw length. Since the relation force-draw length affects the bow's performance, it is one of the most important factors to be controlled in the design of a bow. The area under the force-draw curve determines the bows' efficiency for propelling an arrow, which can be measured by the fraction of available potential energy transferred into kinetic energy of the arrow. Furthermore, the shape of the force-draw curve – which depends primarily on the dimensions and geometry of the bow – indicates the possibility of the bow becoming difficult to control or risk to break (Klopsteg 1943, Bardi 2000b).

Figures 4C.50 and 4C.51 show the maximum distance along the path made by the limbs in response to variations in force and wood species, not the actual draw length of the bow – i.e., fistmele – as it is much dependant on the string's length, type, and how it was made. Each curve is plotted as a graph of force against displacement. The curves show a linear or nearly linear relation, which usually indicates the nonoccurrence of sudden rise in force at high draws (also known as 'stack'). The graph also indicates that it is necessary to exert higher forces on *Fraxinus* (< 95N; 159,867 mm), *Pinus* (< 84N; 157,895 mm), *Quercus* (< 72,5N; 134,799 mm), and

Ulmus (< 64,5N; 130,347 mm) to fully draw the bow. Instead, *Corylus* (< 58N; 206,205 mm) and French *Taxus* (< 52N; 181,649 mm) require lower force to fully draw while being capable of achieving greater displacement. Catalan *Taxus* and *Salix* are the wood species which require lowest force, with the former achieving the shortest displacement (< 33,6N; 126,35 mm) and the latter the greatest displacement (< 36N; 242,308 mm).

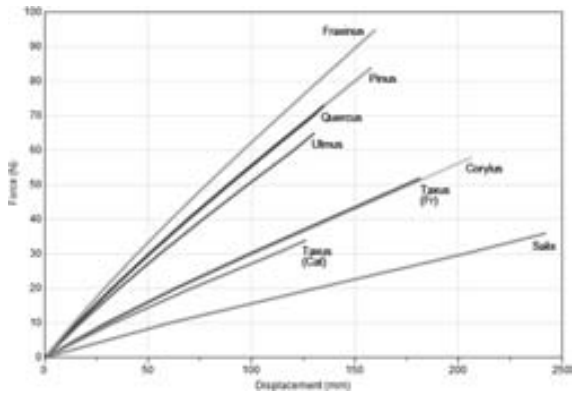

Fig. 4C.50 Displacement response of artefact D12_JF-JG-81 FE model to variations in force and wood species.

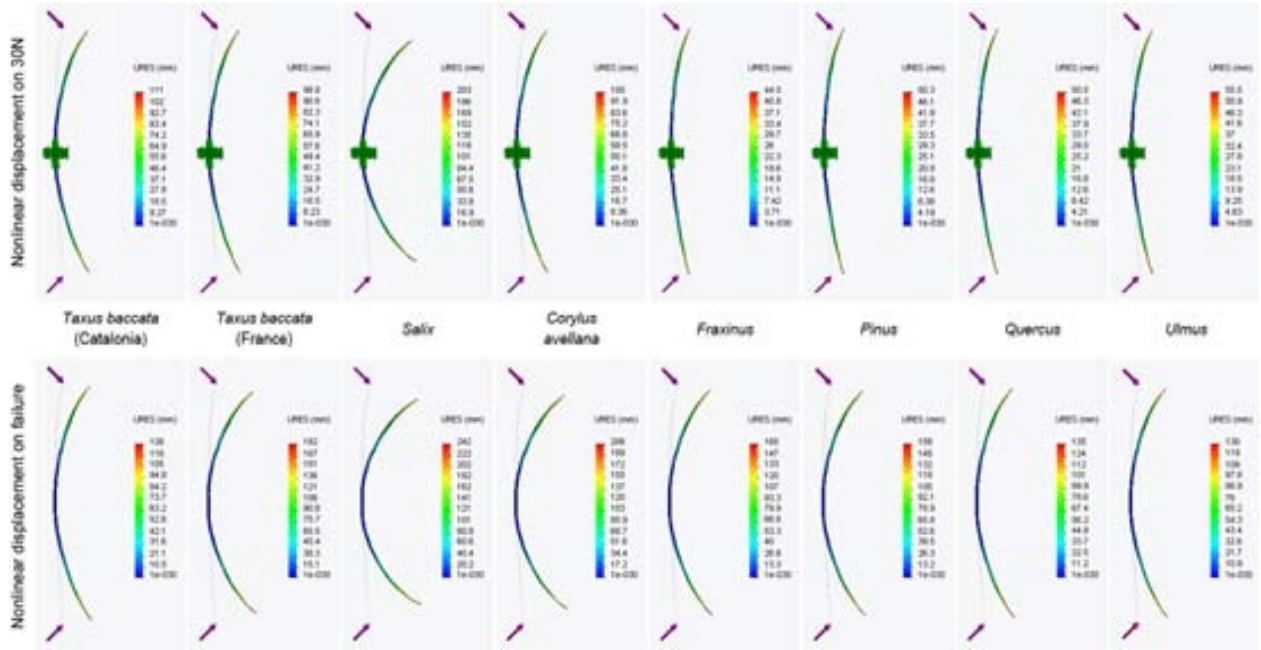

Fig. 4C.51 Displacement plot displaying the mechanical response of artefact D12_JF-JG-81 FE model to variations in force and wood species: nonlinear displacement on 30N (top), and nonlinear displacement on failure (bottom).

As expected, these results indicate that the resistance to failure of bow D12_JF-JG-81 is not the same upon different types of wood under the same conditions. Nevertheless, all graphs show stress, strain and displacement curves rising continuously as the bow is drawn. At this point it is important to have in mind that bows require flexibility, resistance to fracture, and ability to store energy that can be explosively released and transmitted to the arrow in a more or less efficient way. Consequently, the overall results allowed distinguishing two major groups of wood species to manufacture the bow:

1) Adequate – this group can be divided in two other groups. One comprises *Fraxinus*, *Pinus*, *Quercus*, and

Ulmus; whereas the other includes *Taxus* and *Corylus*.

The first group requires higher force to fully draw the bow. *Pinus* and *Fraxinus* are capable of storing more energy than *Ulmus* and *Quercus*. A heavier draw, especially on longbows, can sometimes be a disadvantage in that it is more difficult to hold steadily while pulling back the string until it is fully drawn. Though it can eventually suggest the use of stiffer arrows, and the increased weight of an arrow will impart a greater amount of energy to the target, and therefore do more damage.

The differences between the FE model's response to the Catalan and French *Taxus baccata* are in agreement with the results already presented in section *C.3.3 Material – Wood*. The French *Taxus* is able to bow under higher stress without easily fracturing. Since the overall response of the French *Taxus* bow is closer to those of *Fraxinus*, *Pinus*, *Quercus*, and *Ulmus* – wood species also used in other archaeological bows – than the Catalan *Taxus*, I assume that the first represents best a yew bow.

In this study, the advantage of the French *Taxus baccata* over the other wood species was confirmed by its ability to store higher strain energy while undergoing lower stress. The superior toughness and high resilience of yew allows the bow to withstand greater displacements under lower forces, and to achieve higher ranges compared with bows made from other species (Baugh et al. 2006, Bjurhager et al. 2013). As refered by Kamminga and Cotterell (1990, p.182), "the efficiency of a bow depends on its design and the materials of its construction. The bow material must be light and resilient so that the bow has as small a mass as possible". The results herein presented suggest that this material could have been selected on the basis of how well it fitted the requirements for this particular artefact.

As Piqué et al. (2013) have noted, the bows of La Draga show a manufacturing process that continued to be used subsequently. They were made with a segment of *Taxus baccata*, which seemed to take advantage of the unique properties of sapwood and heartwood parts. In fact, D02_KA89-11 and D12_JF-JG-81 have their belly made from heartwood, which is better suited to handle compressive stress; while their back face is from sapwood, which is very strong and elastic under tensile stress. Exception is made for artefact D05_KE90-7 which has its back face and belly made of sapwood and heartwood, respectively – but this difference might be due to the restoration process, when reassembling all five fragments of the bow. The recent work of Bjurhager et al. (2013) additionally demonstrates that the mechanical performance at least of a longbow made from yew "is influenced by the juvenile-to-mature wood ratio rather than by the heartwood-to-sapwood ratio. A yew bow is predicted to have maximized performance at a juvenile wood content of 30–50%, and located at the concave side".

According to Stemmler (1947) and Gordon (1978), because the mechanical properties of *Taxus* deteriorate more rapidly with increasing temperature than do those of other species, yew bows cannot be used reliably as a weapon above 35° C as it loses weight and cast, hence making it unsuitable for use in the Mediterranean summer. On the other hand, using a yew bow in winter when there is any frost can cause a bow to brake (Ascham 1545).

Although not specifying the chronology, Gordon (1978) also mentions that much later "most English bows were made from Spanish yew and it was legally compulsory to import consignments of Spanish

bow-stave with each shipment of Spanish wine" – to put forward the hypothesis, this could eventually help to understand at which point and why *Taxus baccata* began to decrease in the Iberian Peninsula.

Unexpectedly, the overall results of *Corylus* fall in the group of 'favourite' wood species to manufacture a one piece bow, if it wasn´t the fact that this wood specie consists in a shrub or a small tree and consequently very difficult if not impossible to find a log with the required dimensions. In the scope of bows and arrows, this fact – together with its availability and, of course, the mechanical properties of this wood specie – can eventually explain the use of *Corylus* for making a possible spear in La Draga.

2) Inadequate – *Salix*. "The longer draw length would apparently contribute significantly to the energy transferred to the arrow allowing for a faster shot and longer cast" (Prior 2000), but the results of the previous material tests and the above graphs show a very high risk of breakage. Again, the properties and behaviour of *Salix* suggest that it could instead be suitable for making shafts – as it seems to be corroborated by the ones discovered in La Draga. The efficiency of a bow increases with the design and mass of an arrow, as well as the purpose of the projectile, along with other factors (Bergman et al. 1988, Cotterell and Kamminga 1990).

Within the limits of this experiment, the design parameters of artefact D12_JF-JG-81 which determined the mechanical action of the bow fit very well the selected material, i.e., *Taxus baccata*. Though, it is not possible to isolate these features from the combination of many other ones, such as draw length, type of string, type of arrow, materials sensitivity to changing weather conditions, or material availability.

C.4 Conclusions

The approach herein presented demonstrates the interest of the proposed framework towards a better comprehension of archaeological artefacts, by bringing quantitative 3D digital methods and techniques and now computer simulation to functional analysis. To this end, I have investigated the geometry, material, and behaviour of a set of archaeological wooden artefacts.

Once again, 3D scanning allowed to acquire meaningful shape, form, and texture information from the Neolithic bows from La Draga. This enabled to differentiate from one another, by describing and analysing quantitatively their geometrical features.

Comprehensive analytical methods and techniques used in material science were applied to the analysis of the physical and mechanical properties of a set of wood species. The significance of these properties in the selection and use of raw materials is evident, although one should not ignore the perception of the raw material's characteristics, the potential importance of the resources location (Henderson 2000), and exchange networks.

FEA has emerged as a powerful tool in the prediction of the mechanical behaviour of a specific bow upon distinct forces and several wood species. Because the physical world is invariably too complex to model at every level of detail (Biomesh 2010), it was necessary to simplify assumptions according to the mechanics of

the bow, available data, and computational resources. While these experimental studies using computer simulation are still at a preliminary stage, they have already enabled to draw some novel and useful results from an archaeological bow, which was chosen as an optimal test case. I have demonstrated how computer simulation can be a powerful tool in archaeological research – in this particular case study, not only to get insight into the influence of a set of wood species and exerted forces on a specific artefact, but also for understanding the design choices and changes of bows in the past.

Ideally, the achieved results should be compared and supported by other sorts of data, to enable more complete "what if?" scenarios and therefore a comprehensive understanding of the subject. Moreover, if feasible, one should also conduct real world testing to completely validate the results (Wroe et al. 2007, McHenry et al. 2007, Degrange et al. 2010). Howbeit, I hope that these preliminary results contribute to the understanding of complex issues: (i) of bow-and-arrow using in Neolithic times, and ultimately (ii) related to prehistoric cognition (Yonekura 2008).

In this vein, future computer simulation studies may include:

- The whole set and dynamics of bow and arrow, which will require to consider wood, stone, and bone arrowheads too;
- Fragmented artefacts D02_KA89-11 and D05_KE90-7, which will require to digitally reconstruct the remaining form and dimension, while conveying information about levels of empirical certainty in each hypothetical reconstruction (Frisher et al. 2002, Bentkowska-Kafel et al. 2012, Niccolucci et al. 2004);
- If possible, other archaeological bows.

As an inter and multidisciplinary investigation, I believe that further studies – from hunting and defence strategies of the Neolithic people from La Draga, to material-related activities, the entire *chaîne operatoîre* (Leroi-Gourhan 1966) related to each bow and arrow, and corresponding functional analysis – will definitely benefit reasoning, among many other issues, on:

- How to get the best bow for one needs out of the materials available, with the minimum of effort;
- Wether different forms of bow represented a careful choice of materials adapted to its function, or different materials represented a careful change of form adapted to its function, and eventually leading to the later emergence of the composite bow;

According to Bergman et al. (1988) variations in bow and arrow design represent a unique adaptation within the limitations of the available raw materials, while Baker (1992) adds manufacturing tools, and skills. "We compare the performance of bows used in the past with that of modern competition bows. It appears that the superb features of man-made materials contribute most to the better performance of the modern bow and not its geometric shape" (Kooi 1994, p.1). Concerning the Neolithic site of La Draga, it has already provided many evidence for a greater selection of raw materials, on the basis of how well their properties and morphology fitted the requirements for a particular function (Piqué 2000, Bosch et al. 2006, Terradas et al. 2012).

Annex C

Systematic Section Measurements of the Bows from La Draga

Table 4C.8 Artefacts D02_KA89-11 and D12_JF-JG-81: width, height, area, perimeter, and Shape Factor measurements of the extracted planar cross-sections, every 10 mm.

	D02_KA89-11					D12_JF-JG-81				
Cross-section	Width	Height	Area	Perimeter	Shape Factor	Width	Height	Area	Perimeter	Shape Factor
1	16,0303	5,8153	58,7613	38,2614	0,5044	-	-	-	-	-
2	20,1742	8,4220	111,9925	49,3581	0,5777	9,2065	4,5006	31,2547	22,2052	0,7966
3	23,9324	11,4007	149,7063	59,9886	0,5228	10,2360	5,7393	46,1119	26,0411	0,8545
4	24,3547	12,8650	161,8249	63,0490	0,5116	12,0119	7,0871	65,3757	30,7394	0,8694
5	24,5010	13,5278	175,1954	64,1753	0,5346	13,6240	8,9790	91,9673	35,6652	0,9086
6	24,5066	14,1829	187,0527	65,5490	0,5471	14,2498	9,7074	108,4505	38,3514	0,9266
7	24,2780	14,6368	195,0551	64,3196	0,5925	14,6565	9,7899	117,9469	40,0591	0,9236
8	24,1959	15,5546	202,1716	66,3830	0,5765	15,5674	9,9003	120,5201	41,1047	0,8964
9	23,8316	16,6837	208,9453	68,0860	0,5664	15,8889	10,2286	130,7917	42,7844	0,8979
10	23,4996	17,0763	214,8974	69,1538	0,5647	16,3452	10,5251	140,1772	44,3596	0,8952
11	23,5332	18,0467	225,6544	69,2443	0,5914	16,8247	10,7574	146,9700	45,3533	0,8979
12	23,5633	18,7882	235,6492	69,8665	0,6066	16,5408	10,9634	152,4297	45,9445	0,9074
13	23,7335	19,8254	255,5869	69,6807	0,6615	16,4238	11,5689	160,1214	46,6551	0,9244
14	23,9160	20,6424	277,9143	70,0481	0,7118	16,2460	11,6803	158,3604	46,4473	0,9224
15	24,2150	21,4641	296,8812	73,5154	0,6903	16,3878	11,7341	163,7507	47,3328	0,9185
16	24,6166	21,6432	316,5934	73,8324	0,7298	17,0284	12,3263	175,3264	48,8422	0,9236
17	25,0251	22,0286	341,7658	77,9631	0,7066	17,6071	13,2298	188,6208	50,9384	0,9135
18	25,7925	21,9610	351,4187	78,0431	0,7250	18,6942	15,0657	223,5527	54,7972	0,9356
19	26,2730	21,2902	341,7214	76,3970	0,7357	18,9729	14,1188	223,1387	54,8898	0,9307
20	26,0061	20,2240	321,1313	73,9813	0,7373	18,9853	13,5865	213,1078	54,3807	0,9056
21	25,9206	19,2508	309,1923	72,3941	0,7414	18,9648	13,3719	209,6960	53,9367	0,9058
22	27,3376	18,8008	307,7459	74,1856	0,7027	19,0960	13,3243	209,0929	53,7271	0,9103
23	27,8674	18,9110	308,8655	74,9037	0,6918	19,2970	13,4457	209,4633	53,5774	0,9170
24	28,3232	19,6920	319,3081	77,0321	0,6762	19,3258	13,4741	208,2615	53,3654	0,9190
25	28,9522	20,8045	351,9327	81,1182	0,6721	19,2936	13,4415	203,4983	52,8589	0,9152
26	30,9590	23,0425	442,0363	88,5024	0,7092	19,3828	13,1380	201,0899	52,8939	0,9032
27	30,2645	23,6300	458,1459	86,9374	0,7617	19,2337	13,0436	198,8556	52,5744	0,9041
28	29,8452	21,4099	393,7964	82,9978	0,7184	19,6780	12,9421	205,7273	53,9253	0,8890
29	28,3025	20,2301	354,7699	77,2443	0,7472	20,7802	13,0887	219,9202	56,1683	0,8760
30	27,3286	20,0106	356,0692	75,6549	0,7818	21,8690	13,6535	231,6279	57,3081	0,8863
31	27,1348	20,5402	372,9509	75,7885	0,8159	21,8635	14,4469	244,2200	58,2926	0,9032
32	27,8110	21,2232	395,8719	77,0876	0,8371	21,4625	14,0199	236,0320	57,7245	0,8901
33	28,5500	21,4464	405,9978	78,7096	0,8235	21,9120	13,3459	225,2887	57,2925	0,8625
34	27,2144	20,3243	385,3904	75,8472	0,8418	22,0188	12,9122	216,4572	56,1909	0,8615
35	27,4170	19,5054	382,0883	75,4225	0,8441	21,8815	12,3665	209,6062	55,6069	0,8518
36	27,2440	19,0778	377,3029	74,6370	0,8511	22,3409	12,2326	211,0261	56,4307	0,8328

	D02_KA89-11					D12_JF-JG-81				
Cross-section	Width	Height	Area	Perimeter	Shape Factor	Width	Height	Area	Perimeter	Shape Factor
37	27,6839	19,8416	403,8240	76,9273	0,8575	22,9557	12,6343	219,9801	57,4325	0,8381
38	28,7083	22,8331	483,5323	84,6822	0,8473	23,8675	13,3020	232,4215	58,9418	0,8407
39	29,0229	21,7055	479,5624	82,5115	0,8852	24,7277	14,3098	242,2648	60,8210	0,8230
40	28,7198	19,8099	452,7422	80,1086	0,8865	23,8836	14,3742	245,6218	60,5886	0,8408
41	28,5672	19,2836	428,1618	77,6648	0,8920	23,8079	13,7749	242,2773	59,7707	0,8522
42	28,7236	19,9767	420,6294	76,8520	0,8950	23,5867	13,6386	238,1319	59,8166	0,8363
43	28,9337	21,5215	439,6558	78,1997	0,9035	23,7327	13,3742	237,8929	59,8571	0,8344
44	28,6032	19,3831	408,6954	75,5861	0,8989	23,7983	13,6418	238,9441	59,6834	0,8429
45	28,5067	19,3034	410,3200	76,0825	0,8908	23,4573	13,7317	234,3603	58,9227	0,8483
46	28,2583	18,4322	375,0078	73,3784	0,8752	22,9601	13,9755	233,3569	58,9930	0,8426
47	27,6833	18,2096	352,3700	71,5568	0,8648	22,7653	14,0514	232,6433	58,6423	0,8501
48	27,7090	18,2178	364,1225	71,9046	0,8850	22,8988	14,1408	233,9529	58,4010	0,8620
49	27,8511	19,2224	397,0743	74,2158	0,9059	22,8492	13,9710	237,5038	58,9009	0,8603
50	27,6038	19,5298	399,2368	74,0174	0,9157	22,8826	14,1223	242,3605	59,1318	0,8710
51	27,3974	18,7114	381,6222	72,4723	0,9131	22,9159	13,9698	247,1513	59,5832	0,8748
52	27,3132	18,6130	374,4474	71,5347	0,9195	22,9980	14,1850	252,1576	60,6311	0,8620
53	27,1085	18,6264	373,5985	71,3871	0,9212	23,1932	14,8824	256,7431	60,9098	0,8696
54	26,8595	18,2558	360,0946	70,5012	0,9104	23,9096	14,0120	254,7057	60,8856	0,8634
55	26,9915	18,3312	360,3309	70,6136	0,9081	24,6112	14,4011	270,7293	63,2312	0,8509
56	26,9409	18,4310	359,7934	70,4644	0,9106	23,9876	14,9942	278,9385	63,2451	0,8763
57	27,1444	19,1681	375,0917	71,7592	0,9154	22,9951	14,8316	257,7561	60,8680	0,8743
58	27,5095	20,7001	422,1024	75,9388	0,9198	22,8443	14,4414	246,9460	59,7129	0,8703
59	27,2225	20,6196	412,2285	75,6367	0,9055	22,8341	13,5334	238,0539	58,9954	0,8595
60	26,7231	20,1649	398,2032	79,7508	0,7868	22,7615	13,5169	235,9919	58,6340	0,8626
61	26,8009	19,9995	391,9239	85,0686	0,6806	22,9767	13,4440	240,0375	59,3427	0,8566
62	26,6367	19,6396	377,6381	81,3240	0,7175	22,8768	13,4177	242,7360	59,2428	0,8691
63	26,7734	18,7757	366,5931	78,5282	0,7470	22,7771	13,7354	246,6780	59,3070	0,8813
64	26,8332	18,5771	360,0368	81,0101	0,6894	22,6160	13,9735	245,4649	59,1382	0,8820
65	26,8924	18,5119	354,0059	81,1105	0,6762	22,3733	13,7440	237,1214	59,0128	0,8556
66	26,6626	18,6421	354,3844	78,7968	0,7172	22,2688	13,1781	228,1582	57,5292	0,8663
67	26,3443	18,4084	356,7547	79,8592	0,7030	22,2016	12,8615	218,4722	56,3787	0,8637
68	26,4418	18,4033	355,2687	81,1120	0,6786	22,4716	12,9381	221,2332	56,6982	0,8648
69	26,5965	17,8681	345,6728	78,1356	0,7115	22,8257	13,6151	225,8512	57,4876	0,8588
70	25,7286	17,5923	325,0412	70,9718	0,8109	22,9745	14,2127	247,0211	60,0040	0,8622
71	25,0039	16,9889	312,2983	70,0743	0,7992	21,5967	14,1846	226,8158	57,3914	0,8653
72	24,5008	16,8487	302,7086	67,7685	0,8283	20,8885	14,1898	215,7044	55,3215	0,8857
73	24,4966	17,0079	300,3197	67,1722	0,8364	20,3989	13,8425	206,8555	54,0751	0,8890
74	24,8338	17,1628	311,4811	68,8932	0,8247	20,1985	13,5395	201,9285	53,6217	0,8825
75	24,7755	17,3513	312,0957	69,5164	0,8116	20,2408	13,6521	201,1135	54,3680	0,8550
76	24,5882	17,4556	315,5171	69,7754	0,8144	20,7900	13,9088	213,0495	55,7611	0,8610
77	24,8283	17,4787	343,1374	68,3479	0,9231	21,9503	13,9787	233,8713	58,0805	0,8712
78	24,4259	17,8981	328,9828	67,3525	0,9113	21,9610	13,9528	227,9145	57,3557	0,8706
79	23,8837	16,0887	294,6538	67,2592	0,8185	20,4479	13,3258	205,1206	54,3266	0,8734
80	23,8592	15,2245	285,1085	65,5047	0,8350	20,1984	12,6386	189,8888	52,4561	0,8672
81	23,7916	14,5432	272,7875	66,7696	0,7689	20,0139	12,2095	183,3620	52,0478	0,8506

	D02_KA89-11					D12_JF-JG-81				
Cross-section	Width	Height	Area	Perimeter	Shape Factor	Width	Height	Area	Perimeter	Shape Factor
82	22,9247	12,5614	234,1728	63,2553	0,7354	19,9081	11,6830	173,3520	50,7205	0,8468
83	22,9922	12,4883	208,0361	63,6982	0,6443	19,3314	11,5976	164,7846	49,4731	0,8460
84	21,5566	11,7661	180,2257	56,6238	0,7064	19,1230	11,7475	161,9735	49,4156	0,8335
85	20,7915	11,4112	173,7362	56,4006	0,6863	18,7859	11,9898	160,6991	48,9759	0,8419
86	20,4665	10,9461	167,4443	54,7788	0,7012	18,9338	11,8803	162,3937	49,1304	0,8454
87	20,5593	10,3664	165,5641	54,6922	0,6955	19,5259	11,8764	170,0799	51,4903	0,8061
88	20,7779	10,1037	163,6838	54,3092	0,6974	19,8204	12,3581	189,9106	52,2508	0,8741
89	20,6727	10,3612	160,7059	53,2547	0,7121	18,2063	12,4602	174,8586	49,3602	0,9019
90	20,4698	11,1121	158,0815	54,5331	0,6680	18,1183	11,8400	160,7798	48,0415	0,8754
91	19,2719	10,3747	152,2772	50,7135	0,7440	18,0966	11,1342	149,6723	47,0542	0,8495
92	18,2796	10,2555	143,2091	49,0127	0,7491	17,7988	10,9365	142,3039	45,8116	0,8521
93	17,2084	10,4486	135,0819	47,3756	0,7563	17,8831	11,0207	139,3388	45,5655	0,8434
94	15,7837	10,6383	123,0023	45,0603	0,7613	17,6936	10,8753	136,0643	45,6135	0,8218
95	14,9402	10,6658	120,9126	42,5529	0,8391	17,4713	10,5524	131,2015	44,1765	0,8448
96	13,6080	9,8037	102,2359	39,1469	0,8383	17,0455	10,3934	126,2256	43,1888	0,8504
97	12,2892	9,2357	77,5580	34,8844	0,8009	16,4365	9,6368	118,5646	41,8120	0,8522
98	10,9545	8,7595	65,7501	32,5720	0,7788	16,1464	9,2160	113,4169	40,9257	0,8509
99	8,4481	5,6497	30,5930	22,4853	0,7604	15,8511	8,7573	111,8487	40,5784	0,8536
100	-	-	-	-	-	15,8686	9,6721	113,1249	40,5312	0,8653
101	-	-	-	-	-	14,8682	8,0937	93,8114	37,3527	0,8449
102	-	-	-	-	-	14,0643	8,0111	81,0353	34,6130	0,8500
103	-	-	-	-	-	12,7651	7,3038	66,7843	31,9050	0,8245
104	-	-	-	-	-	12,1280	6,7117	57,9841	30,0890	0,8048
105	-	-	-	-	-	11,3333	6,2807	50,0312	28,2873	0,7857
106	-	-	-	-	-	10,0994	5,8002	40,0966	25,3517	0,7840
107	-	-	-	-	-	9,1889	4,9536	32,9964	23,0947	0,7774
108	-	-	-	-	-	7,2635	4,0457	20,5772	19,1266	0,7068

Table 4C.9 Artefact D05_KE90-7: width, height, area, perimeter, and Shape Factor measurements of the extracted planar cross-sections, every 10 mm.

	D05_KE90-7				
Cross-section	Width	Height	Area	Perimeter	Shape Factor
1	12,9163	6,4487	65,1133	31,4569	0,8269
2	14,0979	8,9578	99,4240	37,5899	0,8842
3	14,4883	9,9630	114,7334	39,2054	0,9380
4	14,2281	11,0750	119,3078	40,5127	0,9135
5	15,2053	9,8158	113,7886	40,3366	0,8788
6	15,5253	10,0028	118,6510	40,6973	0,9002
7	15,8812	10,3142	126,2052	42,5565	0,8757
8	16,8166	9,8202	126,2170	42,9910	0,8582
9	16,5692	11,2992	126,4617	44,6481	0,7972

	D05_KE90-7				
Cross-section	Width	Height	Area	Perimeter	Shape Factor
10	14,4844	10,9370	118,9280	41,5156	0,8671
11	19,7091	12,0078	150,2080	49,9924	0,7553
12	20,6273	11,9832	157,1346	52,7919	0,7085
13	20,4930	12,1560	164,0095	53,6370	0,7164
14	20,2776	12,1191	163,8646	55,5403	0,6675
15	20,2118	12,1297	170,5172	54,8569	0,7121
16	19,8390	12,4376	167,3435	52,8323	0,7534
17	20,6639	13,7510	185,1727	58,0956	0,6894
18	19,4035	13,7581	181,8555	53,9446	0,7853
19	21,6825	12,2206	187,3958	56,3045	0,7428
20	22,1775	12,6984	206,2763	59,3112	0,7369
21	22,6138	11,1010	188,9049	58,0538	0,7044
22	23,1451	11,4128	179,3596	59,4910	0,6368
23	21,8620	12,3949	188,1639	56,9686	0,7286
24	22,5293	11,5730	178,9534	56,6154	0,7016
25	24,0251	11,7791	175,6372	59,1038	0,6318
26	23,7945	11,3878	181,5410	58,1409	0,6749
27	24,0449	11,4775	169,8987	60,1271	0,5906
28	24,6100	10,2407	178,5541	59,2267	0,6397
29	25,6676	11,9454	189,2192	63,0468	0,5982
30	25,1539	11,6351	180,6369	62,9632	0,5726
31	26,1847	11,9559	196,3333	62,8674	0,6242
32	26,3852	12,3636	197,9582	63,1577	0,6236
33	25,4464	12,9733	207,4496	64,2389	0,6317
34	19,4247	11,1412	89,6206	58,8885	0,3248

Table 4C.10 Artefact D02_KA89-11, nocks A and B: width, height, area, perimeter, and Shape Factor measurements of the extracted planar cross-sections, every 1 mm.

	Nock A					Nock B				
Cross-section	Width	Height	Area	Perimeter	Shape Factor	Width	Height	Area	Perimeter	Shape Factor
1	7,6428	4,4970	25,0245	19,7360	0,8073	2,4120	2,3909	4,5521	7,8387	0,9310
2	10,2512	4,8503	37,2381	24,7695	0,7627	7,1625	3,7332	19,1362	19,3551	0,6419
3	12,0842	5,2250	44,9025	29,0840	0,6671	9,0926	6,0691	35,6851	23,8371	0,7892
4	13,3059	5,7878	49,7924	32,1463	0,6055	10,2512	7,0532	48,7812	27,9613	0,7841
5	14,2705	5,9776	53,6897	34,0910	0,5805	11,0021	7,7392	55,7752	30,1526	0,7709
6	14,7171	5,7929	55,2130	34,9568	0,5678	11,0147	7,6959	58,3765	31,5761	0,7358
7	15,1825	5,7029	55,6298	36,1001	0,5364	10,9636	8,0430	61,7519	33,1938	0,7043
8	15,5426	5,7760	56,7965	36,9365	0,5231	10,8375	8,3300	65,7138	32,4037	0,7865
9	15,8365	5,7155	57,7714	37,5766	0,5141	10,8244	8,5152	67,2270	32,4090	0,8043
10	16,0303	5,8153	58,7613	38,2614	0,5044	10,8541	8,6863	66,7646	32,4246	0,7980
11	16,2334	5,9193	59,9895	38,7219	0,5028	10,8306	8,7339	66,2114	32,4392	0,7907

	Nock A					Nock B				
Cross-section	Width	Height	Area	Perimeter	Shape Factor	Width	Height	Area	Perimeter	Shape Factor
12	16,4266	6,0728	61,2763	39,1484	0,5024	10,9010	8,7490	65,8507	32,4915	0,7838
13	16,6577	6,2544	64,0094	39,7922	0,5080	10,9866	8,7767	65,7193	32,6108	0,7766
14	16,9143	6,4972	67,4111	40,5582	0,5150	11,1274	8,7882	65,8042	32,7014	0,7733
15	17,2355	6,7807	71,7307	41,3913	0,5261	11,2605	8,8040	66,3229	32,8497	0,7723
16	17,6956	7,1291	77,3991	42,7499	0,5322	11,3786	8,8640	67,2889	33,1187	0,7709
17	18,2629	7,3958	83,5667	44,2921	0,5353	11,4853	8,9065	68,3476	33,2825	0,7754
18	18,9196	7,7162	90,6569	45,8405	0,5421	11,6148	8,9757	69,7363	33,4734	0,7821
19	19,4986	8,0685	100,2131	47,5969	0,5559	11,7545	9,0629	71,2291	33,7444	0,7861
20	20,1742	8,4220	111,9925	49,3581	0,5777	11,9306	9,1706	72,9408	34,0678	0,7898
21	20,7396	8,7562	119,8413	50,7310	0,5852	12,0840	9,2551	74,7928	34,4143	0,7936
22	21,1237	9,0915	122,6659	52,4023	0,5613	12,2052	9,2711	76,4542	34,6836	0,7987
23	21,4436	9,3496	125,4746	53,4745	0,5514	12,3393	9,2109	78,2236	35,0368	0,8008
24	21,7601	9,7145	128,7981	54,4472	0,5460	12,5119	9,2426	79,9417	35,4058	0,8014
25	22,0187	10,0555	131,8941	55,5701	0,5367	12,6538	9,2493	81,4217	35,6364	0,8057
26	22,2357	10,3378	135,1869	56,3701	0,5346	12,7993	9,2794	83,4055	35,9140	0,8126
27	22,5540	10,5886	138,8018	57,2787	0,5316	12,9076	9,3515	85,6611	36,2760	0,8180
28	23,0612	10,7845	142,9539	58,3398	0,5278	13,0150	9,4220	88,2512	36,7186	0,8225
29	23,6260	11,1716	147,1903	59,3717	0,5247	13,1240	9,4732	91,0486	37,1775	0,8278
30	23,9324	11,4007	149,7063	59,9886	0,5228	13,2671	9,5826	94,1898	37,7991	0,8284
31	24,0453	11,5739	150,6519	60,8087	0,5120	13,4025	9,5997	97,2092	38,3205	0,8319
32	24,0599	11,7809	151,9065	61,0258	0,5126	13,5340	9,7205	100,2915	38,8094	0,8368
33	24,0677	11,9881	153,5248	61,5015	0,5101	13,6680	9,8501	103,2819	39,3334	0,8389
34	24,1391	12,1523	154,9217	61,9324	0,5076	13,8154	10,1150	104,7486	39,8085	0,8306
35	24,1894	12,3867	155,7924	62,2725	0,5049	13,9178	10,2352	106,3642	40,2976	0,8231
36	24,2759	12,5684	156,7172	62,5951	0,5026	14,0806	10,2544	109,1310	40,9261	0,8188
37	24,2770	12,6814	158,2044	62,7362	0,5051	14,2353	10,2319	111,7224	41,5763	0,8122
38	24,3135	12,7635	159,3469	63,0027	0,5045	14,3582	10,1627	114,9515	41,5523	0,8366
39	24,3530	12,7068	160,5792	62,8323	0,5111	14,4883	10,0539	117,5054	41,7452	0,8473
40	24,3547	12,8650	161,8249	63,0490	0,5116	14,6237	10,2752	120,1042	42,0234	0,8546
41	24,3701	13,0274	163,2723	63,3696	0,5109	14,7681	10,4548	121,3573	42,2375	0,8548
42	24,3733	13,0164	164,9509	63,7039	0,5108	14,8899	10,6068	121,1698	42,4339	0,8456
43	24,3989	13,0692	166,4748	64,0141	0,5105	14,9598	10,6762	120,7006	42,6464	0,8340
44	24,4354	13,0438	167,6985	64,1139	0,5127	14,9980	10,6794	120,2314	42,9076	0,8207
45	24,3894	13,1276	169,0339	63,5708	0,5256	15,0416	10,6568	119,9353	43,1120	0,8109
46	24,4336	13,2424	170,1730	64,0293	0,5216	15,0919	10,6396	119,9985	43,3428	0,8027
47	24,4394	13,3020	171,6393	64,0927	0,5251	15,1239	10,7282	120,2148	43,5504	0,7965
48	24,4724	13,3691	172,9267	63,5107	0,5387	15,2405	10,7772	120,6078	43,8525	0,7881
49	24,5685	13,4432	173,9698	63,6367	0,5398	15,3406	10,7501	120,9258	44,1006	0,7813
50	24,5010	13,5278	175,1954	64,1753	0,5346	15,4478	10,7203	121,0758	44,3577	0,7733

Table 4C.11 Artefact D05_KE90-7, nock C: width, height, area, perimeter, and Shape Factor measurements of the extracted planar cross-sections, every 1 mm.

	Nock C				
Cross-section	Width	Height	Area	Perimeter	Shape Factor
1	3,9062	3,2365	6,7019	13,7904	0,4428
2	5,7886	3,9842	18,7632	16,2006	0,8984
3	7,0161	4,6355	26,6303	19,1981	0,9080
4	8,1852	5,0117	32,9701	21,5883	0,8890
5	9,1057	5,3163	38,6294	23,3940	0,8870
6	10,0345	5,5947	44,1184	25,2531	0,8694
7	10,6838	5,7942	48,8663	26,7900	0,8556
8	11,5112	6,0256	53,5954	28,3068	0,8405
9	12,3261	6,2309	59,8711	30,0215	0,8348
10	12,9163	6,4487	65,1133	31,4569	0,8269
11	13,2806	6,7155	69,6719	32,3780	0,8352
12	13,4927	6,9634	74,1869	33,1671	0,8475
13	13,6613	7,2643	78,6433	33,8867	0,8606
14	13,5818	7,5657	81,0518	34,0520	0,8784
15	12,7389	7,8058	78,4194	33,0640	0,9014
16	11,8069	8,0684	76,3707	32,2273	0,9240
17	11,0215	8,3763	76,0252	31,6601	0,9531
18	11,7991	8,5711	82,2000	33,2553	0,9340
19	12,9978	8,7813	91,4064	35,7221	0,9001
20	14,0979	8,9578	99,4240	37,5899	0,8842
21	14,9150	9,0699	104,9467	38,7513	0,8782
22	15,3651	9,1486	108,4700	39,5069	0,8733
23	15,5880	9,2330	111,0383	39,9509	0,8742
24	15,6646	9,3381	112,6388	40,0715	0,8815
25	15,5650	9,3821	112,6334	39,8445	0,8915
26	15,2882	9,4420	111,8295	39,4226	0,9042
27	15,0230	9,4577	111,2703	39,1788	0,9109
28	14,8205	9,5869	111,5433	39,1405	0,9150
29	14,6424	9,7530	113,0658	39,1921	0,9250
30	14,4883	9,9630	114,7334	39,2054	0,9380
31	14,2884	10,1633	116,0406	39,3076	0,9438
32	14,2025	10,3570	116,7878	39,6068	0,9356
33	14,1989	10,6707	117,8312	39,8742	0,9313
34	14,2252	10,8184	118,2718	40,0381	0,9271
35	14,2225	10,9145	119,2155	40,1954	0,9272
36	14,2646	10,9944	120,3300	40,2348	0,9341
37	14,2829	11,0446	120,9458	40,4787	0,9276
38	14,1834	11,1130	120,4729	40,4518	0,9252
39	14,1011	11,1059	119,6092	40,3864	0,9215
40	14,2281	11,0750	119,3078	40,5127	0,9135
41	14,5171	11,0463	119,8019	40,6458	0,9113
42	14,6774	11,0178	119,2443	40,5316	0,9121
43	14,7152	10,8739	119,0492	40,4672	0,9135

	Nock C				
Cross-section	Width	Height	Area	Perimeter	Shape Factor
44	14,7643	10,7407	117,8720	40,5552	0,9006
45	14,8357	10,4824	116,5993	40,4164	0,8970
46	14,8606	10,2670	115,2575	40,6305	0,8774
47	14,9421	10,1210	113,9297	40,7531	0,8620
48	15,0447	9,9992	113,5828	40,4237	0,8735
49	15,1254	9,9024	113,5968	40,4433	0,8727
50	15,2053	9,8158	113,7886	40,3366	0,8788

Table 4C.12 Artefact D12_JF-JG-81, nocks D and E: width, height, area, perimeter, and Shape Factor measurements of the extracted planar cross-sections, every 1 mm.

	Nock D					Nock E				
Cross-section	Width	Height	Area	Perimeter	Shape Factor	Width	Height	Area	Perimeter	Shape Factor
1	5,5017	3,0013	11,4972	14,4516	0,6918	6,0905	3,0557	10,9883	14,8461	0,6265
2	6,7530	2,6333	13,5651	15,8857	0,6755	6,6097	3,5548	17,1117	16,8086	0,7611
3	7,4161	3,2785	17,5930	17,4894	0,7228	6,9674	3,8583	19,2622	17,9845	0,7484
4	7,7986	3,6459	20,3041	18,6198	0,7359	7,4315	4,0880	21,3584	19,3985	0,7133
5	8,1966	3,7634	22,4036	19,5689	0,7352	7,8162	4,3797	22,9501	20,3263	0,6980
6	8,5433	3,9064	24,6076	20,3514	0,7466	8,0247	4,3237	24,1093	20,7062	0,7066
7	8,9564	4,0529	26,9775	21,1988	0,7544	8,3131	4,4482	25,4178	21,2754	0,7057
8	9,0051	4,1824	28,6577	21,4754	0,7809	8,3900	4,3425	26,7961	21,2065	0,7488
9	9,0300	4,3843	29,9923	21,8364	0,7904	8,7627	4,4669	27,7028	21,5880	0,7470
10	9,2065	4,5006	31,2776	22,2088	0,7969	8,8223	4,5618	29,0906	22,3046	0,7348
11	9,3368	4,6536	32,6731	22,6103	0,8031	8,9499	4,7019	30,0406	22,5759	0,7407
12	9,3983	4,7959	33,9149	22,9200	0,8113	9,0524	4,8107	30,8719	22,5507	0,7629
13	9,5146	4,9325	35,2575	23,3417	0,8132	9,1648	4,8669	32,1240	22,7841	0,7776
14	9,5952	5,0654	37,0078	23,6718	0,8299	9,2165	5,0374	33,3982	23,1369	0,7840
15	9,5385	5,2330	38,5361	23,9099	0,8471	9,2585	5,1986	33,7874	23,3042	0,7818
16	9,5370	5,3789	39,7591	24,1597	0,8560	9,2923	5,3524	34,2095	23,4651	0,7807
17	9,6146	5,4716	41,3231	24,5799	0,8595	9,3876	5,5032	35,4749	23,8062	0,7866
18	9,8975	5,5569	42,9262	25,1754	0,8511	9,4734	5,6037	35,9841	24,0322	0,7829
19	10,0450	5,6296	44,4879	25,6450	0,8501	9,4946	5,7005	37,2718	24,3046	0,7929
20	10,2360	5,7393	46,1421	26,0484	0,8546	9,6691	5,7679	37,9633	24,7059	0,7816
21	10,4039	5,8801	47,9089	26,3845	0,8648	9,8697	5,7772	38,6364	24,8982	0,7832
22	10,6133	5,9878	49,6752	26,8386	0,8666	9,8731	5,7709	39,0764	25,0428	0,7830
23	10,7093	6,0829	51,6267	27,3542	0,8670	9,9445	5,8433	39,5290	25,1006	0,7884
24	10,9010	6,1860	53,4233	27,8717	0,8642	10,2154	5,8020	40,4530	25,5092	0,7812
25	11,1888	6,2948	55,0804	28,3608	0,8605	10,3649	5,7656	41,0447	25,9079	0,7684
26	11,4046	6,3727	56,9031	28,9001	0,8561	10,4889	5,8750	41,7854	26,3268	0,7576
27	11,5726	6,5170	58,8647	29,4427	0,8533	10,6148	5,8871	43,0832	26,4664	0,7729
28	11,6867	6,6778	61,1756	29,9356	0,8579	10,7952	5,9326	44,3470	26,7059	0,7814
29	11,8244	6,7988	63,1541	30,3342	0,8625	10,7806	6,0077	45,0213	26,7172	0,7926

	Nock D					Nock E				
Cross-section	Width	Height	Area	Perimeter	Shape Factor	Width	Height	Area	Perimeter	Shape Factor
30	12,0119	7,0871	65,4144	30,7468	0,8695	10,8994	6,1857	46,4852	27,3511	0,7809
31	12,2100	7,2527	67,6127	31,1987	0,8729	11,1304	6,3462	47,3982	27,8614	0,7673
32	12,3988	7,4258	70,1282	31,6922	0,8774	11,3377	6,3171	47,9745	28,1618	0,7602
33	12,5870	7,6569	72,7657	32,1701	0,8836	11,3412	6,2678	49,1582	28,2478	0,7742
34	12,7666	7,9799	76,1956	32,8241	0,8887	11,3478	6,3236	50,5703	28,1844	0,8000
35	12,8671	8,2348	79,4128	33,3405	0,8978	11,5320	6,4005	51,2680	28,3644	0,8008
36	13,0501	8,4878	82,4494	33,8706	0,9031	11,7343	6,3876	52,2655	28,6131	0,8022
37	13,1619	8,5926	84,8379	34,3170	0,9053	11,8161	6,4400	53,0552	28,9759	0,7941
38	13,3123	8,7338	87,1767	34,7367	0,9079	11,8258	6,4198	53,4062	28,9708	0,7996
39	13,4527	8,8820	89,6940	35,2027	0,9095	11,7540	6,5075	53,9967	29,0414	0,8045
40	13,6240	8,9790	92,0035	35,6736	0,9085	11,7589	6,5231	54,5924	29,1513	0,8073
41	13,8228	8,9955	93,9388	36,0974	0,9059	11,8462	6,5883	55,7410	29,4309	0,8087
42	13,9717	9,0187	96,0088	36,4615	0,9075	12,0286	6,6175	56,7450	29,7324	0,8066
43	14,0478	9,0927	98,3168	36,8501	0,9098	12,0174	6,6775	57,6561	29,8208	0,8147
44	14,1244	9,2393	100,6140	37,1795	0,9147	12,1258	6,7297	58,1185	30,0981	0,8062
45	14,1289	9,3046	102,9483	37,5341	0,9183	12,1505	6,7900	58,3596	30,0974	0,8096
46	14,1937	9,4186	104,9546	37,9207	0,9172	12,1330	6,7780	58,9689	30,2211	0,8114
47	14,2199	9,5335	106,1765	38,2011	0,9143	11,9847	6,8452	59,6607	30,0929	0,8279
48	14,2575	9,6219	107,4813	38,4032	0,9158	12,0548	6,9738	60,8689	30,3211	0,8320
49	14,2928	9,6834	107,9008	38,4600	0,9167	12,1118	7,0243	62,4216	30,6024	0,8376
50	14,2498	9,7074	108,4698	38,3524	0,9267	12,2112	7,0299	62,4216	30,6024	0,8376

References

3D-COFORM (2009). *D.2.1 – Initial version of "User Requirement analysis and Functional Specifications" (version 8)*. 3DCOFORM Consortium. http://www.3d-coform.eu/downloads/D_2_1_User_Req_and_Fnctl_Specs_online.pdf

AENOR (1979). *UNE 56 533 79 – Características físico-mecánicas de la Madera. Determinación de las contracciones lineal y volumétrica*. Asociación Española de Normalización y Certificación.

AENOR (1979a). *UNE 56 534 79 – Características físico-mecánicas de la Madera. Determinación de la dureza*. Asociación Española de Normalización y Certificación.

AENOR (1979b). *UNE 56 535 79 – Características físico-mecánicas de la Madera. Determinación de la resistencia a la compresión axial*. Asociación Española de Normalización y Certificación.

AENOR (1979c). *UNE 56 536 79 – Características físico-mecánicas de la Madera. Determinación de la resistencia a la flexión dinámica*. Asociación Española de Normalización y Certificación.

AENOR (1979d). *UNE 56 537 79 – Características físico-mecánicas de la Madera. Determinación de la resistencia a la flexión estática*. Asociación Española de Normalización y Certificación.

AENOR (1979e). *UNE 56 538 79 – Características físico-mecánicas de la Madera. Determinación de la resistencia a la tracción perpendicular a las fibras*. Asociación Española de Normalización y Certificación.

AENOR (1979f). *UNE 56 539 79 – Características físico-mecánicas de la Madera. Determinación de la resistencia a la hienda*. Asociación Española de Normalización y Certificación.

Aicher, R.R., Dill-Langer, G., Ranta-Maunus, A. (1988). Duration of Load Effect in Tension Perpendicular to the Grain of Glulam in Different Climates. *Holz Roh Werkst* 56:295-305.

Alakangas, E. (2005). *Properties of Wood Fuels Used in Finland - BIOSOUTH - project*. Project Report PRO2/P2030/05. VTT Processes.

Alrune, F. (1992). A Mesolithic Elm Bow Approximately 9000 years old. *Journal of the Society of Archer-Antiquaries* 35:47-50.

Amendas, G., McConnachie, G., Pournou, A. (2013). Selective Reburial: a potential approach for the *in situ* preservation of waterlogged archaeological wood in wetland excavations. *Journal of Archaeological Science* 40:99-108.

Antolín, F., Buxó, R. (2011). L'Explotació de les Plantes: contribució a la Història de l'agricultura i de l'alimentació vegetal del Neolític a Catalunya. In El Poblat Lacustre Neolític de la Draga. Excavacions de 2000-2005. Bosch, À., Chinchilla, J., Tarrús, J. (eds.). MAC, CASC, Girona. *Monografies del CASC* 9:147-176.

Arno, J. (1993). *Encyclopedia of Wood*. Time-Life Books.

Ascham, R. (1545). *Toxophilus*. Ed. E. Arber (1869), London.

Askeland, D.R. (1998). *The Science and Engineering of Materials*. (SI edition) Nelson Thornes, London.

ASME (2010). *ASME-B46-1-2009 – Surface Texture (Surface Roughness, Waviness, and Lay)*. American Society of Mechanical Engineers (ASME), New York (NY).

ASTM (1994). *ASTM D 5536-94 – Standard Practice for Sampling Forest Trees for Determination of Clear Wood Properties, (reapproved 2004)*. American Society for Testing and Materials (ASTM) International, Pennsylvania (PA).

ASTM (2009). *ASTM D143-09 – Standard Test Methods for Small Clear Specimens of Timber*. ASTM International, Pennsylvania (PA).

Baena, J., Cuartero, F. (2009). Perspectivas Metodològiques de l'Experimentació en Arqueologia. *Cota Zero* 24:21-30.

Baena Preysler, J., Carrión Santafé, E. (2010). Experimental Approach to the Function and Technology of Quina Side-scrappers. In *Experiments and Interpretation of Traditional Technologies: essays in honor of Errett Callahan*. H.G. Nami (ed.), Ediciones de Arqueología Contemporánea, Buenos Aires, pp.171-201.

Baena Preysler, J., Terradas, X. (2005): ¿Por qué experimentar en Arqueología? *Proceedings of the 15th cursos monográficos sobre el Patrimonio Histórico* (2004), Santander, pp.141-160.

Baker, T. (1992). Bow Design and Performance. In *The Traditional Bowyer's Bible, Volume 1*. The Lyons Press (2000), Connecticut (CT).

BAM (2001). *Testing and Chemical Analysis – catalogue of reference procedures*. BAM, Berlin.

Baño, V., Argüelles-Bustillo, R., Regueira, R., Guaita, M. (2012). Determinación de la curva tensión-deformación en madera de *Pinus sylvestris* L. para la simulación numérica de vigas de madera libre de defectos. *Materiales de Construcción* 62(306):269-284.

Barceló, J. A. (2009). *Computational Intelligence in Archaeology*. IGI Global, Hershey (PA).

Barceló, J.A. (2010). Visual Analysis in Archaeology. An Artificial Intelligence Approach. In *Morphometrics for Nonmorphometricians*. E.M.T. Elewa (ed.). Springer Verlag, Berlin. Lecture Notes in Earth Sciences 124:92-156.

Barceló, J.A., Moitinho de Almeida, V. (2012). Functional Analysis from Visual and Non-visual Data. An Artificial Intelligence Approach. *Mediterranean Archaeology & Archaeometry* 12(2):273-321.

Bardi, U. (2000a). *Short Bows and Long Bows: scaling effects in archery*. http://www3.unifi.it/surfchem/solid/bardi/archery/scalingbows/index.html

Bardi, U. (2000b). *Reverse Engineering the Bow: a simple static model*. http://www.unifi.it/surfchem/solid/bardi/archery/modelingbows/

Beismann, H., Wilhelmi, H., Baillères, H., Spatz, K.-C., Bogenrieder, A., Speck, T.. (2000). Brittleness of twig bases in the genus *Salix*: fracture mechanics and ecological relevance. *Journal of Experimental Botany* 51(344):617-633.

Bellintani, P., Benini, S., Gonzalez, O.M. (2002). L'arco e le frecce dell'abitato palafitticolo di Fiavè. Indagine sperimentale su aspetti ricostruttivi e funzionali. *Incontro di Archeologia Sperimentale*, San Lorenzo in Banale e Fiavè, Trento, pp.167-200.

Bentkowska-Kafel, A., Denard, H., Baker, D. (eds.) (2012). *Paradata and Transparency in Virtual Heritage*. Ashgate

Bergman, C.A., McEwen, E., Miller, R. (1988). Experimental Archery: projectile velocities and comparison of bow performances. *Antiquity* 62(237):658-670.

Biblis, E.J. (2001). Tension parallel to grain, pure flexural stiffness, and modulus of rigidity of clear wood of seven eastern red oaks. *Forest Products Journal* 51(4):87-89.

Biomesh (2010). *FEA in Biology*. University of Massachusetts, Amherst (MA). http://www.biomesh.org/fea-basics

Bjurhager, I., Gamstedt, E.K., Keunecke, D., Niemz, P., Berglund, L.A. (2013). Mechanical performance of yew (*Taxus baccata* L.) from a longbow perspective. *Holzforschung* 0(0):1-8.

Blateyron, F. (2006). New 3D Parameters and Filtration Techniques for Surface Metrology. *Quality Magazine*. http://www.qualitymag.com/ext/resources/files/white_papers/New3DParametersandFiltrationTechniquesforSurfaceMetrology-DigitalSurf.pdf

Blateyron, F. (2013). The Areal Field Parameters. In *Characterisation of Areal Surface Texture*. Leach, R. (ed.). Springer. pp.15-43.

Blunt, L., Jiang, X. (eds.) (2003). *Advanced Techniques for Assessment Surface Topography*. Elsevier, London.

Bogdanovic, I., Bosch, A., Buxó; R., Chinchilla, J., Palomo, A., Piqué, R., Saña, M., Tarrús, J., Terradas, X. (2011). La Draga en el contexto de las evidencias de ocupación del lago de Banyoles. *Proceedings of the 5th Congreso del Neolítico Peninsular*, Lisbon.

Bosch, À., Buxó, R., Chinchilla, J., Palomo, A., Piqué, R., Saña, M., Tarrús, J., Terradas, X. (2012). Dinàmica d'Ocupació de l'Entorn Lacustre de Banyoles i del Jaciment Neolític de La Draga. *Proceedings of the XI Jornades d'Arqueologia de les Comarques de Girona*, Girona.

Bosch, À., Chinchilla, J., Tarrús, J. (editors) (2000). El Poblat Lacustre Neolític de la Draga. Excavacions de 1990 a 1998. MAC, CASC, Girona. *Monografies del CASC* 2.

Bosch, À., Chinchilla, J., Tarrús, J. (eds.) (2006). Els objectes de fusta del poblat neolític de la Draga. Excavacions de 1995-2005. MAC, CASC, Girona. *Monografies del CASC* 6.

Bosch, À., Chinchilla, J., Tarrús, J. (eds.) (2011). El Poblat Lacustre Neolític de la Draga. Excavacions de 2000-2005. MAC, CASC, Girona. *Monografies del CASC* 9.

Bosch, À., Chinchilla, J., Tarrús, J., Piqué, R. (2006). Matèries Primeres, Fabricació i Funcionalitat. In Els objectes de fusta del poblat neolític de la Draga. Excavacions de 1995-2005. Bosch, À., Chinchilla, J., Tarrús, J. (eds.). MAC, CASC, Girona. *Monografies del CASC* 6:127-132.

Breukmann (2009). *Brief Instruction Manual: stereoSCAN3D, smartSCAN3D, optoTOP, naviSCAN - Optocat 2009*. Breukmann.

Britannica (2013). *Encyclopaedia Britannica online*. http://www.britannica.com/

Callister, W.D., Jr. (2007). *Materials Science and Engineering. An introduction*. John Wiley & Sons, New York.

Carmichael, C. (ed.) (1950). *Kent's Mechanical Engineers' Handbook*. (12nd ed.) John Wiley & Sons, New York.

Cassen, S., Robin, G. (2010). Recording Art on Neolithic Stelae and Passage Tombs from Digital Photographs. *Journal of Archaeological Method and Theory* 17:1-14.

Casteren, A. van, Sellers, W.I., Thorpe, S.K.S, Coward, S., Crompton, R.H., Ennos, A.R. (2012). Why don't branches snap? The mechanics of bending failure in three temperate angiosperm trees. *Trees* 26:789-797.

Cattelain, P. (2006). Apparition et évolution de l'arc et des pointes de flèches dans la Préhistoire européenne (Paléo-, Méso-, Néolithique). In *Catene operative dell'arco preistorico*. Proceedings of the Incontro di Archeologia Spérimentale (2002), Trento. Provincia Autonomia di Trento, Soprintendenza per i Beni Archeologici (eds.).

Coffey, D.J. (1962). *Effects of Knots and Holes on the Fatigue Strength of Quarter-scale Timber Bridge Stringers*. M.Sc. Thesis. Department of Civil Engineering, University of Wisconsin.

Chopra, S., Marfurt, K.J. (2007). Using Curvature to Map Faults, Fractures. *Explorer - Geophysical Corner*, B.A. Hardage (ed.). http://www.aapg.org/explorer/geophysical_corner/2007/11gpc.cfm

Cotterell, B., Kamminga, J. (1990). *Mechanics of Pre-industrial Technology: An Introduction to the Mechanics of Ancient and Traditional Material Culture*. Cambridge University Press.

Cretté, S.A., Näsänen, L.M., González-Pereyra, N.G., Rennison, B. (2013). Conservation of Waterlogged Archaeological Corks using Supercritical CO_2 and Treatment Monitoring using Structured-light 3D Scanning. *The Journal of Supercritical Fluids* 79:299-313.

Curtis, N., Jones, M.E.H., Lappin, A.K., O'Higgins, P., Evans, S.E., Fagan, M.J. (2010). Comparison between *in vivo* and theoretical bite performance: Using multi-body modelling to predict muscle and bite

forces in a reptile skull. *Journal of Biomechanics* 43:2804-2809.

Danielsson, H. (2013). *Perpendicular to Grain Fracture Analysis of Wooden Structural Elements. Models and Applications*. Ph.D. Thesis. Department of Construction Sciences - Structural Mechanics, Lund University.

Degrange, F.J., Tambussi, C.P., Moreno, K., Witmer, L.M., Wroe, S. (2010). Mechanical Analysis of Feeding Behavior in the Extinct "Terror Bird" *Andalgalornis steulleti* (Gruiformes: Phorusrhacidae). *PLoS ONE* 5(8):1-7, e11856.

Demkin, N.B., Izmailov, V.V. (2010). The Relation between the Friction Contact Performance and the Microgeometry of Contacting Surfaces. *Journal of Friction and Wear* 31(1):48-55.

Dennet, D.C. (1991). Cognitive Science as Reverse Engineering: Several Meanings of 'Top-Down' and 'Bottom-Up'. Paper presented at the *9th International Congress of Logic, Methodology and Philosophy of Science*. http://users.ecs.soton.ac.uk/harnad/Papers/Py104/dennett.eng.html

Denny, M. (2003). Bow and Catapult Internal Dynamics. *European Journal of Physics* 24:367-378.

Derome, D., Rafsanjani, A., Hering, S., Dressler, M., Patera, A., Lanvermann, C., Sedighi-Gilani, M., Wittel, F.K., Niemz, P., Carmeliet, J. (2013). The Role of Water in the Behavior of Wood. *Journal of Building Physics* 36(4):398-421.

Dias-Meirinho, M.-H. (2011). *Des Armes et des Hommes. L'archerie à la transition fin du Néolithique - Age du Bronze en Europe occidentale.* Ph.D. Thesis. Université de Toulouse.

Dinwoodie, J.M. (2000). *Timber: Its Nature and Behaviour*. Taylor & Francis, Oxon.

Dumont, E.R., Grosse, I.R., Slater, G.J. (2009). Requirements for Comparing the Performance of Finite Element Models of Biological Structures. *Journal of Theoretical Biology* 256:96-103.

EH - English Heritage (2010). *Waterlogged Wood. Guidelines on the recording, sampling, conservation and curation of waterlogged wood*. English Heritage, Swindon.

Eilam, E. (2005). *Reversing: Secrets of Reverse Engineering*. Wiley Publishing, Indianapolis (IN).

Elmer, R.P. (1952). *Target Archery*. Hutchinson, London.

Eriksson, J. (2005). *Moisture Transport and Moisture Induced Distortions in Timber - An Experimental and Numerical Study*. Ph.D. Thesis. Chalmers University of Technology, Gothenburg.

Feynman, R., Leighton, R., Sands, M. (1963). *The Feynman Lectures on Physics*. Addison-Wesley, Reading (MA).

French, R.M., Curtis, B., Pham, V. (2006). Mechanics of a Simple Bow. *Proceedings of the IMAC-XXIV: Conference & Exposition on Structural Dynamics* 30(6):66-68.

Frisher, B., Niccolucci, F., Ryan, N.S., Barceló, J.A. (2002). From CVR to CVRO: The Past, Present and Future of Cultural Virtual Reality. *Virtual Archaeology*. Franco Niccolucci (ed.). Oxford. pp.7-18.

FPL - Forest Products Laboratory (2010). *Wood Handbook - Wood as an Engineering Material*. General Technical Report FPL-GTR-190. U.S. Department of Agriculture, Forest Service, Madison (WI).

Gadelmawla, E.S., Koura, M.M., Maksoud, T.M.A., Elewa, I.M., Soliman, H.H. (2002). Roughness Parameters. *Journal of Materials Processing Technology* 123:133-145.

Gamstedt, K., Bjurhager, I., Berglund, L., Keunecke, D., Niemz, P. (2010). Beam theory modelling of the performance of medieval yew longbows. *International workshop on "Modeling mechanical behavior of wooden cultural objects"*, Krakow.

García Díez, M., González-Morales, M., Straus, L.G. (2012). El Grafismo Rupestre Paleolítico de la Cueva de El Mirón (Ramales de la Victoria, Cantabria, España): una propuesta para su datación estratigráfica. *Trabajos de Prehistoria* 69:21-36.

Gerhards, C.C. (1982). Effect of Moisture Content and Temperature on the Mechanical Properties of Wood: an analysis of immediate effects. *Wood and Fiber* 14(1):4-36.

Gibson, L.J., Ashby, M.F. (1988). *Cellular Solids. Structure and Properties*. Pergamon Press.

Goldstein, H., Poole, C., Safko, J. (2001). *Classical Mechanics*. (3rd ed.) Addison Wesley, Reading (MA).

González-Morales, M., Straus, L.G. (2009). Extraordinary Early Magdalenian finds from El Mirón Cave, Cantabria (Spain). *Antiquity* 83:267-281.

Gordon, J.E. (1978). *Structures, or Why Things Don't Fall Down*. Penguin Books, London.

Grayson, C.E., French, M., O'Brien, M.J. (2007). *Traditional Archery from Six Continents. The Charles E. Grayson Collection*. University of Missouri Press, Columbia, Missouri (MO).

Greenland, H. (2002). *The Traditional Archer's Handbook: a practical guide*. Sylvan Archery.

Gunduz, G., Yaman, B., Ozden, S., Donmez, S.C. (2013). Anatomy of Wooden Core of Ottoman Composite Archery Bows. *Sains Malaysiana* 42(5):547-552.

Hamm, J. (2007). *Bows & Arrows of the Native Americans: A Step-By-Step Guide to Wooden Bows, Sinew-Backed Bows, Composite Bows, Strings, Arrows & Quivers*. Lyons Press, New York (NY).

Haselein, C.R., Berger, R., Goulart, M., Sthal, J., Trevisan, R., Santini, E.J., Lopes, M.C. (2002). Propriedades de flexão estática da madeira úmida e a 12% de umidade de um clone de *Eucalyptus saligna* Smith sob o efeito do espaçamento e da adubação. *Ciência Florestal* 12(2):147-152.

Henderson, J. (2000). *The Science and Archaeology of Materials: an investigation of inorganic materials*. Routledge, London.

Hickman, C.N. (1937). The Dynamics of a Bow and Arrow. *Journal of Applied Physics* 8:404-409.

Hickman, C.N., Nagler, F., Klopsteg, P.E. (1947). *Archery: the technical side*. National Field Archery Association, Redlands (CA).

Ho, H.T., Gibbins, D. (2009). A Curvature-based Approach for Multi-scale Feature Extraction from 3D Meshes and Unstructured Point Clouds. *Computer Vision, IET* 3(4):201-212.

Hoadling, R.B. (2000). *Understanding Wood: a craftsman's guide to wood technology*. The Taunton Press, Newtown (CT).

Ingersoll, D., Yellen, J.E., Macdonald, W. (eds.) (1977). *Experimental Archaeology*. Columbia University Press, New York (NY).

ISO (2012). *25178-2:2012 - Geometrical Product Specifications (GPS) - Surface texture: Areal - Part 2: Terms, definitions and surface texture parameters*. ISO.

Jakubczyk, B. (1966). Technical properties of the yew wood from the preserve Wierzchlas. *Sylwan* 10:79-86.

Jönsson, J., Thelandersson, S. (2005). The Effect of Moisture Gradients on Tensile Strength Perpendicular to the Grain in Glulam. *Holz Roh Werkst* 61:342-348.

Junkmanns, J. (2001). *Arc et Flèche. Fabrication et utilisation au Néolithique*. Ed. Musée Schwab, Bienne.

Kamat, V. R., Martinez, J.C. (2007). Variable-speed Object Motion in 3D Visualizations of Discrete-event Construction Simulation Models. *ITcon* 12:293-303. http://www.itcon.org/2007/20

Karasik, A., Smilansky, U. (2008). 3D Scanning technology as a standard archaeological tool for pottery analysis: practice and theory. *Journal of Archaeological Science* 35:1148-1168.

Keunecke, D., Sonderegger, W., Pereteanu, K., Lüthi, T., Niemz, P. (2007). Determination of Young's and shear moduli of common yew and Norway spruce by means of ultrasonic waves. *Wood Science and Technology* 41:309-327.

Keunecke, D. (2008a). *Elasto-mechanical characterisation of yew and spruce wood with regard to structure-property relationships*. Ph.D. Thesis. Department of Civil, Environmental and Geomatic Engineering, Swiss Federal Institute of Technology Zurich.

Keunecke, D., Hering, S., Niemz, P. (2008b). Three-dimensional elastic behaviour of common yew and Nor-

way spruce. *Wood Science and Technology* 42:633-647.

Klopsteg, P.E. (1943). Physics of Bows and Arrows. *America Journal of Physics* 11(4):175-192.

Kohdzuma, Y. (2005). *Characteristics of Archaeological Waterlogged Wood*. http://www.nara.accu.or.jp/elearning

Kooi, B.W. (1983). *On the Mechanics of the Bow and Arrow*. Ph.D. Thesis. Mathematisch Instituut, Rijksuniversiteit Groningen.

Kooi, B.W. (1991). Archery and Mathematical Modeling. *Journal of the Society of Archer-Antiquaries* 34:21-29.

Kooi, B.W. (1994). The Design of the Bow. *Proceedings Koninklijke Nederlandse Akademie van Wetenschappen* 97(3):1-27.

Kooi, B.W. (1998a). Bow-arrow interaction in archery. *Journal of Sport Sciences* 721–731.

Kooi, B.W. (1998b). The Archer's Paradox and Modelling, a Review. *History of Technology* 20:125-137.

Kooi, B.W., Sparenberg, J.A. (1980). In the Static Deformation of the Bow. *Journal of Engineering Mathematics* 14(1):27-45.

Kooi, B.W., Sparenberg, J.A. (1997). On the Mechanics of the Arrow. *Journal of Engineering Mathematics* 285-306.

Kord, B. (2011). Variation of Physical and Biometrical Properties of *Salix* Wood Along the Stem. *World Applied Sciences Journal* 13:1404-1408.

Korkut, S., Hiziroglu, S. (2009). Effect of heat treatment on mechanical properties of hazelnut wood (*Corylus colurna* L.). *Materials and Design* 30:1853-1858.

Kretschmann, D.E. (2008). The influence of juvenile wood content on shear parallel, compression and tension perpendicular to grain strength and mode I fracture toughness of loblolly pine at various ring orientations. *Forest Products Journal* 58(7/8):89-96.

Kúdela, J., Lagaňa, R. (eds.) (2010). Wood Structure and Properties '10. *Proceedings of the 6th IUFRO Symposium "Wood Structure and Properties '10"*, Podbanské. Arbora Publishers, Zvolen.

Leroi-Gourhan, A. (1966). O Gesto e a Palavra. Edições 70, Lisbon (1985).

Longman, C.J., Walrond, H. (1894). *Archery*. The Badminton Library of Sports and Pastimes. http://www.archerylibrary.com/books/badminton/

Lupo, K.D., Schmitt, D.N. (2005). Small prey hunting technology and zooarchaeological measures of taxonomic diversity and abundance: Ethnoarchaeological evidence from Central African forest foragers. *Journal of Anthropological Archaeology* 24(4):335-353.

Mackenzie-Helnwein, P., Eberhardsteiner, J., Mang, H.A. (2005). Rate independent mechanical behavior of biaxially stressed wood: Experimental observations and constitutive modeling as an orthotropic two-surface elasto-plastic material. *Holzforschung* 59(3):311-321.

Marlow, W.C. (1981). Bow and Arrow Dynamics. *American Journal of Physics* 49(4):320-333.

Masad, E., Al-Rousan, T., Little, D. (2007). *Test Methods for Characterizing Aggregate Shape, Texture, and Angularity*. NCHRP Report 555, National Cooperative Highway Research Program. Transportation Research Board of the National Academies, Washington D.C. (WA).

MatWeb (2013). *MatWeb: Material Property Data*. MatWeb, LLC. http://www.matweb.com/index.aspx

McEwen, E., Miller, R., Bergman, C. (1991). Early Bow Design and Construction. *Scientific American* 264(6):76-82.

McHenry, C.R., Wroe, S., Clausen, P.D., Moreno, K., Cunningham, E. (2007). Supermodeled sabercat, predatory behaviour in *Smilodon fatalis* revealed by highresolution 3-D computer simulation. *PNAS* 104:16010-16015.

Mélard, N. (2010). L'étude microtopographique et la visualisation 3D dans l'analyse de gravures préhisto-

riques – L'exemple des pierres gravées de La Marche. *In Situ, Revue des Patrimoines* 13. http://insitu.revues.org/6837

Miller, R., McEwen, E., Bergman, C. (1986). Experimental Approaches to Ancient Near Eastern Archery. *World Archaeology* 18(2):178-195.

Moitinho de Almeida, V., Barceló, J.A. (2012a). Understanding Virtual Objects through Reverse Engineering. Proceedings of the 3rd Congreso Internacional de Arqueología, Informática Gráfica, Patrimonio e Innovación - Arqueológica 2.0 2011, Sevilla. *Virtual Archaeology Review - special issue on Virtual Museums* 3(7):14-17.

Moitinho de Almeida, V., Barceló, J.A. (2012b). 3D Scanning and Computer Simulation of Archaeological Artefacts. *Proceedings of the 1st International Conference on Best Practices in World Heritage: Archaeology*, Menorca, 384-399. A. Castillo (ed.), Editorial Complutense, Madrid.

Moitinho de Almeida, V., Barceló, J.A., Rosillo, R., Palomo, A. (2013a). Linking 3D Digital Surface Texture with Ancient Manufacturing Procedures. *IEEE Digital Heritage International Congress*, Marseille. A.C. Addison, G. Guidi, L. De Luca, S. Pescarin (eds.). pp.735-738.

Moitinho de Almeida, V., Rosillo, R., Palomo, A. (2013b). Analysis and Production. In *La Serra del Mas Bonet (Vilafant) i Els Banys de la Mercè (Capmany), dues ocupacions a l'aire lliure emmarcades en la prehistòria recent a l'Alt Empordà*. Monographic series on Archaeological Excavations in Catalonia. Archaeological Museum of Catalonia, Barcelona. (*in press*)

Moitinho de Almeida, V., Rosillo, R., Palomo, A. (2012c). 3D Macrowear Analysis of Sculpture Techniques in the Manufacture of the Neolithic Stelae with Horns of the Serra del Mas Bonet (Vilafant, Catalonia). *Computer Applications and Quantitative Methods in Archaeology Congress* (CAA'12), Southampton.

Moitinho de Almeida, V., Teira, L., González-Morales, M., Straus, L.G., Millán, M., Blasco, A. (2012d). (Re)seeing the engraved block of El Mirón Cave (Ramales de la Victoria, Cantabria, Spain). *Proceedings of the Computer Applications and Quantitative Methods in Archaeology Congress* (CAA'12), Southampton. Amsterdam University Press (AUP), Pallas Publications.

MountainsMap (2013). *MountainsMap manual*. Digital Surf.

Müllner, H.W., Kohlhauser, C., Fleischmann, M., Eberhardsteiner, J. (2006). Influence of the Characteristic Length on the Strength Properties of a Material Model for Spruce Wood. *The Archive of Mechanical Engineering* 53(3):247-262.

Myshkin, N.K., Petrokovets, M.I., Kovalev, A.V. (2005). Tribology of Polymers: Adhesion, friction, wear, and mass-transfer. *Tribology International* 38:910-921.

Newton, I. (1687). *Mathematical Principles of Natural Philosophy*. Trans. Andrew Motte, Daniel Adee (ed., 1846), New York (NY).

Niccolucci, F., Hermon, S. (2004). A Fuzzy Logic Approach to Reliability in Archaeological Virtual Reconstruction. *Proceedings of the Computer Applications and Quantitative Methods in Archaeology Conference* (CAA'04), Prato. F. Nicolucci (ed.), ArchaeoLingua, Budapest. pp.26-33.

Niemz, P. (1993). *Physik des Holzes und der Holzwerkstoffe*. DRW-Verlag, Leinfelden-Echterdingen.

O'Brien, M. (2003). *Finite Element Analysis of Wood and Composite Structured Hockey Sticks*. http://www.ecs.umass.edu/mie/labs/mda/fea/fealib/obrien/obrienPresentation.pdf

Ozyhar, T., Hering, S., Niemz, P. (2013). Moisture-dependent orthotropic tension-compression asymmetry of wood. *Holzforschung* 67(4):395-404.

Palomo, A. (2012). *Tecnologia lítica i de la fusta de la prehistòria recent al nord-est peninsular. Anàlisi tecnomorfològicat i experimental*. Ph.D. Thesis. Departament d'Antropologia Social i de Prehistòria,

Universitat Autònoma de Barcelona.

Palomo, A., Piqué, R., Bosch, A., Chinchilla, J., Gibaja, J.F., Saña, M., Tarrús, J. (2005). La Caza en el Yacimiento Neolítico de La Draga (Banyoles-Girona). P. Aria, R. García (ed.), in *Proceedings of the III Congreso del Neolítico Peninsular*, Santander (2003), pp.135-144.

Perros, H. (2009). *Computer Simulation Techniques: The definitive introduction!* Computer Science Department, NC State University, North Carolina.

Piqué, R. (2000). La Gestió dels Recursos Llenyosos a La Draga. In El Poblat Lacustre Neolític de La Draga. Excavacions de 1990 a 1998. Bosch, À., Chinchilla, J., Tarrús, J. (eds.). MAC, CASC, Girona. *Monografies del CASC* 2:140-149.

Piqué, R., Palomo, A., Terradas, X., Tarrús, J., Saña, M., Buxó, R., Bosch, A., Chinchilla, J., Bodganovic, I., López, O., (2013). The Oldest Neolithic Bows of Europe. *Current Anthropology*. (*in press*)

Plumb, O.A., Spolek, G.A., Olmstead, B.A. (1985). Heat and Mass Transfer in Wood Drying. *International Journal of Heat Mass Transfer* 28:1669-1678.

Pope, S. (1923). *Hunting with the Bow and Arrow*. Project Gutenberg *e*Book (2005), *e*Book #8084. http://www.gutenberg.org/ebooks/8084

Prior, S.J. (2000). The Skill of the Neolithic Bowyers - Reassessing the past through Experimental Archaeology. In *Somerset Archaeology: Papers to Mark 150 Years of the Somerset Archaeological and Natural History Society*. C.J. Webster (ed.). SCC, Taunton. pp.19-24.

Raja, V., Fernandes, K. J. (eds.) (2008). *Reverse Engineering: an industrial perspective*. Springer-Verlag, London.

Record, S.J. (1914). *The Mechanical Properties of Wood*. John Wiley & Sons, New York (NY).

Reichenbach, T., Kovačić, Z. (2003). Derivation of Kinematic Parameters from a 3D Robot Model Used for Collision-free Path Planning. Paper presented at the *11th Mediterranean Conference on Control and Automation*, MED '03. http://med.ee.nd.edu/MED11/pdf/papers/t2-039.pdf

Rendtroff, E.J. (1913). The Toxophilist's Paradox. *Forest and Stream* (February 8th).

Requicha, A.A.G. (1980). Representations for Rigid Solids: Theory, Methods, and Systems. *Computing Surveys* 12(4):437-464.

Rheingans, W.R. (1936). Exterior and Interior Ballistics of Bows and Arrows - Review. *Archery Review* (March-April).

Ripoll Perelló, E. (1972). Un palimpsesto rupestre de la Cueva del Castillo (Puente Viesgo, Santander). *Santander Symposium*, 457-464.

Rosendahl, G., Beinhauer, K.-W., Löscher, M., Kreipl, K., Walter, R., Rosendahl, W. (2006). Le plus vieil arc du monde? Une pièce intéressante en provenance de Mannheim, Allemagne. *L'Anthropologie* 110:371-382.

Rosillo, R., Tarrús, J., Palomo, A., Bosch, À., García de Consuegra, R. (2010). Les Esteles amb Banyes de la Serra del Mas Bonet (Vilafant, Alt Empordà) dins de l'Art Megalític de Catalunya. *Cypsela* 18. Museu d'Arqueologia de Catalunya, Barcelona.

Rosillo, R., Palomo, A., Moitinho, V. (2013). Técnicas Escultóricas en la Fabricación de las Estelas con Cuernos Neolíticas de la Serra del Mas Bonet (Vilafant, Alt Empordà - nordeste peninsular). In *Experimentación en arqueología. Estudio y difusión del pasado.* A. Palomo, R. Piqué, X. Terradas (eds.). Sèrie Monogràfica del MAC, Girona, pp.141-147. (*in press*)

Russ, J.C. (2011). *The Image Processing Handbook*. CRC Press, Boca Ratón (FL).

Saña, M. (2011). La Gestió dels Recursos Animals. In El Poblat Lacustre Neolític de la Draga. Excavacions

de 2000-2005. Bosch, À., Chinchilla, J., Tarrús, J. (eds.). MAC, CASC, Girona. *Monografies del CASC* 9:177-212.

Saranpaa, P. (2003). Wood density and growth. In *Wood Quality and its Biological Basis*. G. Jeronimidis, J.R. Barnett (eds.). Blackwell Publishing, Oxford. pp.87-117.

Schuster, B.G. (1969). Ballistics of the Modern-Working Recurve Bow and Arrow. *American Journal of Physics* 37(4):364-373.

Shapiro, V. (2001). *Solid Modeling*. Technical Report SAL 2001-2. Spatial Automation Laboratory, University of Wisconsin-Madison (WI).

Shmulsky, R., Jones, P.D. (2011). *Forest Products and Wood Science: an introduction*. John Wiley & Sons, Sussex.

Sjödin, J., Serrano, E. (2006). A Numerical Study of the Effects of Stresses Induced by Moisture Gradients in Steel-Timber Dowel Joints. *Holzforschung* 60:694-697.

SolidWorks (2012). *SolidWorks*. Dassault Systèmes. http://www.solidworks.com/

Stemmler, L.E. (1947). *The Essentials of Archery: how to use and make bows and arrows*. Manorville, New York (NY). http://www.stavacademy.co.uk/mimir/archeryessentials.htm

Straus, L.G., González Morales, M.R. (eds.) (2012). *El Mirón Cave, Cantabria, Spain*. University of New Mexico, Albuquerque (NM).

Straus, L.G., González Morales, M.R., Carretero, J.M (2011). Lower Magdalenian secondary human burial in El Mirón Cave, Cantabria, Spain. *Antiquity* 85:1151-1164.

Straus, L.G., González-Morales, M.R. (2012). *El Mirón Cave, Cantabrian Spain. The Site and its Holocene Archaeological Record*. University of New Mexico Press, Albuquerque (NM).

Subic, A.J., Cooke, A.J. (2003). Materials in Cricket. In *Materials in Sports Equipment*. M. Jenkins (ed.). Woodhead Publishing, Cambridge, and CRC press, Boca Raton (FL). pp.342-372.

Tapley, J. (2000). *Topics on Archery Mechanics*. http://www.tap46home.plus.com/mechanics/#

Tarrús, J. (2008). La Draga (Banyoles, Catalonia), an Early Neolithic Lakeside Village in Mediterranean Europe. Institut d'Estudis Catalans, Barcelona. *Catalan Historical Review* 1:17-33.

Taskini, J., Ghanadzadeh, H., Haghi, R.K., Haghi, A.K. (2006). Experimental Study on the Effect of Thermal Drying on the Mechanical Properties of Wood. *Proceedings of The 14th Annual International Mechanical Engineering Conference I.U.T*, Isfahan.

Taskini, J. (2007). Effect of Drying Methods on Wood Strength: a comparison between microwave, infrared, and convectional drying. *Mechanical & Aerospace Engineering Journal* 3(1):83-90.

Terradas, X., Antolín, F., Bosch, À., Buxó, R., Chinchilla, J., Clop, X., Gibaja, J.F., Oliva, M., Palomo, A., Piqué, R., Saña, M., Tarrús, J. (2012). Áreas de Aprovisionamiento, Territorios de subsistencia y Producciones Técnicas en el Neolítico Antiguo de La Draga. Congrés Internacional Xarxes al Neolític - "Neolithic Networks Rubricatum". *Revista del Museu de Gavà* 5:441-448.

Terradas, X., Clemente, I. (2001). La Experimentación como Método de Investigación Científica: aplicación a la tecnología lítica. In *Prehistoire et approche expérimentale*. L. Bourguignon, I. Ortega, M.C. Frère-Sautot (eds.). *Préhistoires* 5:89-94.

Uddeholm (2004). *Polishing Mould Steel*. Uddeholm. http://www.uddeholm.com.ar/files/polishing-eng_040608.pdf

USAITA (n.a.). *Glossary*. U. S. Army Information Technology Agency. http://ita.army.mil/CatalogService.aspx?service_Id=122&serviceGroup_Id=9

Váradi, K., Palásti-Kovács. B., Czifra, Á., Néder, Z., Kovács, K. (2004). 3D Characterization of Engineering Surfaces. *Budapest Tech Jubilee Conference*.

Wang, W. (2011). *Reverse Engineering: Technology of Reinvention*. CRC Press, Boca Ratón (FL).

Whitehouse, D.J. (2002). *Handbook of Surface Metrology*. Institute of Physics, Bristol.

Wroe, S., Moreno, K., Clausen, P.D., McHenry, C.R. (2007). High-resolution Three-dimensional Computer Simulation of Hominid Cranial Mechanics. *The Anatomical Record* 290:1248-1255.

Yonekura, K., Hasegawa, H., Hotta, A., Suzuki, T. (2008). A Novel Approach to Studies of Prehistoric Exploitation of Stone Tool Materials Using Material Composition, Surface Morphology, Microstructure and Mechanical Properties. *Archaeometry* 50(5):727-746.

Zaniewski, I. (2009). Modeling of the Archery Bow and Arrow Vibrations. *Shock and Vibration* 16:307-317.

Ø5
Final Reflections

> *Yet I exist in the hope that these memoirs, in some manner, I know not how, may find their way to the minds of humanity in Some Dimension, and may stir up a race of rebels who shall refuse to be confined to limited Dimensionality.*
>
> Edwin A. Abbot (1838-1926), in Flatland. A Romance of Many Dimensions (1884, 2nd ed.)

The first chapter initiated with the problem statement and general remarks, followed by the objectives of this research, and work dissemination. A theoretical approach was presented in the second chapter, while a framework was proposed in the third chapter where aspects dealing with methods, processes, techniques and tools were described in a way that makes them useful. A full integration of the method was presented in the fourth chapter, in the form of three case studies. Each case study was built in the information described in the previous chapters. However, only the parts of the method needed to accomplish its initial goals were used. Due to time constraints, the discussion of each case study was also dependant on the breadth and depth of investigations which have been carried out in each topic. Notwithstanding, they were intended to highlight the flexibility of the proposed method, and preliminary results show clearly its potential and strength.

The results of each case study have been presented in the corresponding sections, while related conclusions

and future works have been presented at the end of each case study.

*

Ever since the studies of materials from direct observation and handling has provided data of great and unquestionable relevance. Visual perception makes us aware of many fundamental properties of material evidences from past human activities. Different characteristics have almost certainly been of great importance for different explanations. For their study it is essential to measure, to compare and to classify the various attributes of archaeological materials, as much as to quantify them, since these allow to describe its (ir)regularity and to some extent making possible the study of its causes.

Why archaeological artefacts are the way they are? In this research I tried to solve such a question by investigating the relationship between geometry (shape, form, and texture), material and function. I have proposed new ways of studying the way behaviour in the past can be asserted on the examination of archaeological observables in the present. In any case, I took into account that there are also non-visual features characterizing ancient objects and materials. Information that should make us aware of many functional properties of objects is multidimensional in nature: size, shape, form, texture, visual appearance of surfaces, and material. With the exception of material data, the other relevant aspects for functional reasoning have been traditionally described in rather ambiguous terms, without taking into account the advantages of quantitative measurements.

Reasoning about the functionality of archaeological objects recovered at the archaeological site requires a cross-disciplinary investigation. The approach I adopted here was to follow current computational theories of object perception to ameliorate the way archaeology can deal with the explanation of human behaviour in the past (function) from the measurement and analysis of visual and non-visual data, taking into account that visual appearances and even compositional characteristics only constrain the way an object may be used, but never fully determine it.

In a wide perspective, the aim of this research has been to contribute to a better knowledge about the function of archaeological objects. In a more confined sense, to develop a comprehensive framework based on Reverse Engineering processes, where the initial objectives were achieved:

1. A framework based on specific methods and techniques has been developed and used to generate three dimensional geometrical digital models; to measure and quantify shape, form, and texture features; to measure and quantify the physical and mechanical properties of materials; to test and analyse the use and behaviour of archaeological artefacts.
2. Different approaches have been applied, in order to understand possible relationships between the geometry, material, and function(s) of archaeological artefacts.
3. Digital models of archaeological artefacts have been documented for future reuse and repurpose.

The framework was applied to three distinct case studies spanning a broad diachrony ranging from the Palaeolithic in Cantabria to the Neolithic in Catalonia, Spain, whereas the archaeological objects of study

encompass rock art, sculptures, lithics, and bows, as well as a variety of raw-materials. Since each case study had its own archaeological questions and aims, and was strongly limited by time, different parts of the framework have been tackled and therefore implemented. The case studies described were neither intended to be exhaustive nor to be limiting in scope, but to be exemplary and illustrative of the potentialities and effectiveness of the proposed framework. At the end, the framework proved to be both efficient and flexible, allowing for its implementation in other archaeological contexts.

The approach involved applying Reverse Engineering processes from the physical-to-digital stage to the interpretation stage. In the context of the present research, it consisted in recapturing how the object was made and its function(s), by analysing its shape, form, texture, material, and behaviour.

When planning survey strategies, there were technical issues, operational imperatives and environmental conditions which were taken into account, in order to prevent or troubleshoot problems. Likewise, on the one hand, it was fundamental to have a thorough understanding and knowledge of how the workflow functioned, since each stage of the process depends on the outcome of the previous ones and determines the subsequent ones. On the other, to set clear objectives when tailoring each step's parameters. Every selection of parameters and variables should always depend on the archaeological question behind and be adequate to describe specific features of the objects of study. It was of paramount importance to ensure data consistency and best results, by applying the same methods, techniques, and measurement schemes within each stage and step of the framework.

Dealing with various equipment and computer programs throughout the framework was not always straightforward. A full operability between hardware-software and software-software urges for a fast solution. Considering that the amount of digital data collected and generated is enormous, resulting in questions of processing, post-processing, data storage, accessibility and preservation, hardware and software capacities should not be overestimated. On the contrary, it is undoubtedly a very critical technical issue – as they presently are a common working tool, thus part of the research process – and almost likely the Achilles heel of the framework.

It has happened more than once that people seemed to be expecting too much of 3D data capture and were bound to be disappointed with the 'scanning in action'. It takes indeed time, effort, planning, sometimes patience with the weather forecast and overall logistics, among other issues, to obtain a good 3D digital model. 3D Scanning and processing are a most labour-intensive work, urging for instance for a fast and global registration, with an entirely automated on-the-fly multiview alignment. I have taken the approach of starting with as rich a data set as possible and then simplifying it as needed in each subsequent step using derivative 3D models. All 3D scanned raw data, derivative digital models, and corresponding metadata and paradata were saved in a specific repository. However, there is a challenge for standardization of policies and strategies for long-term digital preservation, as well as for transparency and access to 3D digital data.

Although a 3D digital model does not provide a complete picture of the object, it should be understood as a highly powerful tool – potentially, with valid data – for archaeological research, and complementary to other measurement techniques. It has been common practice to use 3D digital models to extract traditional 2D information. But why not use the potentialities of these multidimensional digital models, instead of insisting in mainly replicating 2D work if this is not the information that we actually seek? The 3D models allowed

achieving stimulating results, as they enabled to acquire meaningful (and quantitative) geometrical information from distinct archaeological artefacts and differentiate from one another.

The undertaken shape and form basic measurements and indices were representative, in order to characterize morphologically the artefacts considered and differentiate from one another. It was surprising to verify how sometimes a single or simple descriptor permitted to infer a conceptual frame in the manufacturing planning and shaping of archaeological objects.

Curvature analysis enabled to semi-automatically detect use-wear macro traces, and to visually differentiate surface texture regions. Although the interest of this 3D analytical technique, it has revealed insufficient, in that it did not allow to quantitatively describe and compare between surface texture patterns.

This prompted me to delve deeper into 3D areal parameters and specialized metrology software, which provided a new insight into the quantitative description and analysis of the three-dimensional digital surface textures. Surface metrology applications have the ability to greatly contribute to our understanding of ancient manufacturing procedures, among other archaeological issues. Measurement standards demonstrated to be useful tools to this end. The potential of the ISO 25178-2 surface texture parameters and measurement of texture direction is vast, and can undoubtedly shed light on distinct archaeological issues.

Comprehensive analytical methods and techniques used in material science were applied to the analysis of the physical and mechanical properties of a set of wood species. The significance of these properties in the selection and use of raw materials is evident, although one should not ignore the perception of the raw material's characteristics, the importance of the resources location, and exchange networks.

Three-dimensional digital models of archaeological artefacts provided unique experimental approaches for studies in their functional aspects. As I have demonstrated across this framework, different techniques permit to detect distinct features on the surface models. The power of solid models – in the sense of being close surrogates of both form and material of the real object – allowed to apply theory to real-world situations, by virtually integrate the data, test hypothesis, and understand the object as a whole. While the experimental studies presented using computer simulation are still at a preliminary stage, they have already enabled to draw some novel and useful results. FEA has emerged as a powerful tool in the prediction of the material and mechanical behaviour of archaeological artefacts. The computer simulation results were able to provide comprehensive knowledge on practical material selection and usage, adding exact meaning (i.e. quantitative data) and interpretation (i.e. simulation tests) to conventional studies.

Ideally, the achieved results should be compared and supported by other sorts of data, to enable more complete *what if?* scenarios and therefore a comprehensive understanding of the subject. The possibility to include physical experimental work permitted to raise and test interesting hypothesis, which undoubtedly enriched this investigation by yielding valuable information.

*

The approach herein presented demonstrates the interest of the proposed framework towards a better comprehension of archaeological objects, by bringing quantitative 3D digital methods and techniques to functional

analysis, as well as to ancient manufacturing processes analysis. To this end, I have investigated the geometry, material, and behaviour of a set of archaeological artefacts.

3D Scanning will likely become as common as microscopes in archaeological research groups or University departments, as an increasing number of researchers are already working with some of these technologies on an everyday basis. I have demonstrated that there are fields where 3D digital data analysis is an obvious upgrade on the way things are currently being done. Besides costs and training, there is probably some education that still needs to be done.

Every equipment and software mentioned in this research was used as a means (tools) for attaining very specific objectives. Their use does not imply that they are the 'best' available for all purposes within this framework, but that they enable to achieve the objectives set for each stage of the framework, were made available for this research, and in a few cases I was prior acquainted with – the latter exempting me from spending time learning how to use even more software, therefore allowing to focus on further issues. There are indeed other free, proprietary/commercial and non-comercial software which can be utilized to achieve similar purposes.

I explicitly did not intend to rewrite a step-by-step manual on how to use each equipment or software. If doing so, both chapters 3 and 4 would most certainly be obsolete even before being finished, since new technologies, equipment, software, models and versions appear in the market every year. Those interested in more detailed technical procedures should consult the corresponding user´s manuals.

The novelty of the framework lies in the integration of several unconventional methods and procedures in archaeological research, towards the study of functional analysis and working processes of multidimensional digital models of archaeological objects. New tools and new techniques require new workflows, to enable new researches which may permit new results and understandings. A chain of procedures from data acquisition to information extraction has been described and illustrated. In addition, the non-invasive nature of the approach – from 3D scanning to computer simulation – renders it of particular value in archaeological studies.

Personally, one of the real values of this research lies on the merge of seemingly unlikely but yet so intertwined scientific domains – an interdisciplinary approach between different branches of archaeology, history of technology, material and mechanical engineering, physics, and software developers, among others, encompassing a wide range of specialists. This interdisciplinary approach proved extremely useful enabling a real progress in the whole broad spectrum of the subjects herein investigated.

Even though this is the final chapter, I am well aware that I barely began to tackle some important issues. I hope I have managed, on the one hand, to take a first step toward a systematic procedure for functional analysis, by Reverse Engineering archaeological objects. On the other hand, that the results of this research contribute to the current body of knowledge in the relevant field of study. At the same time, aware that technologies, software and devices are in constant development, I am sure that many and much interesting scientific results covering these topics will be published within the near future.

5.1 Future works

Besides those specifically related to each particular case study, and already described, future works may include:

- To continue disseminating the outcomes of this research to the academic scientific community, as well as to the general public, through conferences, papers, and the Internet.
- To delve further into some of the many complex issues presented;
- To continue investigating issues related to the *hows*, *whys* and *what-ifs* of surface phenomena;
- To integrate further types of visual and non-visual data;
- Regarding the simulation of the use-function of archaeological objects, to investigate the type of kinect technology and wiimote tracking as an entry point to gather further information about causality and work space environment.